

# HYDROGEOLOGY, GROUNDWATER CHEMISTRY, AND WATER BUDGET OF JUAB VALLEY, EASTERN JUAB COUNTY, UTAH

*by Hugh A. Hurlow, Paul C. Inkenbrandt, and Trevor H. Schlossnagle*



**SPECIAL STUDY 170**  
**UTAH GEOLOGICAL SURVEY**  
UTAH DEPARTMENT OF NATURAL RESOURCES  
**2022**

*Blank pages are intentional for printing purposes.*

# HYDROGEOLOGY, GROUNDWATER CHEMISTRY, AND WATER BUDGET OF JUAB VALLEY, EASTERN JUAB COUNTY, UTAH

by

*Hugh A. Hurlow, Paul C. Inkenbrandt, and Trevor H. Schlossnagle*

**Cover image:** *Perspective of a drop of water starting out at the top of Mt. Nebo, flowing down to Mona Reservoir. View to the west.*

Suggested citation:

Hurlow, H.A., Inkenbrandt, P.C., and Schlossnagle, T.H., 2022, Hydrogeology, groundwater chemistry, and water budget of Juab Valley, eastern Juab County, Utah: Utah Geological Survey Special Study 170, 101 p., 1 appendix, 2 plates, <https://doi.org/10.34191/SS-170>.



**SPECIAL STUDY 170**  
**UTAH GEOLOGICAL SURVEY**  
UTAH DEPARTMENT OF NATURAL RESOURCES  
**2022**



**STATE OF UTAH**  
Spencer J. Cox, Governor

**DEPARTMENT OF NATURAL RESOURCES**  
Joel Ferry, Executive Director

**UTAH GEOLOGICAL SURVEY**  
R. William Keach II, Director

**PUBLICATIONS**

contact

Natural Resources Map & Bookstore  
1594 W. North Temple  
Salt Lake City, UT 84116  
telephone: 801-537-3320  
toll-free: 1-888-UTAH MAP  
website: [utahmapstore.com](http://utahmapstore.com)  
email: [geostore@utah.gov](mailto:geostore@utah.gov)

**UTAH GEOLOGICAL SURVEY**  
contact

1594 W. North Temple, Suite 3110  
Salt Lake City, UT 84116  
telephone: 801-537-3300  
website: [geology.utah.gov](http://geology.utah.gov)

*Although this product represents the work of professional scientists, the Utah Department of Natural Resources, Utah Geological Survey, makes no warranty, expressed or implied, regarding its suitability for a particular use. The Utah Department of Natural Resources, Utah Geological Survey, shall not be liable under any circumstances for any direct, indirect, special, incidental, or consequential damages with respect to claims by users of this product.*

*The Utah Geological Survey does not endorse any products or manufacturers. Reference to any specific commercial product, process, service, or company by trade name, trademark, or otherwise, does not constitute endorsement or recommendation by the Utah Geological Survey.*



## CONTENTS

ABSTRACT.....	1
INTRODUCTION .....	2
Study Area .....	2
Hydrology .....	4
Objectives .....	4
HYDROGEOLOGIC SETTING .....	4
Geography, Climate, and Surface Water.....	4
Stratigraphy and Structural Geology .....	5
Hydrostratigraphy .....	12
Groundwater .....	16
Hydrogeographic Areas .....	22
BASIN-FILL HYDROLOGY.....	22
Introduction.....	22
Lithology.....	23
Introduction .....	23
Methods .....	23
Results.....	23
Lithologic Profiles .....	23
Grain-size Maps .....	29
Interpretation .....	30
HYDRAULIC PROPERTIES.....	30
Introduction.....	30
Methods .....	30
Results.....	30
STRUCTURE .....	32
Introduction.....	32
Methods .....	32
Well Data .....	32
Gravity and Seismic-Reflection Data .....	32
Gravity Model Profiles .....	32
Results.....	35
Interpretation of Seismic-Reflection Profile and Gravity Model .....	35
Isopach Map .....	36
Discussion.....	36
GROUNDWATER LEVELS .....	38
Introduction.....	38
Previous Work.....	38
Methods .....	38
Groundwater Level Measurement .....	38
Potentiometric Surface Map.....	38
Groundwater Level Change.....	38
Groundwater Storage Change .....	39
Inundation Changes.....	39
Results.....	40
Groundwater-Level Map for 2015 .....	40
Groundwater-Level Changes from 1993 to 2015.....	40
Groundwater-Level Monitoring .....	40
Transient Electromagnetic Survey .....	52
Rates of Groundwater-Level Decline based on U.S. Geological Survey Data .....	52
Reduction in Size of Discharge Area, Southwestern Juab Valley .....	52
Change in Groundwater Storage .....	54
Discussion.....	54
Levan Ridge Groundwater Divide .....	54
Groundwater-Level Changes.....	54
GROUNDWATER CHEMISTRY .....	55

Introduction.....	55
Previous Work.....	55
Methods .....	55
Sample Collection .....	55
Bayesian Mixing Model .....	55
Results and Discussion .....	57
Temperature .....	57
Major Solute Chemistry and Total Dissolved Solids .....	57
Stable Isotopes.....	63
Radiogenic Isotopes .....	71
MONA RESERVOIR WATER BUDGET .....	73
Introduction.....	73
Previous Work.....	73
Methods .....	73
Bathymetric Survey.....	73
Hypsometric Curve.....	73
Stream Gaging.....	75
Budget Calculation .....	75
Results and Discussion .....	76
GROUNDWATER BUDGET .....	76
Previous Work.....	76
Methods .....	77
MODFLOW Model .....	77
Recharge .....	79
Seepage from Streamflow .....	79
Recharge and Irrigation .....	79
Subsurface Inflow.....	84
Discharge .....	85
Groundwater Pumping .....	85
Flow to Goshen Valley .....	88
Springs and Seeps.....	88
Evapotranspiration.....	88
Results and Discussion .....	88
Recharge.....	88
Discharge.....	89
Storage Change.....	91
Error Quantification.....	94
SUMMARY .....	94
ACKNOWLEDGMENTS .....	98
REFERENCES .....	98
APPENDIX.....	102

## FIGURES

Figure 1. Geographic and hydrologic setting of Juab Valley, Juab County, Utah .....	3
Figure 2. Precipitation records for Juab Valley climate stations.....	6
Figure 3. Hydrographs for Salt Creek in Juab Valley .....	7
Figure 4. Hydrographs for Currant Creek in Juab Valley .....	9
Figure 5. Hydrographs for Chicken Creek .....	11
Figure 6. Stratigraphic column for Juab Valley study area .....	13
Figure 7. Estimates of annual groundwater pumping in Juab Valley .....	17
Figure 8. Histograms and statistics for well depths and the top of open or screened intervals for wells in Juab Valley .....	17
Figure 9. Analysis of water-level trends for wells in Juab Valley.....	18
Figure 10. Pie-diagram maps showing relative proportions of fine, mixed, and coarse-grained deposits interpreted from driller's logs.....	24

Figure 11. Transmissivity estimates for the Juab Valley basin-fill aquifer calculated from data in drillers' logs and aquifer test data .....	31
Figure 12. Map of gravity stations, model profiles, and wells for which depth to bedrock was interpreted from drillers' logs .....	33
Figure 13. Grid of complete Bouguer gravity anomaly values for Juab Valley and adjacent areas .....	34
Figure 14. Gravity model profile trending east-west through Nephi, along the seismic-reflection line published by Zoback (1992) .....	35
Figure 15. Isopach map of the Juab Valley upper basin fill from gravity model profiles .....	37
Figure 16. Water-level map for Juab Valley from March to April 2015, and interpretations of the potential groundwater divides .....	41
Figure 17. Map of Levan Ridge area, showing wells having 2015 groundwater levels, interpreted water-level contours, and alternative positions, including our preferred position, of the groundwater divide .....	42
Figure 18. The Levan Ridge area showing TEM stations and alternative interpretations of water-level contours and groundwater divide .....	43
Figure 19. Changes in Juab Valley groundwater levels from 1993 to 2015, including change values at anomalous wells and interpreted contours .....	47
Figure 20. Map of wells monitored monthly and both monthly (manually) and continuously (by pressure transducers) .....	48
Figure 21. Hydrographs for wells monitored for depth to water by the UGS .....	49
Figure 22. Seasonally flowing wells H2-S1 and H2-S2 northeast of Chicken Creek Reservoir in the southwest part of the Levan hydrogeographic area .....	50
Figure 23. Change in surface-water classes from 1984–99 to 2000–19 based on Joint Research Centre European Commission (JRC) data .....	51
Figure 24. Location and site type of Juab Valley water chemistry samples .....	56
Figure 25. Map of groundwater temperatures measured during chemical sampling in 2015 and 2017 .....	58
Figure 26. Piper diagram for groundwater and surface water samples collected in 2015 and 2017, categorized by hydrogeographic area and site type .....	59
Figure 27. Pie map showing relative concentrations of major solutes of groundwater and surface water samples collected in 2015 and 2017 .....	60
Figure 28. Map of TDS concentrations of groundwater and surface water samples collected in 2015 and 2017 .....	61
Figure 29. Results of cluster analysis of Juab Valley chemical samples collected in 2015 and 2017 .....	64
Figure 30. Map of cluster assignments of groundwater and surface water samples collected in 2015 and 2017 .....	66
Figure 31. Sites where stable isotope data were collected, symbolized by site type .....	67
Figure 32. Stable-isotope compositions of groundwater and estimated seasonal precipitation end-members .....	70
Figure 33. Map of tritium-unit values (TU) for Juab Valley water chemistry samples collected in 2015 and 2017 .....	72
Figure 34. Carbon-isotope compositions and simple mixing lines between modern soil gas and carbonate minerals .....	73
Figure 35. Map of lumped parameter model ages for Juab Valley water chemistry samples collected in 2015 and 2017 .....	74
Figure 36. Mean residence time of samples and age progression with indicative flow velocities along the flow path from Levan to Chicken Creek Reservoir .....	75
Figure 37. Best-fit model of age progression for samples along the flow path from Levan to Chicken Creek Reservoir .....	75
Figure 38. Hypsometric curve for Mona Reservoir .....	76
Figure 39. Frequency analysis for Currant Creek inflow data collected by the UGS .....	77
Figure 40. Flow components for the water balance of Mona Reservoir .....	78
Figure 41. Model grid of the updated USGS 3-dimensional groundwater flow model .....	80
Figure 42. Subwatersheds analyzed using StreamStats .....	81
Figure 43. Validation of StreamStats models against measured monthly flow in the Salt Creek and Chicken Creek watersheds .....	82
Figure 44. Regression analysis of the Chicken Creek watershed against yearly discharge estimates .....	83
Figure 45. Exponential relationship between precipitation and subsurface inflow (solid lines) for each area of subsurface input, and resulting time-series .....	86
Figure 46. Relationship between valley-wide groundwater pumping and precipitation .....	87
Figure 47. Regression model results for temporal groundwater pumping model .....	90
Figure 48. Distribution of pumping intensity estimated using spatial groundwater pumping model .....	92
Figure 49. Estimated groundwater evapotranspiration over time .....	93
Figure 50. Hydrographs showing modeled and measured changes of potentiometric surface elevation over time in select wells .....	95
Figure 51. Modeled groundwater storage change for Juab Valley over time .....	96

## TABLES

Table 1. Hydrogeologic Units .....	14
Table 2. Rates of water-level change from U.S. Geological Survey data .....	53
Table 3. Results of radiogenic-isotope analyses and models .....	57
Table 4. Results of factor analysis of major-solute concentrations.....	62
Table 5. Mean solute concentrations of statistical clusters .....	63
Table 6. Mona Reservoir budget for water years 2019 and 2020 .....	79
Table 7. Stress periods for the revised Thiros and others (1996) model.....	79
Table 8. Yearly streamflow estimates aggregated to major areas of Juab Valley and adjusted for different years.....	84
Table 9. Groundwater recharge in Juab Valley from distribution-system loss and unconsumed irrigation return flow .....	85
Table 10. Groundwater budget for Juab Valley.....	89
Table 11. Water-related events in history of Juab Valley .....	94

## PLATES

- Plate 1. Generalized geologic map of study area.
- Plate 2. Cross sections of Juab Valley.

# HYDROGEOLOGY, GROUNDWATER CHEMISTRY, AND WATER BUDGET OF JUAB VALLEY, EASTERN JUAB COUNTY, UTAH

by Hugh A. Hurlow, Paul C. Inkenbrandt, and Trevor H. Schlossnagle

## ABSTRACT

Juab Valley is a north-south-trending basin in the eastern Basin and Range Province. Juab Valley is bounded on the east by the Wasatch normal fault and the Wasatch Range and San Pitch Mountains, bounded on the west by Long Ridge and the West Hills. Juab Valley is at the southern end of Utah's Wasatch Front, an area of projected rapid population growth and increased groundwater use. East-west-trending surface-water, groundwater, and water-rights boundaries approximately coincide along the valley's geographic midline at Levan Ridge, an east-west trending watershed divide that separates the north and south parts of Juab Valley. The basin includes, from north to south, the towns of Mona, Nephi, and Levan, which support local agricultural and light-industrial businesses. Groundwater use is essential to Juab Valley's economy.

The Juab Valley study area consists of surficial unconsolidated basin-fill deposits at lower elevations and various bedrock units surrounding and underlying the basin-fill deposits. Quaternary-Tertiary basin-fill deposits form Juab Valley's primary aquifer. Tertiary volcanic rocks underlie some of the basin-fill deposits and form the central part of Long Ridge on the northwest side of the valley. Paleozoic carbonate rocks that crop out in the Mount Nebo area of the Wasatch Range, which receives the greatest average annual precipitation in the study area, likely accommodate infiltration of snowmelt and subsurface groundwater flow to the basin-fill aquifer. The Jurassic Arapien Formation also crops out in the Wasatch Range and San Pitch Mountains, and dissolution of gypsum and halite in the formation and sediments derived from it increases the sulfate, sodium, and total-dissolved-solids concentrations of surface water and groundwater. We grouped the stratigraphy of the Juab Valley study area into 19 hydrostratigraphic units based on known and interpreted hydraulic properties.

Streamflow and groundwater recharge to the Juab Valley is derived from the annual snowpack in the eastern-bounding mountains. Stream gage data from the U.S. Geological Survey indicate that flow of Salt Creek and Currant Creek declined from the early 1990s to 2015. Recharge to the valley's basin-fill aquifer occurs mainly along the eastern mountain front, by infiltration of streamflow on the alluvial-fan heads and by underflow from bedrock across the Wasatch normal-fault system into the aquifer. Previous work by the U.S. Geological Survey identified two major groundwater-flow paths: in the northern part of the valley, from a recharge zone along the eastern mountain front between Salt Creek and North Creek, flowing to the west and northwest to a major discharge zone in

the valley bottom that includes the spring-fed Burraston Ponds and Mona Reservoir; and in the southern part of the valley, from the Pigeon Creek and Chicken Creek alluvial fans near Levan, southwest to a major groundwater-discharge area at and northeast of Chicken Creek Reservoir.

Seven profiles constructed from driller's logs for water wells illustrate spatial and depth variations in the lithology of the upper ~400 ft of the basin fill. At the Mona Reservoir-Burraston Ponds discharge area, basin-fill deposits transition abruptly from predominantly coarse- and mixed-grain-size deposits in the southeast and east to predominantly fine-grained deposits below the discharge area. The reduced transmissivity likely forces groundwater toward the surface. A similar transition in grain size occurs east of Mona Reservoir. At the Chicken Creek Reservoir discharge area, basin-fill deposits transition abruptly from predominantly coarse- and mixed-grain-size deposits in the northeast and east to predominantly fine-grained deposits below the discharge area. Basin-scale groundwater flow likely occurs mainly between 100- and 300-ft depth, because the basin-fill deposits in that depth range are overall coarser than those in the upper 100 ft.

Transmissivity of the basin-fill aquifer estimated from selected well tests reported on drillers' logs ranges from 14 to 116,110 ft<sup>2</sup>/day, and the median value is 1580 ft<sup>2</sup>/day. Transmissivity is typically greater in the proximal parts of the alluvial fans that emanate from the ranges bounding the eastern valley margin.

Historical and newly acquired gravity data were used to construct an isopach map of basin-fill thickness. A previously published seismic-reflection line that trends east-west through Nephi shows a prominent reflection in the basin fill that is interpreted here to represent the unconformity between the syn-tectonic basin-fill sediments that form the principal aquifer above (upper basin fill), and the less transmissive Tertiary volcanic and/or sedimentary rocks (lower basin fill) below. The isopach map gives an estimate of the thickness of these upper basin-fill deposits. Basin-fill thickness ranges from 2000 to 3250 ft below the valley center from the latitude of Mona to Levan. An east-west-trending concealed bedrock high exists below the southern part of Mona Reservoir, and basin fill is as much as 2000 ft thick below the northern part of the reservoir.

The Utah Geological Survey (UGS) performed a valley-wide groundwater-level campaign during March and April 2015. Groundwater-level contours indicate flow to the north-northeast north of the groundwater divide near Levan Ridge, and

flow to the southwest south of the divide. Most contours are horseshoe-shaped, trending parallel to valley margins and approximately perpendicular to the valley-floor axis. Complicated contour patterns exist below areas of intensive agricultural pumping and interspersed residential development. Two viable interpretations exist for the position of the Levan Ridge groundwater divide. The preferred interpretation places the divide as much as 4 miles north of its interpreted location based on 1965 groundwater levels, and north of the administrative and surface-water boundary.

Samples collected in 2015 and 2017 characterize the major-solute composition of groundwater in Juab Valley and surface water in the ranges that bound the valley on the east. Groundwater and surface water are predominantly Mg-HCO<sub>3</sub> type and mixed Mg-Ca-HCO<sub>3</sub>-SO<sub>4</sub> type, with distinct trends toward increasing Na, Cl, and SO<sub>4</sub>. Five statistically distinct major-solute composition types reflect differences in water chemistry by geographic area and due to differing amounts of chemical interaction with Paleozoic carbonates, sediment, and the evaporite-rich Arapien Formation. Groundwater in the Levan area is more sulfate-rich than in the rest of the valley.

The stable isotopes of hydrogen and oxygen (<sup>2</sup>H and <sup>18</sup>O, respectively) generally become more depleted from east to west, reflecting progressively lower temperatures at the time of recharge. Due to relatively smaller amounts of precipitation, low hydraulic conductivity, and a low hydraulic gradient, little recharge occurs from the mountains bounding the valley on the west. Also, based on existing regional isotope studies, the recharge in the west has more enriched stable-isotope composition in contrast to the observed overall trend. Based on that information, the east-to-west variation probably reflects increasing age of groundwater that was recharged under overall cooler ambient temperatures. The stable-isotope composition of groundwater at Burrison Ponds and an adjacent well is more similar to streams in the Wasatch Range than to groundwater samples from the northern and southern parts of the valley. This may indicate a zone of comparatively high groundwater flow rate supplying the springs that form Burrison Ponds.

We collected samples of the radiogenic isotopes <sup>3</sup>H (tritium) and <sup>14</sup>C to evaluate groundwater ages and travel times along flow paths. Tritium values decrease along the groundwater flow path from the Salt Creek alluvial-fan recharge area to the Burrison Ponds–Mona Reservoir discharge area, reflecting progressively older groundwater; a major exception is at a well just east of Burrison Ponds which shows the highest tritium value of the 14 samples. This result may reflect the highly transmissive flow path from the Wasatch Range front to Burrison Ponds springs indicated by the stable-isotope data, or local recharge of irrigation water. Tritium values in the Levan Ridge area are low and reflect recharge ages of >60 years. Tritium values decrease along the groundwater flow path from the Pigeon Creek–Chicken Creek alluvial-fan recharge area to the Chicken Creek Reservoir discharge area, reflecting progressively older groundwater.

Carbon-14 model ages could be calculated for 6 of the 13 samples and range from about 1200 to 15,000 years. The remaining samples contained some <sup>14</sup>C generated during above-ground nuclear weapon testing, and their ages could only be constrained as <1000 years. The oldest samples occur in the western part of the valley, consistent with the hypothesis that little if any groundwater recharge occurs along the western valley margin. Model ages along the groundwater flow path from Pigeon Creek–Chicken Creek to Chicken Creek Reservoir increase progressively with increasing distance from the mountain front, although the model age of the southwestern sample is substantially greater than the other samples, suggesting input of deeper, older groundwater.

The Juab Valley groundwater budget is in deficit on average of about 7080 ac-ft/yr. The loss in discharge and decrease in storage is driven by increased groundwater pumping and decreasing precipitation over time. Relatively wet water years can temporarily increase storage but will likely not cause a complete water level recovery to levels observed prior to the 1990s. Despite groundwater discharge to Mona Reservoir, it has been completely emptied at least twice in the past decade, and if current conditions persist, this will likely happen again.

## INTRODUCTION

This report summarizes the findings of a hydrogeologic study of Juab Valley in eastern Juab County, Utah, conducted in 2015–20 by the Utah Geological Survey (UGS). The principal work included a valley-wide campaign to (1) measure groundwater levels and sample for groundwater chemistry and isotope composition, (2) delineate basin-fill lithology using well driller's logs, (3) estimate basin-fill thickness and structure using gravity and well data, and (4) conduct a three-year study to calculate water budget components of the valley with emphasis on the northern part of the valley including Mona Reservoir. Hugh Hurlow (UGS) and Brittany Dame (former UGS) performed the initial work of the study, including the groundwater-level campaign, chemical sampling, and well-log interpretation. Christian Hardwick (UGS Energy and Minerals Program) and assistants collected and processed new gravity and electromagnetic data. Paul Inkenbrandt and Trevor Schosnagle, with assistance from J. Lucy Jordan, Will Hurlbut, and Emily McDermott (all UGS) measured streamflow and collected stable isotope samples. Stan Smith (former UGS) interpreted the stable and radiogenic isotope data.

## Study Area

Juab Valley (figure 1) is at the southern end of Utah's Wasatch Front, an area of strong economic activity and rapid projected population growth. Compared to the central Wasatch Front, Juab Valley is predominantly rural and sparsely populated

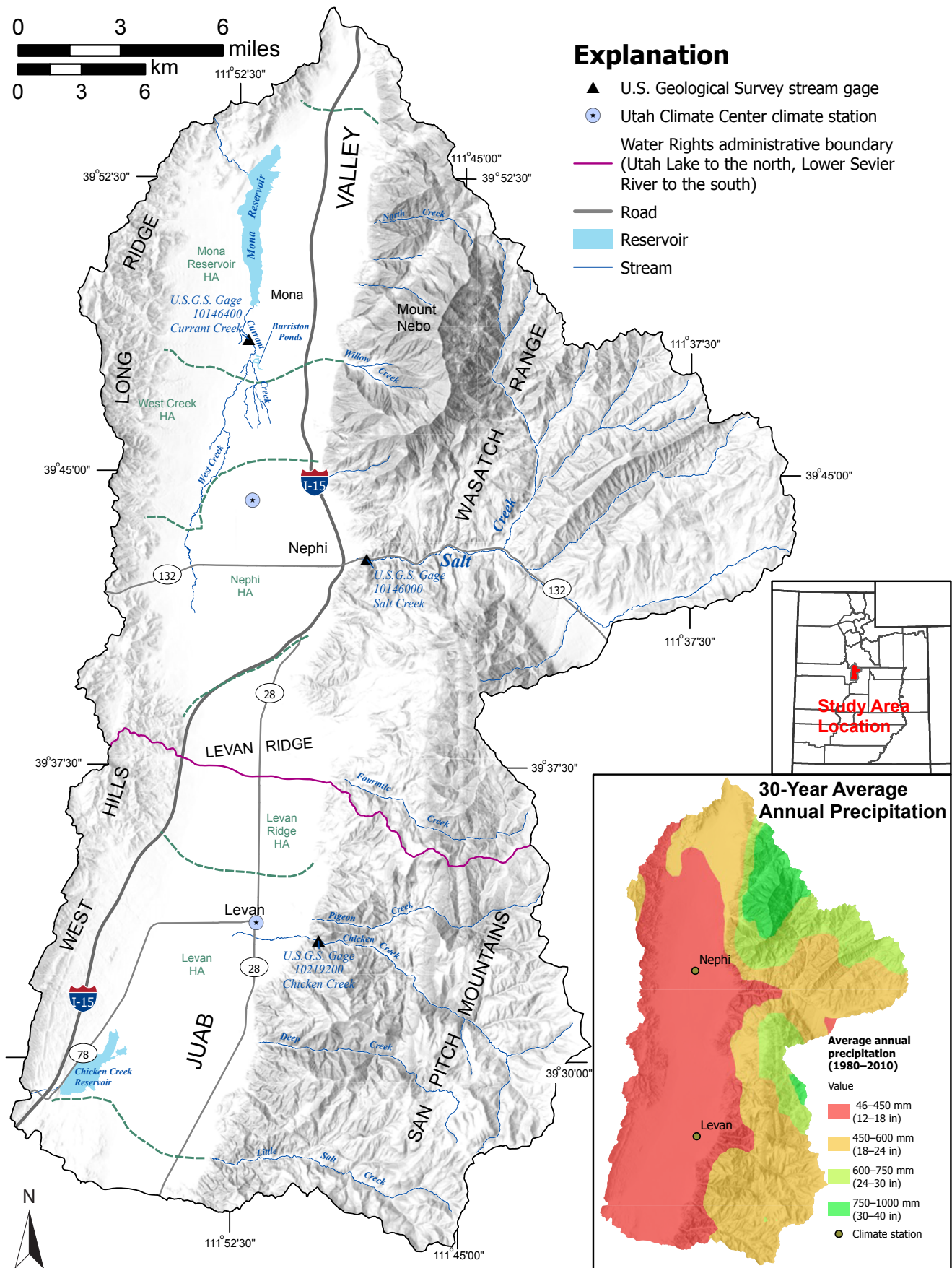


Figure 1. Geographic and hydrologic setting of Juab Valley, Juab County, Utah. Inset: Average annual precipitation from 1980 to 2010 (PRISM Climate Group, 2012).

(about 10,873 people in 2020 [U.S. Census, 2020]). The economy is based primarily on agriculture and light industry including manufacturing and mining. The population is projected to increase to about 23,400 by 2050 (Utah Foundation, 2014a), and water use, mostly derived from groundwater, is expected to increase during the next 30 years along with that of the rest of Utah (Utah Foundation, 2014b).

## Hydrology

The study area is set in the Great Basin hydrologic area and covers 488 square miles. The southern half of the area, covering 183 square miles, drains to Chicken Creek, a tributary of the Sevier River drainage, and the northern half of the area, covering 304 square miles, drains to Currant Creek, which terminates into the southern end of Utah Lake. The valley part of the study area covers about 169 square miles.

Annual monitoring by the U.S. Geological Survey (USGS) of 30 wells in Juab Valley demonstrates that groundwater levels have declined steadily in many locations for nearly 30 years (Smith and others, 2019). Recharge to groundwater and the source of streams that enter Juab Valley are predominantly in the geologically complex Wasatch Range and San Pitch Mountains that border the valley on the east. The recharge water quality is adversely affected by salt- and gypsum-rich layers of the Jurassic Arapien Formation (Sprinkel and others, 2011), which crops out in the southern Wasatch Range and the western San Pitch Mountains. The basin-fill deposits below the valley floor also include sediment derived from the formation, which affects groundwater quality as well.

## Objectives

The lack of current information created a need for an updated evaluation of the groundwater and surface-water resources and water budget of Juab Valley. Bjorklund (1967) summarized the hydrogeologic conditions and water budget of the northern part of Juab Valley. A comprehensive study of groundwater conditions and a valley-wide water budget of the study area has not been conducted since the early 1990s (Thiros and others, 1996). The primary objectives of the UGS hydrogeologic study were to evaluate the hydrogeologic setting in greater detail than previous studies, update groundwater levels and chemistry throughout the valley, and evaluate changes in groundwater levels, hydrologic budgets, and chemistry since 1993, the time of data collection reported by Steiger (1995) and Thiros and others (1996).

This report includes:

1. Summaries of the hydrogeologic setting and hydrostratigraphy of Juab Valley, including evaluation of lithologic variations in the upper 400 ft of the basin fill based on analysis of water-well drillers' logs, and of the large-scale basin structure based on previously existing and newly collected gravity data.
2. Results of a valley-wide water-level survey conducted in spring 2015 (157 water levels measured by the UGS and 16 water levels measured by the USGS).
3. An evaluation of the position of a groundwater divide near Levan Ridge in the central part of the valley.
4. Results of valley-wide chemical sampling of groundwater, including major solutes (i.e., Na, K, Ca, Mg, HCO<sub>3</sub>, CO<sub>3</sub>, Cl, and SO<sub>4</sub>) (71 sites, including 5 springs), stable-isotope (82 sites) and radiogenic-isotope (17 tritium, 13 carbon-14) composition, and sampling of streams for major-solute chemistry and stable-isotope compositions (12 sites each).
5. Hydrologic budget for the Mona Reservoir system.
6. Hydrologic budget for the entire valley, with an emphasis on the groundwater system and the northern end of the valley.

## HYDROGEOLOGIC SETTING

### Geography, Climate, and Surface Water

Juab Valley is in eastern Juab County, central Utah (figure 1). The valley trends north-northeast, and its dimensions are about 35 miles northeast-southwest and 7 miles east-west. The valley is bounded on the northeast by the Wasatch Range including Mount Nebo (elevation 11,928 ft) and associated highlands; on the east and southeast by the San Pitch Mountains (peak elevations range from about 8300 to 10,000 ft); on the southwest by the West Hills (peak elevations range from about 5400 to 6350 ft), and on the west, northwest, and north by Long Ridge (peak elevations range from about 5450 to 7050 ft). Elevations in Juab Valley range from 4867 ft near the Mona Lake outflow to about 5400 ft in the foothills of the mountains. Juab Valley and the bounding ranges to the west are in the Basin and Range physiographic province, whereas the Wasatch Range is in the Middle Rocky Mountains physiographic province and the San Pitch Mountains are in the Basin and Range–Colorado Plateau Transition physiographic province.

The central part of Juab Valley includes a water-rights administrative boundary that trends roughly northwest-southeast (figure 1). The boundary follows a surface-drainage divide on Levan Ridge, a large alluvial fan that emanates from the San Pitch Mountains. The northern part of Juab Valley (about 300 square miles) is in the southeastern part of the Utah Lake drainage basin, and the southern part (about 174 square miles) is in the northeastern part of the Lower Sevier drainage basin. The southern study-area boundary is along a low topographic divide between Little Salt Creek on the north (figure 1), which drains toward Chicken Creek Reservoir, and Chriss Creek on the south (south of the study area boundary and not shown on figure 1), which drains southwest toward the Sevier River (although both streams rarely flow into the valley).

Average annual precipitation from 1980 to 2010 (PRISM Climate Group, 2012) ranged from 12 to 18 inches on the valley floor and western bounding ranges, 30 to 40 inches on Mount Nebo, and intermediate values depending on elevation in the Wasatch Range and San Pitch Mountains. Climate stations at Nephi and Levan indicate average annual precipitation of  $14.1 \pm 3.3$  and  $14.5 \pm 3.4$  inches per year, respectively, from 1945 to 2021 (figure 2) (Utah Climate Center, 2021).

The study area for this report includes the surface-drainage basins that flow to Mona Reservoir in the northwestern part of the study area and to Chicken Creek Reservoir in the southwestern part of the study area. Major streams include Salt Creek, which drains a large area in the southern Wasatch Range and northern San Pitch Mountains; Currant Creek, which originates on the valley floor south of Mona, flows to Mona Reservoir, and exits the valley north through Long Ridge to Goshen Valley; and Chicken Creek, which drains the central San Pitch Mountains and enters the valley floor only under peak flow conditions. Perennial and intermittent streams originate in the Wasatch Range and San Pitch Mountains, and dry to intermittent drainages occur in these ranges and along the eastern flanks of the West Hills and Long Ridge (figure 1). Flow data for Salt Creek, Currant Creek, and Chicken Creek were compiled from the USGS (figures 3, 4, and 5, respectively) and are summarized in the following paragraphs. The Levan Irrigation Company has assumed measurement of Chicken Creek and Pigeon Creek flow; the data from their measurements are presented in the water budget report.

The USGS operates gage 10146000 on Salt Creek, about 0.25 miles east of the canyon mouth (figures 1 and 3). During water years 1951 through 1979, geometric mean flow was 17.7 cubic feet per second (cfs) and increased slightly during this time period by about 0.15 cfs per year, equivalent to 103 acre-ft per year (ac-ft/yr). Flow data are not available for water years 1981 through 1992. During water years 1993 through 2015, geometric mean flow was 10.6 cfs and decreased slightly during this time period by about 0.29 cfs per year (206 ac-ft/yr).

Monthly flow in Salt Creek was greatest in May and June, and average monthly flow was less in 1993–2015 than in 1951–1980 (figure 3C) for all months. Base flow is the groundwater contribution to a stream and generally sustains streamflow when flow created by snowmelt and precipitation is unavailable. Median base flow, roughly estimated by average flow during December, was 9.9 cfs ( $0.28 \text{ m}^3/\text{s}$ ) during water years 1951 through 1979 and 5.5 cfs ( $0.16 \text{ m}^3/\text{s}$ ) during water years 1993 through 2015. Salt Creek flow is derived predominantly from snowmelt and precipitation in the southern Wasatch Range and northern San Pitch Mountains, and the lower average flow during 1993 to 2015 may have resulted from decreased average annual precipitation in its catchment area. The decreased flow may partly contribute to declining groundwater levels in the Nephi area. Most Salt Creek flow, however, is diverted into irrigation canals and pipes where it

enters the valley (Thiros and others, 1996, p. 11) so seepage to groundwater and, therefore, impact on groundwater levels may be minor.

The USGS operates gage 10146400 on Currant Creek, about 1 mile southeast of Mona (figures 1 and 4). During water years 1983 to 1985, average monthly flow was much greater than normal and highly variable (figure 4A). Before and after this anomalous period, average monthly flow ranged from about 1 to 50 cfs ( $0.03\text{--}1.4 \text{ m}^3/\text{s}$ ), was punctuated by several unusually high months, and then declined slowly (figure 4A). During water years 1993 through 2015 (same period of record analyzed for Salt Creek), geometric mean flow was 11.1 cfs and decreased slightly during this time period by about 0.6 cfs per year (412 ac-ft/yr), based on poorly defined linear regression. Base flow, estimated by average December flow, was 9.1 cfs during water years 1993 through 2015. Currant Creek originates on the valley floor about 3.5 miles south of the southern end of Mona Reservoir (figure 1) and is not connected to other streams, so its flow is derived from groundwater. Decreasing flow during water years 1993 through 2015 may reflect increased groundwater pumping (see Groundwater section) and decreased precipitation.

The USGS operated gage 10219200 on Chicken Creek, about 2 miles southeast of Levan (figures 1 and 5), from 1962 through 1995. Geometric mean flow during water years 1987 through 1995 was 1.1 cfs. Levan Irrigation Company currently operates this gage.

Flow of many streams in the Wasatch Range and San Pitch Mountains ranges from perennial to ephemeral and is diverted into aqueducts in the mountains for agricultural use on the valley floor.

## Stratigraphy and Structural Geology

Juab Valley is a syntectonic sedimentary basin, composed of interlayered alluvial and lacustrine gravel, sand, and clay. The basin formed due to Basin and Range normal faulting during Quaternary-Tertiary time, which uplifted the adjacent ranges and caused the valley floor to subside. The Wasatch Range on the eastern valley margin is composed mainly of Paleozoic carbonate rocks and Mesozoic siliciclastic rocks that were faulted and folded during Mesozoic and Cenozoic time. The San Pitch Mountains—the southern continuation of the Wasatch Range—are composed of Cenozoic volcanic rocks, Mesozoic siliciclastic rocks, and the Mesozoic Arapien Formation which includes gypsum- and halite-bearing mudstone and sandstone. Previous work indicated that the Arapien Formation underwent diapirism in this region, but more recent work indicates that Late Mesozoic and Early Cenozoic thrusting structurally thickened the salt rich Arapien (Sprinkel and others, 2011). Mountains bounding Juab Valley on the west are composed of Paleozoic sedimentary rocks, Cenozoic volcanic and volcanoclastic rocks, and Cenozoic sedimentary rocks, from north to south.

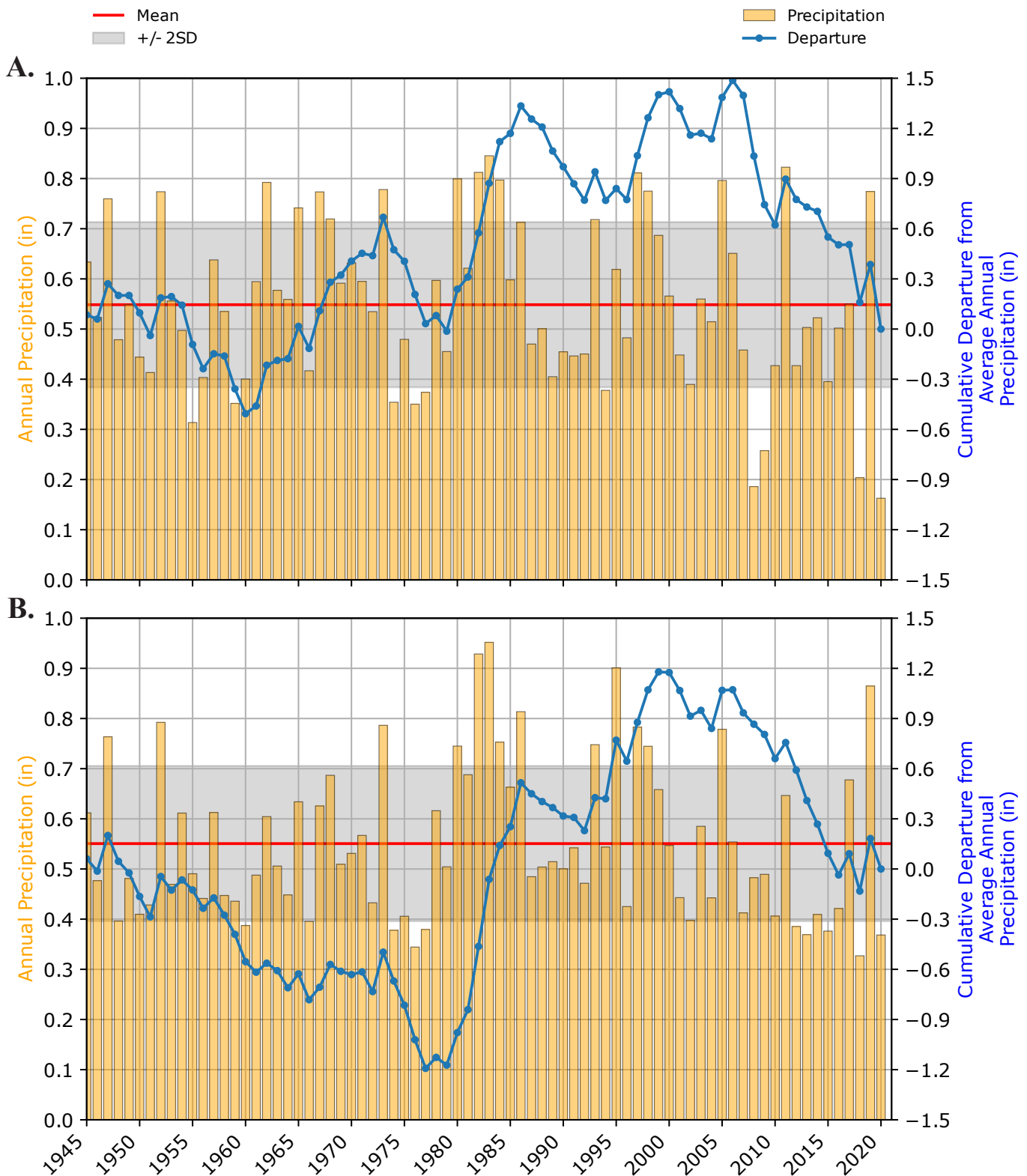


**Figure 2.** Precipitation records for Juab Valley climate stations for water years 1945 through 2021 (Utah Climate Center, 2021). Station locations are shown on figure 1. Plots show annual precipitation, average, and  $\pm 2$  standard deviations annual precipitation, and cumulative departure from average annual precipitation. **A)** Precipitation records from Nephi Co-op station. **B)** Precipitation records from Levan Co-op station.

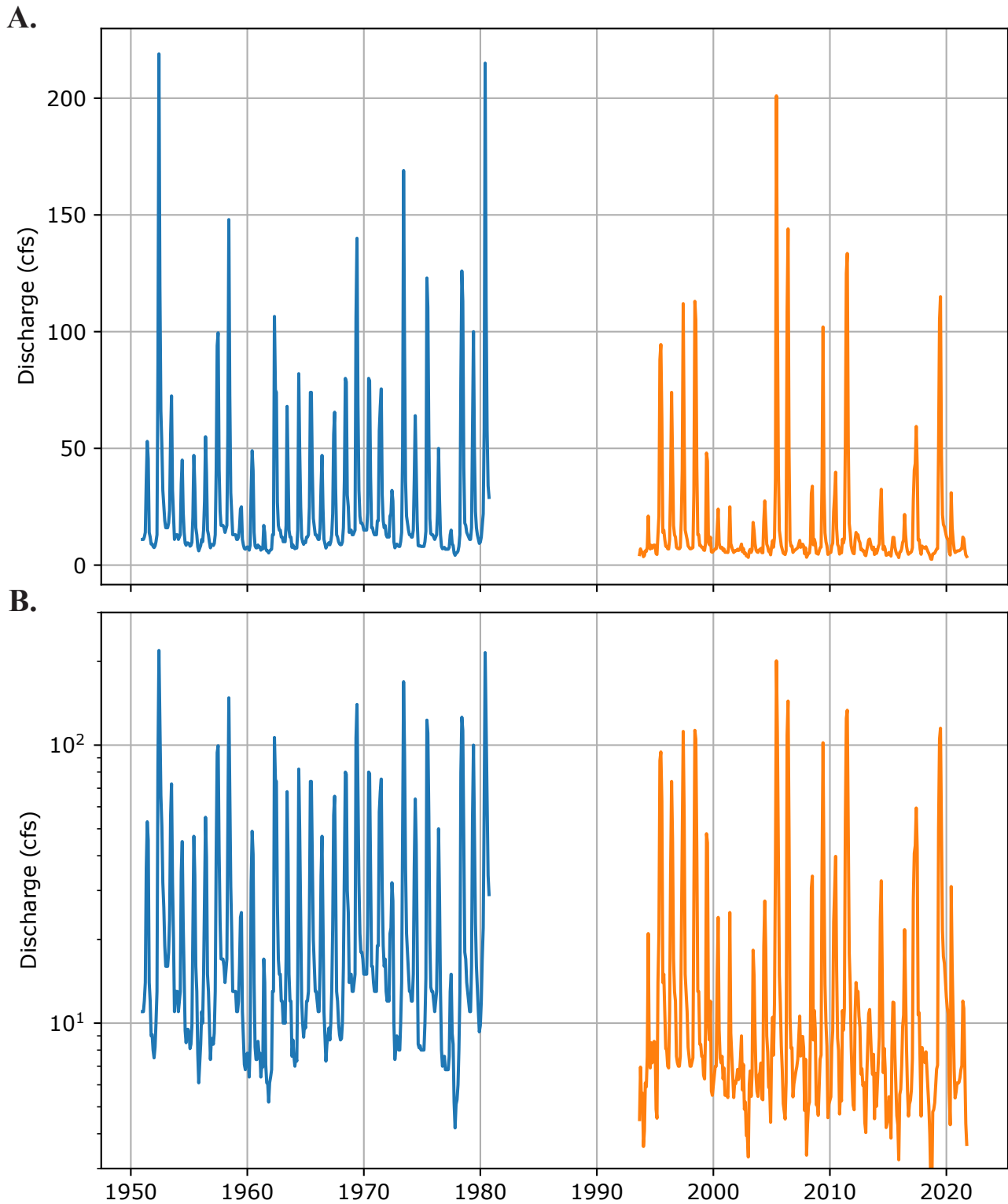


**Figure 3. A)** Hydrographs for Salt Creek in Juab Valley, water years 1951 to 1980 and 1993 to 2021. Data are from the U.S. Geological Survey's National Water Information System (NWIS) (USGS, 2021) for gage 10146000, "Salt Creek at Nephi, UT." Gage location is shown on figure 1. Geometric mean flow was 17.7 cfs from 1951 to 1980, and 14.2 cfs from 1993 to 2021, a decrease of 20%. Simple linear regression suggests approximate changing flow rates of 0.15 cfs (103 ac-ft/yr) from 1951 to 1980, and -0.29 cfs (-206 ac-ft/yr) from 1993 to 2021. **B)** Logarithmic y-axis (discharge) showing detail of lower flow range from A. **C)** Median flow by day. Median flow for each day was 28% to 45% lower in 1993 to 2021 than in 1951 to 1980. **D)** Hydrograph for December discharge, approximating base flow.

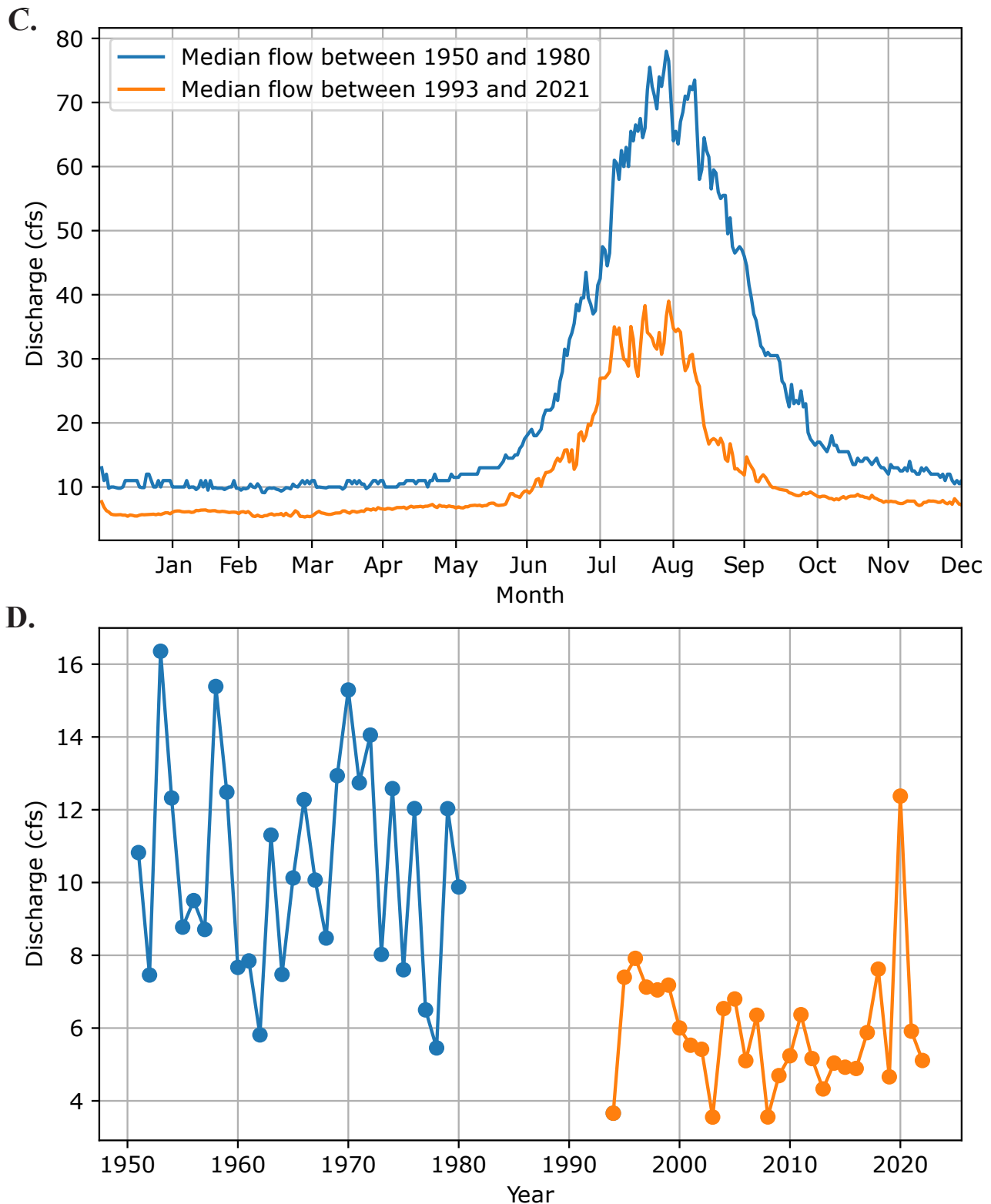


**Figure 3 continued.** **A)** Hydrographs for Salt Creek in Juab Valley, water years 1951 to 1980 and 1993 to 2021. Data are from the U.S. Geological Survey's National Water Information System (NWIS) (USGS, 2021) for gage 10146000, "Salt Creek at Nephi, UT." Gage location is shown on figure 1. Geometric mean flow was 17.7 cfs from 1951 to 1980, and 14.2 cfs from 1993 to 2021, a decrease of 20%. Simple linear regression suggests approximate changing flow rates of 0.15 cfs (103 ac-ft/yr) from 1951 to 1980, and -0.29 cfs (-206 ac-ft/yr) from 1993 to 2021. **B)** Logarithmic y-axis (discharge) showing detail of lower flow range from A. **C)** Median flow by day. Median flow for each day was 28% to 45% lower in 1993 to 2021 than in 1951 to 1980. **D)** Hydrograph for December discharge, approximating base flow.

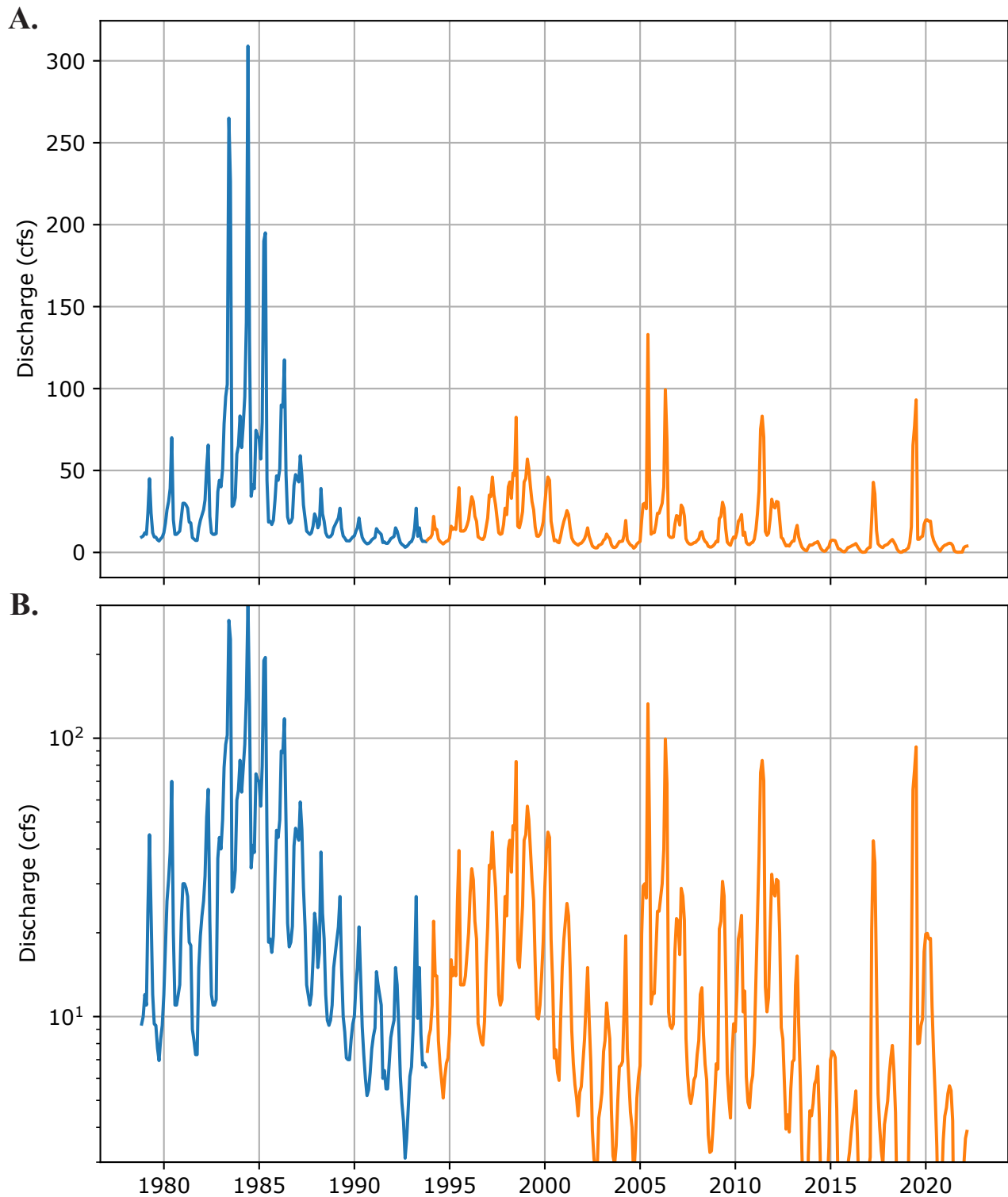


**Figure 4.** Hydrographs for Currant Creek in Juab Valley, water years 1978 to 2021. Data are from the NWIS, for gage 10146400, “Currant Creek Near Mona, UT.” Gage location is shown on figure 1. **A)** Hydrograph for Currant Creek. Geometric mean flow was 11.1 cfs from 1993 to 2021. We used this timeframe for comparison to the Salt Creek data periods. Simple linear regression suggests an approximate changing flow rate of  $-0.6$  cfs ( $-412$  ac-ft/yr) from 1993 to 2021. **B)** Logarithmic y-axis (discharge) showing detail of lower flow range from A. **C)** Median flow by day of year. Peak flow occurred over a greater time range than for Salt Creek (skewness of geometric means by month was 0.45 cfs for Currant Creek, and 1.7 cfs for Salt Creek), reflecting the dependence of flow on groundwater discharge rather than surface runoff. **D)** Hydrograph for December flows (approximating base flow). Geometric mean flow during “low flow” years (arbitrarily defined as less than 10.0 cfs) after 1990 was 7.3 cfs and decreased at a rate of approximately 1 cfs/year.

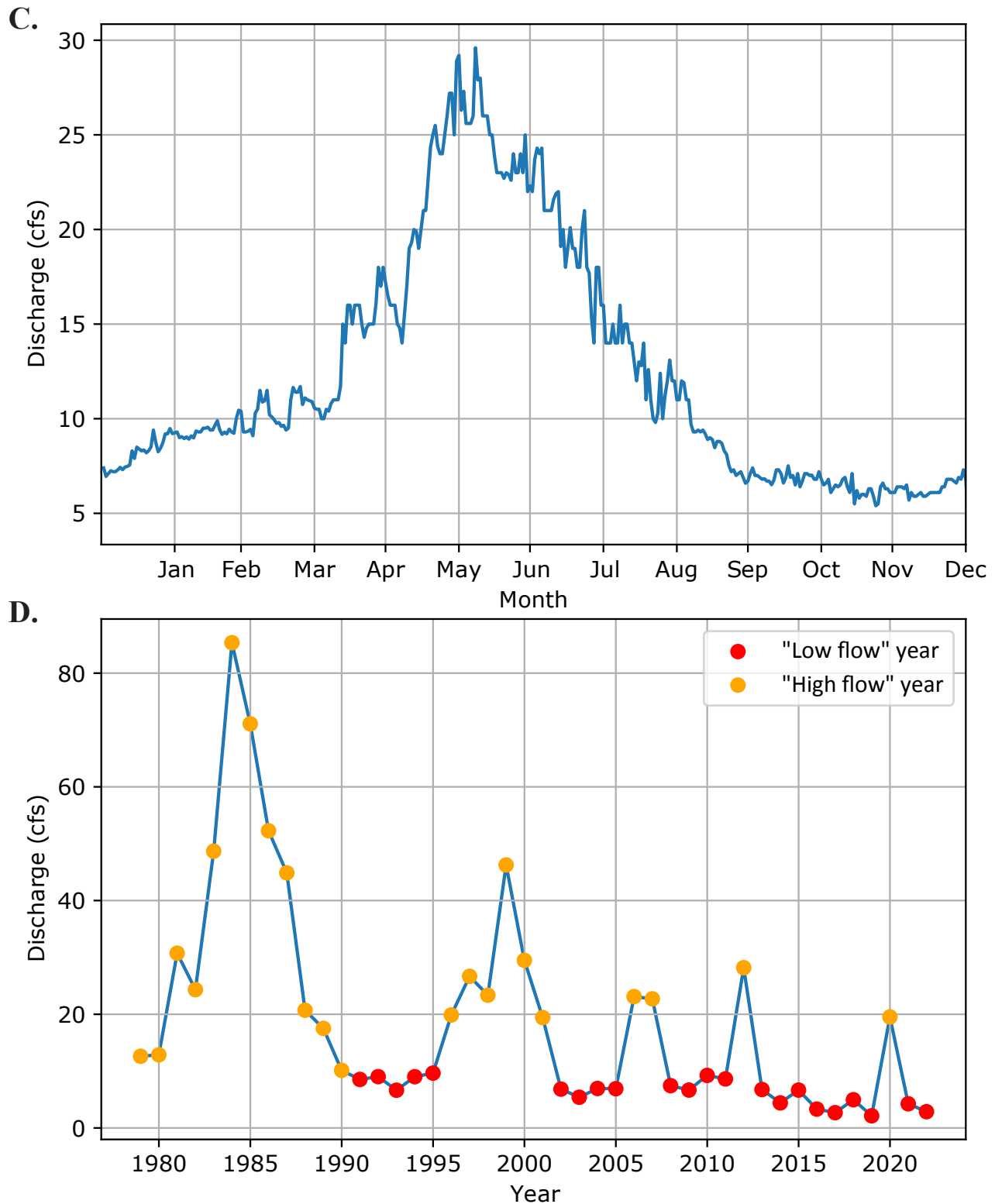


**Figure 4 continued.** Hydrographs for Carrant Creek in Juab Valley, water years 1978 to 2021. Data are from the NWIS, for gage 10146400, "Carrant Creek Near Mona, UT." Gage location is shown on figure 1. **A)** Hydrograph for Carrant Creek. Geometric mean flow was 11.1 cfs from 1993 to 2021. We used this timeframe for comparison to the Salt Creek data periods. Simple linear regression suggests an approximate changing flow rate of  $-0.6$  cfs ( $-412$  ac-ft/yr) from 1993 to 2021. **B)** Logarithmic y-axis (discharge) showing detail of lower flow range from **A**. **C)** Median flow by day of year. Peak flow occurred over a greater time range than for Salt Creek (skewness of geometric means by month was 0.45 cfs for Carrant Creek, and 1.7 cfs for Salt Creek), reflecting the dependence of flow on groundwater discharge rather than surface runoff. **D)** Hydrograph for December flows (approximating base flow). Geometric mean flow during "low flow" years (arbitrarily defined as less than 10.0 cfs) after 1990 was 7.3 cfs and decreased at a rate of approximately 1 cfs/year.

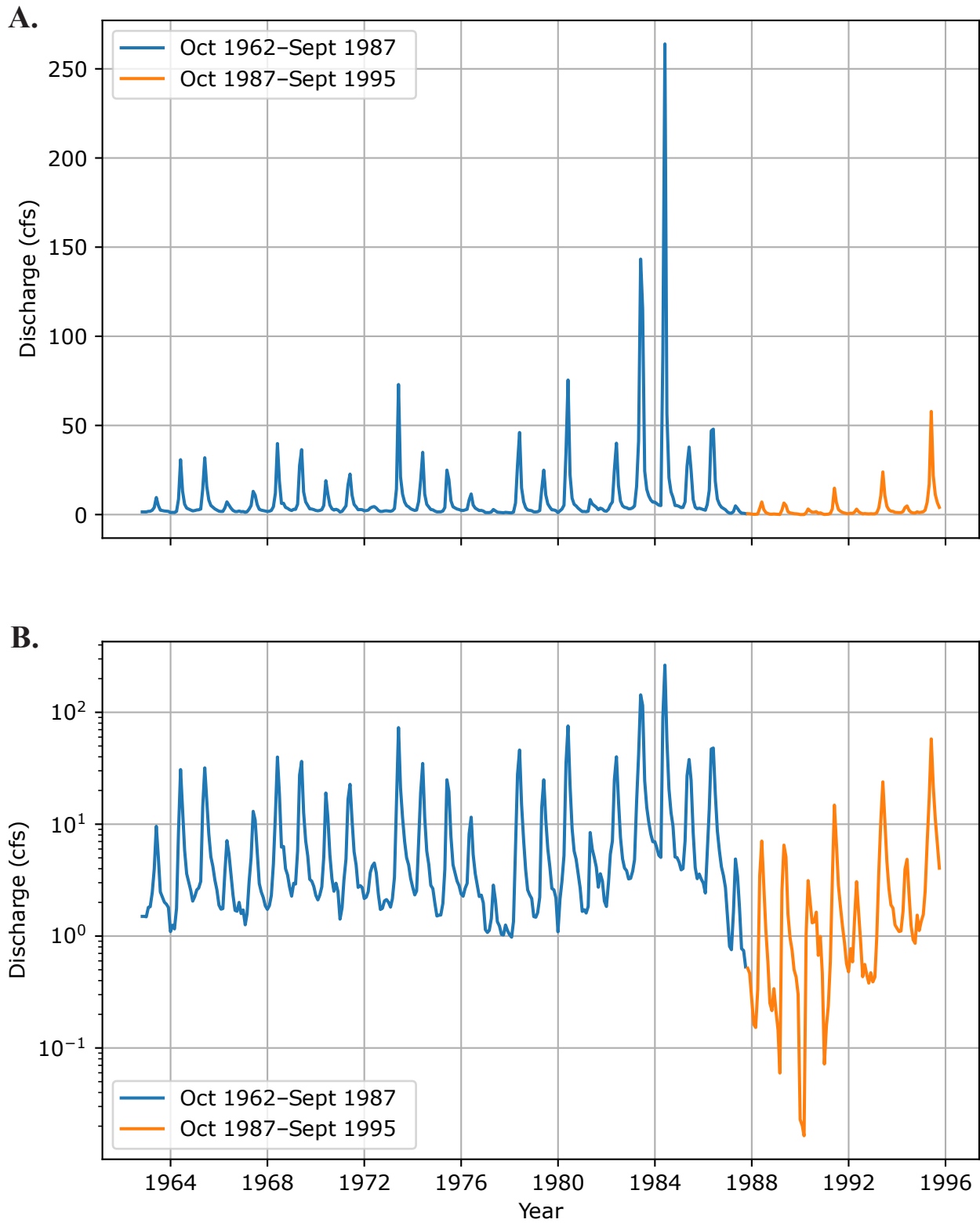


**Figure 5.** Hydrographs for Chicken Creek. Data are from the NWIS, for gage 10219200, “Chicken Creek Near Levan, UT.” **A)** Hydrograph for water years 1962 to 1995. **B)** Logarithmic y-axis showing detail of low-flow range from A.

Geologic maps of the Manti and Nephi 30' x 60' quadrangles (Witkind and others, 1987; Witkind and Weiss, 1991, respectively) are the sources for the compiled hydrogeologic map (plate 1). Figure 6 shows the simplified stratigraphy and hydrostratigraphy. Smaller scale geologic maps within the study area include two surficial geologic maps along the Wasatch fault zone (Harty and others, 1997; Hylland and Machette, 2008) and geologic maps of the Juab (Clark, 1990), Levan (Auby, 1991), Nephi (Biek, 1991), and Mona (Felger and others, 2004) 7.5' quadrangles. Select publications that describe the regional stratigraphic and tectonic setting and the geologic evolution of Juab Valley include Smith and Bruhn (1984), Machette and others (1992), Zoback (1992), Constenius (1996), DeCelles and Coogan (2006), Hintze and Kowallis (2009), and Sprinkel and others (2011).

The geology of the Juab Valley drainage basin is characterized by stratigraphic and structural elements common in the Basin and Range geologic province: (1) a north-trending, normal-fault-bounded valley having steep mountain fronts that transition from steep to moderately steep mountain ranges, all having high length-to-width ratios; (2) basin fill derived from erosion of adjacent ranges during Quaternary-Tertiary normal faulting and associated range uplift/valley subsidence, composed of complexly interlayered clay, gravel, and sand deposited in alluvial-fan, fluvial, and lacustrine environments, ranging up to several thousand feet thick; and (3) below the basin fill and in the adjacent ranges, Tertiary volcanic and volcanoclastic rocks that are moderately to highly faulted, and variably faulted and folded early Cenozoic, Mesozoic, Paleozoic, and Proterozoic carbonate and siliciclastic sedimentary rocks. Early Cenozoic and Mesozoic rocks are interlayered siliciclastic (chiefly sandstone, mudstone, and shale) and carbonate (chiefly limestone) rocks. The Paleozoic rocks are predominantly carbonate in the upper two-thirds and siliciclastic in the lower one-third of the stratigraphic section.

The ranges and valleys have a complex stratigraphic and structural evolution that includes: (1) deposition of late Proterozoic through early Paleozoic siliciclastic rocks in shallow to deep marine, subsiding continental-margin environments; (2) deposition of middle through late Paleozoic rocks in carbonate reef and nearshore to deep marine, continental-margin environments; (3) deposition of Mesozoic rocks in a variety of nearshore marine and fluvial environments; (4) folding and thrusting during the Late Jurassic to early Tertiary Sevier orogeny; (5) calc-alkalic volcanism and normal faulting during the early Tertiary; and (6) normal faulting that formed the present Basin and Range topography, and fluvial and lacustrine deposition in syntectonic basins on the hanging walls of the range-bounding normal faults during the late Tertiary and Quaternary.

### Hydrostratigraphy

We grouped the geologic units into informal hydrostratigraphic units (table 1), defined here as consecutive or later-

ally gradational geologic map units or formations grouped according to their interpreted hydraulic properties (i.e., hydraulic conductivity and storativity) (Seaber, 1988, p. 13; Macfarlane, 2000, p. 3). Because aquifer-test data in Juab Valley are sparse, grouping of units and evaluation of hydraulic properties is informal and is based on data and experience from similar basins along and near the Wasatch Front. Units are classified into three informal hydrogeologic types: aquifer (yields substantial water to wells and/or accommodates basin-scale groundwater flow), confining unit (does not yield substantial water to wells and/or greatly slows or forms a barrier to basin-scale groundwater flow), and heterogeneous (the unit contains stratigraphic and/or facies variations or variable fracture density at scales too small to show on the map, that may result in different hydraulic properties at different locations and/or depths).

The most important hydrostratigraphic units in the study area are (1) Quaternary alluvial and lacustrine deposits and Quaternary-Tertiary alluvial-fan deposits (units Qal, Ql, and QTaf, respectively, table 1) that together form the Juab Valley basin-fill aquifer, (2) the Jurassic Arapien Formation [unit Ja], and (3) Cretaceous siliciclastic rocks (unit Ks), Permian-Pennsylvanian carbonate rocks (units Pcs and PPO), and Mississippian-Ordovician carbonate and siliciclastic rocks (unit MOcs).

Unconsolidated, Quaternary and Quaternary-Tertiary alluvial and alluvial-fan deposits make up most of the basin fill in the depth range covered by the drillers' logs (as deep as about 1000 ft). Where saturated, these gravel, sand, and clay sediments form the principal basin-fill aquifer of Juab Valley. Quaternary lacustrine deposits of Lake Bonneville and possibly earlier lake cycles are chiefly clay or clay with variable but lesser amounts of silt, sand, and gravel. These laterally discontinuous deposits are interlayered with the alluvial and alluvial-fan deposits in the upper 100 to 200 ft of the basin fill, and collectively form a confining zone. The "Basin-Fill Hydrogeology" section below describes the lithology of the basin-fill deposits in greater detail.

The Jurassic Arapien Formation (unit Ja) is composed of mudstone and sandstone and includes gypsum and halite in bedded and vein form (Witkind and others, 1987; Witkind and Weiss, 1991; Sprinkel and others, 2011). This unit was originally named the Arapien Shale, but Sprinkel and others (2011) recommended redefining it as the Arapien Formation and including the limestone in the San Pitch Mountains previously mapped as Twin Creek Limestone. Gypsum mines are present in Arapien Formation outcrops in Salt Creek and canyons to the south. Witkind and others (1987) and Witkind and Weiss (1991) interpreted highly deformed Arapien Formation exposed in the southern Wasatch Range and San Pitch Mountains as diapirs that were mobile from Jurassic through late Tertiary time, and accordingly gave it a map unit having a compound age. However, Sprinkel and others (2011) indicate that this deformation is more likely related to

Era	Period	Epoch	Age (Ma)	Geologic Unit	Hydrogeologic Units			Lithology	Thickness (feet)	Depositional Setting	Tectonic Setting	
					Aquifers	Confining Units	Heterogeneous Units					
Cenozoic	Quaternary	Holocene	0.01	Qal Qcl Qf Qvf	Qcs	Qfs			≤150	Alluvial & lacustrine	Basin & Range normal faulting	
		Pleistocene	2.6	Qb Qe Qj Qmw Qao Qg Qbo Qbs Qbn								
	Tertiary	Pliocene	5.3	unconformity			QTs		~4000	Volcanic & alluvial	Volcanism & normal faulting	
		Miocene	23.0	Tsp Tlm Tmp Td		Ti						
		Oligocene	33.9	Tls Tlsv Tgr Tm Thmp Tvg		Tv						
		Eocene			Tg		Tsu					
					Tc							
					Tf							
	Paleocene	65.5	TKn									
	Mesozoic	Cretaceous		146	Kpr Ki Kcm	Ksc			~7000	Shallow marine	Sevier orogeny - foredeep basin, thrust faulting & folding, uplift & erosion	
				Jtg	Jsm							
				Jtc	Jl	Ja						
Jurassic				200	T(Ja) JRn			500-1000 4500 1400-1500	Erg	Stable continental margin		
		Triassic			Ra Rt Rw		TRs	2850	Shallow marine			
informal subdivisions			Permian	Upper	251	unconformity				1900	Deep-to shallow-marine carbonate/sandy basins	Oquirrh Basin/ Ancestral Rockies orogeny
				Middle	260							
	Lower	271		Ppc Pdc Pk	pdk	Psu						
	Pennsylvanian	Upper	299					~11,000	Deep marine	Foredeep Basin - Antler orogeny (west of study area)		
		Middle	307	PIPo	PIPs							
		Lower	312	IPMmc	IPMs							
	Mississippian	Upper	318	Mgb Mh Md				2200-3200				
		Lower	340	Mg	MDold							
	Devonian	Upper	359	MDf								
				Du DO								
Middle		385										
Lower		398										
Silurian	Upper	416	unconformity									
	Lower	423										
Ordovician	Upper	444										
	Middle	461										
	Lower	472										
Cambrian	Upper	488	DO	MDold			100					
	Middle	501	€u		€ld	950-1700						
	Lower	513	€mu €df €t	Cot		€Ysq	2150-2400					
Mesoproterozoic			542	unconformity						Post-Rift continental margin		
				Ybc								

Figure 6. Stratigraphic column for Juab Valley study area, compiled from Witkind and others (1987), Clark (1990), Auby (1991), Biek (1991), Witkind and Weiss (1991), and Felger and others (2004). Geologic unit symbols are from compiled geologic maps, hydrostratigraphic symbols shown on plate 1 and described in table 1.

Table 1. Summary descriptions of hydrostratigraphic units shown on plate 1.

Hydrostratigraphic Unit <sup>1</sup>	Age	Lithology <sup>2</sup>	Thickness (ft) <sup>2</sup>	Hydrogeologic Type <sup>3</sup>	Source-Map Units <sup>4</sup>
Qal	Quaternary	Sand, gravel, and cobbles with variable amounts of clay and silt. Well sorted in discrete sedimentary layers, to unsorted, intermixed gravel and clay.	≤50	Aquifer	Nephi 30' x 60': Qal Manti 30' x 60': Qal
Qm	Quaternary	Heterogeneous, unsorted mixture of large blocks and gravel- to clay-sized fragments.	≤50	Variable	Nephi 30' x 60': Qe, Ql, Qmw Manti 30' x 60': none
Ql	Quaternary	Clay, silt, sand, and gravel, typically well layered and sorted.	≤250	Variable	Nephi 30' x 60': Qbn, Qbs, Qbo Manti 30' x 60': none
QTaf	Quaternary-Tertiary	Gravel, sand, and cobbles with minor silt and clay. Varies from well sorted in discrete sedimentary layers, to unsorted, intermixed gravel, sand, and clay.	≤50	Aquifer	Nephi 30' x 60': Qcl, Qf, Qcf, Qrf, Qg, Qsw, Qb, QTcf, QTpm. Manti 30' x 60': Qcl, QTcf, QTr, QTpm
Ti	Tertiary	Dikes, sills, and stocks of monzonite or monzonite porphyry.	n/a	Aquitarid	Nephi 30' x 60': Tmp Manti 30' x 60': Tlm, Tmp, Td
Tv	Tertiary	Pyroclastic ash-flow tuff, welded tuff, and flows; volcanoclastic breccia, fluvial conglomerate, and sandstone.	~4000	Variable	Nephi 30' x 60': Tmp Manti 30' x 60': Tlm, Tmp, Td
Ts	Tertiary	From top to bottom, includes the Green River Formation (limestone, sandstone, and tuff overlying calcareous shale), Colton Formation (claystone, mudstone, sandstone, and shale), Flagstaff Limestone (limestone and dolomite), and North Horn Formation (mudstone, claystone, sandstone, and conglomerate).	1475–4850	Variable	Nephi 30' x 60': Tg, Tc, Tf, TKn Manti 30' x 60': Tg, Tc, Tf
Ks	Cretaceous	Conglomerate, sandstone, and shale.	2850–4000	Aquifer	Nephi 30' x 60': Ki, Kpr Manti 30' x 60': Ki, Kpr
Js	Jurassic	Sandstone, siltstone, and shale.	3000	Variable	Nephi 30' x 60': Jtg Manti 30' x 60': Jtg
Jlc	Jurassic	Limestone and shale.	500–1000	Variable	Nephi 30' x 60': Jlc Manti 30' x 60': Jlc
Ja	Jurassic	Calcareous mudstone to fine sandstone, gypsum- and halite-bearing mudstone, and gypsum and halite veins and bedded deposits. Deposited during Jurassic time.	"4000–13,000 (structural thickness)"	Aquitarid	Nephi 30' x 60': T(Ja) Manti 30' x 60': T(Ja)
JFn	Jurassic-Triassic	Well-sorted sandstone.	1400–1500	Aquifer	Nephi 30' x 60': JFn Manti 30' x 60': none
TRC	Triassic	Shaly sandstone, shale, and limestone.	2850	Variable	Nephi 30' x 60': Ra, Rt, RW Manti 30' x 60': none

Table 1 continued. Summary descriptions of hydrostratigraphic units shown on plate 1.

Hydrostratigraphic Unit <sup>1</sup>	Age	Lithology <sup>2</sup>	Thickness (ft) <sup>2</sup>	Hydrogeologic Type <sup>3</sup>	Source-Map Units <sup>4</sup>
Pcs	Permian	Cherty limestone and sandstone.	1900	Aquifer	Nephi 30' x 60': Ppc, Pdc, Pdk, Pk Manti 30' x 60': none
PPO	Permian-Pennsylvanian	Limestone and sandstone.	11,000	Aquifer	Nephi 30' x 60': PPO Manti 30' x 60': none
PMmc	Pennsylvanian-Mississippian	Shale, quartzite, and limestone.	1000–1700	Aquitard	Nephi 30' x 60': PMmc Manti 30' x 60': none
MOcs	Mississippian-Ordovician	Limestone, dolomite, and sandstone.	2080–2680	Aquifer	Nephi 30' x 60': Mgb, Mh, Md, Mg, MDf, MDu, Du, DO Manti 30' x 60': none
€c	Cambrian	Dolomite and limestone.	1260–2110	Aquifer	Nephi 30' x 60': €u, €mu Manti 30' x 60': none
€ys	Cambrian-Proterozoic	Quartzite, shale, and sandstone.	2420–2630	Variable	Nephi 30' x 60': €o, €df, €t, €ot, Ybc Manti 30' x 60': none

## Notes

<sup>1</sup> Consecutive or coeval geologic map units or formations grouped into hydrogeologic units based on interpreted hydraulic properties. Hydrogeologic units consisting of a single map unit or formation retain the formation name. Hydrogeologic units consisting of several map units or formations are given generalized names denoting their age and dominant rock type.

<sup>2</sup> Lithologic descriptions and thicknesses are from Witkind and others (1987) and Witkind and Weiss (1991).

<sup>3</sup> Informal hydrogeologic designation based on interpreted capacity to yield water to wells and accommodate groundwater flow over basin-scale flow paths (for example, from the Wasatch Range western range front east of Mona, to the springs at Burrington Ponds). Few wells are in bedrock in this study area, so designations are based on data from other parts of the Wasatch Front and back valleys. Variable/heterogeneous implies that hydraulic conductivity and porosity vary spatially within the unit, due to variations in stratigraphy, composition, secondary porosity, or fracture density and type.

<sup>4</sup> Sources: geologic maps of Manti (Witkind and others, 1987) and Nephi (Witkind and Weiss, 1991) 30' x 60' quadrangles.

structural thickening of the Laramide and Sevier orogenies. The Arapien Formation is poorly resistant, and its detritus likely makes up a significant part of the basin fill in the Salt Creek alluvial fan and in the southern half of the study area.

Gypsum and halite dissolve in groundwater, increasing its sulfate, sodium, chloride, and total-dissolved-solids concentrations. This process likely occurs in the mountain ranges where precipitation and snowmelt infiltrate into the Arapien Formation, and in mountain streams and the basin-fill aquifer where water flows through Arapien Formation-derived sediment. Dissolution of gypsum and halite is likely enhanced in and around the gypsum mines where abundant fresh outcrop surfaces and fine-grained detritus are present. Groundwater chemistry and reaction modeling by Thiros and others (1996) and data from this study (see “Groundwater Chemistry” section) confirm the strong influence of the Arapien Formation on Juab Valley groundwater chemistry.

The southern Wasatch Range in the northeast part of the study area is composed of Permian through Ordovician carbonate rocks (hydrostratigraphic units *Pcs*, *PIPo*, and *MOcs*) that are folded and fractured. This area has the highest average annual precipitation in the study area (figure 1 inset). The carbonate rocks here are likely permeable by virtue of high fracture density and solution widening of fractures by groundwater and, therefore, accommodate recharge of snowmelt and precipitation to a greater degree than hydrostratigraphic units classified as aquitards or heterogeneous.

The high country of the northeastern San Pitch Mountains is composed predominantly of conglomerate and sandstone of the Cretaceous siliciclastic rocks hydrostratigraphic unit (*Ks*). These rocks likely have both primary and secondary fracture porosity and permeability and accommodate infiltration of snowmelt. The high country of the southeastern San Pitch Mountains is composed predominantly of the Tertiary sedimentary rocks unit (*Ts*), which includes interbedded sandstone, mudstone, and limestone that together do not form a large, physically continuous aquifer, but some formations yield sufficient water to stock watering and industrial wells in the southwestern part of the study area.

## Groundwater

Thiros and others (1996) described the hydrologic conditions and chemistry of Juab Valley groundwater, as paraphrased below (their report also includes measurements of surface water, a water budget, and conceptual and numerical models of groundwater flow, none of which are summarized here). Recharge to the basin-fill aquifer occurs directly on the alluvial fans by infiltration of stream flow and of local snowmelt and precipitation, and by subsurface flow from bedrock aquifers across the Wasatch fault zone that forms the eastern structural boundary of the basin fill. Groundwater flows through the basin-fill aquifer from the mountain front toward the valley floor,

to major discharge areas at Mona Reservoir and adjacent areas to the south including Burraston Ponds, and at Chicken Creek Reservoir and adjacent areas to the northeast. Thiros and others (1996) estimated that the discharge from the springs of Burraston Ponds and the diffuse groundwater discharge area to the south was 10,570 ac-ft/yr, based on stream gage data from Currant Creek downstream from Burraston Ponds (USGS gage 10146400; see figure 4A and the Geography, Climate, and Surface Water section; Thiros and others, 1996, table 4, p. 60, and p. 68). The principal basin-fill aquifer is composed of unconsolidated gravel, sand, and clay derived from erosion of bedrock in adjacent ranges and deposited in fluvial and lacustrine environments. Some groundwater may flow northeast out of the northwestern part of the valley through the Paleozoic carbonate-rock aquifer below Long Ridge.

Groundwater in the basin fill flows either north-northwest or south-southwest depending on location relative to a groundwater divide near Levan Ridge that is about 5 miles south of Nephi. North of the divide, groundwater flows toward the Mona Reservoir discharge area in the northwestern part of the valley, whereas south of the divide groundwater flows toward the Chicken Creek Reservoir discharge area in the southwestern part of the valley.

Based on recent and historical groundwater levels, Thiros and others (1996, p. 34) noted seasonal groundwater fluctuations related to groundwater pumping for irrigation but concluded that “long-term water-level fluctuations reflect climatic trends and a decline caused by increased ground-water withdrawal from wells generally is not apparent.” Groundwater conditions in Juab Valley have changed since the time of their report, and groundwater levels are now substantially lower, likely impacted by increased withdrawals over time. The USGS has estimated average annual groundwater withdrawal (chiefly groundwater pumping by wells for irrigation) for Juab Valley since 1963 (Smith and others, 2019). Smith and others (2019) cite an average value of 21,000 ac-ft/yr for 1963 to 2015, during which annual withdrawal varied substantially (figure 7). Withdrawal was as low as 8000 ac-ft/yr from 1983 to 1986, and as great as 29,000 ac-ft/yr from 2012 to 2015 (figure 7).

Data from 201 driller’s logs entered into a well database for this study show that the median well depth in Juab Valley is 224 ft, and 92% of the wells are between 110 and 575 ft deep. The median midpoint of the screened or open interval is 175 ft, and the screened or open interval for most wells is 100 ft or less (figure 8). These statistics define the current withdrawal zone in the basin-fill aquifer.

The USGS measures groundwater levels in 30 wells in Juab Valley annually, most of which have been measured continuously since the late 1970s (figure 9) (Smith and others, 2019; USGS, 2018). Groundwater levels show various trends but have declined overall at many locations throughout the valley since 1990 (figures 9B–O). Most wells show peak groundwater levels in 1984 and 1999 (plus-or-minus two years depending

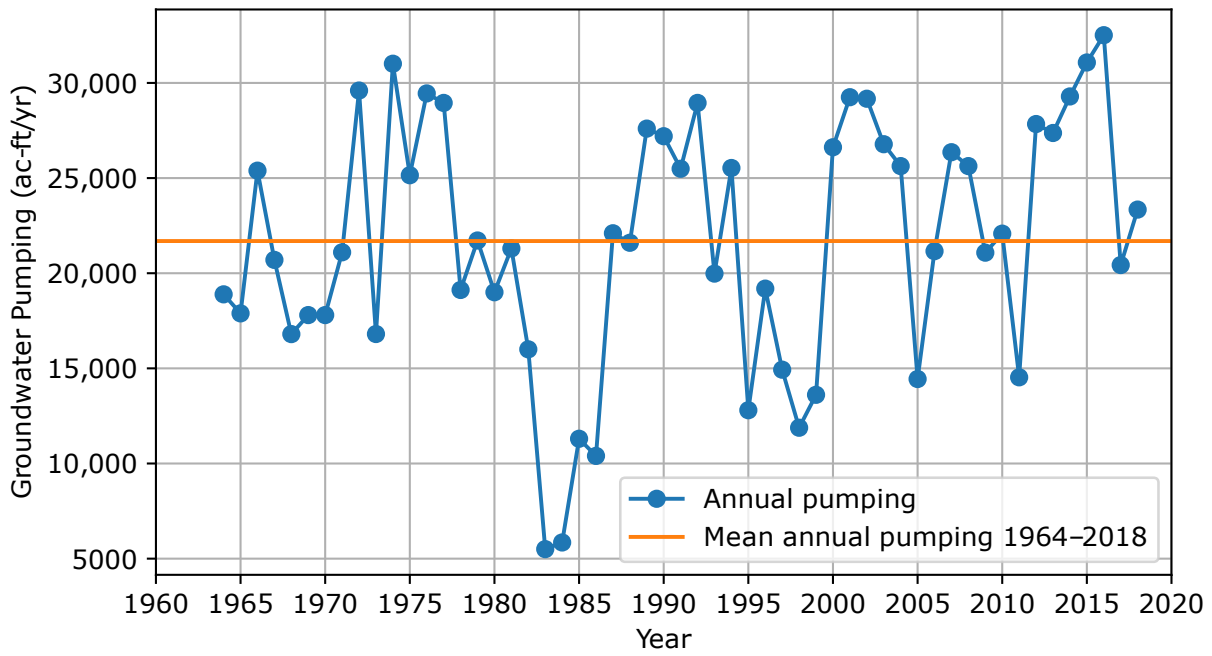


Figure 7. Estimates of annual groundwater pumping in Juab Valley, 1964 to 2018 (Smith and others, 2019).

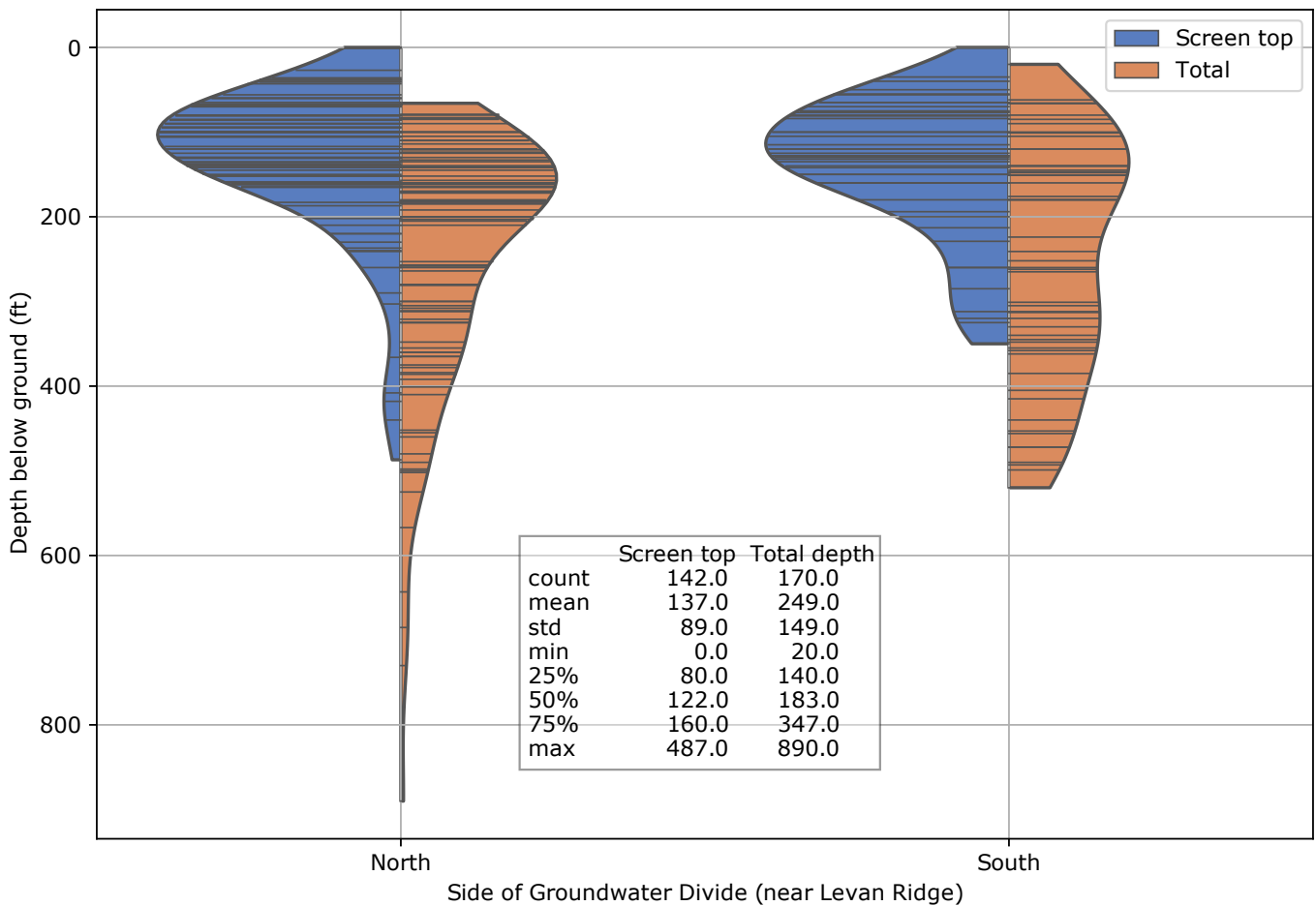
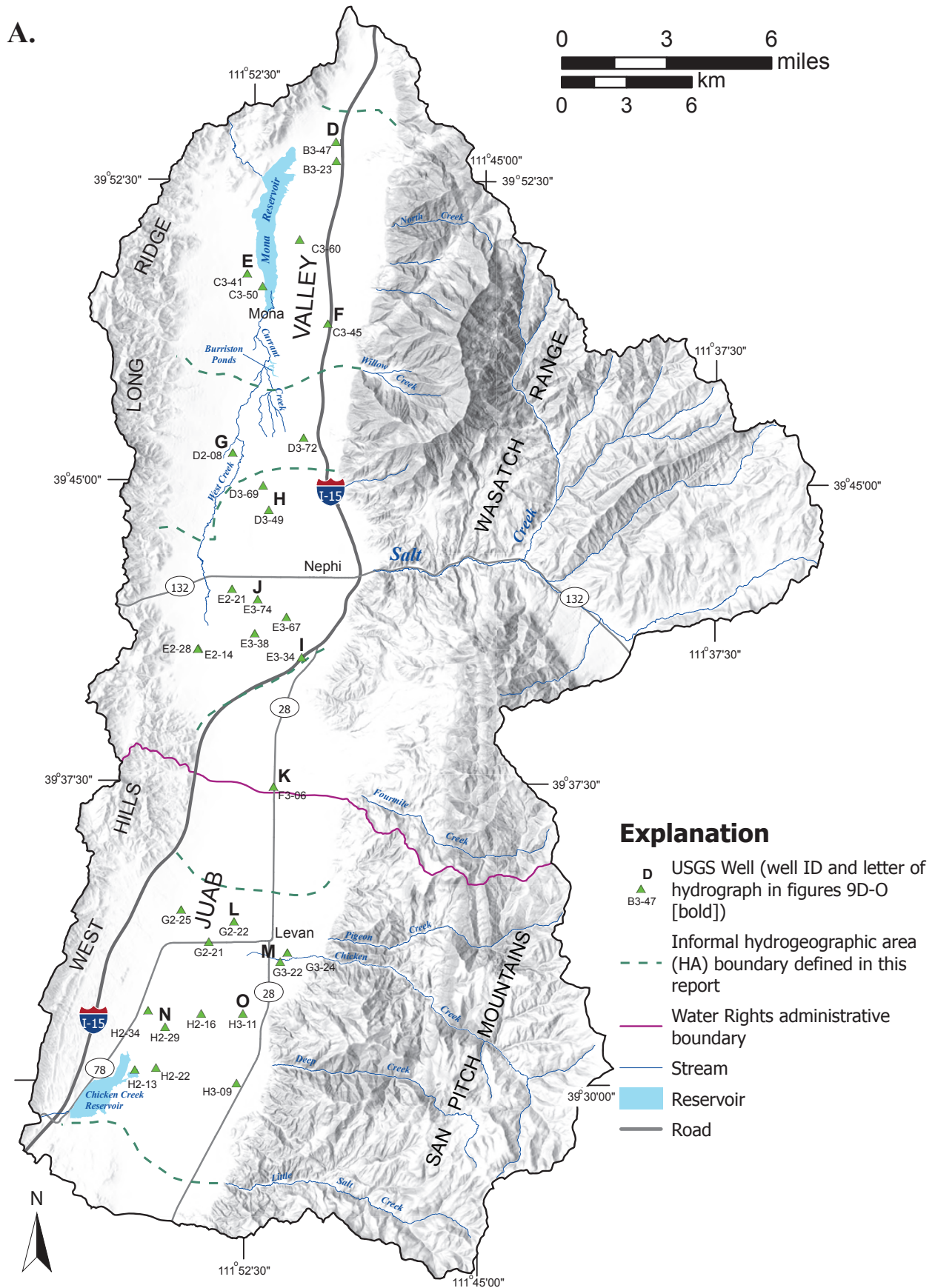
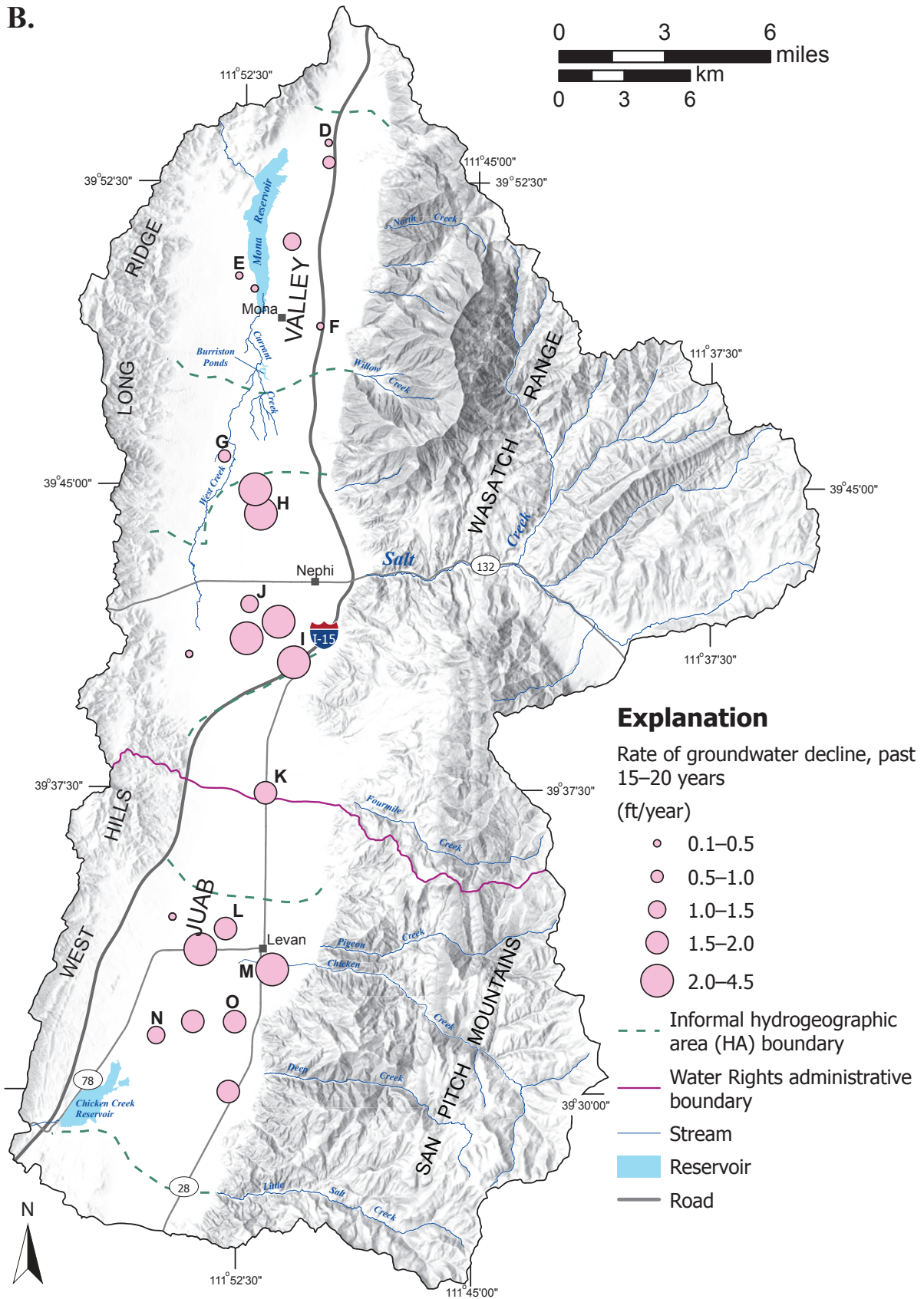


Figure 8. Histograms and statistics for well depths and the top of open or screened intervals for wells in Juab Valley recorded in the well database for this study. The number of screened/open intervals is greater than the number of wells because many wells have more than one screened interval. Data are from drillers' logs obtained from the Utah Division of Water Rights (2021).



**Figure 9.** Analysis of water-level trends for wells in Juab Valley measured annually by the U.S. Geological Survey (2021). Estimates of average decline rates are by Hurlow (table 2). **A)** Location of wells currently monitored annually by the USGS. Bold letter denotes hydrograph shown on figures 9D–O. Smaller label is well ID (table 2).



**Figure 9 continued. B)** Average rates of groundwater decline from about 2000 to 2021 (depending on the well) based on linear regression of March water levels from U.S. Geological Survey water-level data. The beginning year selected for the regression depended on when the overall declining trend began and on data availability. Several wells do not have data from about 2016 to 2021 but are included because their earlier records are complete, they illustrate a clear trend, and their locations provide improved spatial coverage of water-level trend data.

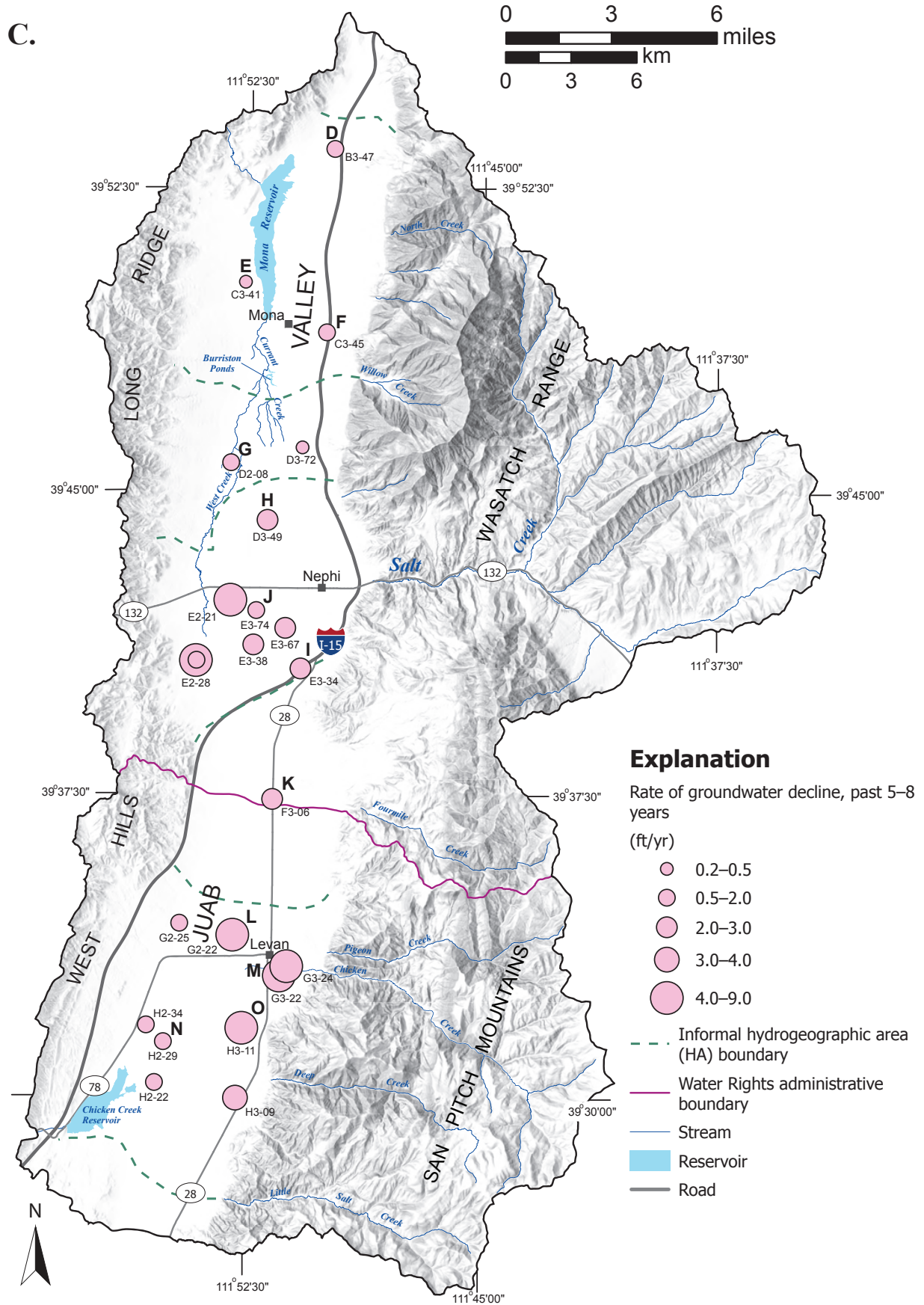


Figure 9 continued. C) Average rates of groundwater decline from about 2012 to 2021 (depending on the well) based on linear regression of March water levels from U.S. Geological Survey annual water-level data. Most rates of decline are greater than the longer time period shown on A.

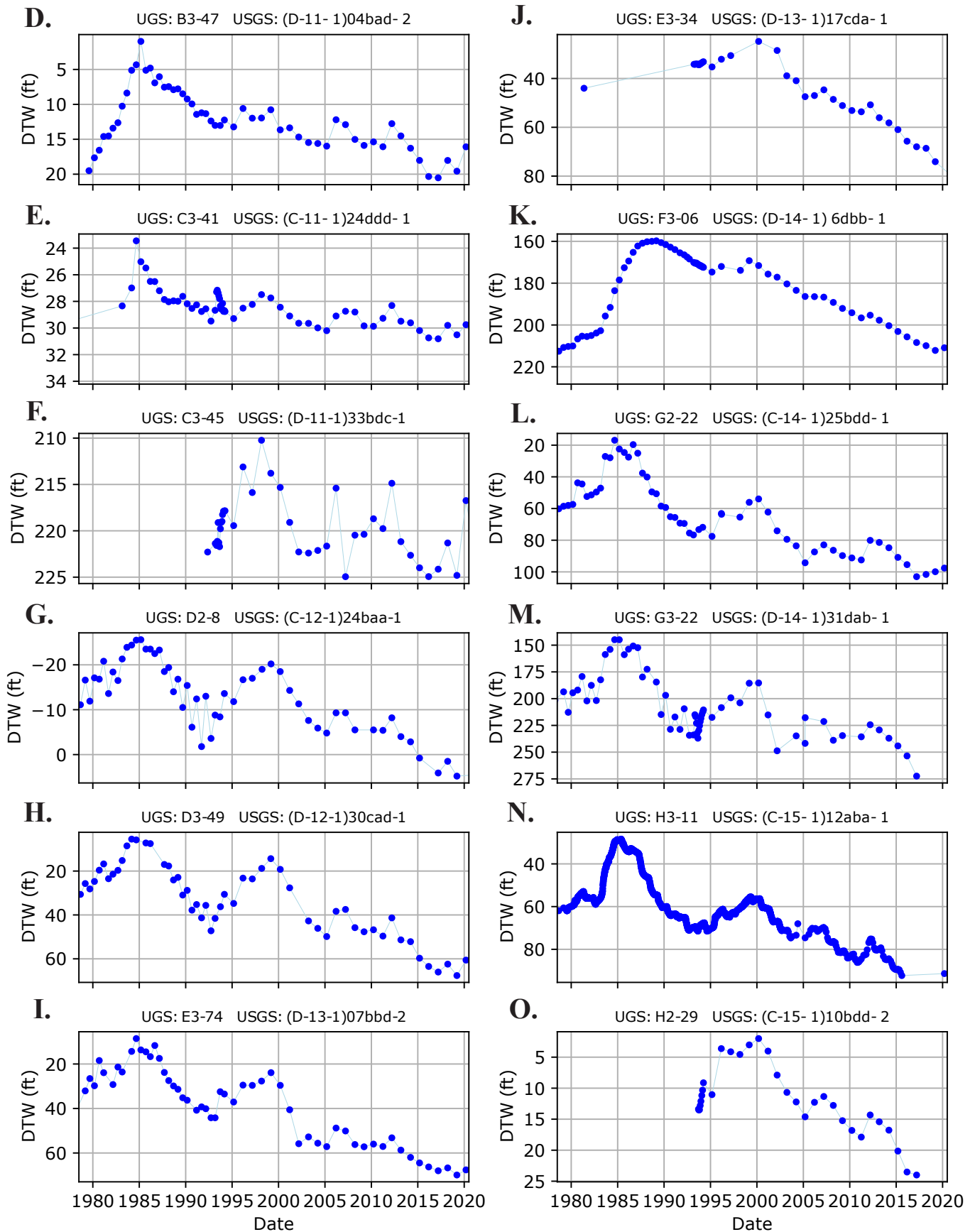


Figure 9 continued. D–O) Hydrographs from 1978 to present of selected wells measured annually by the U.S. Geological Survey. “DTW” is depth to water; Locations are on figure 9A.

on location), with periods of overall decline from approximately 1984 to 1998 and from 1999 to present. The Interpretations subsection of the Groundwater Levels section below describes trends and spatial distribution of groundwater-level declines in Juab Valley, based on these long-term data.

### Hydrogeographic Areas

Topography, surface-drainage patterns, hydrogeology, and groundwater conditions vary along the length of Juab Valley and five informal hydrogeographic areas can be delineated for descriptive purposes (figure 1). From north to south, these are:

1. Mona Reservoir hydrogeographic area, from north of Mona Reservoir to about 0.5 miles south of the central part of Burraston Ponds. Topography is characterized by a narrow, north-south- to northeast-trending valley-floor axis (i.e., the locus of low-elevation points and adjacent, flat parts of the valley floor) near the valley meridian. Steep alluvial fans form the mountain front along the eastern valley margin and transition abruptly to the very steep Wasatch Range. Thiros and others (1996) delineated a groundwater flow path from recharge areas on the Salt Creek and Willow Creek alluvial fans, northwest to the valley-floor discharge area at Burraston Ponds. Smaller springs and distributed seeps occur west, northwest, and southwest of Burraston Ponds. Several flowing wells are present along the eastern margin of Mona Reservoir. The southern boundary of the hydrogeographic area is placed approximately where Currant Creek becomes perennial (this location likely changes year to year depending on precipitation and antecedent groundwater levels).
2. West Creek hydrogeographic area, from about 0.5 miles south of Burraston Ponds to an arcuate southern boundary in about a 3-mile radius from central Nephi. The valley-floor axis and mountain front have similar geometry to those of the Mona Reservoir hydrogeographic area. The valley-floor discharge area is characterized by numerous distributed small springs and seeps. The ephemeral West Creek and the ephemeral part of Currant Creek originate on the valley floor, presumably from groundwater discharge, in the southwestern part of the West Creek hydrogeographic area.
3. Nephi hydrogeographic area, from the southern boundary of the West Creek hydrogeographic area to about 4 miles southwest of Nephi, where topography is defined by the Salt Creek alluvial fan that slopes radially away from where Salt Creek enters Juab Valley, and a narrow, arcuate valley-floor axis near the eastern valley margin. Salt Creek enters the valley through Salt Creek Canyon east of Nephi, where bedrock is predominantly the Jurassic Arapien Formation, described in the Hydrostratigraphy section above. The Wasatch Range is composed of Mesozoic sedimentary rocks and Tertiary volcanic and volcanoclastic rocks, and tapers southward to Salt Creek Canyon. The San Pitch Mountains, composed of Mesozoic and Cenozoic rocks, rise southward from Salt Creek Canyon. The Arapien Formation influences surface-water and groundwater chemistry in the Nephi hydrogeographic area (Thiros and others, 1996). Groundwater flows to the west from the range fronts and flows radially outward from the Salt Creek alluvial fan toward areas of heavy agricultural pumping west of Nephi. The groundwater discharge areas are along the valley-floor axis including the southern West Creek hydrogeographic area and in the northwestern part of Juab Valley toward Burraston Ponds in the Mona Reservoir hydrogeographic area.
4. Levan Ridge hydrogeographic area, from about 4 miles southwest of Nephi to about 1.5 miles north of Levan, comprising the Levan Ridge geographic feature shown on most topographic maps, which is a large, gently west-sloping alluvial fan that emanates from the Fourmile Creek drainage basin in the San Pitch Mountains. The valley-floor axis is comparatively narrow and arcuate and is on the west side of the valley. The western part of the Fourmile Creek drainage basin in the San Pitch Range is composed largely of the Jurassic Arapien Formation, and the eastern part is composed of Cretaceous siliciclastic rocks. The groundwater divide briefly described in the "Groundwater" section above occurs in the Levan Ridge hydrogeographic area, as do the surface-flow and administrative boundaries between the southern part of the Utah Lake basin to the north and the northeastern part of the Lower Sevier basin to the south. Groundwater flows north from the northern part of Levan Ridge to the Nephi hydrogeographic area and south from the southern part of Levan Ridge to the Levan hydrogeographic area. The nature of this groundwater divide is discussed in greater detail in the "2015 Groundwater-Level Map" subsection of the "Groundwater Levels" section below.
5. Levan hydrogeographic area, from the southern end of Levan Ridge to the southern part of the study area including Chicken Creek Reservoir. Topography is characterized by a broad, gently southwest-sloping valley floor and southwest-trending valley-floor axis, comparatively small and gently sloping alluvial fans along the eastern valley mountain front, and the western part of the San Pitch Mountains which is composed predominantly of the Jurassic Arapien Formation. Groundwater flows from the mountain front to the southwest toward a discharge area at and northeast of Chicken Creek Reservoir (Thiros and others, 1996).

## BASIN-FILL HYDROLOGY

### Introduction

A major objective of this study was to characterize the basin fill in greater detail than previous work. Specific goals were to characterize (1) basin fill lithology—chiefly grain size varia-

tions over depth and area, based on water well driller's logs, (2) hydraulic properties—chiefly transmissivity estimated from well-test data from water well driller's logs, and (3) large-scale basin structure—using well-log and gravity data combined with a published seismic-reflection profile.

## Lithology

### Introduction

The primary lithologic data came from well driller's logs obtained from the Utah Division of Water Rights, which we then entered into a well-information database. The approach of this analysis was to (1) construct hydrogeologic cross sections through critical areas such as the groundwater-divide area, along the groundwater flow paths delineated by Thiros and others (1996), and through other major natural discharge and groundwater pumping areas; and (2) create maps showing the relative proportions of fine, mixed, and coarse deposits for defined depth intervals. The difficulties and uncertainties of using well drillers' logs to delineate hydrogeology are well known, but useful results can be derived using proper quality control (Hurlow, 2017). In short, it is important to verify the well's location, generalize the data, not overly rely on a single log for interpretation (except those logged in detail by an on-site geologist), and discard logs that appear too simplified or that contradict several nearby logs.

### Methods

Data from 201 well driller's logs throughout Juab Valley were entered into a database that was imported into Rockworks Borehole Manager to construct lithologic profiles through the basin fill. Data entered included the location, diameter, depth, and construction of the well, the lithologic log, and the water level (well-test data, if available, were entered into a separate spreadsheet for estimation of transmissivity; see next section). Land-surface elevation was determined from lidar imagery for wells within the available coverage. For wells outside of the lidar coverage, elevation was determined by GPS ( $\leq 4$  in. resolution) for wells in which the UGS measured water levels, and from USGS National Water Information System (NWIS) data or 1:24,000-scale topographic maps for wells we did not measure. The lithologic logs were entered by coding each lithology type with a number and forming a composite number to represent the lithology of each reported depth interval. For example, clay was coded as 1, gravel as 4, and intervals containing both were coded as 14. For intervals having both gravel and clay where gravel was listed as the primary component, the code was 41. Most logs do not, however, include relative proportions when more than one grain size is present, an important limitation of this method. Such intervals were coded with the number corresponding to the finer grain size first. The overall bias of the lithologic data is, therefore, to emphasize the fine-grained deposits.

The lithologic profiles (plate 2) were constructed in the Rockworks Borehole Manager application, which projects the wells into the profile line, plots a vertical strip log for each well that illustrates the interpreted driller's logs, and plots the screened or open interval and the water level. Water levels on the profiles are UGS measurements from 2015 or extrapolated from the 2015 water-level contours (see Groundwater Levels section). In all, 18 profiles were constructed, 8 of which are shown on plate 2 at 5:1 vertical exaggeration.

## Results

### Lithologic Profiles

The initial profiles illustrated the lithologic logs' grain-size information and, where available, sediment or rock type, using the compound numerical codes described above and unique colors and/or patterns assigned to each code. The next level of interpretation was to attempt to assign stratigraphic units to intervals in each well. Initial stratigraphic units were based on grain size and relative depth in the well; for example, the shallowest predominantly fine-grained (i.e., mainly clay) interval was denoted f1, the next deepest fine-grained interval was denoted f2, etc., and the same convention was applied to mixed and predominantly coarse-grained intervals. The goal of this approach was to evaluate whether laterally continuous hydrostratigraphic units could be identified in the basin fill. Correlation of lithologic types using this technique was generally poor. For example, although the f1, m1, and c1 layers commonly occur at similar elevations and have similar thicknesses in two to five consecutive wells, they typically do not form laterally continuous layers across more than one-third of any profile. As a result, fine, mixed, and coarse-grained layers were delineated but were not correlated into a basin-wide stratigraphy. Instead, the logs were further simplified into predominantly fine (clay and silt), mixed (unknown relative proportions of fine- and coarse-grain sizes), and predominantly coarse (sand, gravel, cobble, and boulder) intervals. Intervals coded as mixed deposits could be either intermixed clay and gravel such as debris-flow deposits, or interlayered, well-sorted beds such as fluvial deposits.

The resulting profiles (plate 2, figure 10) show the distribution of predominantly fine, mixed, and coarse-grained deposits in the upper 400 to 500 ft of the basin fill. Lateral pinch out of units is common. The interpretation of lithology between wells is geologically reasonable based on the predominant alluvial-fan, lacustrine, and fluvial depositional environments in which these deposits formed, but is speculative. Where abrupt changes occur—e.g., between wells C3-34 and C3-70 in the central part of profile A–A' (plate 2)—the lithologic boundaries are illustrated as roughly vertical, sawtooth shapes that indicate the nature and location of the contact is uncertain. Such abrupt changes typically occur between wells having different levels of detail in their lithologic logs. Lithologic patterns are not given solid or dashed boundaries to emphasize the speculative

A.

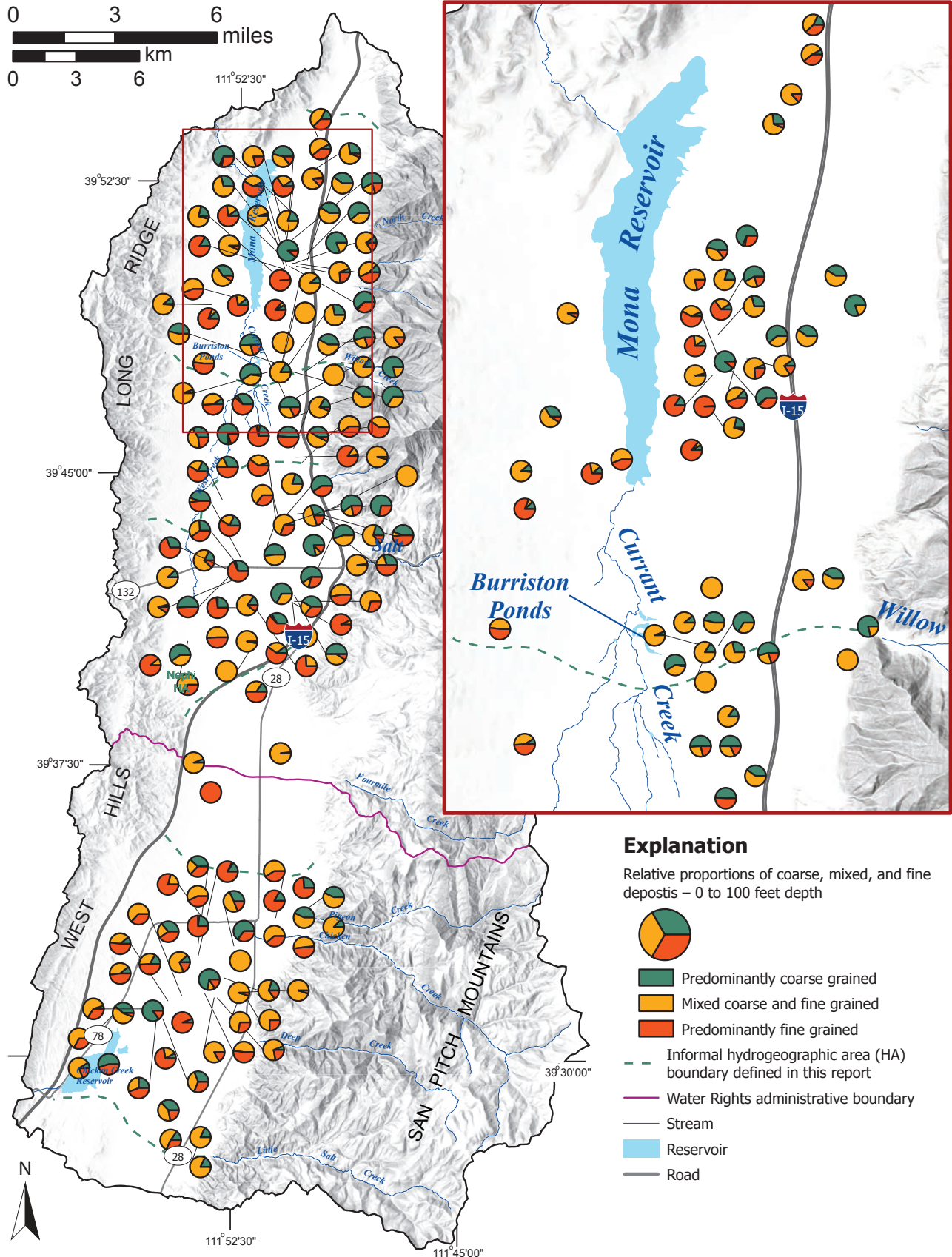


Figure 10. Pie-diagram maps showing relative proportions of fine, mixed, and coarse-grained deposits interpreted from driller's logs. A) Depths of 0 to 100 feet. B) Depths of 100 to 200 feet. C) Depths of 200 to 300 feet. D) Depths of 300 to 400 feet.

**B.**

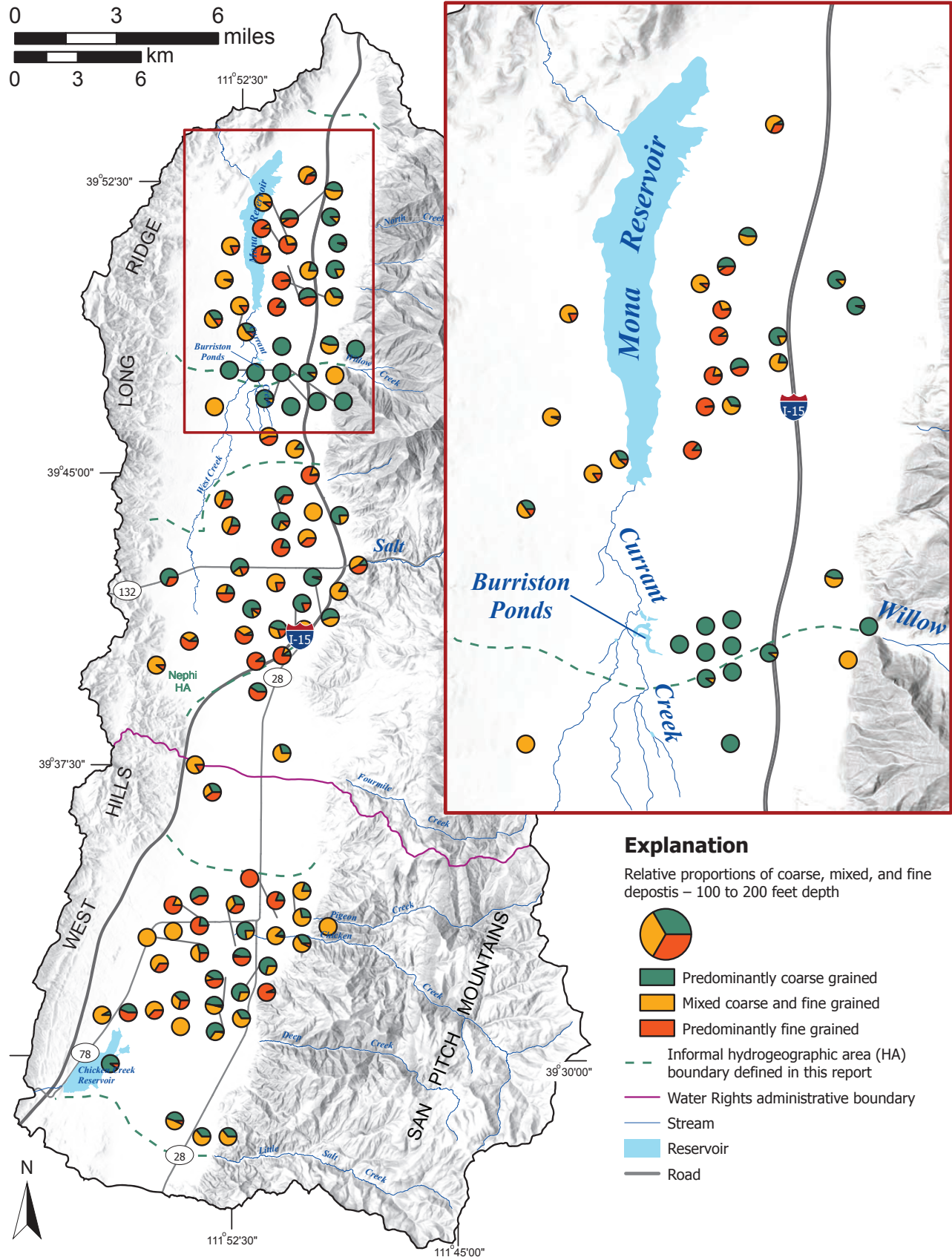


Figure 10 continued. Pie-diagram maps showing relative proportions of fine, mixed, and coarse-grained deposits interpreted from driller's logs. A) Depths of 0 to 100 feet. B) Depths of 100 to 200 feet. C) Depths of 200 to 300 feet. D) Depths of 300 to 400 feet.

C.

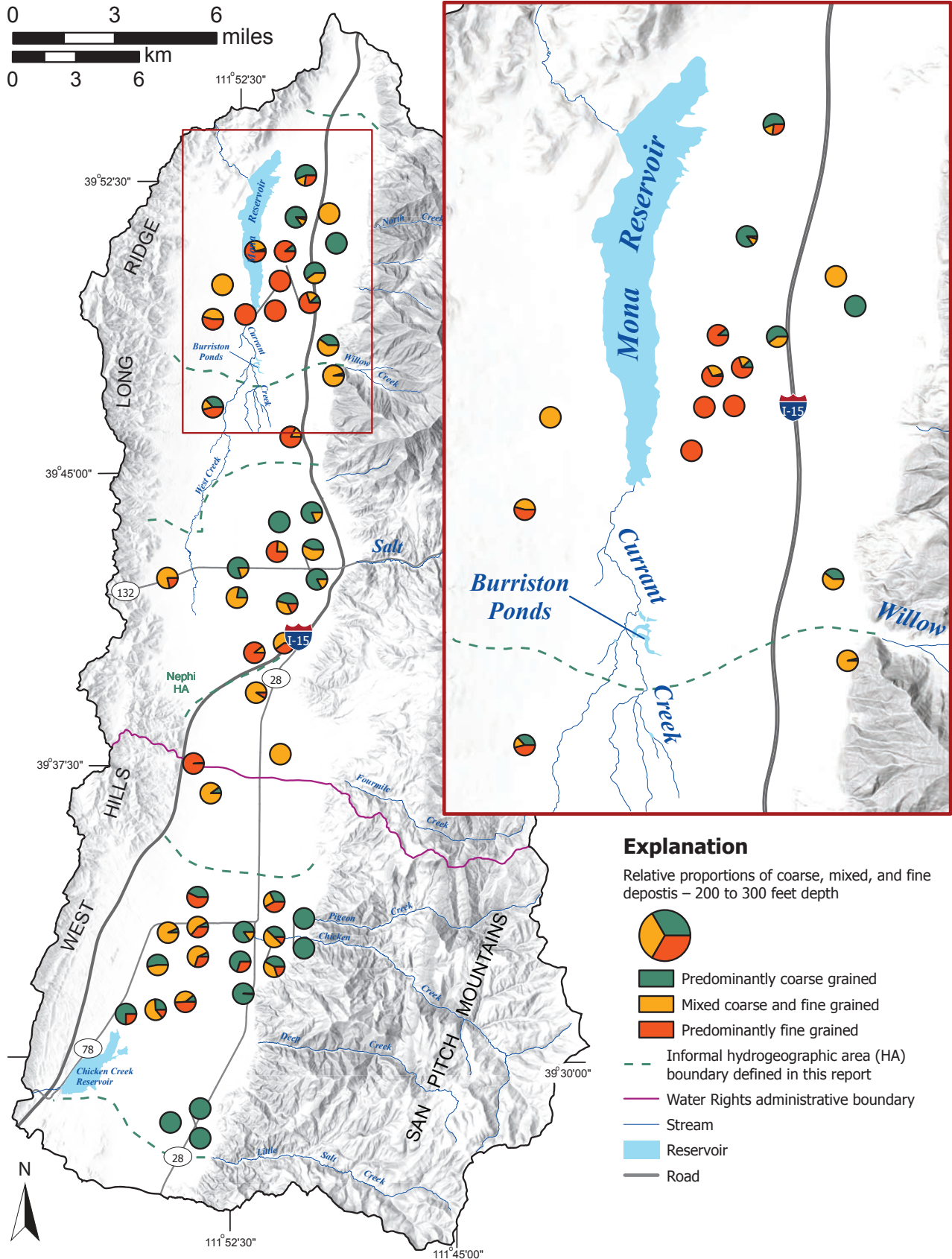


Figure 10 continued. Pie-diagram maps showing relative proportions of fine, mixed, and coarse-grained deposits interpreted from driller's logs. A) Depths of 0 to 100 feet. B) Depths of 100 to 200 feet. C) Depths of 200 to 300 feet. D) Depths of 300 to 400 feet.

D.

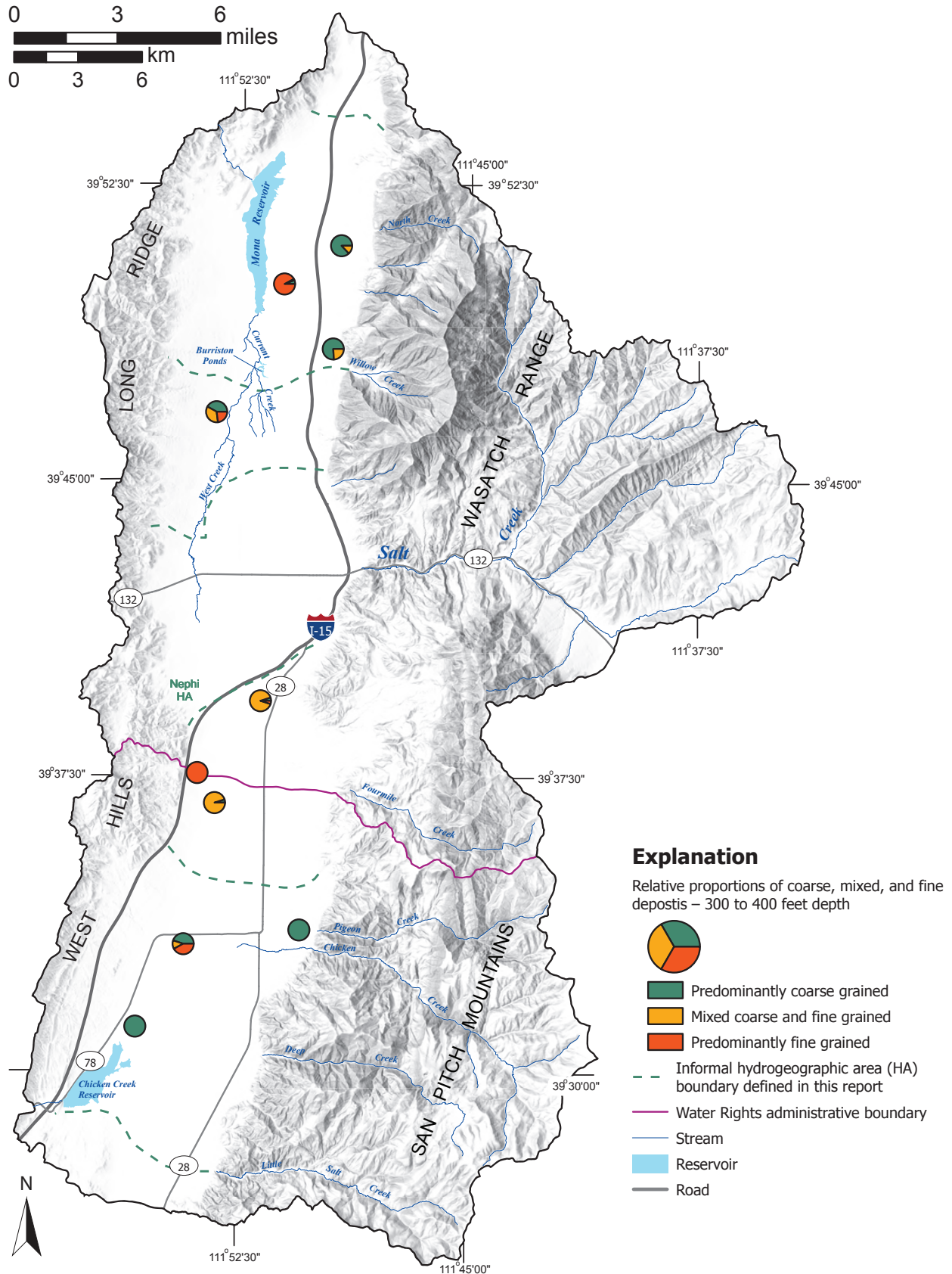


Figure 10 continued. Pie-diagram maps showing relative proportions of fine, mixed, and coarse-grained deposits interpreted from driller’s logs. A) Depths of 0 to 100 feet. B) Depths of 100 to 200 feet. C) Depths of 200 to 300 feet. D) Depths of 300 to 400 feet.

nature of the contacts away from the wells. Water levels illustrate depth to water and the saturated thickness of the basin-fill aquifer within about 300 ft of land surface.

Despite the limitations described in the preceding paragraphs, the profiles yield useful information about the lithology of the principal basin-fill aquifer including lateral and vertical variations. The following paragraphs describe the general characteristics and possible hydrogeologic significance of each profile.

Profile A–A' (plate 2) trends southwest-northeast through the southern part of the Mona Reservoir hydrogeographic area. Coarse-grained and mixed deposits dominate the northeastern part of the profile in the distal part of the North Creek alluvial fan that emanates from the Wasatch Range. From well C3-64 southwest to well C3-10, the deposits grade to predominantly fine grained. In the southwestern part of the profile, fine-grained deposits dominate the upper ~200 ft and overlie ~100 ft of coarse-grained and mixed deposits. The water table is flat compared to topography; the substantially greater depth to water below the alluvial fan reflects the greater transmissivity of these deposits than of the clay-rich deposits in the basin center. The water table is close to the land surface near Mona Reservoir, indicating that seepage to the surface likely occurs in this area. Thiros and others (1996) noted several flowing wells near Mona Reservoir, though many of these are now only intermittently or no longer flowing. Depth to groundwater below the alluvial fan on the southwestern end of the profile likely reflects low local recharge rates.

Profile B–B' (plate 2) trends north-northwest from the northern part of Nephi to Burrison Ponds, along one of the major flow paths within the basin-fill aquifer proposed by Thiros and others (1996, figure 8). The southeastern part of profile B–B' is in the mountain-front alluvial fan that originates where Salt Creek flows into Juab Valley and is composed of predominantly coarse- and mixed-grain-size deposits. Fine-grained deposits make up a greater proportion of the upper ~100 ft of the basin fill between wells D3-38 and D3-75 in the central part of the profile, and coarse- and mixed-grain-size deposits dominate the northwestern part of the profile. A 30-foot-thick fine-grained layer occurs at the top of well D3-80, east of Burrison Ponds, at land surface elevation 4922 ft. Groundwater in this well is confined and about 18 ft below land surface. The spring heads are about 400 to 1500 ft to the northwest, west, and southwest at about 4900 to 4880 ft land surface elevation, roughly at the base of the fine-grained layer in well D3-80. If the fine-grained layer in well D3-80 is laterally persistent, the Burrison Ponds springs may be a localized valley depression where the land surface cuts down to the confined aquifer. The source of the springs may, however, be deeper. Thiros and others (1996, p. 68) suggested that unspecified geologic structures, indicated by a local gravity high, focus groundwater flow to the springs. Profile B–B' is too shallow to illustrate bedrock structures, and well coverage at its northwestern end is too sparse to interpret whether faults that cut the basin fill are present.

Profile C–C' (plate 2) trends southwest-northeast, approximately perpendicular to the long axis of Juab Valley north of Nephi. This area has intensive crop growing, supported by surface water in a canal system fed by Salt Creek (Thiros and others, 1996, figure 6) and by groundwater pumping. Fine-grained deposits dominate the upper 20 to 50 ft of the basin fill in the northeastern half of the profile and overlie as much as ~200 ft of predominantly coarse- and mixed-grain-size deposits. Mixed-grain-size deposits occur in the upper ~100 ft of the basin fill in the southwestern half of the profile, above coarse and mixed deposits. Most well screens are 200 ft or more below land surface and 25 to 100 ft below the local water table. Sediment size distributions with water level and screen data indicate confined conditions. Groundwater levels in this area have declined by as much as 35 ft since 1993 (see Groundwater Levels section).

Profile D–D' (plate 2) trends north-northwest–south-southeast, from an intensive agricultural area southwest of Nephi, where the valley floor is nearly flat, abundant wells exist, and groundwater levels have declined by as much as 30 ft since 1993 (see Groundwater Levels section), to Levan Ridge, where wells are sparse. In the northwestern part of the profile, the basin fill is composed primarily of fine-grained deposits, but coarse-grained deposits are present in several wells. In the southeastern part of the profile, basin-fill deposits are predominantly mixed to fine grained, and depth to groundwater is greater than in the northwestern part of the profile. The profile crosses the Levan Ridge groundwater divide between wells F3-05 and F3-02. The elevation and position of the divide are not closely constrained here. Southwest of the divide, the profile trends toward the upper part of the Levan Ridge fan where groundwater levels increase markedly toward the range front (see Groundwater Levels section). The existence and location of the normal faults in the southeastern part of the profile are speculative. The faults are drawn based on the offset of the top of a thick section of mixed deposits between wells E3-30 and F3-05 and between wells F3-05 and F3-02, and on the apparent offset of the top of interpreted Tertiary volcanic or sedimentary rocks between wells F3-05 and F3-02. The interpreted faults are along strike with a southwest-northeast-trending section of the San Pitch Mountains range front, which could be defined by subsidiary strands of the Wasatch fault zone. Neither Witkind and others (1987) nor Hylland and Machette (2008) show Quaternary faults along this part of the range front but concealed Quaternary normal faults are likely present.

Profile E–E' (plate 2) trends east-west along the topographic crest of Levan Ridge. The profile is approximately parallel to the groundwater divide, and between the past and current locations of the divide as interpreted by Bjorklund (1967) and this study, respectively (see Groundwater Levels section). The perplexing discordance in lithologic logs between well F2-01 and wells F2-02 and F2-04 may be due to lack of reporting of relative proportions of different grain-size categories, and/or lumping of large depth intervals in the driller's log of well

F2-01. The profile shows a transition from fine-grained deposits in the west to mixed-grain-size deposits in the east. Normal faults interpreted on either side of well F2-02 are based on offset of interpreted Tertiary volcanic or sedimentary rocks in the driller's logs. The normal fault west of well F2-02 may be the same fault between wells E3-30 and F2-02 shown on profile D–D'. The normal fault, like the one between wells F3-02 and F4-02, is along strike with several Quaternary faults shown by Witkind and others (1987) and Hylland and Machette (2008). A single fault is shown on the profile, for simplicity. The steep westward slope of the groundwater table between wells F3-02 and F4-02 is consistent with the presence of mixed-grain-size deposits, Tertiary volcanic and sedimentary rocks, and faults in this part of the alluvial fan, all of which likely result in lower transmissivity of the basin-fill deposits compared to younger unconsolidated deposits.

Profile F–F' (plate 2) trends north-south from the west-central part of Levan Ridge to an area of intensive agricultural activity southwest of Levan, where irrigation wells are abundant and groundwater levels declined by as much as 40 ft from 1993 to 2015 (see Groundwater Levels section). In the northern part of the profile, in the distal part of the Levan Ridge alluvial fan, up to 140 ft of predominantly fine-grained deposits overlie mixed deposits. The upper ~250 ft of the southern part of the profile is composed of predominantly fine-grained deposits having lens-shaped deposits of coarse- and mixed-grain-size deposits. Below about 250 ft depth, the basin fill is composed primarily of coarse- and mixed-grain-size deposits. Groundwater levels in most wells are higher than the screened intervals and overlying fine-grained deposits, indicating confined conditions. Local perched conditions occur in the upper 100 ft of the basin fill, based on continuous monitoring of groundwater levels in wells southwest of Levan (see Groundwater Levels section).

Profile G–G' (plate 2) trends southwest from Levan to Chicken Creek Reservoir. Basin-fill deposits in the northeastern part of the profile have predominantly coarse and mixed grain size. This area is a composite alluvial fan built from the Pigeon Creek, Chicken Creek, and Spring Hollow drainages in the San Pitch Mountains. Groundwater levels are as much as 210 ft below land surface at the northeastern end of the profile, and progressively shallow toward the southwest. Groundwater levels in the northeastern part of the profile declined by as much as 30 ft from 1993 to 2015 (see Groundwater Levels section). Basin-fill deposits in the southwestern part of the profile are predominantly fine grained within about 150 ft of land surface and are predominantly coarse and mixed grain size at greater depths. Groundwater levels are at or near the land surface in much of the southwestern one-third of the profile, which is a major discharge area in southwestern Juab Valley, though it contains many former springs that no longer flow. Seasonally flowing wells H2-S1 and H2-S2 are shown in the profile and are discussed in the Groundwater Levels section. March groundwater levels in this area declined by less than 5 ft from 1993 to 2015 based on available well data,

but likely declined by greater amounts based on the overall reduction of surface discharge. Monitoring by the UGS indicates seasonal fluctuations of as much as 15 ft in H2-S1. The southwestern end of the profile obliquely crosses the western mountain front between the West Hills and southwestern Juab Valley. Two interpreted normal faults shown on the profile are based on the offset of the top of interpreted Tertiary sedimentary rocks between wells H1-02 and H1-08, and the substantial increase in basin-fill thickness between wells H1-08 and H1-04. The existence and positions of these faults are based in part on geologic mapping by Clark (1990). The presence of Tertiary sedimentary rocks, normal faults, and low mean annual precipitation in this area (figure 1 inset) collectively suggest that little groundwater recharge occurs in the West Hills and, therefore, little if any groundwater moves from the West Hills into the basin fill.

### Grain-size Maps

To examine spatial variations in average grain size of the basin fill, the relative proportion of fine-, mixed-, and coarse-grain-size deposits were calculated for each well in the database for depth intervals of 0 to 100 ft, 100 to 200 ft, 200 to 300 ft, and 300 to 400 ft (figure 10).

Considering the uncertainty in the drillers' logs and averaging over significant depth intervals, the results can be interpreted to only show general spatial variations and temporal trends.

Average grain size from 0 to 100 ft (figure 10A) is predominantly fine and mixed in the southwestern and western parts of the Mona Reservoir hydrogeographic area. Predominantly coarse- and mixed-grain-size deposits are present in the northeastern part of the Mona Reservoir hydrogeographic area, in the North Creek and Pole Canyon alluvial fans. Basin-fill deposits are generally coarse- and mixed-grain size in the proximal part of the Salt Creek alluvial fan in the eastern part of the Nephi hydrogeographic area, and the proportion of fine-grained deposits increases toward distal parts of the fan. Basin-fill deposits in the southwestern part of the Levan Ridge hydrogeographic area are predominantly mixed- and fine-grained, suggesting overall lower transmissivity than deposits of the Salt Creek and Willow Creek alluvial fans. Basin-fill deposits in the eastern part of the Levan hydrogeographic area are derived in large part from the fine-grained Arapien Formation along the western margin of the San Pitch Mountains, accounting for the overall finer grain size than in the Salt Creek and Willow Creek alluvial fans.

Based on well statistics (figure 8), the basin fill from 100 to 200 ft depth (figure 10B) is the most-used part of the Juab Valley basin-fill aquifer. Sediments in this depth interval are predominantly fine grained and mixed in the northern part of the Mona Reservoir hydrogeographic area, similar to the deposits in the upper 100 ft (figure 10A). Basin-fill deposits in the Willow Creek alluvial fan and near Burrinston Ponds in the southeastern

part of the Mona Reservoir hydrogeographic area are nearly entirely coarse grained. Deposits of the Salt Creek alluvial fan in the eastern part of the Nephi hydrogeographic area are overall coarser than in the upper 100 ft. Basin-fill deposits in the southwestern Levan hydrogeographic area are also overall coarser grained than in the upper 100 ft. Coarse- and mixed-grain-size deposits occur as much as 5 miles southwest of Levan, just northeast of the discharge area.

Fewer data are available from 200 to 300 ft in Juab Valley wells (figure 10C). Patterns are like those observed between 100 and 200 ft: predominantly fine-grained in the northern Mona Reservoir hydrogeographic area and the southwestern Levan hydrogeographic area, and predominantly coarse-grained to mixed in the Salt Creek (eastern Nephi hydrogeographic area) and Chicken Creek-Pigeon Creek (northeastern Levan hydrogeographic area) alluvial fans. Coarse-grained and mixed deposits are present in the northeastern part of the Mona Reservoir hydrogeographic area, in the North Creek alluvial fan.

Basin-fill deposits from 300 to 400 ft (figure 10D) are fine grained in the northern part of the Mona Reservoir hydrogeographic area, and predominantly coarse in the North Creek, Willow Creek, and Chicken Creek-Pigeon Creek alluvial fans.

## Interpretation

Groundwater flow from the mouths of Salt Creek and Willow Creek to Burrison Ponds, and from the mouths of Chicken Creek and Pigeon Creek to Chicken Creek Reservoir flow paths suggested by Thiros and others (1996) likely occurs primarily between 100- and 300-ft depth where deposits are generally coarser grained than in the upper 100 ft. The Burrison Ponds-southern Mona Reservoir and Chicken Creek Reservoir discharge areas result from the combined effects of (1) lateral change from predominantly coarse- and mixed grain-size deposits to finer-grained deposits in the upper 300 ft of the basin-fill aquifer, which forces groundwater to the surface, and (2) topographic depressions that cut down through the upper part of the basin-fill aquifer to intersect parts of the aquifer that accommodate basin-scale flow. These depressions likely formed during late Pleistocene or early Holocene time when surface flow along the valley-floor axis was more prevalent.

# HYDRAULIC PROPERTIES

## Introduction

Thiros and others (1996, p. 30–34) reported transmissivity estimates for the basin-fill aquifer from specific capacity tests ( $n = 76$ ; values of 40 to 80,000  $\text{ft}^2/\text{d}$ ), slug tests ( $n = 4$ ; values of 150 to 12,400  $\text{ft}^2/\text{day}$ ), and two aquifer tests. One aquifer test reported a transmissivity of 242,000  $\text{ft}^2/\text{day}$  for a well in the west part of Nephi, and the other test reported a transmissivity of 4000  $\text{ft}^2/\text{day}$  for a well 4 miles southwest of Levan.

## Methods

We chose to calculate our own estimates of transmissivity from data on well drillers' logs because Thiros and others (1996) did not provide a table of results, and many new wells have been installed in Juab Valley since the time of their report. Approximately 34 of our 74 wells used for transmissivity estimates were installed after the time of Thiros and others' (1996) report. We used the method of Mace (2001) to estimate transmissivity from specific capacity reported on drillers' logs, excluding tests shorter than two hours and those that were performed using bailers.

Data from longer-duration aquifer tests supplemented our compiled specific capacity estimates of transmissivity and added storativity estimates. We compiled the aquifer test data from drinking-water source protection studies and data provided by consulting firms. The longest and most detailed test we examined was a multi-well aquifer test conducted at the Young Living Lavender Farm east of Mona Reservoir. Bowen Collins and Associates conducted the 21-day constant rate test, measuring groundwater levels in the pumping well and four observation wells. We matched the Theis confined and Papadopulos-Cooper type curves to the raw aquifer test data.

## Results

Our transmissivity estimates of the Juab Valley basin-fill aquifer from specific capacity data ranged from 14 to 116,110  $\text{ft}^2/\text{day}$  (1.3–10,800  $\text{m}^2/\text{day}$ ), the median value was 1580  $\text{ft}^2/\text{day}$  (150  $\text{m}^2/\text{day}$ ) and the geometric mean was 1165  $\text{ft}^2/\text{day}$  (108  $\text{m}^2/\text{day}$ ). Eighty-nine percent of the estimates were less than 7500  $\text{ft}^2/\text{day}$  (700  $\text{m}^2/\text{day}$ ; table A2). Transmissivities from aquifer tests ranged from 3765 to 267,000  $\text{ft}^2/\text{day}$  (350–24,800  $\text{m}^2/\text{day}$ ; table A3). Figure 11 shows the transmissivity estimates, along with the areas of predominantly coarse- and mixed-grain-size basin-fill deposits generalized from figure 10, and the two transmissivity estimates from aquifer tests calculated by Thiros and others (1996, p. 31). Most of the high-transmissivity wells are in the predominantly coarse- and mixed-grain-size alluvial-fan deposits near the Wasatch and San Pitch range fronts, particularly the Willow Creek, Salt Creek, and Pigeon Creek-Chicken Creek fans. Some wells in the alluvial fans, however, have moderate to low transmissivity estimates. Our estimates generally follow the magnitudes and spatial distribution of the estimates of Thiros and others (1996), but direct comparison is difficult lacking a table of their results. In summary, figure 11 illustrates the spatial variation of transmissivity in the Juab Valley basin-fill aquifer; however, the transmissivity estimates and the basin-fill composition proportions include significant uncertainties and generalizations so that the diagram does not necessarily predict transmissivity at any particular location.

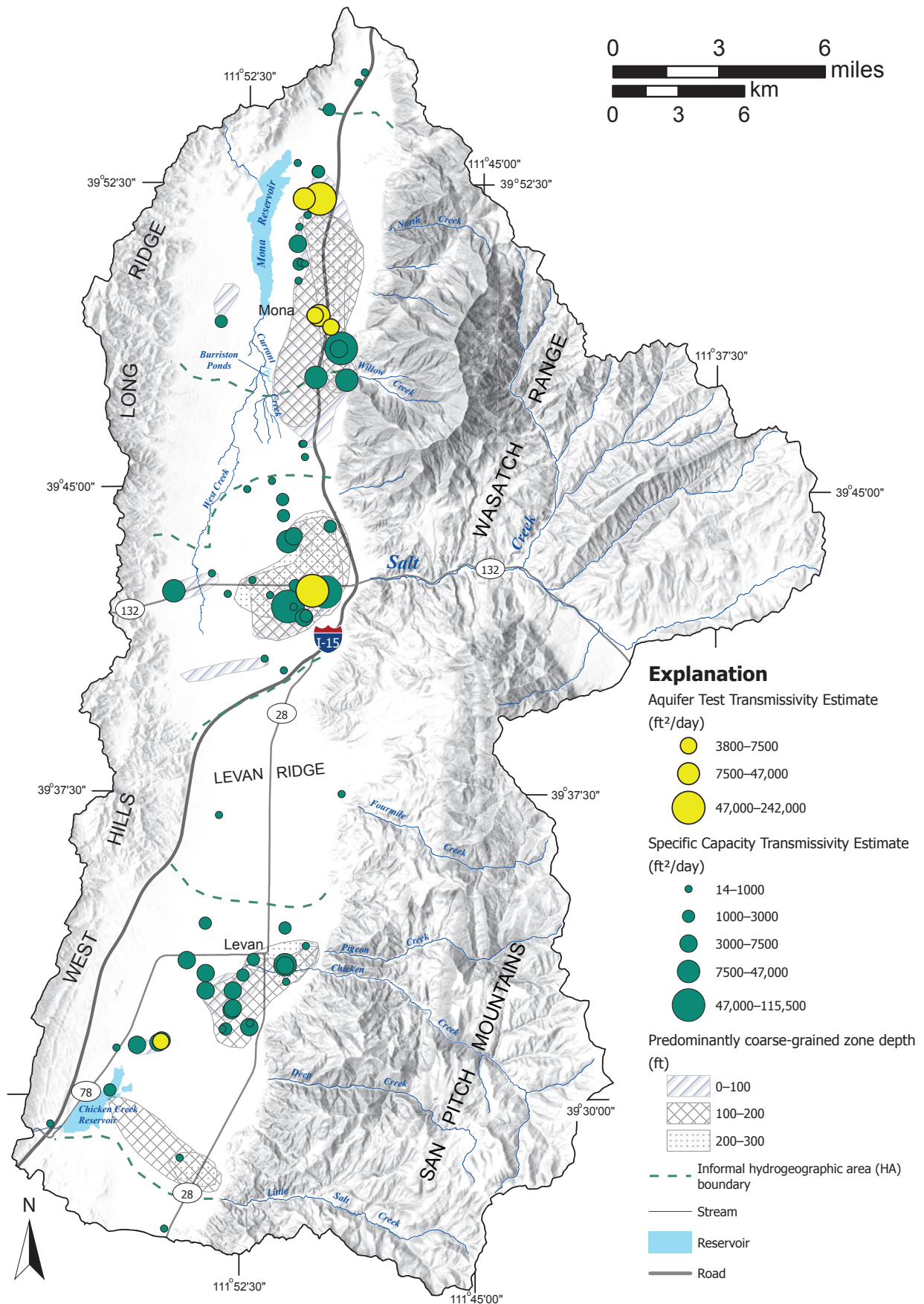


Figure 11. Transmissivity estimates for the Juab Valley basin-fill aquifer calculated from data in drillers' logs and aquifer test data. Zones of predominantly coarse-grained deposits at various depth ranges are derived from figure 10.

## STRUCTURE

### Introduction

Well-construction statistics summarized in the Groundwater subsection of the Hydrogeologic Setting section above show that current groundwater use is primarily in the upper 600 ft of the basin fill (figure 8). Analysis of the lithology and hydraulic properties of the basin fill in the previous section necessarily focused on this upper part of the Juab Valley basin fill. Previous work by Smith and Bruhn (1984) and Zoback (1992) show that the Quaternary-Tertiary fill of the syntectonic depositional basin below Juab Valley is as much as 5000 ft thick in places and is structurally complex. The large-scale structure of the basin fill is important to understand because (1) faults and thickness variations may influence regional groundwater-flow patterns including recharge from bedrock to basin-fill aquifers and flow to springs and discharge areas, (2) the deep basin fill (i.e., below about 750 ft depth) may contain groundwater that is hydraulically connected to the zone of current use, and (3) the total volume of saturated basin fill is an important factor in estimating changes in storage, and possible effects of increased groundwater pumping. Sparse deep well data requires the use of geophysics to estimate the basin-fill structure. Geophysical data provide estimates of the large-scale thickness and geometry but, compared to well data, are less precise for thickness estimates and do not provide direct measurement of the lithology and groundwater conditions of the deep basin fill.

### Methods

#### Well Data

Records of water wells in Juab Valley that penetrate the entire thickness of the basin fill are sparse. We interpreted basin-fill thickness from 37 of the driller's logs examined for this study (figure 12), in which the driller checked "bedrock" at a particular interval and all intervals below, or indicated a particular lithology such as limestone, quartzite, or volcanic rock in the interval notes. These depth-to-bedrock estimates provide important constraints on model profiles of gravity data that show the basin-fill geometry. None of the 19 petroleum-exploration wells within the study-area boundary that have lithologic logs available from the Utah Division of Oil, Gas and Mining are on the Juab Valley floor.

#### Gravity and Seismic-Reflection Data

Zoback (1992, figure 3) published a Complete Bouguer Gravity Anomaly (CBGA) map for Juab Valley. The data are sparse except along two detailed east-west traverses near Nephi, and her interpretations focused on the geometry of the Wasatch fault zone and the structure of bedrock below the basin fill. Zoback (1992, figure 7) constructed a two-dimensional model of basin-fill thickness from gravity data along an east-west

profile through Nephi that coincides with a seismic-reflection profile that was published and interpreted in the same paper.

Because the primary focus of this study is the basin-fill aquifer, and additional gravity data became available after Zoback's (1992) work, the UGS undertook a new compilation of available gravity data and collected and processed new data. Gravity data, including those collected by Zoback (1992), were downloaded from the Pan American Center for Earth and Environmental Studies (PACES, 2012). This data set contains areas of sparse coverage in several parts of Juab Valley, including Levan Ridge and adjacent areas to the north and south that are critical to this study. Christian Hardwick and Will Hurlbut of the UGS collected new gravity data (table A4) during 2016 and 2017 to fill in the spatial data gaps. Hardwick processed the data and ensured consistency with the previously existing data. The result is a new CBGA map (figure 13) that represents the gravity field in the study area, corrected for local variations in elevation, topography, and crustal thickness, projected to a common reference plane. Variations in the CBGA reflect variations in density of subsurface rock and sediment, integrated over a range of depths from a few hundred feet to the base of the continental crust (about 15–19 miles below land surface). Changes in basin-fill thickness produce most of the variations in the CBGA field because they are closer to the surface and the density contrast between basin fill and bedrock is high. The CBGA field also reflects density variations in bedrock, at greater depths and longer wavelengths than the variations in basin-fill thickness. The basin-fill depth model has profiles that cross the entire width of the valley and, therefore, have data points on bedrock (i.e., zero basin-fill thickness) at either end to account for possible variations in bedrock density on either side of the valley. The CBGA map shows that the basin fill is thickest below the geographic center of the valley from the Nephi airport (5 miles northwest of Nephi) to the north end of Chicken Creek Reservoir. Basin fill thins north of the Nephi airport and thickens again below Mona and Mona Reservoir.

#### Gravity Model Profiles

An important goal of this study was to construct an isopach map of the Juab Valley basin fill. This task required estimating basin-fill thickness from the CBGA field by combining the sparse well data with a network of two-dimensional gravity model profiles (locations shown on figures 12 and 13). Zoback's work (1992, figures 6 through 8) provided an ideal starting point with a detailed east-to-west gravity profile across the entire basin, along a seismic-reflection line for which she calculated and interpreted a depth section. The depth section (Zoback, 1992, figure 6) included the inferred base of the basin fill and two prominent reflectors within the basin fill, at about half the total basin-fill depth (reflection X) and near the base of the basin fill (Y). Zoback (1992, figure 7) constructed a two-dimensional gravity model of the basin-fill structure, and projected reflectors X and Y onto the profile but did not interpret details of the basin-fill reflections and stratigraphy.

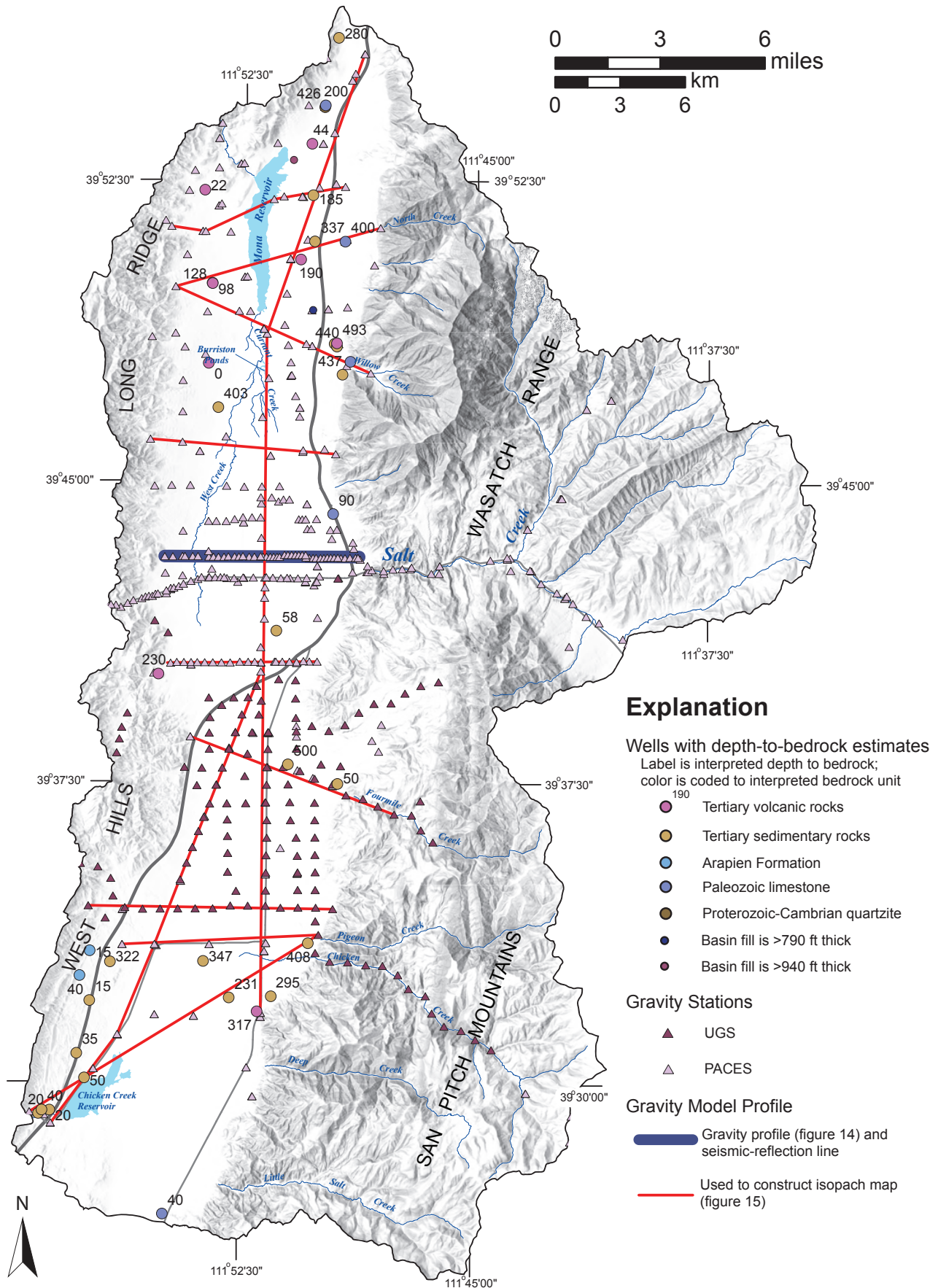


Figure 12. Gravity stations, model profiles, and wells for which depth to bedrock was interpreted from drillers' logs.

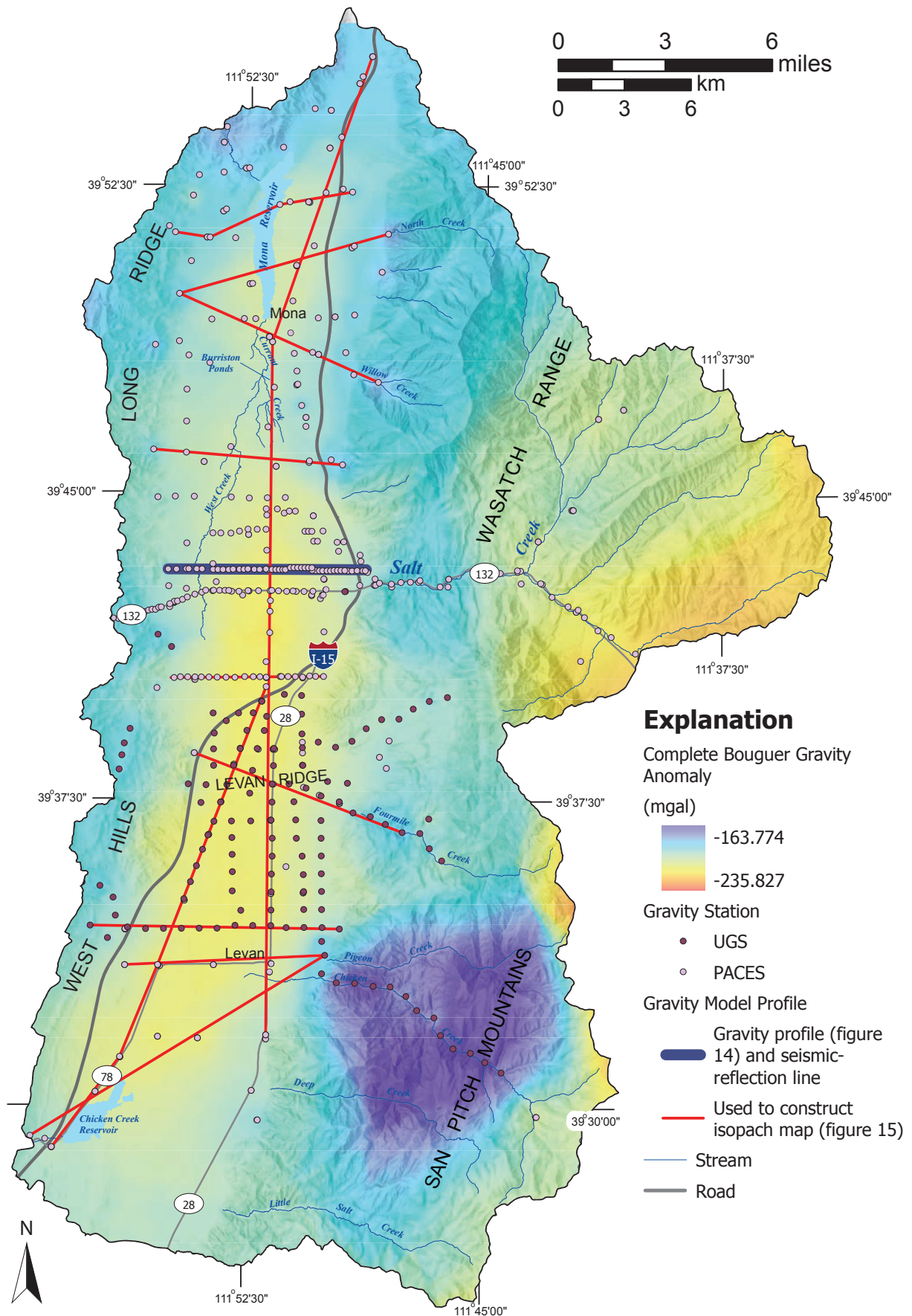


Figure 13. Grid of complete Bouguer gravity anomaly values for Juab Valley and adjacent areas.

Figure 14 shows the two-dimensional gravity model constructed for this study along Zoback's depth section of the seismic-reflection line. The depth section was scanned from the published manuscript (Zoback, 1992, figure 6) and imported into the model as a background layer. Whereas Zoback (1992) used a single density contrast between basin fill and bedrock of 0.4 grams per cubic centimeter, the new models constructed for this study used a stepwise-increasing depth-density model developed for the Basin and Range by the USGS (Saltus and Jachens, 1995) (figure 14). The boundaries between the density layers within the basin fill correspond to the prominent reflectors (X and Y) and the base of the basin fill shown on Zoback's depth section (figure 14). The model fits the gravity data well, as shown by the low root-mean-square error of 0.15, and closely fits Zoback's depth section. Differences between the two models are mainly along the basin fill–bedrock contact and are attributed to the different density-contrast structures used in the two models.

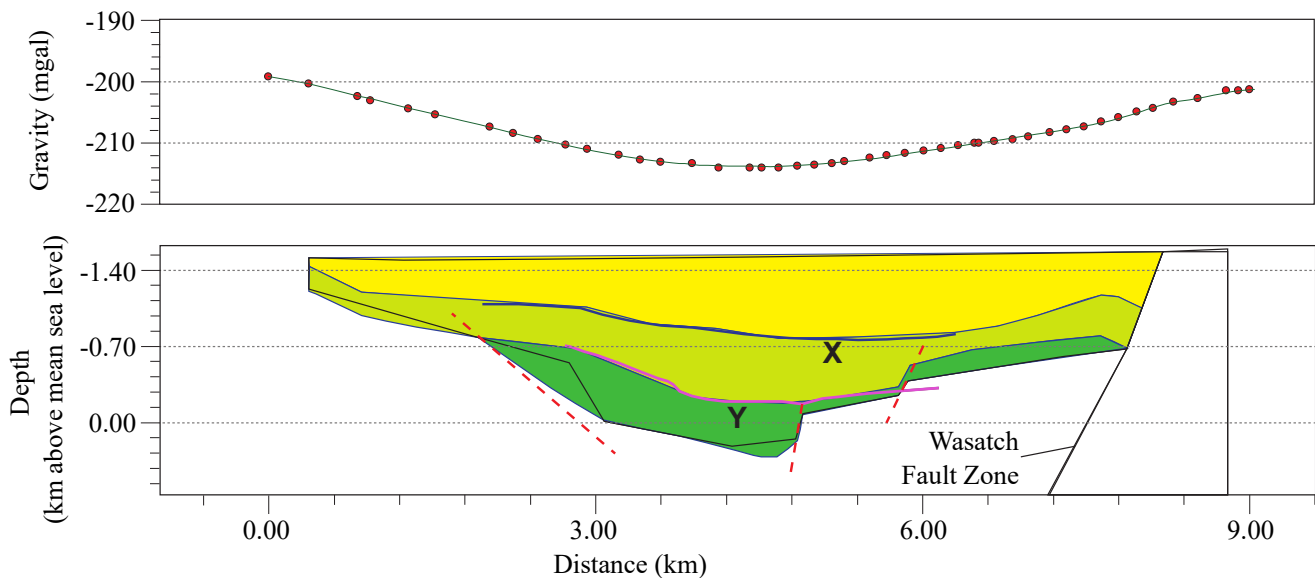
Using this stepwise depth-density model and starting with the model profile along the seismic-reflection line, 12 additional model profiles were constructed through the Juab Val-

ley basin fill (locations on figures 12 and 13). Although relatively poorly constrained by independent estimates of depth to bedrock, the models are internally consistent because they are based on the same assumptions and methodology, use the same depth-density model, and crossing models are exact matches at their tie points.

## Results

### Interpretation of Seismic-Reflection Profile and Gravity Model

The X reflector in the seismic-reflection line as shown in the depth section (figure 14) (Zoback, 1992, figures 6 and 7) is interpreted here to correspond to an unconformity between Quaternary–upper Tertiary unconsolidated to semi-consolidated basin-fill deposits above, and middle Tertiary volcanic, volcanoclastic, and sedimentary rocks below. The X reflector, therefore, divides the basin fill into upper and lower parts, referred to hereafter as the upper and lower basin fill, respectively. The contrast in degree of consolidation between the upper basin fill



### Explanation

• Observed gravity data

#### Features Modeled in this Study

— Gravity signal

— Basin-fill unit contact

- - - Interpreted fault

■ Upper basin fill ( $\Delta\rho = -0.5 \text{ g/cm}^3$ )

■ Lower basin fill 1 ( $\Delta\rho = -0.37 \text{ g/cm}^3$ )

■ Lower basin fill 2 ( $\Delta\rho = -0.34 \text{ g/cm}^3$ )

#### Features from Zoback (1992)

— X reflector

— Y reflector

— Wasatch fault zone

□ Basin fill ( $\Delta\rho = -0.4 \text{ g/cm}^3$ )

□ Arapien Formation ( $\Delta\rho = -0.07 \text{ g/cm}^3$ )

$\Delta\rho$  Density difference between basin fill and bedrock

**Figure 14.** Gravity model profile trending east-west through Nephi, along the seismic-reflection line published by Zoback (1992). Zoback's (1992, figures 6 and 7) depth section and reflectors within (X) and near the base of (Y) the basin fill are shown. Profile location shown on figures 12 and 13.

and the volcanic rocks of the lower basin fill likely results in an abrupt contrast in density and seismic velocity along the contact, producing the X reflector. The upper basin fill is as much as 2500 ft thick, and the total basin fill is as much as 6000 ft thick in the profile shown on figure 14. The lower basin fill is thickest below the geographic midpoint of the profile.

The Y reflector within the lower basin fill is interpreted here as the contact between middle Tertiary volcanic, volcanoclastic, and sedimentary rocks above and lower Tertiary sedimentary rocks below. The base of the basin fill in the gravity models is interpreted as the unconformity between lower Tertiary and Paleozoic sedimentary rocks. Similar interpretations have been presented for other published seismic-reflection lines that are constrained by borehole data and are from basins having a similar geologic history to Juab Valley (Anderson and others, 1983, figure 6; Effimoff and Pinezich, 1986, figures 3, 6, 8, and 9; Liberty and others, 1994; Evans and Oaks, 1996).

### Isopach Map

We created an isopach map of the Juab Valley upper basin fill as interpreted from the gravity model profiles (figure 15). The coordinates and elevations of points along the base of the upper basin fill were exported from each of the 13 model profiles into a text file that was converted into an ArcGIS point feature class. Exported points correspond to gravity data points projected orthogonally onto the profile lines, and additional points added to the contacts in the models. The thickness of the upper basin fill was derived by subtracting the elevations of the points along the contact from the land-surface elevations of the same points (either the elevation of the gravity survey points or the elevation of the land surface in the gravity model above the points added to the surfaces).

Isopach contours were drawn as lines in ArcMap based on the thickness values at the points exported from the models. An inverse-distance-weighted grid of the points was used to guide contour trends and spacing in areas of relatively high point density. The grid does not reflect the geologic structure of the basin near faults, the basin fill-bedrock contacts, or in areas of low point density (figure 15). The effects of these features on basin-fill thickness were interpreted during the contour-drawing process.

### Discussion

The upper basin fill ranges from 2000 to 3200 ft thick below the central part of Juab Valley. The axis of maximum thickness trends west-northwest below the valley northwest of Nephi, north-south near Nephi and below Levan Ridge, and southwest to the south of Levan Ridge. The upper basin fill is thinner (less than 500 ft thick) along an east-west trend below the southern part of Mona Reservoir, and a small area of thicker deposits (as much as 1800 ft thick) occurs below the northern part of Mona Reservoir. The upper basin fill thins

abruptly in the hanging wall of the Wasatch fault zone near the eastern valley margin, and typically thins more gradually toward the western valley margin.

Interpretation of the basin-fill stratigraphy imaged in the seismic-reflection line has important implications for the hydrogeology of Juab Valley. We are particularly interested in the depth to the base of the basin-fill aquifer. Sediments above X reflector are interpreted to comprise the upper basin fill composed of younger, less dense (i.e., less compacted and less cemented) deposits that comprise the Juab Valley basin-fill aquifer. It is important to note, however, that no wells in Juab Valley are sufficiently deep to penetrate the X reflector, and other types of geophysical data to support this interpretation are unavailable if they exist, so that the position of the base of the upper basin fill is not independently constrained.

Saturated basin-fill sediments in hydraulic connection with the actively pumped part of the aquifer may exist at greater depths. The degree of compaction and cementation of the upper basin-fill sediments and, therefore, the transmissivity and storativity of the basin-fill aquifer, likely decrease with increasing depth. The thickness of the upper basin fill shown on the isopach map (figure 15) is, therefore, a maximum estimate of the thickness of the transmissive part of the Juab Valley basin-fill aquifer.

The thickness variations in the upper basin fill are consistent with it having formed as a syntectonic basin during Basin and Range normal faulting. Most range-bounding normal faults in the Basin and Range generally strike north-south, and the axis of maximum basin-fill thickness trends parallel to them. Faults that strike approximately normal to the range-bounding faults and form subsurface bedrock ridges transverse to the predominant north-south structural and topographic grain are common. The east-west-trending zone of thin basin-fill deposits below the southern part of Mona Reservoir may correspond to a bedrock ridge localized by east-west-trending faults. Isopach-contour patterns below and south of Nephi are characterized by multiple, subparallel loci of thick deposits. This pattern suggests a complex buried horst-graben system. The area coincides with the intersection zone between the projected trend of the "Leamington tear fault" (Zoback, 1992, p. E3), a Mesozoic-Cenozoic strike-slip fault zone, and the Wasatch fault zone. A segment boundary between the Nephi and Levan segments of the Wasatch fault zone also occurs here (Machette and others, 1992; Hylland and Machette, 2008). Complex structure is expected in such a zone, along with related variations in basin-fill thickness (Schlische and Anders, 1996). In cross section the thickest part of the lower basin fill is shaped like the keel of a sailboat and suggests a narrow graben below the valley center that cuts the lower basin fill but not the upper basin fill. Hurlow (2014) noted similar profiles in sedimentary basins in west-central Utah. These older normal faults may have formed before and during eruption of the middle Tertiary volcanic rocks, consistent with the interpretation of Best and Christiansen (1991) for west-central Utah and east-central Nevada. The Juab Valley

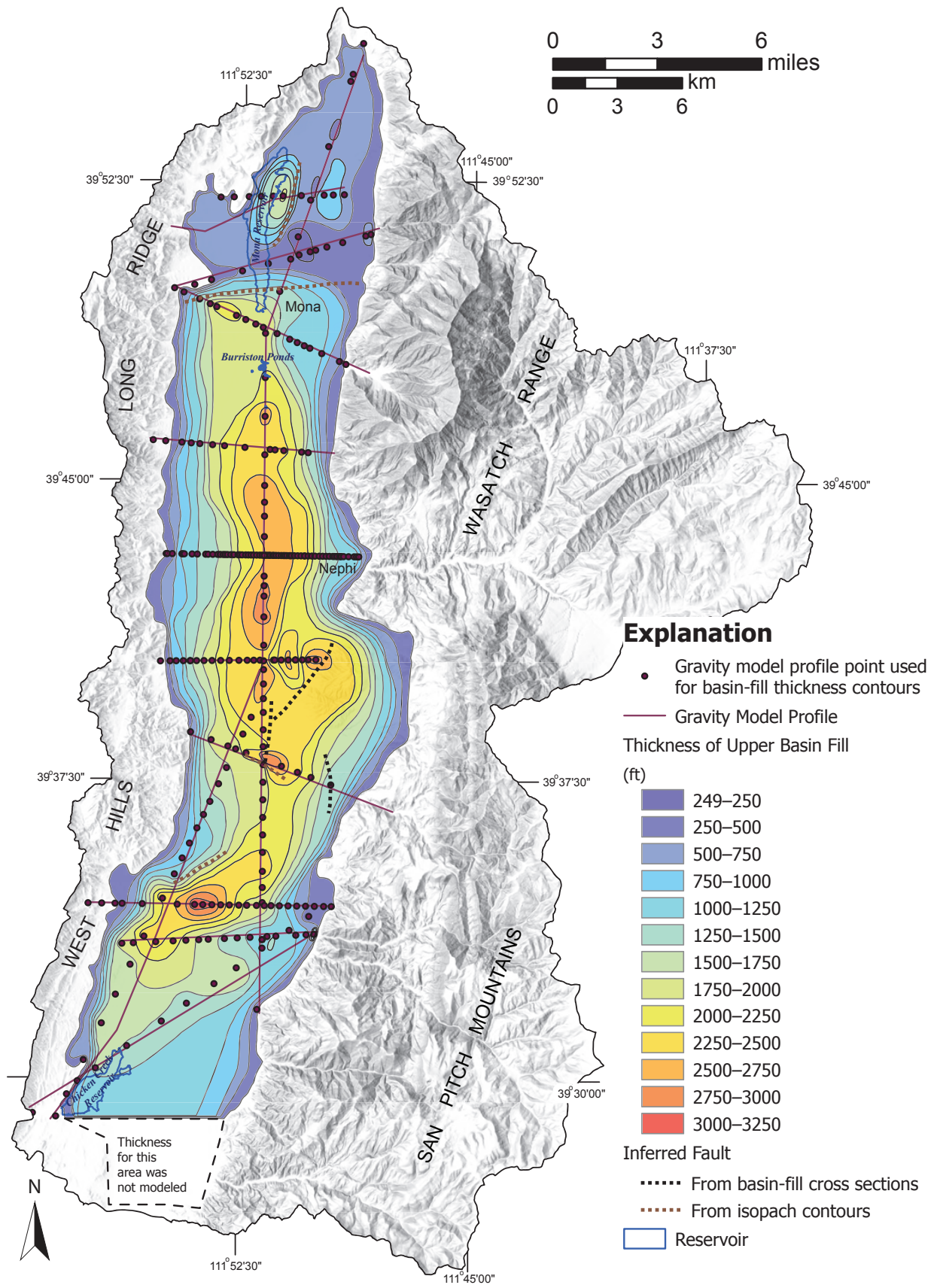


**Figure 15.** Isopach map of the Juab Valley upper basin fill from gravity model profiles. Gravity stations and profile locations are shown on figure 12. The data points shown here are the projections of the gravity data stations onto the profiles. The base of the upper basin fill is interpreted as an unconformity above Tertiary volcanic and volcanoclastic deposits that corresponds to the X reflector in the gravity model shown on figure 14 and the seismic-reflection depth section shown by Zoback (1992).

normal-fault-bounded sedimentary basin then expanded at the onset of Basin and Range faulting in Miocene time.

## GROUNDWATER LEVELS

### Introduction

Groundwater levels in wells can be interpolated to determine the potentiometric surface of groundwater. The potentiometric surface represents the gravitational potential and pressure of groundwater in an aquifer system. The potentiometric surface indicates the direction of groundwater flow, is one component necessary to calculate the amount of available groundwater in the aquifer, and the boundaries of the groundwater system. Climate change, groundwater pumping, and changes in discharge may alter groundwater levels. By measuring groundwater levels in wells, we can determine the changes in the aquifer storage and boundaries over time.

### Previous Work

Bjorklund (1967, plate 2) published a groundwater-level map of Juab Valley between Levan and the northern end of the valley, based on water levels measured in wells in 1965. Thiros and others (1996, figure 8) published a groundwater-level map of Juab Valley based on water levels measured in wells in 1993 (Steiger, 1995).

Bjorklund (1967) and Thiros and others (1996) noted that a groundwater divide exists below Levan Ridge. Water levels north of the divide generally decrease toward Burrinston Ponds and Mona Lake, and water levels south of the divide generally decrease toward Chicken Creek Reservoir. Few wells exist in the Levan Ridge area so the location and seasonal or long-term fluctuations (if any) of the groundwater divide are uncertain. Delineation of the groundwater divide relative to the surface-water divide is important because the groundwater divide roughly corresponds to the surface-water and administrative divide between the Utah Lake and Lower Sevier basins (figure 1). Bjorklund (1967) placed the groundwater divide about one mile north of the latitude of Levan on the eastern margin of Juab Valley and about 3 miles north of the latitude of Levan on the western valley margin. Thiros and others (1996) measured just one water level in Levan Ridge and did not specify the location of the groundwater divide in their water-level map.

The USGS measures groundwater levels annually in early March in 30 wells in Juab Valley (figure 9A). The hydrographs for these wells indicate that groundwater levels have declined in much of Juab Valley since the time of Steiger's (1995) thorough water-level survey (figures 9B–O). Based on this observation Hugh Hurlow and Brittany Dame undertook a water-level measurement campaign to quantify the magnitude and distribution of water-level changes throughout Juab Valley.

## Methods

### Groundwater Level Measurement

We measured water levels in 157 wells during March and early April 2015, before the beginning of seasonal groundwater pumping for irrigation. We used steel tapes to measure water levels in inactive agricultural wells and in domestic wells that presumably had not experienced intensive use during the previous few hours. Depth-to-water measurements were accurate to within a quarter of an inch (6 mm). We carefully measured the height of the measurement point (typically the water-level port on the motor base or outer casing for irrigation wells, and the top of the outer steel casing for domestic wells) above land surface. We estimated land-surface elevation from 3.28-ft (1-meter) resolution lidar data from 2013 and 2014 available from the Utah Automated Geographic Reference Center or using GPS having 0.3-ft-vertical resolution. We calculated depth to water from land surface by subtracting the height of the measuring point above land surface from the measured depth to water, and calculated water-level elevation by subtracting depth to water from the land-surface elevation.

We measured water levels in 76 of the wells that Steiger (1995) measured, to aid direct comparison of the two data sets. Many of the wells measured by Steiger (1995) were plugged or could not be found. We did not measure water levels in 16 of the wells that the USGS measures annually but added those measurements to our data set to prepare a water-level map. Water levels were comparable in 8 of the 11 wells measured by both parties. Differences are attributed to possible recent use unreported by the owner of two of the wells, and difficulty of measurement due to blocking of the tape near the water surface or condensation on the casing wall for the third. For these wells, we used the USGS measurements.

### Potentiometric Surface Map

Contours of equal water-level elevation were hand-digitized in ArcMap, using a grid of water levels computed using the Inverse Distance Weighted algorithm as a guide in areas of comparatively dense well coverage. Contouring assumes that water-level contours are roughly parallel to, and are closely spaced near, the valley margins (i.e., flow is approximately perpendicular to the valley margins and water-level gradients are steep there). These boundary conditions are difficult to build into standard gridding algorithms, which is why the water levels were hand-contoured.

### Groundwater Level Change

To derive changes in groundwater levels from the time of Thiros and others' (1996) study to 2015, we compared water levels in wells measured during both studies. Of the 16 wells that the USGS measured in 2015 and the UGS did not, 15 were also measured in 1993. Thus, we compiled groundwater levels

for 91 wells that were measured in both 2015 and 1993. Contours of water-level changes from 1993 to 2015 were hand-digitized based on data from wells measured in both years. We chose not to subtract grids of water levels from the two studies due to grid inaccuracy near the valley boundaries and in areas having sparse data.

We measured water levels in eight wells on and adjacent to Levan Ridge, six of which did not exist at the time of Steiger's (1995) measurements. Although spatial coverage of groundwater levels in Levan Ridge is still sparse compared to the Neph and Levan areas, it is greatly improved from the previous studies and the groundwater divide is better defined (albeit still somewhat uncertain). We measured water levels monthly in 15 unused wells from May 2015 to December 2018 to quantify seasonal and long-term trends in groundwater levels at and adjacent to the groundwater divide. We installed pressure transducers set to hourly monitoring in wells in the Levan Ridge (F3-06), Levan (H2-S1), and West Creek (D3-41) hydrogeographic areas to provide a more detailed account of seasonal and annual fluctuations and trends in these areas.

Christian Hardwick (UGS) performed transient electromagnetic (TEM) measurements in the Levan Ridge area. The objective was to determine whether the method could be used to map groundwater levels below Levan Ridge where no wells exist. Measurements were made near several wells to calibrate measured groundwater levels with zones of high conductivity, and repeat measurements were made at 10 stations to determine whether seasonal or annual changes in water levels could be detected.

To characterize changes in Juab Valley groundwater levels in a different manner than the snapshot of changes from 1993 to 2015, Hurlow applied simple linear regression to trends evident in the USGS long-term annual data. Later, we applied a Mann-Kendall test to the data to verify these trends with a more statistically robust approach.

During fieldwork in 2015 through 2017 in the southwest Levan hydrogeographic area, Hurlow noticed that some springs described by Thiros and others (1996), and several more shown on topographic maps, were dry year-round. Seasonally flowing wells H2-S1 and H2-S2 were constructed in trenches 20 to 30 ft below adjacent land surface. These observations suggested that declining groundwater levels led to widespread cessation of spring flow. Hurlow estimated the reduction in area having surface flow based on evaluation of the area of now-dry springs from current aerial imagery and comparison with springs noted on topographic maps.

## Groundwater Storage Change

Using the groundwater-level-change map, we estimated groundwater storage change between spring of 1993 (Steiger, 1995) and spring of 2015. Applying a similar approach

to that described above, we also examined groundwater level changes between measurements of Bjorklund (1967) taken in the spring of 1965 and 1993 (Steiger, 1995). To estimate the amount of groundwater storage change between each time, we used the area of the basin-fill extent to calculate volume from groundwater level change. We summarized the volumetric analysis grids using zonal statistics of two polygons, covering the northern and southern areas of the valley. Zonal statistics gave mean values of volumetric change for the north and south parts of Juab valley, which assumed pure water volume change and did not account for the volume of the aquifer. To measure the actual change in water volume, we multiplied the volume change by the storativity value of the aquifer, which is a summation of specific storage (confined portions of the aquifer) times aquifer thickness and specific yield (unconfined portions of the aquifer), based on the equation:

$$\partial V = S\partial hA = \partial hA(S_s b + S_y) \quad (1)$$

where:

S =	storativity
$S_s$ =	specific storage ( $L^{-1}$ )
b =	aquifer thickness (L)
$S_y$ =	specific yield $\approx$ effective porosity
$\partial h$ =	change in head (L)
$\partial V$ =	change in water volume ( $L^3$ )
A =	aquifer area ( $L^2$ )

The storativity of the aquifer is heterogeneous. Storativity values tend to be normally distributed (Neuman, 1982). To account for storage variability in the aquifer, we iteratively randomly sampled from a uniform normal distribution of storage values having a domain between 0.0001 and 0.20. The range of storage values was based on ranges of values from aquifer tests and results of the calibrated USGS model (Thiros and others, 1996), and assumes that parts of the aquifer experiencing groundwater declines are unconfined. The randomly sampled storage coefficient values were multiplied by the calculated volume change over 3000 iterations. The means of the resulting distributions divided by the years between each water level campaign gives estimates of groundwater storage change rates (ac-ft/yr).

## Inundation Changes

Inundation can be a good proxy for groundwater level changes in Juab Valley because the surface water bodies in the valley are predominantly fed by groundwater sources (Thiros and others, 1996). The term "inundation" is the amount of land

area covered by water. We calculated changes of inundation over time using the European Commission's Joint Research Center (JRC) global surface water mapping layers (Pekel and others, 2016). The JRC data are the results of comparisons of monthly data between decades, showing changes in the extent and duration of water inundation. We also made a visual comparison of observations during fieldwork in 2015 through 2018, examined aerial imagery, noted locations of now-dry springs shown on older topographic maps, and compared physical descriptions and spring-flow rates published by Thiros and others (1996). Code for these calculations can be found at <https://code.earthengine.google.com/0562f3f86974e42b3f520377d517f19e>.

## Results

### Groundwater-Level Map for 2015

Figure 16 shows contours of water-level elevations from our work in 2015 and from 16 measurements by the USGS for wells that we did not measure. All these water levels are from wells having open or screened intervals in the basin-fill aquifer.

Water-level contours west of Nephi form a complicated pattern that likely reflects localized drawdown in this mixed agricultural-residential area. From about 3 miles north of Nephi to Mona Reservoir, water-level contours are horseshoe-shaped and concave to the north. Contours in the northeastern part of the valley are parallel to the range front, and water-level elevations decrease toward the northeast part of Long Ridge north of Mona Reservoir.

Water-level contours west and southwest of Levan are generally horseshoe-shaped and concave toward the southwest. Areas of anomalously high groundwater levels exist below and northwest of Levan, defined by two wells each. The well in southeast Levan is not in use, whereas the well in north Levan is pumped annually to irrigate fields to the north and west. The wells in Levan are deep irrigation wells, and their high groundwater levels relative to surrounding areas are difficult to explain. Wells G2-05 and G2-28 northwest of Levan are 70 and 60 ft deep, respectively, and may be in a perched aquifer above the main basin-fill aquifer.

Water-level contours in the Levan Ridge area are horseshoe shaped and concave to the south below the crest of the ridge and to the south and are horseshoe shaped and concave to the north from the northern margin of the ridge to the north. The groundwater divide exists where the water-level surface is saddle-shaped below the northern slope of the ridge. Water-level contours are very steep along the northern margin of Levan Ridge and along the range front east of the ridge. Even with the increased number of water levels compared to previous studies, delineating the groundwater divide was somewhat uncertain and two reasonable alternatives were considered (figure 16). Figures 17 and 18 show the preferred alternative (see discussion below).

### Groundwater-Level Changes from 1993 to 2015

Figure 19 shows the well locations and interpreted contours of valley-wide water-level declines. Groundwater levels declined from 1993 to 2015 in all but one of the wells (G3-25) measured in both years. Declines ranged from about 53 ft to less than 1 foot and were greatest west of Nephi and southwest of Levan, where intensive pumping of groundwater for irrigation occurs. Groundwater levels declined by between 5 and 10 ft along the east margin of Mona Reservoir, and by as much as 25 ft north of Mona. Groundwater levels declined by as much as 53 ft, but more typically between 15 and 32 ft, west and northwest of Nephi. Only one well (F3-06) in Levan Ridge had measurements in both 1993 and 2015 and showed a decline of 33 ft. Continuation of the contours of groundwater-level declines from the area south of Nephi through Levan Ridge, to the area north of Levan as shown on figure 20, is speculative.

### Groundwater-Level Monitoring

In addition to measuring water levels and conducting sampling in spring 2015, we established monthly water-level monitoring of eight wells in and adjacent to the Levan Ridge hydrogeographic area (figures 20 and 21) to characterize the far-field effects of groundwater pumping in the Nephi and Levan hydrogeographic areas and determine whether the location of the groundwater divide changed long-term and/or seasonally. Two of these sites were wells that flow seasonally, so we measured the flow and the depth to water (figures 21 and 22).

In 2017 when the Division of Water Rights indicated they wished to continue the study, emphasizing the northern part of Juab Valley, we established monthly monitoring at four wells in the western part of the West Creek and southern part of the Mona Reservoir hydrogeographic areas (figures 21 and 23). These wells measure groundwater that flows to the east from Long Ridge, to the valley-floor discharge area that sources West Creek and Carrant Creek which in turn provide surface flow into Mona Reservoir. In 2017 we also began monitoring two seasonally flowing wells about 2 miles northeast of Chicken Creek Reservoir to document seasonal and long-term trends in the discharge area in the southwestern part of the study area.

Monthly groundwater levels in wells in and adjacent to the Levan Ridge hydrogeographic area show a variety of seasonal and long-term trends that in part reflect proximity to major areas of groundwater pumping (figure 21A). On the margins of the Levan Ridge hydrogeographic area, wells F2-08, G2-24, and G2-25 show seasonal fluctuations related to groundwater pumping for irrigation, superposed on declining trends of three or four years. Early September groundwater levels in well F2-08 declined steadily at a rate of 1.7 ft per year. In the central part of the Levan Ridge hydrogeographic area, wells F3-01 and F3-06 show little or no seasonal fluctuations. Despite its distance from areas of major groundwater pumping,

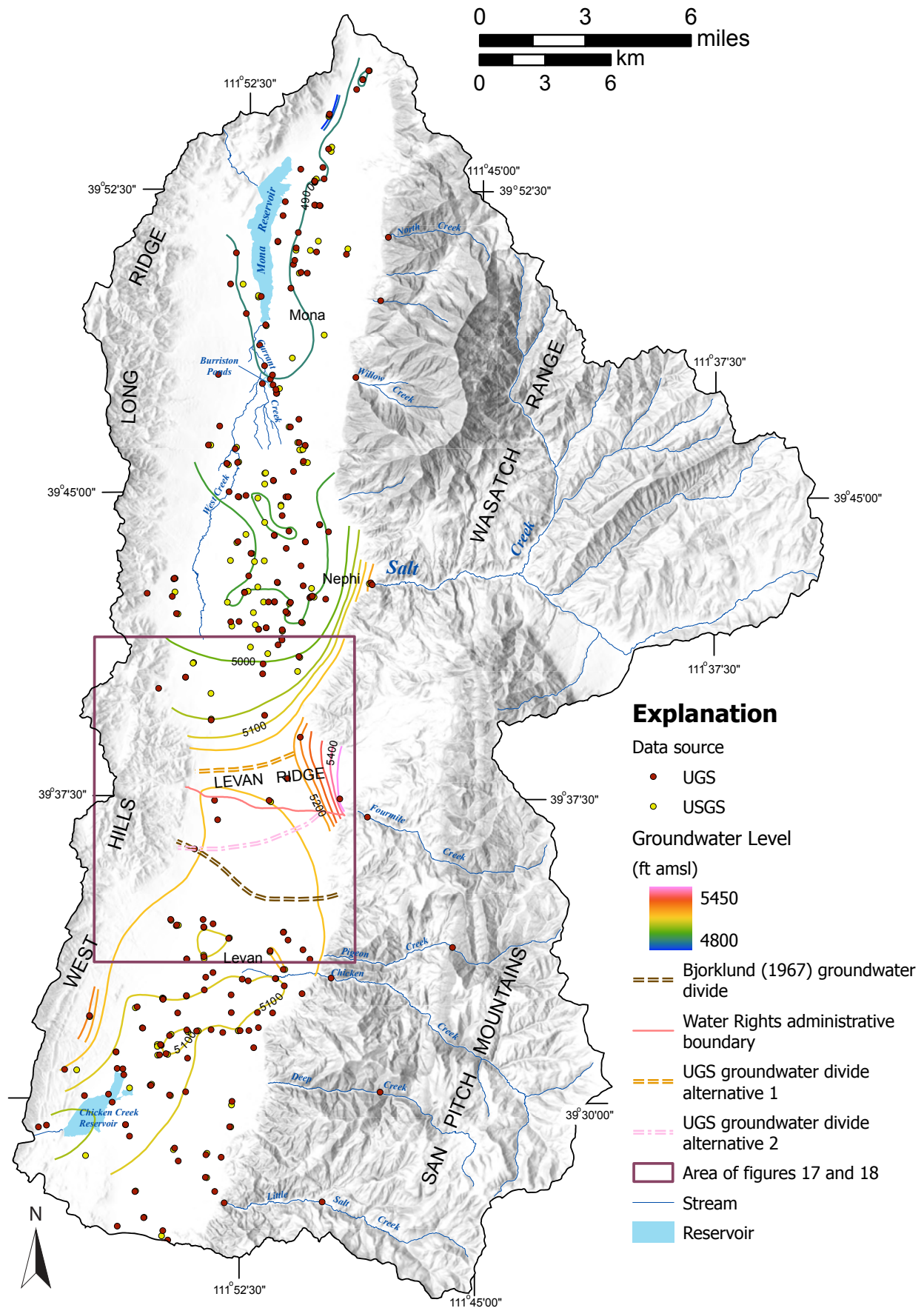


**Figure 16.** Water-level map for Juab Valley from March to April 2015, and interpretations of the potential groundwater divides. The UGS groundwater divide alternative 1 is the preferred interpretation of the divide over the original Bjorklund (1967) divide.

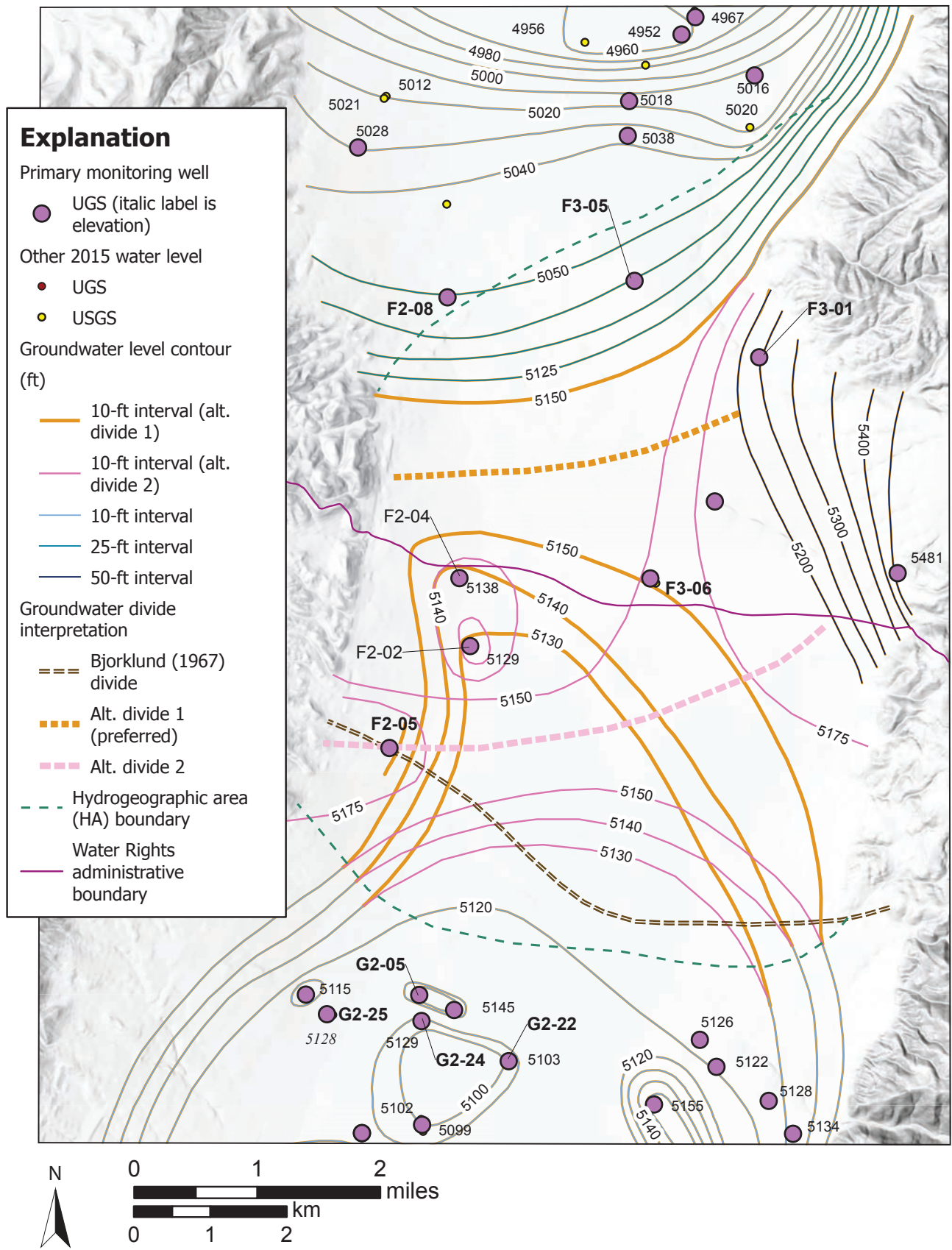
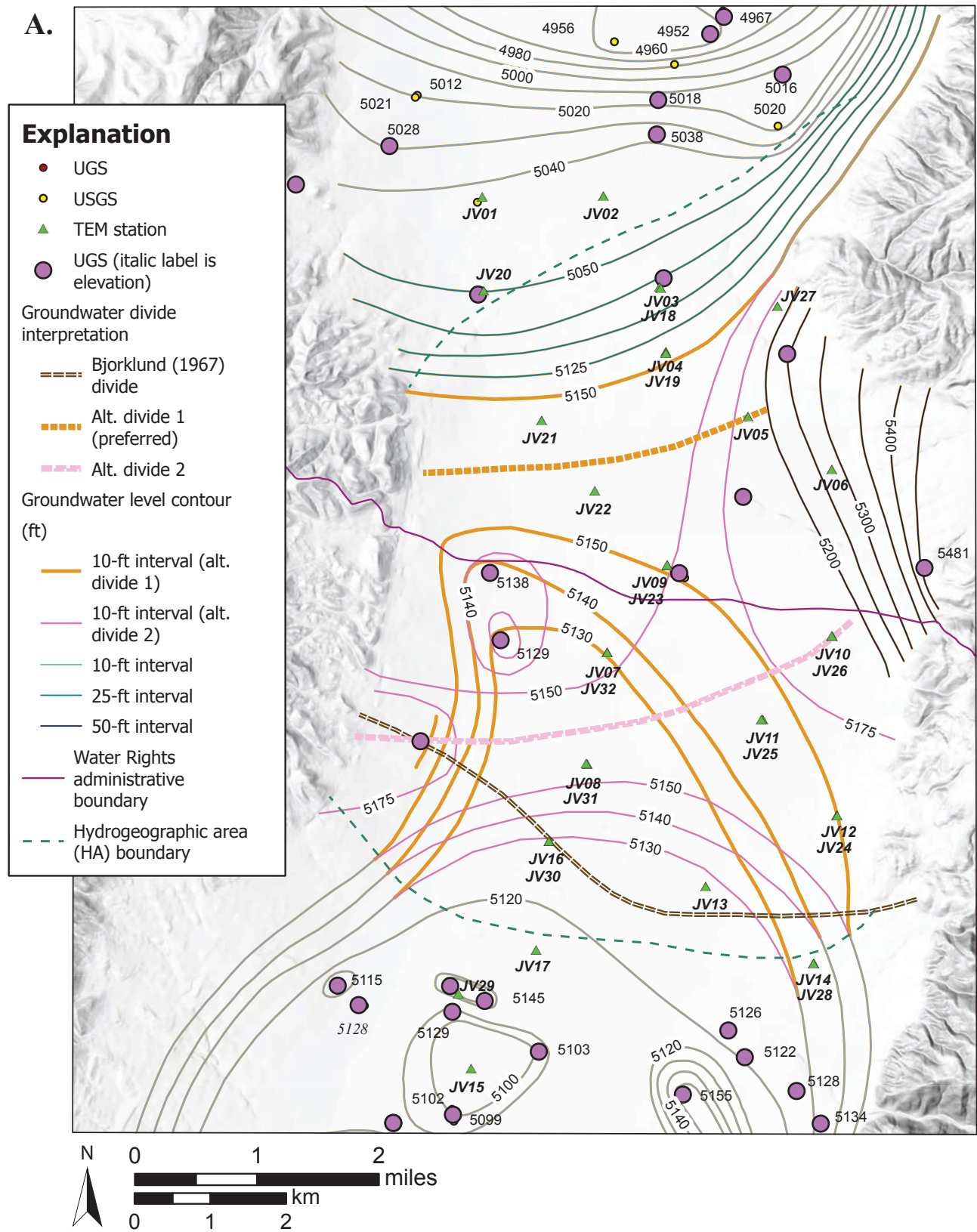
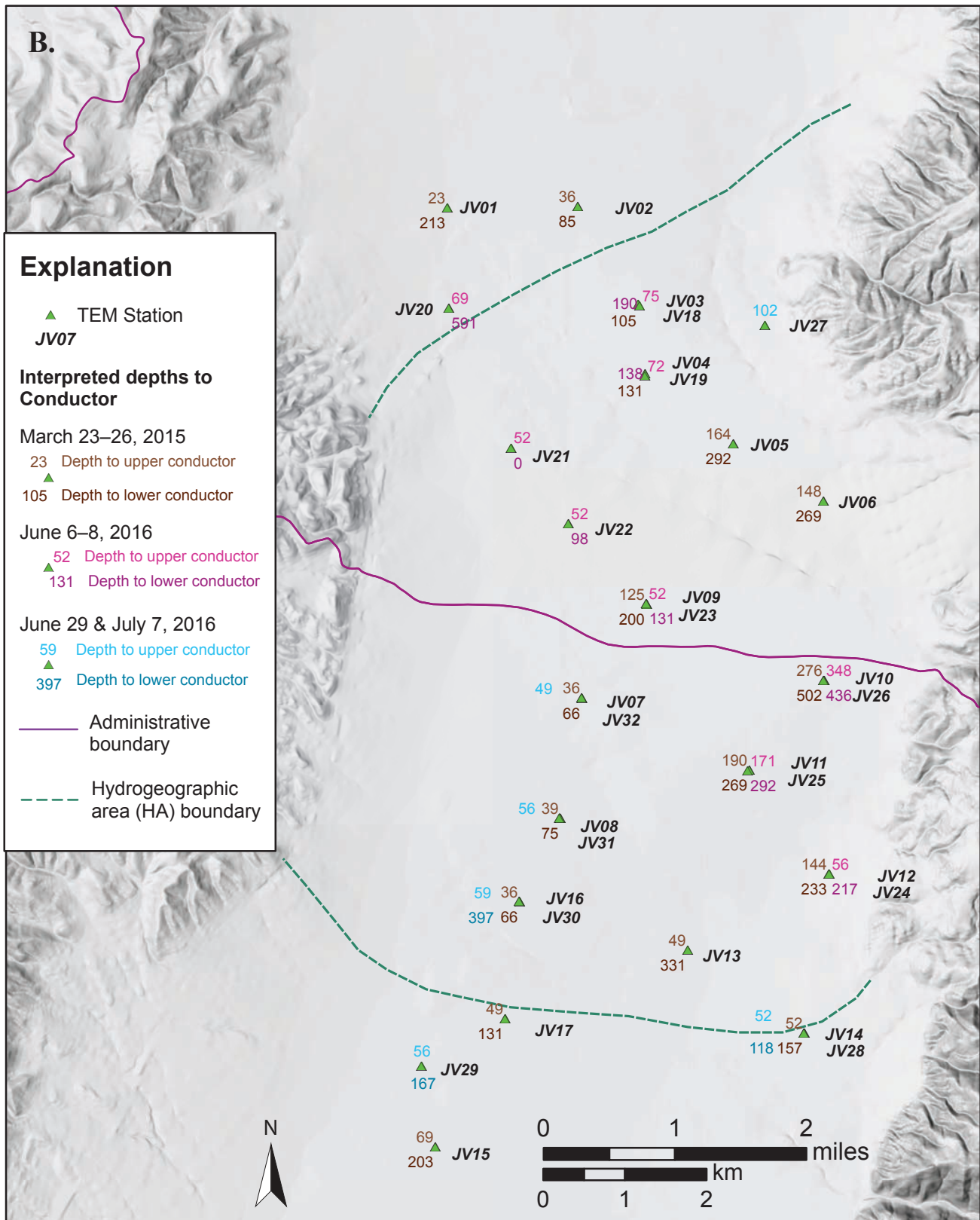


Figure 17. Levan Ridge area wells having 2015 groundwater levels, interpreted water-level contours, and alternative positions, including our preferred position, of the groundwater divide.



**Figure 18. A)** The Levan Ridge area showing transient electromagnetic (TEM) stations and alternative interpretations of water-level contours and groundwater divide. **B)** TEM stations in the Levan Ridge area showing depths (in feet) from land surface to upper and lower conductors from 2015 and 2016 surveys. **C)** TEM stations in the Levan Ridge area showing difference between water-level elevations (in feet) in wells and elevations of interpreted conductors, and differences in elevations (in feet) of upper and lower conductors from 2015 and 2016 surveys. **D).** Plot of differences between water-level elevations in wells and elevations of interpreted conductors from nearby TEM stations in the Levan Ridge area. **E)** Plot of differences in elevations of upper and lower conductors from 2015 and 2016 surveys in the Levan Ridge area.



**Figure 18 continued.** *A)* The Levan Ridge area showing transient electromagnetic (TEM) stations and alternative interpretations of water-level contours and groundwater divide. *B)* TEM stations in the Levan Ridge area showing depths (in feet) from land surface to upper and lower conductors from 2015 and 2016 surveys. *C)* TEM stations in the Levan Ridge area showing difference between water-level elevations (in feet) in wells and elevations of interpreted conductors, and differences in elevations (in feet) of upper and lower conductors from 2015 and 2016 surveys. *D)* Plot of differences between water-level elevations in wells and elevations of interpreted conductors from nearby TEM stations in the Levan Ridge area. *E)* Plot of differences in elevations of upper and lower conductors from 2015 and 2016 surveys in the Levan Ridge area.

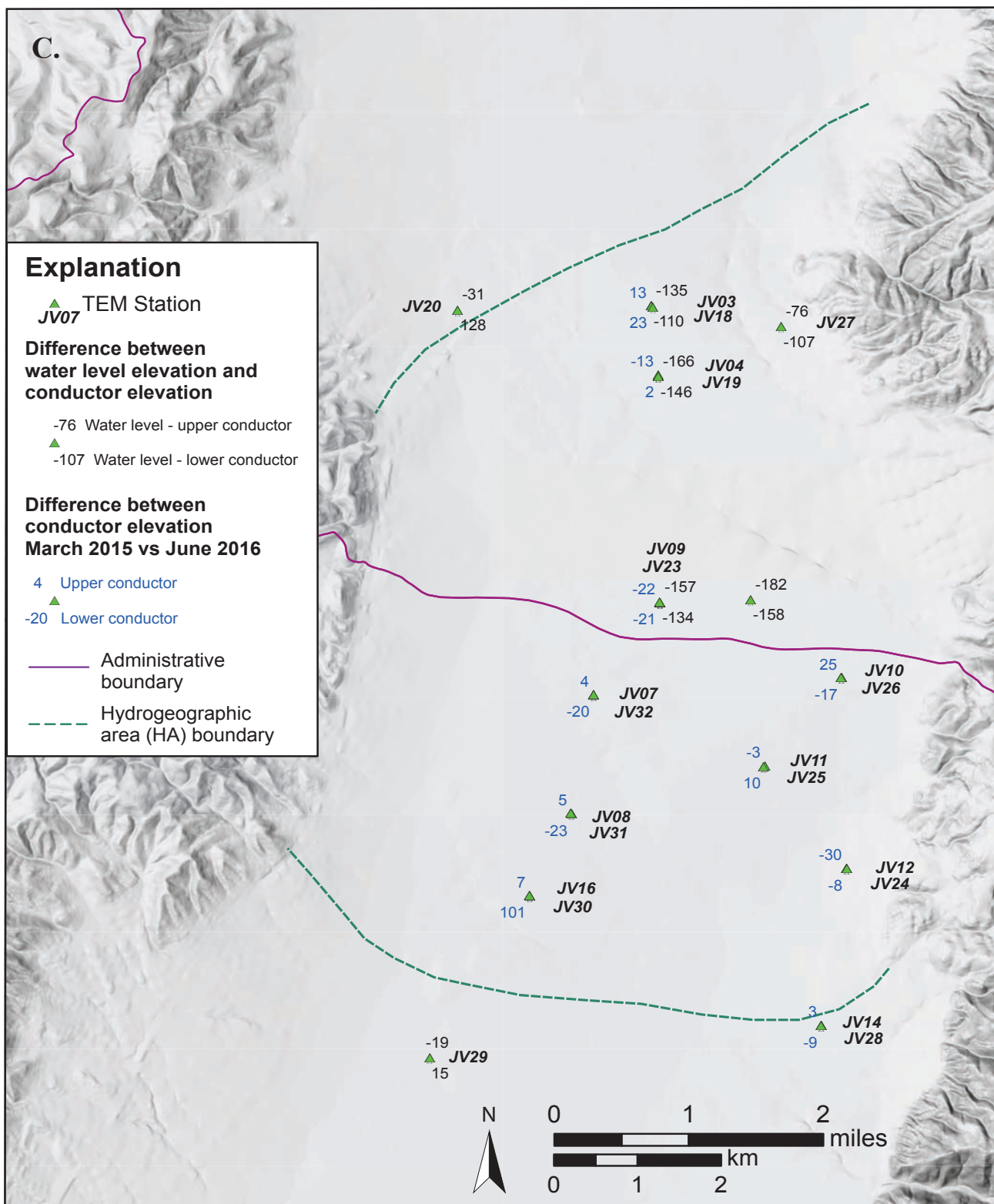


**Figure 18 continued.** *A)* The Levan Ridge area showing transient electromagnetic (TEM) stations and alternative interpretations of water-level contours and groundwater divide. *B)* TEM stations in the Levan Ridge area showing depths (in feet) from land surface to upper and lower conductors from 2015 and 2016 surveys. *C)* TEM stations in the Levan Ridge area showing difference between water-level elevations (in feet) in wells and elevations of interpreted conductors, and differences in elevations (in feet) of upper and lower conductors from 2015 and 2016 surveys. *D).* Plot of differences between water-level elevations in wells and elevations of interpreted conductors from nearby TEM stations in the Levan Ridge area. *E)* Plot of differences in elevations of upper and lower conductors from 2015 and 2016 surveys in the Levan Ridge area.

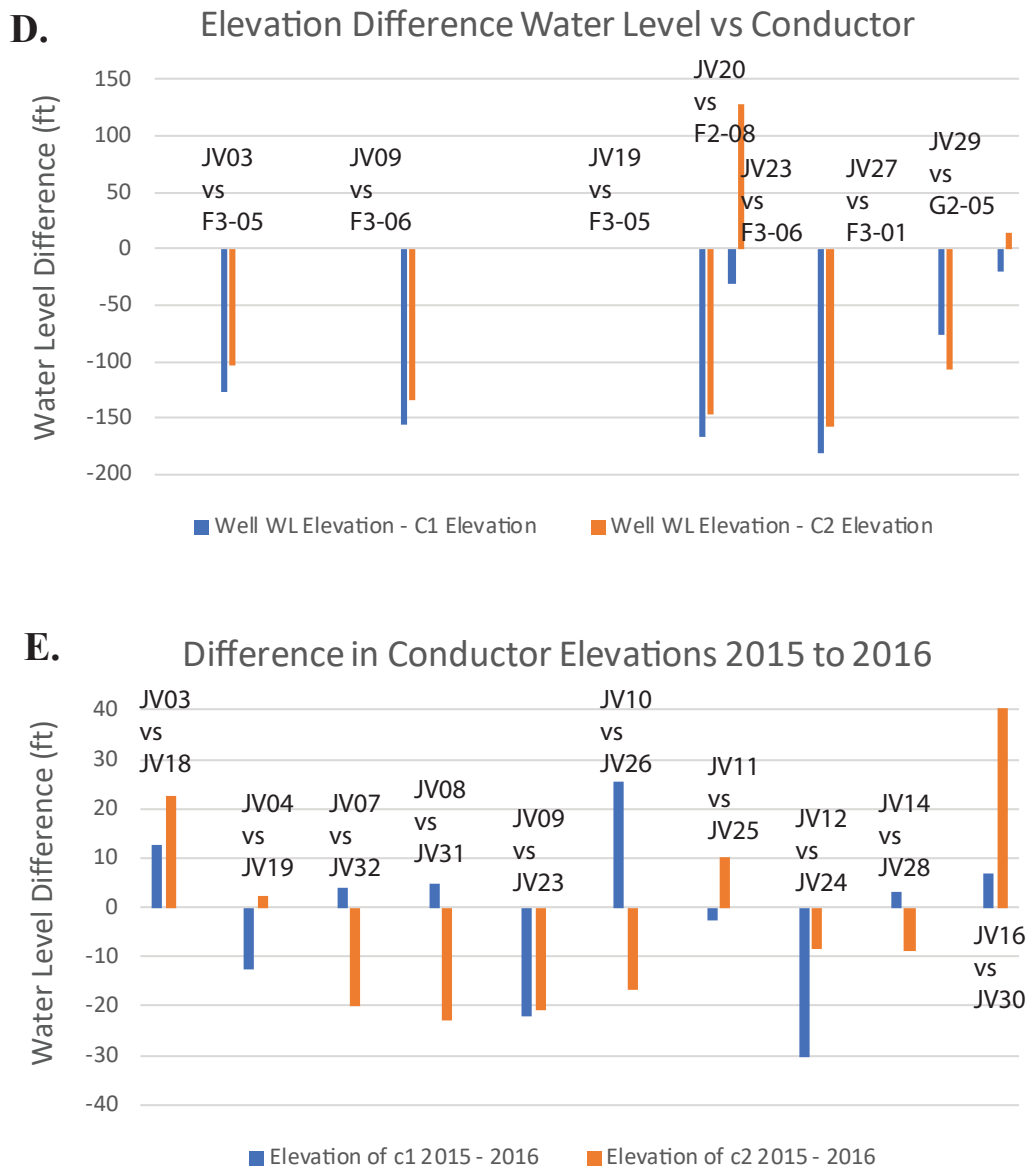


**Figure 18 continued.** *A)* The Levan Ridge area showing transient electromagnetic (TEM) stations and alternative interpretations of water-level contours and groundwater divide. *B)* TEM stations in the Levan Ridge area showing depths (in feet) from land surface to upper and lower conductors from 2015 and 2016 surveys. *C)* TEM stations in the Levan Ridge area showing difference between water-level elevations (in feet) in wells and elevations of interpreted conductors, and differences in elevations (in feet) of upper and lower conductors from 2015 and 2016 surveys. *D)* Plot of differences between water-level elevations in wells and elevations of interpreted conductors from nearby TEM stations in the Levan Ridge area. *E)* Plot of differences in elevations of upper and lower conductors from 2015 and 2016 surveys in the Levan Ridge area.

water levels in well F3-06 declined steadily at a rate of 2.2 ft per year, whereas well F3-01 showed no significant trends. Well F2-05 (depth 38 ft; well may be silted in) on the western margin of the Levan Ridge hydrogeographic area showed clear seasonal fluctuations but was dry after April 2017. Well F3-05 showed variable fluctuations and was pumped at times during 2016, and was re-developed during late 2017. After the re-development, groundwater levels in F3-05 showed a slight overall increasing trend based on limited data. On the southwest margin of the agricultural area southwest of Levan, seasonal fluctuations are superimposed on annual decline rates of 0.33 ft per year at G2-25, 0.7 ft per year at G2-05, and 5 ft per year at G2-24, based on early March water levels.

The seasonally flowing wells in the southwestern part of the Levan hydrogeographic area (H2-S1; and H2-S2A and H2S2B) are 10-inch-diameter steel casing with two rectangles cut into their sides to allow flow (figure 22). The higher set of rectangles were likely cut first, then the lower set as groundwater levels gradually declined. Both sites are set in southwest-trending trenches about 20 to 30 ft below the local land surface, and flow enters a canal system that moves water toward the northeast end of Chicken Creek Reservoir. We measured depth to water monthly, and flow in the trenches downstream of the wells monthly when possible. The wells flowed between early October 2017 and late April 2018, did not flow through the groundwater pumping season, and resumed flow

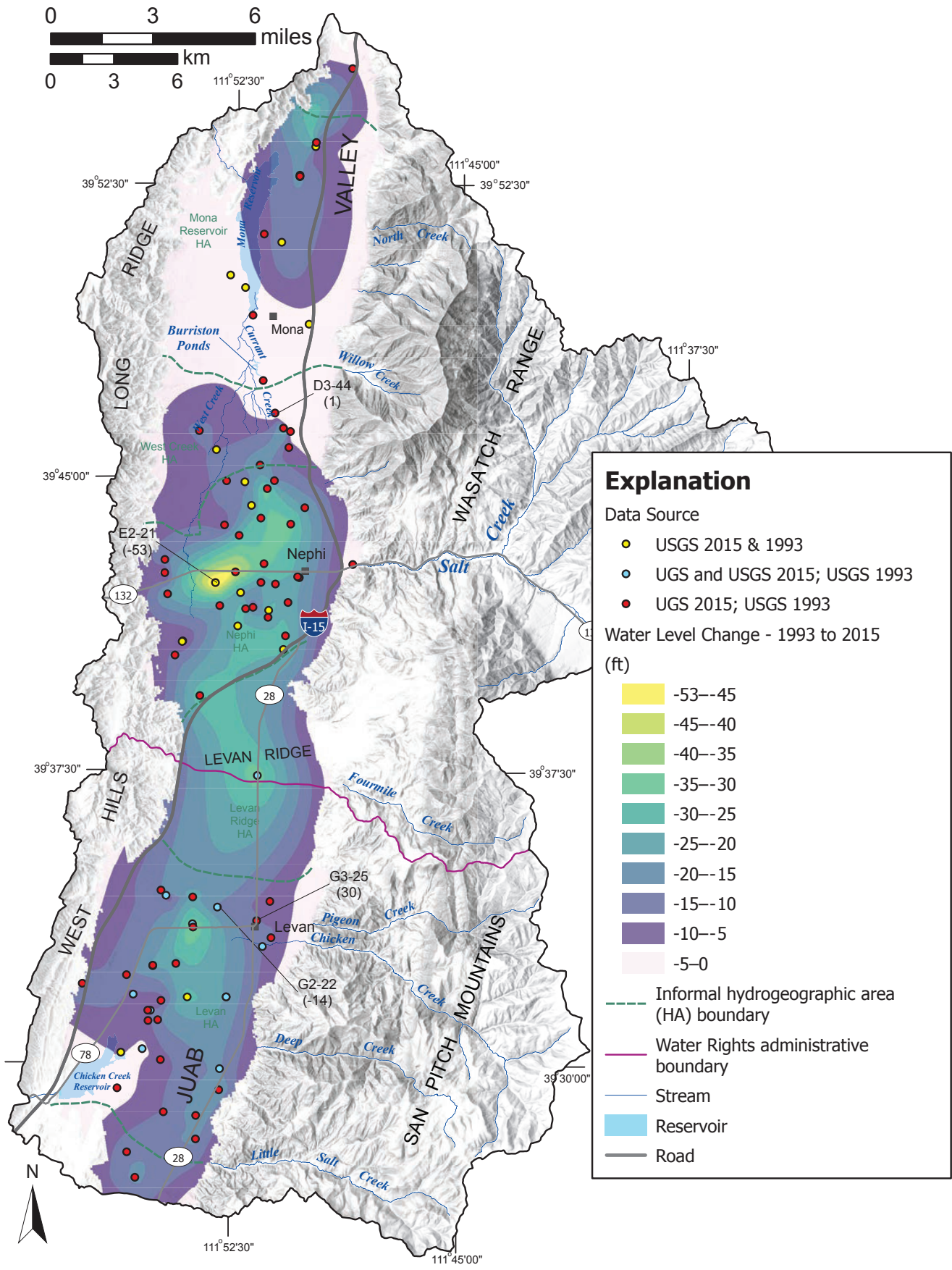


Figure 19. Changes in Juab Valley groundwater levels from 1993 to 2015, including change values at anomalous wells and interpreted contours.

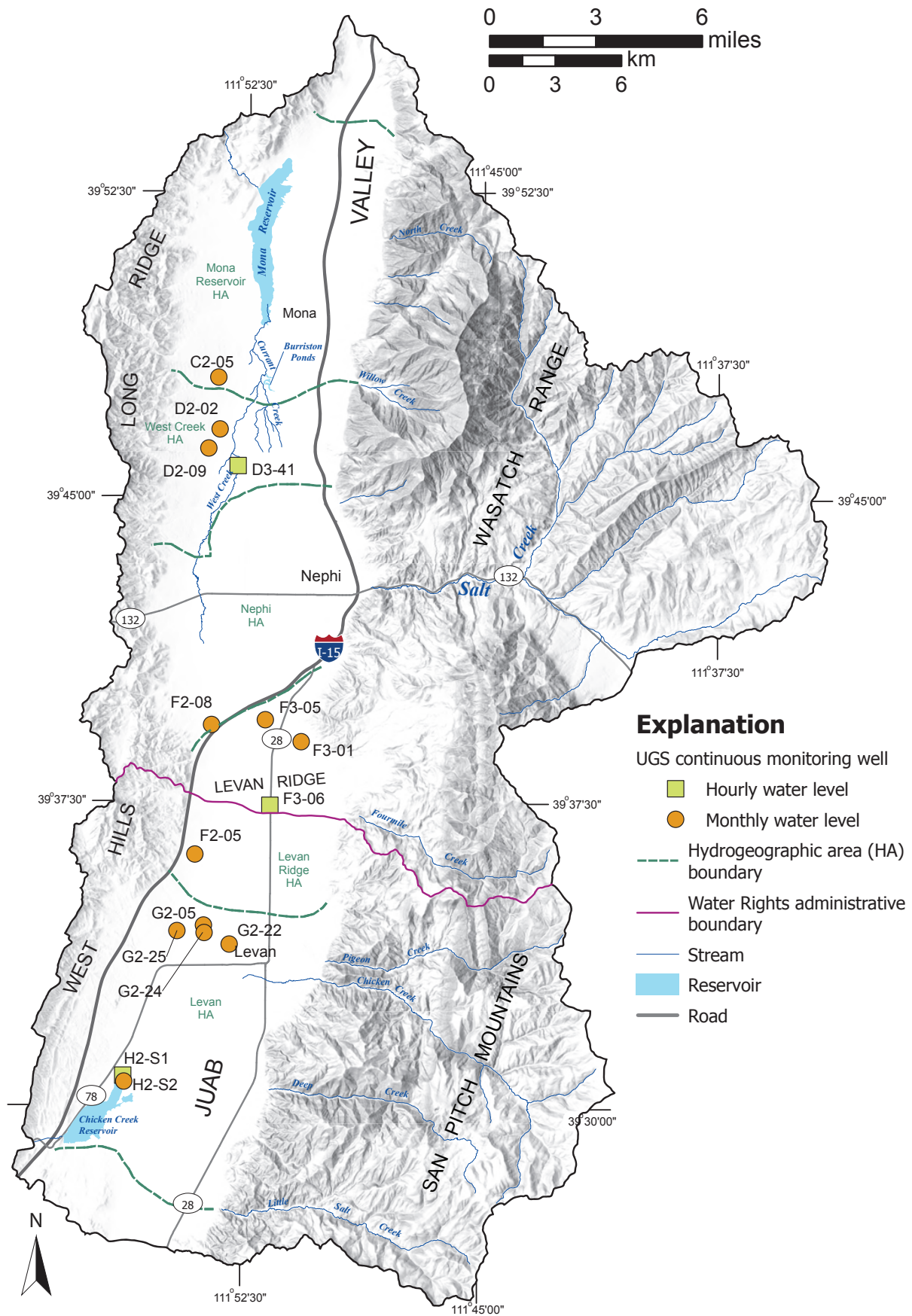


Figure 20. Wells monitored monthly and both monthly (manually) and continuously (by pressure transducers).

in mid-October 2018 (figure 22C). Measured flow from well H2-S1 ranged from 45 to 70 gallons per minute, and the combined flow from wells H2S2A and H2-S2B ranged from 2 to 27 gallons per minute (figure 22C). Water levels in these wells declined by as much as 21 ft during the 2018 pumping season (figure 21B).

Monthly groundwater levels in wells in the West Creek hydrogeographic area showed a variety of seasonal responses, from

slight in well C2-05 to dramatic in well D3-41 (figure 21C). Well D3-41 is about 50 ft from West Creek, which generally flows at that location from October or November through April or May. Water levels in D3-41 are likely closely tied to the stage of West Creek. During the 2017 pumping season, water levels in D3-41 declined by 11.5 ft. The greater decline during 2018 (21.7 ft) was likely due in part to periodic pumping for stock watering (none occurred during 2017). At least two more years of data from these wells are needed to assess long-term trends.

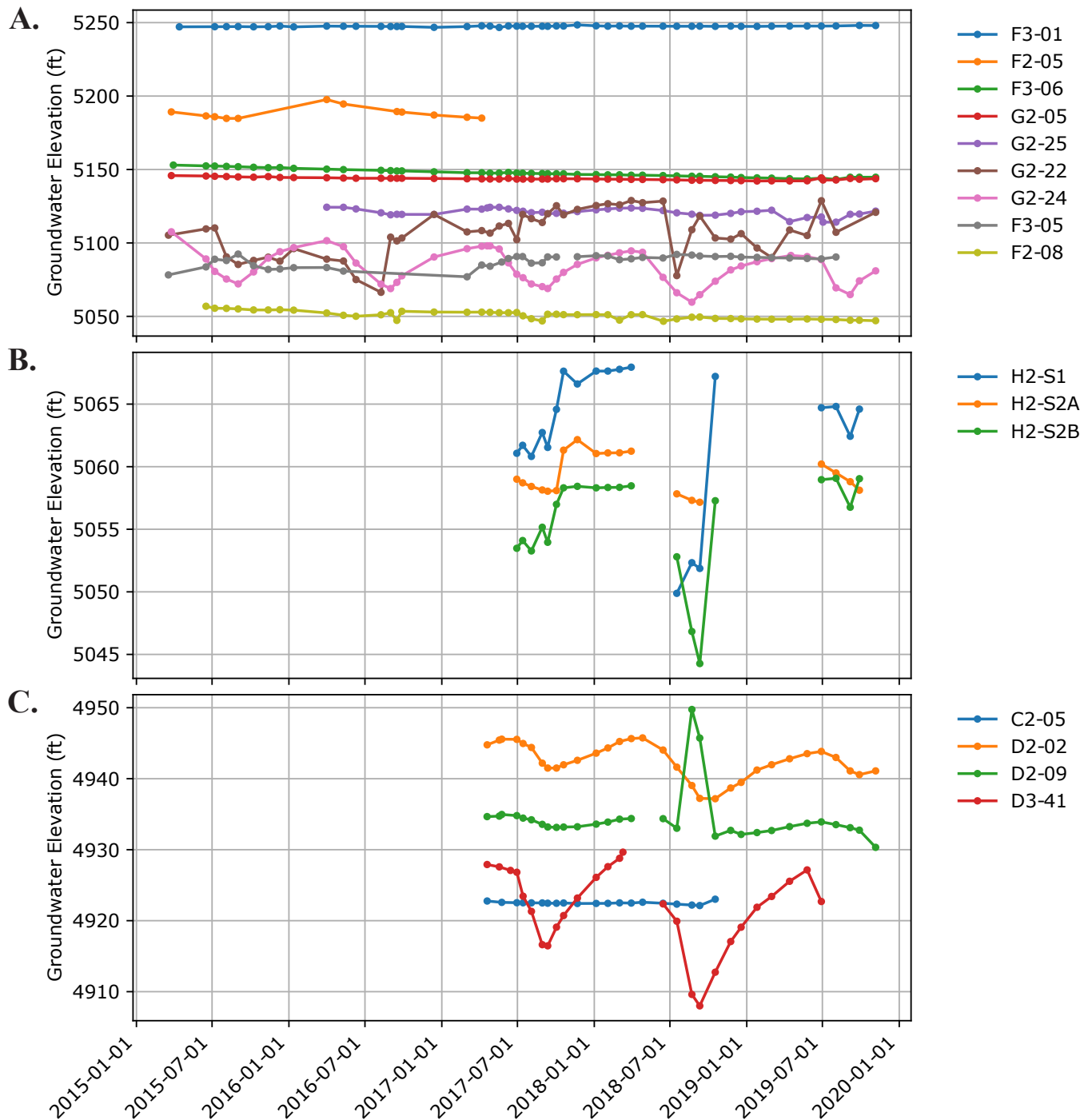


Figure 21. Hydrographs for wells monitored for depth to water by the UGS. Well locations shown on figure 20. Groundwater elevations for A) the Levan Ridge subbasin, B) northeast of Chicken Creek Reservoir, and C) the West Creek subbasin south of Mona.

**A.**



**B.**



**C.**

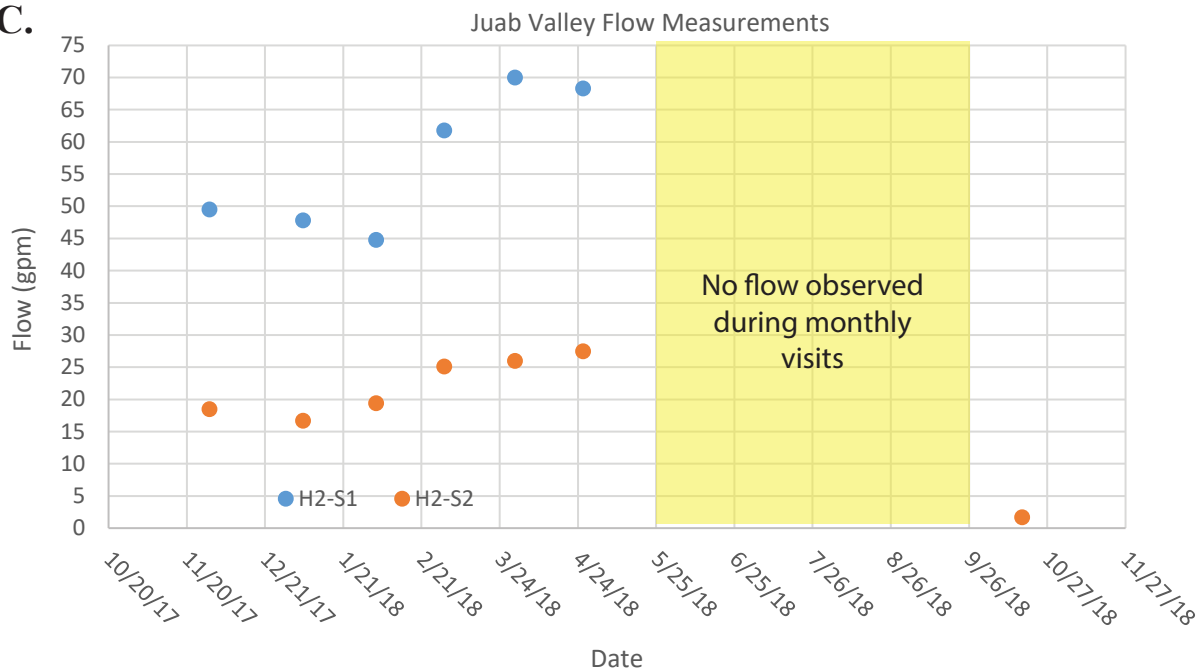


**Figure 22.** Seasonally flowing wells H2-S1 and H2-S2 northeast of Chicken Creek Reservoir in the southwest part of the Levan hydrogeographic area. **A)** Well H2-S1. Note the temporary weir plate to measure flow rate is in the channel to the right of the pin flag. **B)** Wells H2-S2A (left) and H2-S2B (right), which together comprise site H2-S2. The wells were not flowing at the time of the photograph (August of 2018). **C)** Flow records from H2-S1 and H2-S2.

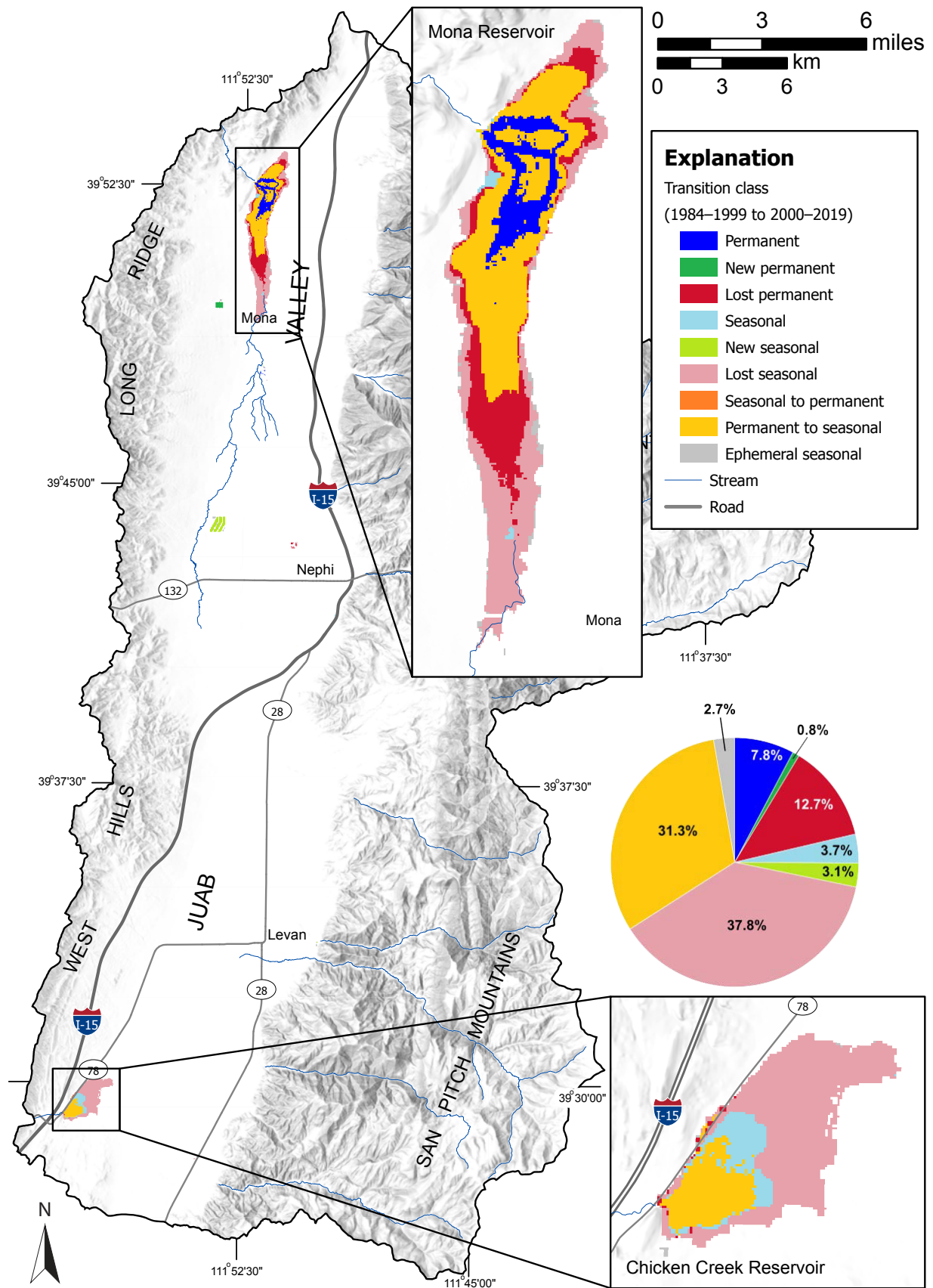


**Figure 23.** Change in surface-water classes from 1984–99 to 2000–19 based on Joint Research Centre European Commission (JRC) data. The surface classes represent the decadal transition of surface water conditions. Two-thirds of the surface-water areas either transitioned from seasonal inundation to dry (pink) or from full-year (permanent) inundation to seasonal inundation.

Data from pressure transducers in wells F3-06, H2-S1, and D3-41 are available from the UGS Groundwater Monitoring Data Portal (<https://apps.geology.utah.gov/gwdp/>). Water levels in well F3-06 in central Levan Ridge (figure 21) declined steadily from June 2015 to early June 2017, increased 0.7 ft during May 2017, and resumed steady decline thereafter at about the same rate as before the increase. The overall rate of decline was 2.2 ft per year during the period of record for the transducer. Well F3-06 is about 3.6 miles south of the southern end of the area of intensive irrigation pumping southwest of Nephi, and about 4.2 miles north of the area of intensive irrigation pumping west and southwest of Levan. Three other wells are present within 1.5 miles of F3-06; one (F2-04) is a domestic well and the other two (F2-02 and F3-02) support light-industrial operations but their use is significantly less than irrigation wells. The majority of drawdown in well F3-06 is likely due to pumping for irrigation, and the lack of seasonal drawdown/recovery fluctuations is likely due to its distance from the pumping.

Water levels in seasonally flowing well H2-S1 about 5 miles southwest of Levan (figure 21) show the influence of pumping for irrigation, and the effects of having the rectangle cut in the outer casing which allows the well to flow from fall through late spring. The nearest irrigation wells are about 1.2 miles to the northeast. The transducer was installed in July 2017, and water levels showed fluctuations related to pumping variations likely related to watering and cutting cycles, superposed on an overall decline of about 12 ft until late September 2017, when water levels began to recover after pumping ended. Water levels stabilized when the well flowed between mid-October 2017 and April 1, 2018, the first day of irrigation season. Water levels declined by as much as 21 ft during the 2018 irrigation season. By combining the detailed water-level records with flow measurements, we will be able to track long-term changes in this part of the Chicken Creek Reservoir discharge area.

Water levels in well D3-41 4.5 miles northwest of Nephi declined by about 11 ft from late June to mid-September 2017, then increased through November 2017 (figure 21). This well is in the southwestern part of the diffuse discharge area southwest of Burraston Ponds, and about 70 ft west of West Creek. The nearest irrigation wells are about 2 miles to the southeast. West Creek ceased flowing at about the same time water levels in D3-41 began to decline. We did not keep a detailed record of flow in West Creek, however, and the degree of hydraulic connection between the well and stream is not known. Declines in groundwater levels and flow both likely result from groundwater pumping to the south near Nephi. West Creek originates about 3.2 miles to the south-southwest on the valley floor, so all of its flow comes from groundwater seepage and, therefore, is likely to be affected by pumping.

### Transient Electromagnetic Survey

Figure 18B shows station locations and interpreted depths to conductive layers or zones in Juab Valley. The TEM data

typically define two discrete conductive layers within 400 ft of land surface. Figure 18B shows the depths below the land surface of the interpreted conductive layers at each station. Figures 18C and 18D show that the elevations of the interpreted conductors do not match groundwater levels at nearby wells. Groundwater in all but one of these wells (G2-05) is likely confined or semi-confined so that the water level is higher than the top of the saturated zone. The differences between water level and the highest conductive layer near well G2-05 is the lowest for the seven well-TEM station pairs. Figures 18C and 18D show that conductor elevations showed significant variation between seasons and years. Most, but not all, changes from March to June or July were negative, suggesting seasonal drawdown of a perched water table. The resistivity-depth models are used to interpret the time-conductivity data from the surveys, providing the estimated depth to conductive layers.

### Rates of Groundwater-Level Decline based on U.S. Geological Survey Data

Average rates of groundwater-level decline from 1999 (plus-or-minus about two years) to present are 0.1 to 1.0 ft per year (four estimates) in the Mona Reservoir hydrogeographic area; 1.0 to 2.1 ft per year (two estimates) in the West Creek hydrogeographic area; 1.0 to 2.5 ft per year (four estimates) in the Nephi hydrogeographic area; 2.0 ft per year (one estimate) in the Levan Ridge hydrogeographic area; and 0.3 to 4.5 ft per year (six estimates) in the Levan hydrogeographic area (figure 9B; table 2). These estimates are based on simple linear regression; uncertainties are substantial, and the exact rate depends on the year chosen as the older endpoint.

### Reduction in Size of Discharge Area, Southwestern Juab Valley

Based on comparison of observations during fieldwork in 2015 through 2018, aerial imagery, locations of now-dry springs shown on older topographic maps, and physical descriptions and spring-flow rates published by Thiros and others (1996), the size of the groundwater discharge area along with spring flows and shallow groundwater levels have declined substantially since 1993 (figure 19) in the southwestern part of the study area, when the majority of the data used for their study was collected.

Analysis of the JRC inundation change data indicates a significant shift to less inundation over time (figure 23). Most of the areas mapped focused on Mona and Chicken Creek Reservoirs. More than one-third of the areas mapped (figure 23) have transitioned from seasonally inundated to only periodically inundated. Another 31% has transitioned from permanently inundated to seasonally inundated, and 12% of the permanently inundated areas have transitioned to only periodically inundated areas.

Table 2. Summary of rates of change in groundwater levels from annual U.S. Geological Survey data, from simple linear regression.

UGS ID	USGS Name	USGS Number	1st Time Period				2nd Time Period				3rd Time Period				To (all)			
			From	Regression		Mann-Kendall p-value	From	Regression		Mann-Kendall p-value	From	Regression		Mann-Kendall p-value				
				Slope (ft/yr)	R <sup>2</sup>			Slope (ft/yr)	R <sup>2</sup>			Slope (ft/yr)	R <sup>2</sup>			Slope (ft/yr)	R <sup>2</sup>	
B3-47	(D-11-1)04bad-2	395328111495402	1984	0.36	0.78	0.36	0.000	1995	0.28	0.62	0.28	0.00	2011	0.49	0.34	0.49	0.25	2020
B3-23	(D-11-1)04cad-1	395259111405701	1984	0.55	0.36	0.82	0.001	1995	0.30	0.16	0.59	0.06	2011	-0.37	0.07	-1.49	0.30	2020
C3-60	(D-11-1)17cdd-1	393358111515001	-	-	-	-	-	-	-	-	-	-	-	-	-	-	-	1993
C3-41	(C-11-1)24ddd-1	395008111524101	1984	0.09	0.65	0.09	0.000	1995	0.07	0.43	0.08	0.00	2011	0.15	0.38	0.16	0.08	2020
C3-50	(D-11-1)30bda-1	394951111521101	1984	0.07	0.59	0.13	0.002	1995	0.09	0.56	0.24	0.05	2013	0.29	0.48	0.26	0.73	2017
C3-45	(D-11-1)33bde-1	394856111500401	-	-	-	-	-	1995	0.29	0.30	0.30	0.00	2011	0.29	0.07	0.50	0.35	2020
D2-08	(C-12-1)24baa-1	394545111531001	1984	0.70	0.80	0.75	0.000	1995	0.88	0.82	1.00	0.00	2011	1.49	0.86	1.83	0.02	2019
D3-72	(D-12-1)17cad-1	394605111504901	-	-	-	-	-	2014	-0.33	0.09	0.09	1.00	2014	-0.33	0.09	0.09	1.00	2020
D3-69	(D-12-1)19cde-1	394455111520701	1984	1.50	0.67	1.53	0.000	1995	1.89	0.64	1.88	0.00	2011	0.57	0.01	0.57	1.00	2013
D3-49	(D-12-1)30cad-1	394417111515501	1984	1.43	0.79	1.52	0.000	1995	1.84	0.82	1.99	0.00	2011	2.32	0.70	2.52	0.02	2020
E2-21	(C-13-1)1cdd-1	394215111530501	-	-	-	-	-	-	-	-	-	-	2014	4.35	0.86	4.65	0.30	2017
E2-28	(C-13-1)14caa-1	394048111541001	-	-	-	-	-	1995	0.22	0.74	0.24	0.00	2011	0.77	0.96	0.84	0.01	2017
E3-74	(D-13-1)076bd-2	394204111521901	1984	1.43	0.84	1.41	0.000	1995	1.65	0.81	1.62	0.00	2011	1.65	0.83	1.72	0.00	2020
E3-67	(D-13-1)07dad-3	394136111512001	1989	1.58	0.63	1.64	0.000	1995	2.37	0.82	2.54	0.00	2011	2.57	0.58	2.93	0.06	2020
E3-38	(D-13-1)18bbe-1	394112111522401	1984	1.72	0.84	1.87	0.000	1995	2.05	0.83	2.14	0.00	2011	2.44	0.61	2.73	0.06	2020
E2-14	(C-13-1)14ddb-2	394048111540901	-	-	-	-	-	-	-	-	-	-	2014	0.88	0.99	0.89	0.01	2020
E3-34	(D-13-1)17cda-1	394037111504901	-	-	-	-	-	1995	1.81	0.90	2.02	0.00	2011	2.78	0.95	2.88	0.00	2019
F3-06	(D-14-1)06ddb-1	393721111514501	1984	1.28	0.78	1.62	0.000	1995	1.79	0.97	1.89	0.00	2011	2.03	0.95	2.27	0.00	2020
G2-25	(C-14-1)27aaa-1	393418111543701	1984	0.53	0.74	0.53	0.000	1995	0.42	0.46	0.45	0.00	2011	0.94	0.55	1.07	0.04	2020
G2-22	(C-14-1)25bdd-1	393401111525501	1984	1.83	0.78	1.85	0.000	1995	1.52	0.67	1.53	0.00	2011	2.09	0.58	2.31	0.02	2020
G3-24	(D-14-1)31ada-1	393315111511601	-	-	-	-	-	-	-	-	-	-	2015	3.41	0.50	3.87	0.46	2020
G3-22	(D-14-1)31dab-1	393301111512501	1984	2.64	0.69	2.99	0.000	1995	2.32	0.56	2.70	0.00	2011	6.55	0.75	7.29	0.01	2017
H2-34	(C-15-1)04ddd-3	393146111554001	1992	0.52	0.94	2.10	0.009	-	-	-	-	-	2015	1.15	0.67	1.50	0.46	2020
H2-13	(C-15-1)16bbb-1	393017111560601	-	-	-	-	-	1993	0.21	0.94	2.01	1.00	-	-	-	-	-	2015
H2-16	(C-15-1)11baa-1	393141111535901	1985	1.28	0.66	1.50	0.000	1995	1.19	0.51	1.59	0.00	-	-	-	-	-	2012
H2-22	(C-15-1)15bcd-2	393023111552101	-	-	-	-	-	1993	-0.05	0.06	-0.19	1.00	2015	0.38	0.13	0.38	1.00	2017
H2-29	(C-15-1)10bdd-2	393122111550601	-	-	-	-	-	1995	0.82	0.78	0.89	0.00	2011	1.34	0.55	1.35	0.03	2016
H3-09	(C-15-1)24abb-1	392957111524101	1984	1.62	0.85	1.62	0.000	1995	1.52	0.80	1.59	0.00	2011	2.80	0.88	3.48	0.00	2020
H3-11	(C-15-1)12aba-1	393143111523301	1984	1.43	0.79	1.51	0.000	1995	1.34	0.79	1.49	0.00	2011	1.22	0.50	3.29	0.03	2020

## Change in Groundwater Storage

Based on storage changes calculated using the 1993 and 2015 potentiometric surface maps, groundwater storage change between 1993 and 2015 was on average 400 ac-ft/yr, with an estimated total loss of 7943 ac-ft. Note that the yearly deficit varies with water availability and water use, where there was less storage decline during years with higher-than-average precipitation. Water years with below average precipitation provide less recharge and require more pumping from storage, resulting in a higher water budget deficit than for a water year with higher-than-average precipitation. It is worth noting that despite higher-than-average precipitation occurring in the early 1980s, in 2011, and again in the 2019 water year, groundwater levels declined, and the volume of groundwater storage decreased. Water levels declined between 1965 and 1993, as well as between 1993 and 2015, and groundwater levels and groundwater storage declined more rapidly between 1993 and 2015 than between 1965 and 1993. See the discussion of groundwater level changes and rates of groundwater level decline for additional details describing these observed changes.

## Discussion

Excessive pumping in a groundwater basin can shift the groundwater divide relative to the surface water divide. In the case of Juab Valley, the surface water divide demarks the location of an administrative boundary for water rights. Groundwater managers need a clear understanding of the location of groundwater divides to best manage the groundwater resource relative to the surface water resources.

### Levan Ridge Groundwater Divide

Alternative 1 for the water-level contours and position of the groundwater divide (see figures 16 through 18) is preferred for three reasons. (1) In the first alternative, the saddle-shaped area of water-level contours that defines the groundwater divide is immediately west of the Fourmile Creek alluvial fan, where presumably more groundwater flows west through the alluvial fan into the valley center than from bedrock to the north and south, resulting in a local groundwater mound that flows either north or south. (2) The long-term groundwater-level decline observed in well F3-06 (see Groundwater-Level Changes from 1993 to 2015 section below) is a far-field effect of pumping in the Levan area, whereas pumping in the Nephi area may have less effect on Levan Ridge due to an east-west zone of low transmissivity south of Nephi, defined by steep hydraulic gradients and closely spaced water-level contours (note increased contour intervals on figure 17). (3) Pumping at wells F2-02 (a domestic well) and F2-04 (an industrial well) is not likely sufficient to produce the local cone of depression required by the second alternative.

## Groundwater-Level Changes

The pattern of groundwater-level declines (figure 19) includes five apparently anomalous points. The water level in well B4-08 in northern Juab Valley declined by nearly 77 ft, whereas declines in nearby wells were less than 5 ft. The anomalously large decline in well B4-08 may result from pumping before or during the water-level measurement, or localized low transmissivity. The water level in well E2-21 northwest of Nephi declined by nearly 52 ft, whereas declines in nearby wells ranged from 21 to 44 ft. Both water levels in E2-21 were measured by the USGS; therefore, we cannot explain the large difference between this and nearby wells. The water level in well G3-25 in north Levan increased by more than 30 ft and is the only water level in the study area that did not decline. In this well, condensation on the inside of the PVC standpipe may have affected the measurement which used a steel tape. The water level in well G2-22 west-northwest of Levan declined by nearly 46 ft using the UGS water-level measurement for 2015 but declined by only 14 ft using the USGS level measurement for March 2015. The change in water level based on the UGS measurement is more consistent with declines in nearby wells; however, we have no reason to doubt the USGS measurement. Figure 19 shows the water-level change based on the USGS measurements, but we cannot explain the anomalously low decline unless the well screen is silted in or located in a low-transmissivity part of the aquifer. In the southwestern part of the Levan hydrogeographic area, the water level in well H1-09 declined by about 58 ft and the water level in well H1-10 declined by about 90 ft. These declines are substantially greater than observed in wells just 1.5 to 2.5 miles to the northeast. Wells H1-09 and H1-10 are likely screened in Tertiary sedimentary rocks having low transmissivity, and/or their water levels had not recovered from pumping during the previous several days.

Continuous monitoring of groundwater levels in wells F3-06 (Levan Ridge, near the groundwater divide), H2-S1 (seasonally flowing well southwest of the Levan agricultural area), and D3-41 (West Creek hydrogeographic area southwest of Burrison Ponds) provide even greater detail on groundwater-level fluctuations and trends. Water levels in well F3-06 do not show seasonal drawdown and recovery cycles, but steady declines; nonetheless, these declines are likely related to groundwater pumping, and the seasonal fluctuations are damped by the distance from the pumping and the hydraulic diffusivity of the aquifer. Water levels in, and flow from, well H2-S1 respond strongly to groundwater pumping southwest of Levan, ranging from flow as great as 70 gallons per minute to water levels as much as 19 ft below the well's outlet. Water levels in D3-41, along with flow in nearby West Creek, responded to pumping in the Nephi area 2 to 4 miles to the southeast, showing as much as 11 ft of drawdown in the well and drying of the stream early in the irrigation season.

## GROUNDWATER CHEMISTRY

### Introduction

We collected water samples for groundwater chemistry analysis because it can indicate the quality of available water, as well as help us draw connections between streams, reservoirs, groundwater, and precipitation. We also measured carbon-14 and tritium in groundwater to determine the age and travel time of groundwater in the Juab Valley system. Groundwater chemistry helped us determine the conceptual groundwater system.

### Previous Work

Bjorklund (1967) and Thiros and others (1996) published major-solute, specific conductance, and total-dissolved-solids data for groundwater in Juab Valley. Thiros and others (1996) collected and analyzed samples for stable isotopes. Miller (2020) examined trends of nitrate, arsenic, and dissolved solids in groundwater in northern Juab Valley, and indicated water quality improvement since the 1970s.

### Methods

#### Sample Collection

We collected water samples for analyses of major-solute concentrations and stable isotope (i.e.,  $^2\text{H}$  and  $^{18}\text{O}$ ) compositions from 62 wells and 2 springs in 2015, and from 4 wells, 4 springs, and 12 streams in 2017 (figure 24; table A5). We sampled 15 wells and 1 spring for tritium ( $^3\text{H}$ ) and  $^{14}\text{C}$  (table 3). In 2018 and 2019, we collected stable isotope samples of precipitation, snowpack, soil water, streams, springs, flowing wells, and Mona Reservoir (figure 24; table A5).

Precipitation samples were collected approximately monthly at three sites, chosen to represent a range of elevation within the basin, and within and just outside of Juab Valley (figure 24) for a total of 28 samples. Precipitation samplers consisted of a 2.5-gallon HDPE carboy, containing approximately 16 ounces of mineral oil to prevent evaporation, connected to a funnel, and sitting in a 30-gallon garbage can with the lid inverted to aid in the collection of rain and snow (modified from those described by Ingraham and Taylor, 1991; Scholl and others, 1996). Snowpack, when present, was also collected at two of the three precipitation sites, for a total of nine samples. Precipitation and snow sample collection began September 2018 and ended November 2019.

We installed two modified passive capillary samplers (PCAPS) to collect infiltrated snowmelt in the Wasatch Range (figure 24). The PCAPS used a design specified by Frisbee and others (2010). We dug soil pits and inserted fiberglass wicks coiled into a “fiddlehead” shape into the soil pit wall at two different depths. The other end of the wicks was pulled through

vinyl tubing connected to carboys containing approximately 16 ounces of mineral oil to prevent evaporation, with each wick going to its own carboy. The carboys were kept in coolers buried in the soil pits. We deployed the PCAPS in the fall of 2018, prior to the first snowfall, and left the samplers alone until retrieving them after the final snowmelt in the spring of 2019. Overall, each carboy contained about 1 liter of water.

We collected stream samples from 44 sites in the Juab Valley catchment, including Currant Creek, North Creek, Bear Creek, West Creek, Fourmile Creek, Willow Creek, Salt Creek, Pigeon Creek, Chicken Creek, Deep Creek, and Little Salt Creek. Most sampling occurred in September and November 2018, and April 2019. We sampled Mona Reservoir at five sites within the reservoir and immediately downstream in Currant Creek (figure 24), for a total of 19 samples between July 2018 and November 2019. We sampled 65 wells, 8 of which were flowing, and 5 springs from 2018 to 2019. Wells that were not actively being pumped or flowing were purged for 15 to 30 minutes depending on well diameter, and history of recent use if known. Spring samples were collected at the closest possible outflow point to the source, and stream samples were collected from clear flowing water (i.e., not from eddies or stagnant pools).

Samples for major-ion-concentration analyses were collected in clean bottles supplied by the laboratory; those for general chemistry were not filtered, and those for metals were filtered using a peristaltic pump and 0.45  $\mu\text{m}$  filters. Samples for stable isotope composition analyses were filtered using 0.45  $\mu\text{m}$  disc filters attached to a syringe, into 10 mL snap-cap vials leaving no head space. Samples for radiogenic isotope analyses were collected in 0.5 L or 1 L amber plastic bottles, rinsed for several volumes by the flowing sample water and sealed with no head space. Samples for major solute concentrations were submitted to the Utah Public Health Laboratory; samples for  $^2\text{H}$  and  $^{18}\text{O}$  compositions were submitted to the University of Utah Department of Geology and Geophysics Stable Isotope Ratio Facility for Environmental Research (SIRFER) laboratory; samples for tritium analyses were submitted to the University of Utah Department of Geology and Geophysics Dissolved and Noble Gas Laboratory; and samples for  $^{14}\text{C}$  analyses were submitted to the Brigham Young University Department of Geology for preparation and submitted to the University of Georgia AMS facility for analysis.

#### Bayesian Mixing Model

Bayesian mixing models create probability density functions of the mixing ratios of sources contributing to mixture, giving the probable percent contribution of each source. We used scripts modified from HydroMix (Beria and others, 2020) to conduct a mixing model between snow and rainwater samples. We ran HydroMix for 20,000 iterations. For the end members of the mixing analysis, we used isotope values from snow, rain, and soil water samples. We estimated the contributing percentages of snow and rain to groundwater and Currant Creek samples.

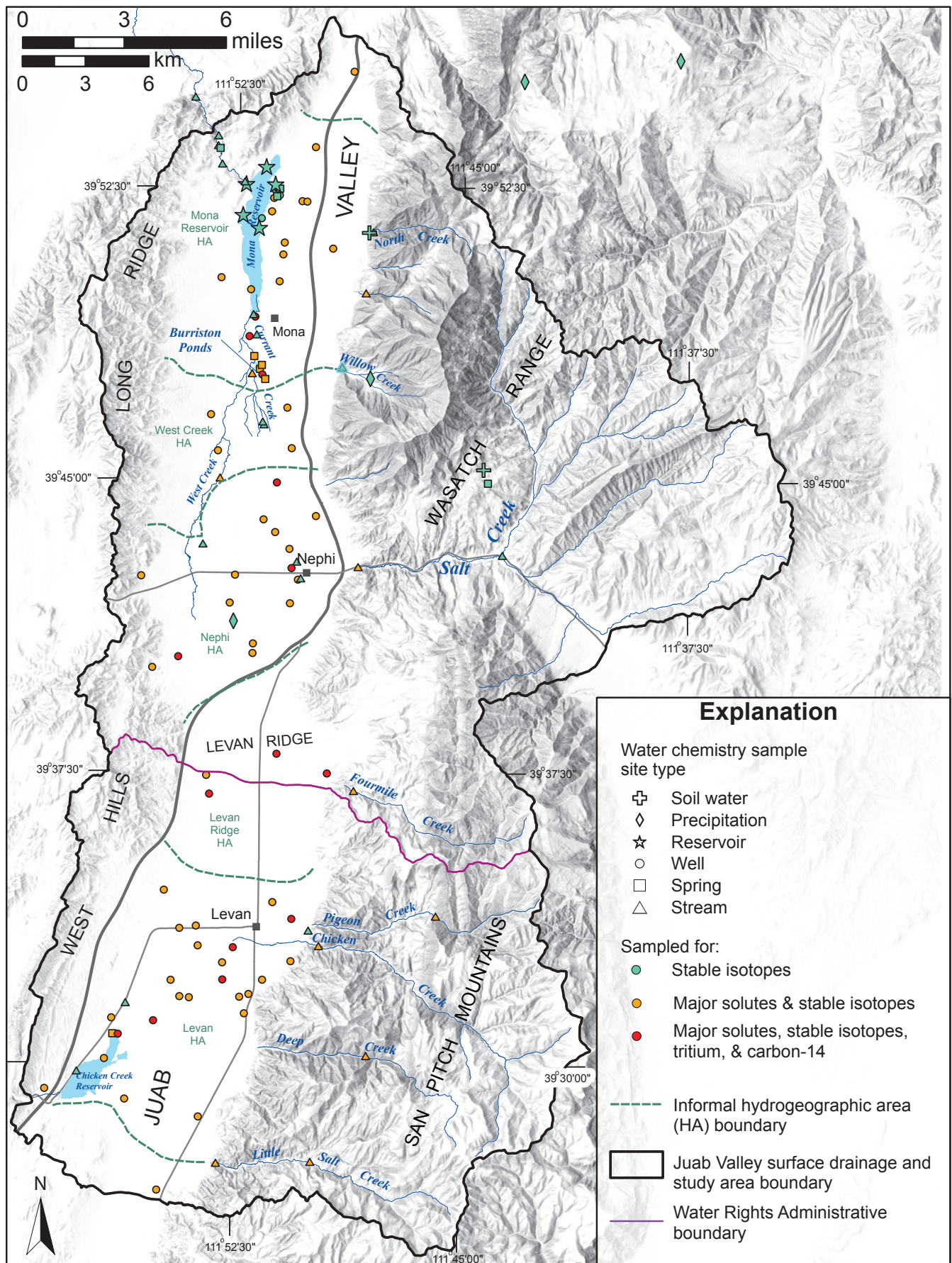


Figure 24. Location and site type of Juab Valley water chemistry samples.

**Table 3.** Analytical and modeling results for radiogenic isotopes.

Well ID <sup>a</sup>	<sup>3</sup> H (TU) <sup>b</sup>	A (pmC) <sup>c</sup>	d <sup>13</sup> C	A <sub>0</sub> <sup>d</sup>	<sup>14</sup> C Age (yr) <sup>e</sup>	LPM <sup>f</sup> Age (yr)
B3-17	0.1	41.36	-7.89	36.9	modern	-
C3-19	1.14	36.37	-8.2	38.3	modern	-
C3-28	0.2	34.22	-9.50	41.8	2200 ± 1300	-
D3-43	2.4	56.26	-9.67	44.8	modern	-
D3-58	4.0	94.17	-13.60	84.7	modern	-
D3-80	5.6	57.99	-9.00	39.7	modern	-
E2-27	0.2	21.49	-10.30	45.1	6500 ± 700	-
E3-09	4.0	100.46	-14.00	60.5	modern	-
F2-02	0.6	7.44	-9.70	42.6	15,000 ± 700	-
F3-02	0.6	41.83	-10.70	46.7	1200 ± 300	-
F4-02	1.0	38.86	-10.10	44.5	1800 ± 800	-
<b>G3-06</b>	3.7	42.33	-8.50	37.7	modern	181
<b>G3-14</b>	4.5	48.84	-10.90	47.7	modern	108
<b>H2-25</b>	2.0	53.71	-9.40	41.7	modern	210
<b>H2-S1</b>	0.2	10.13	-6.60	29.7	10,400 ± 1800	17,700
<b>H3-07</b>	3.4	57.57	-9.50	41.8	modern	202

a Well identification numbers in boldface are included in the southern traverse model (figures 36 and 37) using the Lumped Parameter technique.

b TU is Tritium Units.

c A is measured percent modern carbon of sample.

d A<sub>0</sub> is percent modern carbon at time of recharge to groundwater table.

e Age derived from Fontes and Garnier model (Fontes and Garnier, 1979).

f Lumped parameter modeling

- Model not calculated.

## Results and Discussion

### Temperature

Groundwater temperature, measured using a multiparameter meter during sampling, varied from 9° to 24°C (figure 25). Groundwater temperatures are overall cooler in the eastern and central parts of the Nephi and Mona Reservoir hydrogeographic areas; however, the warmest measured temperatures in the study area occurred in the west to central parts (figure 25). The mean groundwater temperature was 13.4°C and the median groundwater temperature was 13.1°C (figure 25).

### Major Solute Chemistry and Total Dissolved Solids

**Mona Reservoir Hydrogeographic Area (HA):** Groundwater composition in the Mona Reservoir hydrogeographic area is mainly magnesium-bicarbonate type, and compositionally trends toward increasing sodium and chloride (figure 26). Calcium is the predominant cation in the northern half of the hydrogeographic area and sodium is the predominant cation in the southern half (figure 27). Bicarbonate is the predominant anion throughout, though some samples have significant sulfate (figure 27). Total-dissolved-solids (TDS) concentrations range from 232 to 786 mg/L, and values are greater in the southern part than in the northern part (figure 28). The samples having greater proportions of sodium have the higher TDS

values. Surface water has proportionately less sodium and chloride than groundwater (figure 26), bicarbonate is the predominant anion (figure 27), and TDS concentrations are lower (figure 28).

**West Creek HA:** Groundwater composition in the West Creek hydrogeographic area is mixed SO<sub>4</sub>, Cl, Ca, Mg type (figure 26). Cations of sodium and magnesium occur in roughly equal abundance, as do anions of chloride, bicarbonate, and sulfate. TDS concentrations range from 540 to 1204 mg/L (figure 28). Surface-water flow in West Creek is seasonal. One surface-water sample collected from West Creek in April 2017 (D2-11) has generally similar composition to groundwater samples collected in 2015 and 2017.

**Nephi HA:** Groundwater composition in the Nephi hydrogeographic area is mainly magnesium-bicarbonate type, and compositionally trends toward increasing sodium and chloride (figure 26). Calcium and sodium occur in roughly equal proportions (figure 27). Bicarbonate is the predominant anion in the eastern part of the hydrogeographic area, whereas chloride is the predominant anion in the western part (figure 27). TDS concentrations range from 408 to 1230 mg/L and are overall greater than in the Mona Reservoir hydrogeographic area (figure 28). Surface water has sodium and chloride proportions in the middle of the range observed for groundwater (figure 26), bicarbonate is the dominant anion, and TDS concentrations are lower than for groundwater (figure 28).

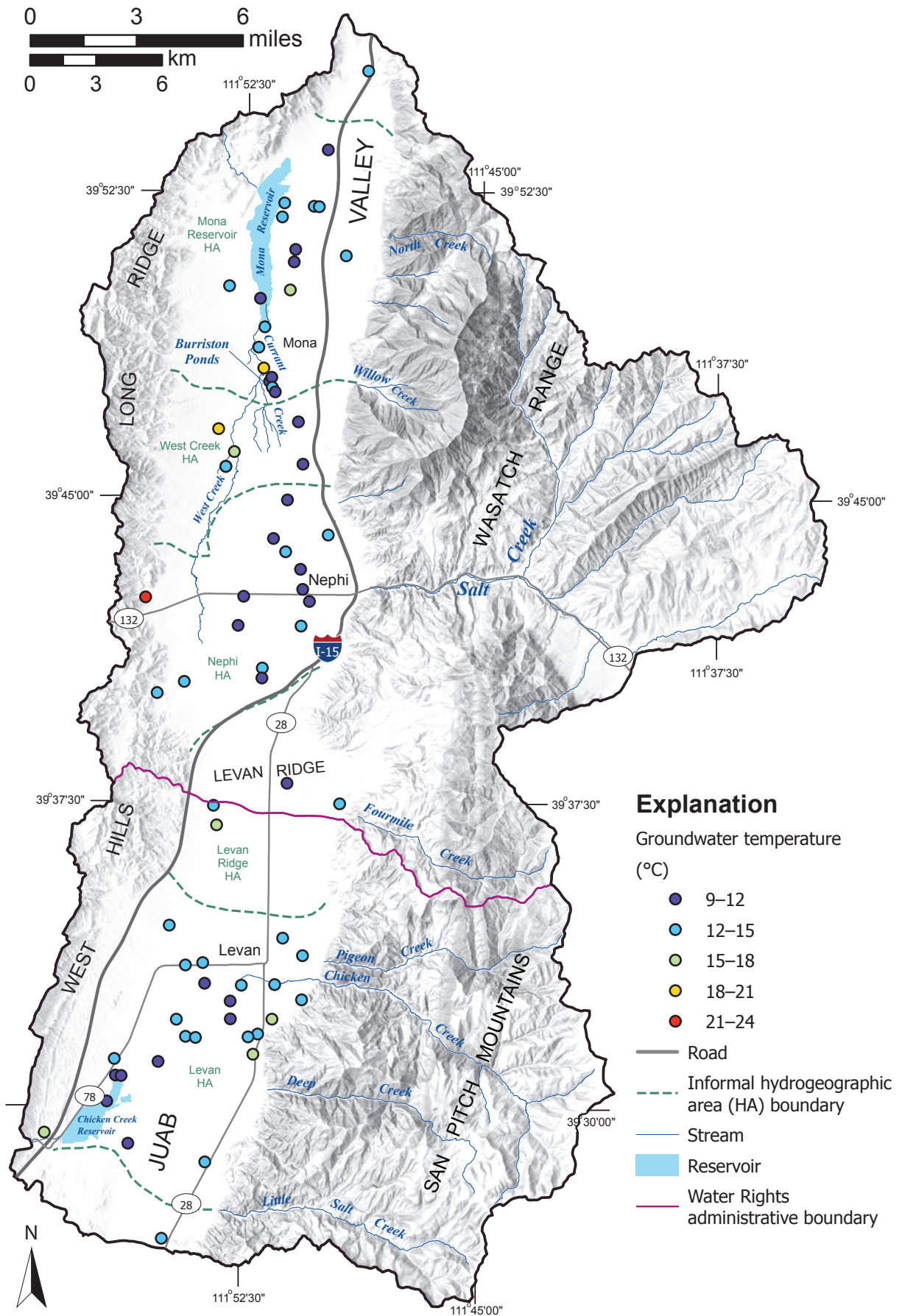


Figure 25. Groundwater temperatures measured during chemical sampling in 2015 and 2017. See table A5 for data.

## Hydrochemical Facies

### Diamond Plot

- Calcium chloride
- Mixed  $\text{SO}_4$ , Cl, Ca, Mg
- Magnesium bicarbonate
- Sodium chloride
- Mixed  $\text{HCO}_3$ ,  $\text{CO}_3$ , Na, K
- Sodium bicarbonate

### Anion Plot

- Bicarbonate
- Sulfate
- Chloride
- Mixed

### Cation Plot

- Calcium
- Magnesium
- Sodium & potassium
- Mixed

## Hydrogeographic Area & Site Type

- Mona Reservoir - groundwater
- ▲ Mona Reservoir - stream
- West Creek - groundwater
- ▲ West Creek - stream
- Nephi - groundwater
- ▲ Nephi - stream
- Levan Ridge - groundwater
- ▲ Levan Ridge - stream
- Levan - groundwater
- ▲ Levan - stream

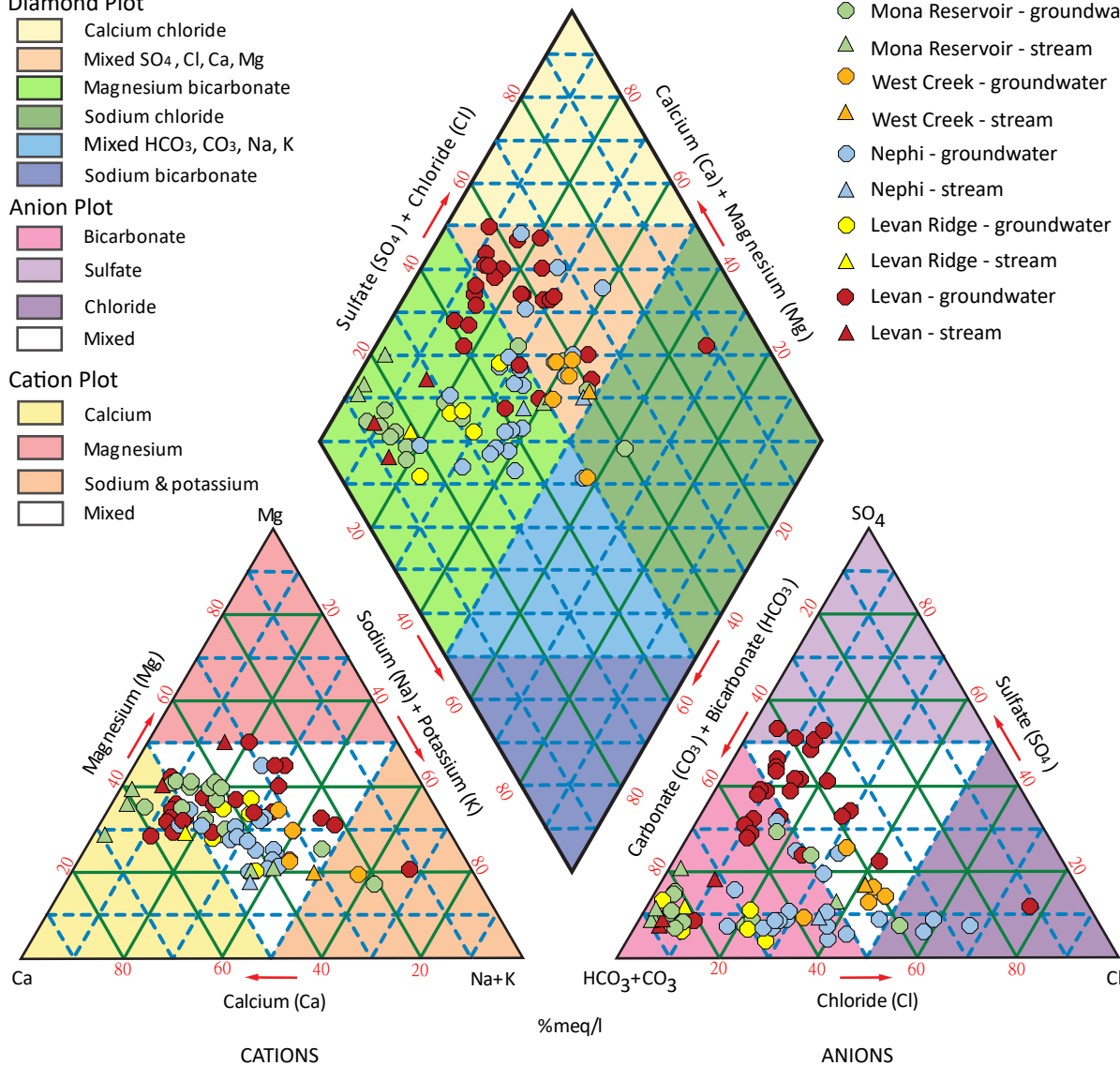


**Figure 26.** Piper diagram for groundwater and surface water samples collected in 2015 and 2017, categorized by hydrogeographic area and site type. See table A5 for data.

**Levan Ridge HA:** Groundwater composition in the Levan Ridge hydrogeographic area is like that in the Mona Reservoir and Nephi hydrogeographic areas: mainly magnesium-bicarbonate type, compositional trends are toward increasing sodium and chloride, and calcium is the predominant cation. Bicarbonate is the predominant anion in the eastern part of the Levan Ridge hydrogeographic area, whereas chloride is the predominant anion in the western part (figure 27). TDS concentrations range from 340 to 472 mg/L, lower than the Mona Reservoir, West Creek, and Nephi hydrogeographic areas (figure 28). Compared to groundwater, surface water (one sample) has lower sodium and chloride (figure 26), bicarbonate is the predominant anion (figure 27), and TDS is lower (figure 28).

**Levan HA:** Groundwater composition in the Levan hydrogeographic area is notably different from that in the other four hydrogeographic areas. Groundwater is mainly mixed calcium- and magnesium-bicarbonate type, with a wider range of proportions. Compositional trends are toward increasing sodium and sulfate. Calcium is the predominant cation in the northeastern part of the hydrogeographic area, whereas sodium is more prevalent in the southwestern part. Sulfate is the predominant anion (figure 27). TDS concentrations range from 500 to 2626 mg/L (figure 28). Compared to groundwater, surface water has significantly lower sodium and chloride (figure 26), bicarbonate is the predominant anion (figure 27), and TDS is substantially lower (figure 28). The preceding description disregards sample G2-15, an industrial supply well for a coal-loading facility that has substantially different composition and greater TDS than all other samples analyzed for this study.

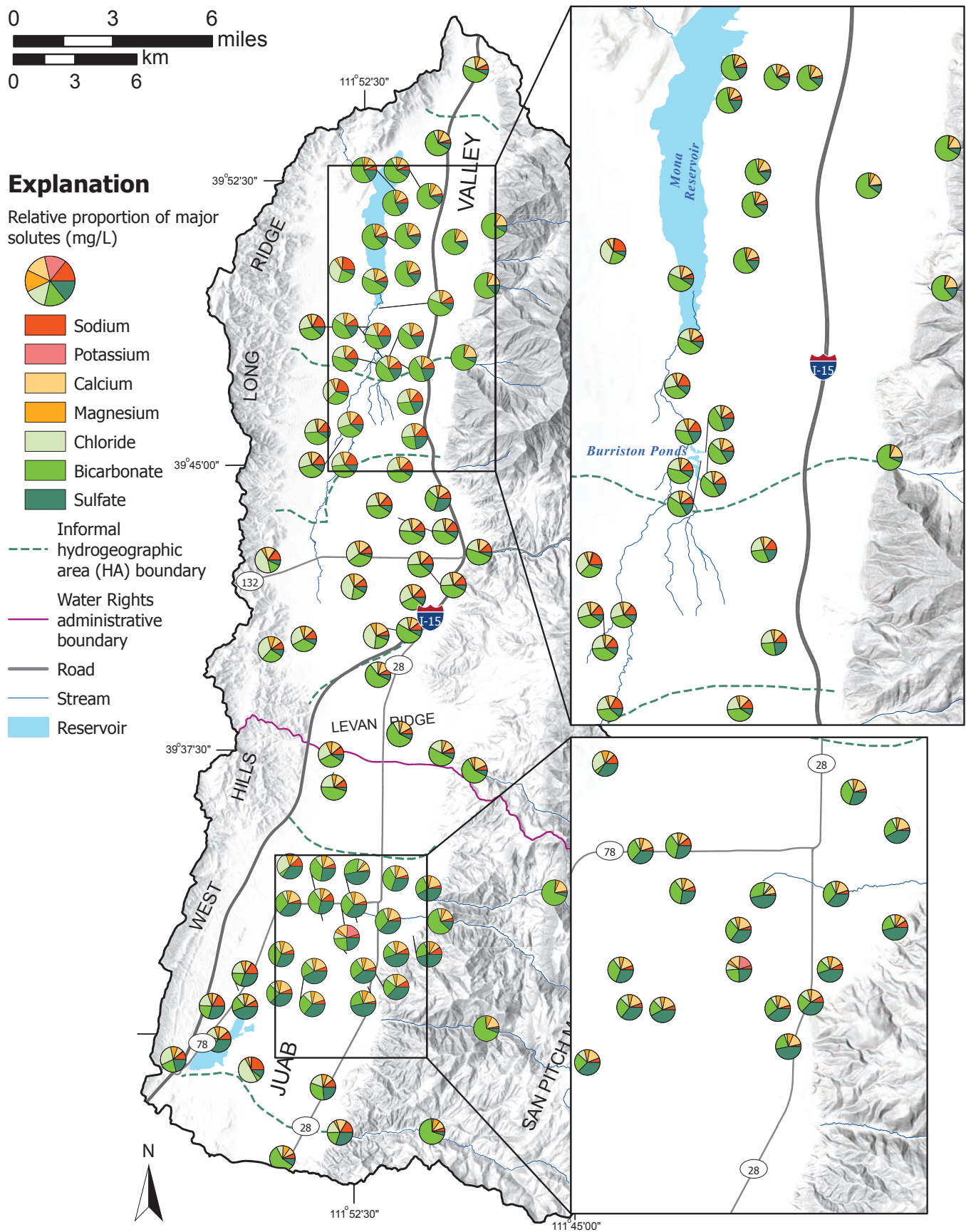


**Figure 27.** Pie map showing relative concentrations of major solutes of groundwater and surface water samples collected in 2015 and 2017. See table A5 for analysis results.

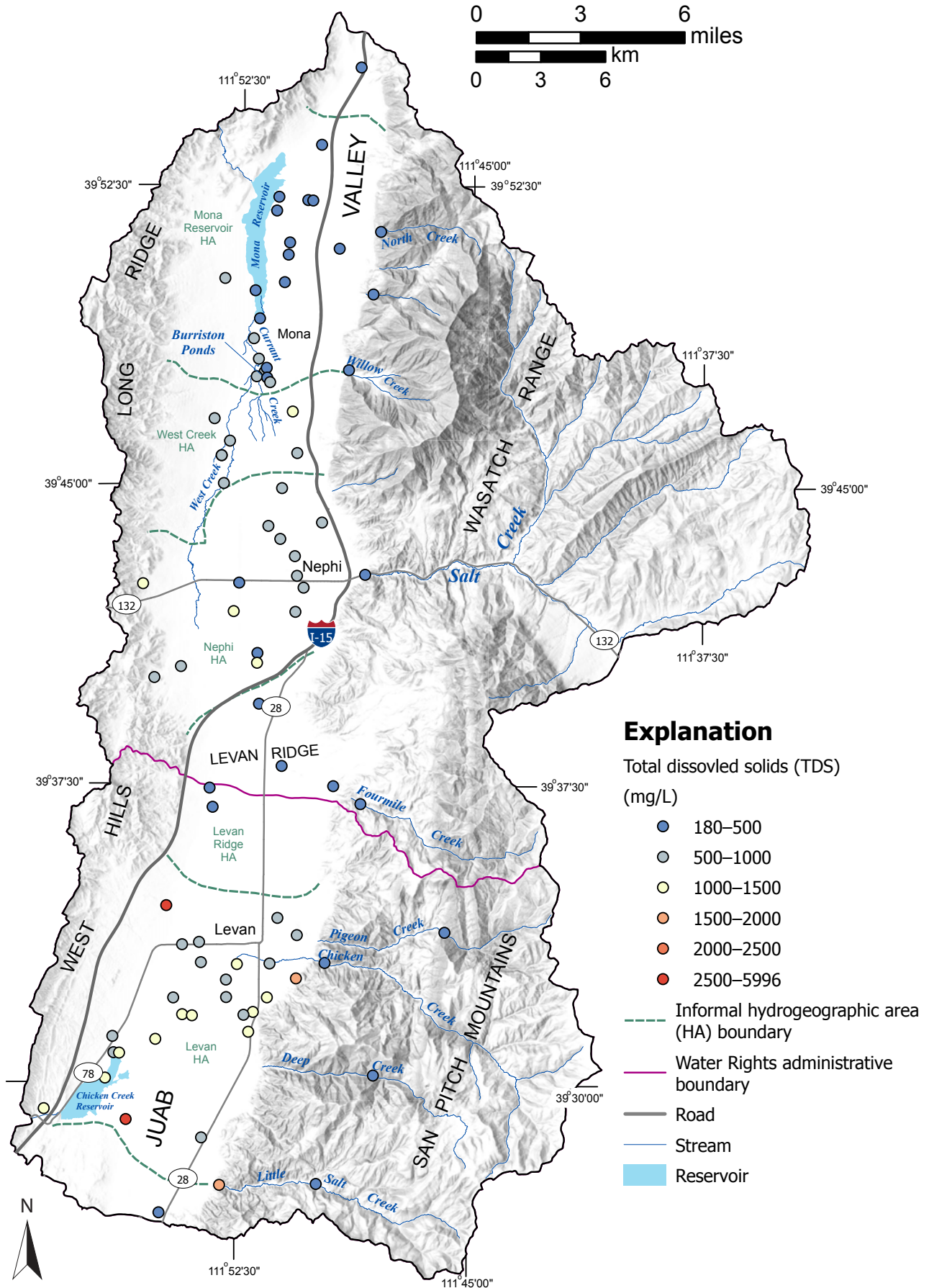


Figure 28. TDS concentrations of groundwater and surface water samples collected in 2015 and 2017.

**Statistical evaluation:** Statistical analysis of the major solute data from groundwater and surface-water samples followed methods outlined by Guler and Thyne (2006) and Kirby (2012), using software packages in R (Anglim, 2009; Quick, 2012; Kodali, 2016). This approach quantifies chemical variations in groundwater and surface water without the bias of pre-determined geographic or other delineations and establishes a data set for process-based analyses in the continuation of this project.

Principal component analysis identified three statistically significant factors that together account for 69% of the observed variance in the solute data (table 4). Factor 1 is predominantly sulfate, magnesium, and calcium; factor 2 is predominantly sodium and chloride; and factor 3 is bicarbonate, carbonate, and calcium (table 4). These factors describe the primary compositional differences among our groundwater samples from Juab Valley and surface-water samples from the Wasatch Range and the San Pitch Mountains.

Cluster analysis identified five statistically distinct compositional groups (table 5; figures 29 and 30). Clusters 1, 2, 3, and 5 are magnesium-bicarbonate type water, and cluster 4 is mixed magnesium-calcium-sulfate-bicarbonate type water (figure 29C). Cluster 2 has distinctly the lowest concentrations of sodium, chloride, and sulfate, whereas clusters 1, 3, and 5 differ primarily by their sodium concentrations, and cluster 4 has a distinctly higher sulfate concentration. Cluster 2 has the distinctly lowest mean TDS concentration, whereas cluster 4 has the highest.

Cluster 1 composition water has the widest geographic distribution and occurs in all five hydrogeographic areas, predominantly but not exclusively in the western part of the valley (figure 30). Cluster 2 composition water occurs exclusively in the northeastern part of the Mona Reservoir hydrogeographic area and in surface water. Cluster 3 composition water occurs in the southern half of the Mona Reservoir

**Table 4.** Results of principal component analysis of Juab Valley major-solute data.

Solute	Factor 1	Factor 2	Factor 3
Sodium	0.26	0.90	-
Potassium	-	-	-
Calcium	0.73	0.18	0.30
Magnesium	0.80	0.35	0.12
Chloride	0.10	0.99	-
Bicarbonate	0.13	-	0.99
Carbonate	0.31	-	0.35
Sulfate	0.99	-	-
Sum of Squares Loadings	2.36	1.95	1.22
Proportion of Variance	0.30	0.24	0.15
Cumulative Variance	0.30	0.54	0.69

hydrogeographic area and the central West Creek hydrogeographic area, and in two surface-water samples in the Levan hydrogeographic area (Little Salt Creek and Pigeon Creek). Cluster 4 composition water occurs in the southeastern part of the Mona Reservoir hydrogeographic area, the eastern part of the West Creek and Nephi hydrogeographic areas, and throughout the Levan hydrogeographic area. Cluster 5 composition water occurs exclusively in the eastern part of the Nephi hydrogeographic area.

Statistical analysis of major-solute data identifies five distinct clusters, or composition types (figure 30). Cluster 2 has distinctly lower Mg-Ca-SO<sub>4</sub> content; clusters 2, 3, and 5 are Mg-HCO<sub>3</sub> type and have comparatively greater Na, Ca, and SO<sub>4</sub> content; and cluster 4 is mixed Mg-Ca-HCO<sub>3</sub>-SO<sub>4</sub> type. Cluster 2 composition water occurs mainly in the northeastern part of the valley and in mountain streams and reflects chemical interaction with Paleozoic carbonate rocks and Mesozoic siliciclastic rocks. Cluster 2, 3, and 5 composition water occurs in the central part of the valley and reflects chemical interaction with Paleozoic carbonate and Arapien Formation bedrock and sediment in varying proportions. Cluster 4 composition water occurs mainly in the southeastern part of the valley and reflects comparatively more dissolution of gypsum from the Arapien Formation and its sediments.

The numbers of samples in each cluster reflect sampling bias and do not necessarily represent the relative proportions of volume or area of the different cluster compositions. Surface water is almost exclusively cluster 2 composition. Surface water samples having cluster 3 or 4 composition are downstream of active gypsum mines.

The compositions and spatial variations of major-solute concentrations in groundwater and surface water in Juab Valley reflect the dominant sedimentary-rock composition in the mountains bounding the east side of the valley and the corresponding mineralogic composition of detritus in the basin-fill sediments. Bedrock in the mountains immediately east of Juab Valley and the basin-fill sediment in the adjacent part of the valley is (a) predominantly limestone in the northeastern quarter of the study area, (b) a mixture of limestone, siliciclastic sedimentary rocks, and the Arapien Formation in the central quarter, and (c) predominantly Arapien Formation in the southeastern half of the study area. Magnesium-bicarbonate-type water in the northern part of the Mona Reservoir hydrogeographic area reflects chemical interaction of groundwater with limestone and dolomite in the Wasatch Range and basin-fill sediments derived from them. Major-solute compositions in the southern part of the Mona Reservoir hydrogeographic area and in the West Creek, Nephi, and Levan Ridge hydrogeographic areas represent chemical interaction of groundwater with a mixture of limestone, dolomite, gypsum, and halite (the latter two derived from the Arapien Formation). Major-solute compositions in the Levan hydrogeographic area represent chemical interaction of groundwater with gypsum and halite. Variations in groundwater composition observed on the Piper diagrams within individual

hydrogeographic areas and in the data as a whole (figures 26 and 29C, respectively) illustrate these trends. Thiros and others (1996) confirmed these basic conclusions using mineral-equilibrium modeling of groundwater compositions.

Statistical analysis of major-solute compositions provides additional confirmation of the basic conclusions above. The three factors derived from principal component analysis have the dominant compositions (1) Ca, Mg and SO<sub>4</sub>, reflecting dissolution into groundwater of gypsum from Arapien Formation bedrock and/or detritus in the basin fill derived from it; (2) Na and Cl, reflecting dissolution into groundwater of halite from Arapien Formation bedrock and/or detritus; and (3) HCO<sub>3</sub>, CO<sub>3</sub>, and Ca, reflecting dissolution into groundwater of calcite and dolomite in Paleozoic limestone bedrock and/or detritus.

The mean solute concentrations and spatial variations of mean cluster compositions reflect the north-to-south variations in bedrock and adjacent basin fill in the ranges bounding Juab Valley to the east, as described above. Mean TDS concentrations of the clusters are correlated with mean Na and Cl and/or SO<sub>4</sub> concentrations, reflecting progressively changing composition due to mineral dissolution during groundwater recharge and flow.

## Stable Isotopes

Stable-isotope compositions are expressed as  $\delta^2\text{H}$  and  $\delta^{18}\text{O}$  in per-mil units (‰), which represents the difference between the sample and globally accepted standard compositions. Stable-isotope compositions of groundwater and surface-water samples collected in 2015 and 2017 (table A5) generally vary from less negative (more enriched in the heavier isotopes, i.e., containing a relatively greater proportion of water molecules having the <sup>2</sup>H and <sup>18</sup>O isotopes) in the east to more negative (more depleted, i.e., containing a relatively lower proportion of water molecules having the <sup>2</sup>H and <sup>18</sup>O isotopes) in the west (figure 31). Several variations cause the trend to deviate toward the west or east. For example, samples from the Burrison Ponds and an adjacent well, and from northeast of Nephi are more enriched than samples from areas to the north and south, whereas surface and groundwater samples from the central part of the San Pitch Mountains are more depleted than samples from areas to the north and south. Several other localized complications in the trend exist but the overall pattern shows westward-decreasing  $\delta^2\text{H}$  and  $\delta^{18}\text{O}$  values.

Stan Smith of the UGS analyzed the groundwater samples collected in 2015. The compositional ranges of the 2015 samples for  $\delta^2\text{H}$  and  $\delta^{18}\text{O}$  are -131.0 to -112.8‰ and -17.2 to -14.2‰,

**Table 5.** Results of cluster analysis.

Cluster	N	Wells	Springs	Streams	TDS (mg/L)		Average of Std Devs
					Mean	Dev (%)	
1	24	23	1	0	672	74	1.78
2	14	7	0	7	264	16	2.56
3	11	5	2	4	560	26	1.55
4	28	26	1	1	1030	25	1.92
5	6	6	0	0	852	6	1.09

### Cations (mg/L)

Cluster	Sodium			Potassium			Calcium			Magnesium		
	Mean	Median	Std Dev	Mean	Median	Std Dev	Mean	Median	Std Dev	Mean	Median	Std Dev
1	65.01	55.42	2.23	4.05	4.22	1.87	70.49	64.72	1.42	38.08	32.30	1.54
2	9.90	11.02	2.19	0.85	1.28	3.29	53.56	54.33	1.23	23.82	23.10	1.33
3	70.55	95.58	1.78	2.08	1.88	1.59	71.65	74.44	1.15	27.96	28.22	1.34
4	75.94	78.26	1.81	3.55	2.76	2.63	143.46	148.41	1.32	63.59	62.49	1.38
5	129.67	131.63	1.04	4.28	3.97	1.13	127.74	134.96	1.15	38.03	38.28	1.04

### Anions (mg/L)

Cluster	Chloride			Bicarbonate			Carbonate			Sulfate		
	Mean	Median	Std Dev	Mean	Median	Std Dev	Mean	Median	Std Dev	Mean	Median	Std Dev
1	130.43	135.64	2.65	217.93	207.47	1.25	106.43	101.49	1.25	58.02	49.40	2.03
2	8.44	9.25	1.75	239.33	238.65	1.21	17.59	36.42	7.98	35.67	37.15	1.46
3	95.32	125.21	1.92	272.90	273.14	1.12	1.22	1.00	1.95	71.33	75.19	1.57
4	109.75	111.61	1.78	299.29	288.59	1.19	101.02	141.17	3.71	342.43	363.22	1.56
5	209.21	203.36	1.08	415.72	417.80	1.04	205.07	206.44	1.04	86.34	86.06	1.19



### C. Hydrochemical Facies

#### Diamond Plot

- Calcium chloride
- Mixed SO<sub>4</sub>, Cl, Ca, Mg
- Magnesium bicarbonate
- Sodium chloride
- Mixed HCO<sub>3</sub>, CO<sub>3</sub>, Na, K
- Sodium bicarbonate

#### Anion Plot

- Bicarbonate
- Sulfate
- Chloride
- Mixed

#### Cation Plot

- Calcium
- Magnesium
- Sodium & potassium
- Mixed

#### Statistical Cluster

- 1
- 2
- 3
- 4
- 5

- Proportional to average TDS of cluster (see table 5)
- Proportional to average of standard deviations of solute mean concentrations (see table 5)

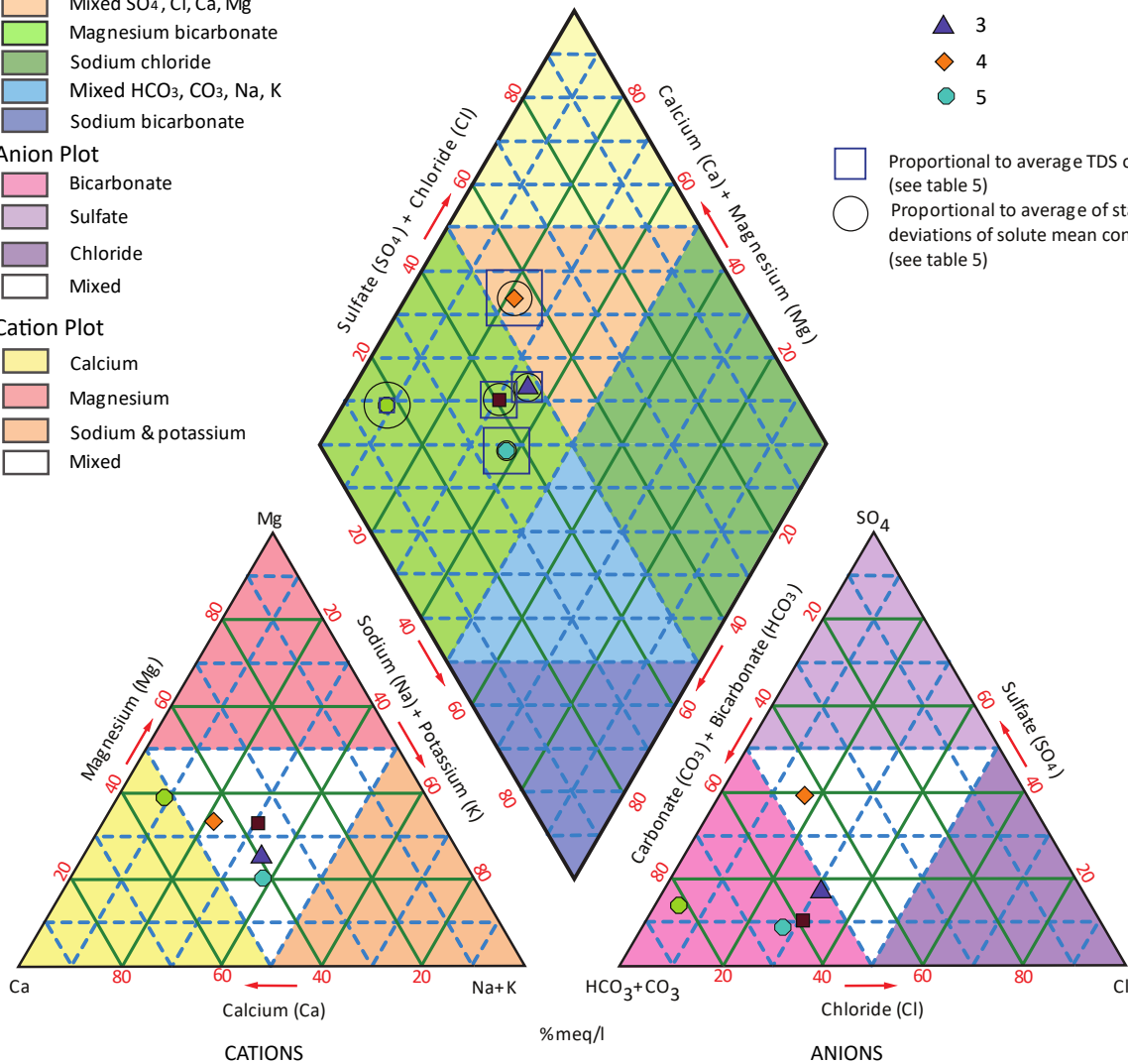


**Figure 29 continued.** Results of cluster analysis of Juab Valley chemical samples collected in 2015 and 2017. **A)** Plot of sum of squares of residuals versus number of clusters used to determine the optimum number of clusters in the analysis. The curve shows pronounced slope changes at 3 and 5 clusters. Increasing from 3 to 5 clusters reduces the sum of squares by about 33%, whereas increasing to more than 5 clusters reduces the sum of squares only slightly. **B)** Cluster dendrogram showing cluster assignments of each sample. **C)** Piper diagram of mean solute concentrations of clusters (table 5). The size of the square centered on the mean composition points is proportional to the average of the TDS concentrations of each cluster. The diameter of the circle around the mean composition points is proportional to the average of the standard deviations of the mean solute concentrations for each cluster, providing a measure of the compositional variance in each cluster.

0.09 and  $-42.85 \pm 1.39\%$ , respectively, with an r-squared value of 0.989. The slope compares well to the value of 4.663 estimated for the area near Mona Reservoir (Bowen and others, 2018). The intersection between the evaporation regression lines and the LMWL is at  $-16.5\%$  for  $\delta^{18}\text{O}$  and  $-122.4\%$  for  $\delta^2\text{H}$ , which is very slightly more depleted than the mean groundwater values of  $-16.13 \pm 0.06\%$  for  $\delta^{18}\text{O}$  and  $-121.45 \pm 0.35\%$  for  $\delta^2\text{H}$ . The near intersection of the LEL with the mean groundwater concentration indicates that Currant Creek and Mona Reservoir water is primarily derived from groundwater, with a minor component of precipitation.

Most groundwater samples are more enriched than winter precipitation, with the offset in  $\delta^2\text{H}$  values approximately 8%. The weighted Bayesian mixing model yields different mixing proportions when using the snow and soil water derived from snowmelt stable isotope compositions as inputs. For the snow isotopic compositions, the model estimates that groundwater is composed of 78% snow and 22% rain. For the soil water composition, the model estimates 90% soil water and 10% rain. The difference in model results may be due to sampling technique or, more likely, the isotopic evolution of snowpack and snowmelt prior to and during infiltration. The soil water samples were more enriched than the snow samples we collected.

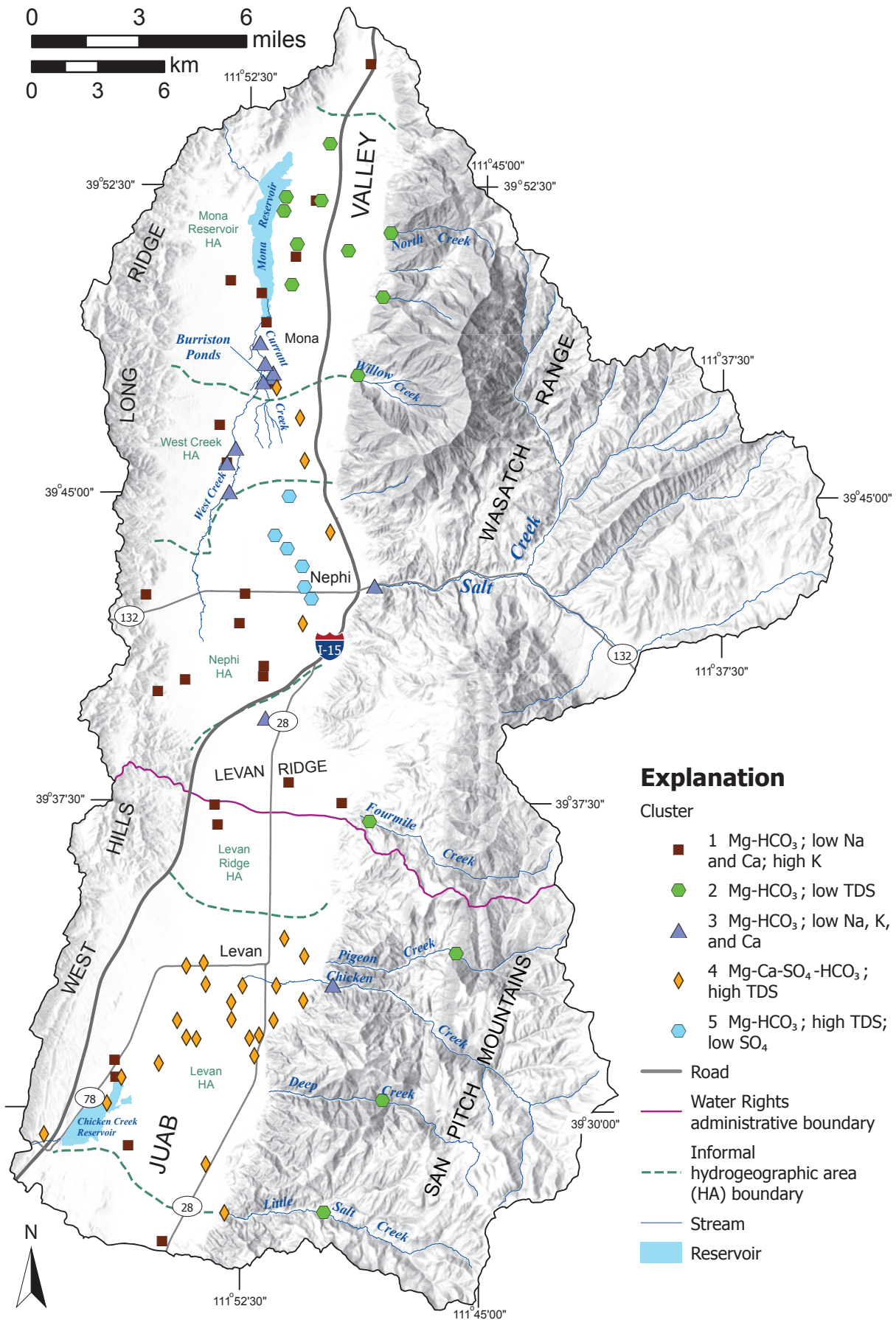
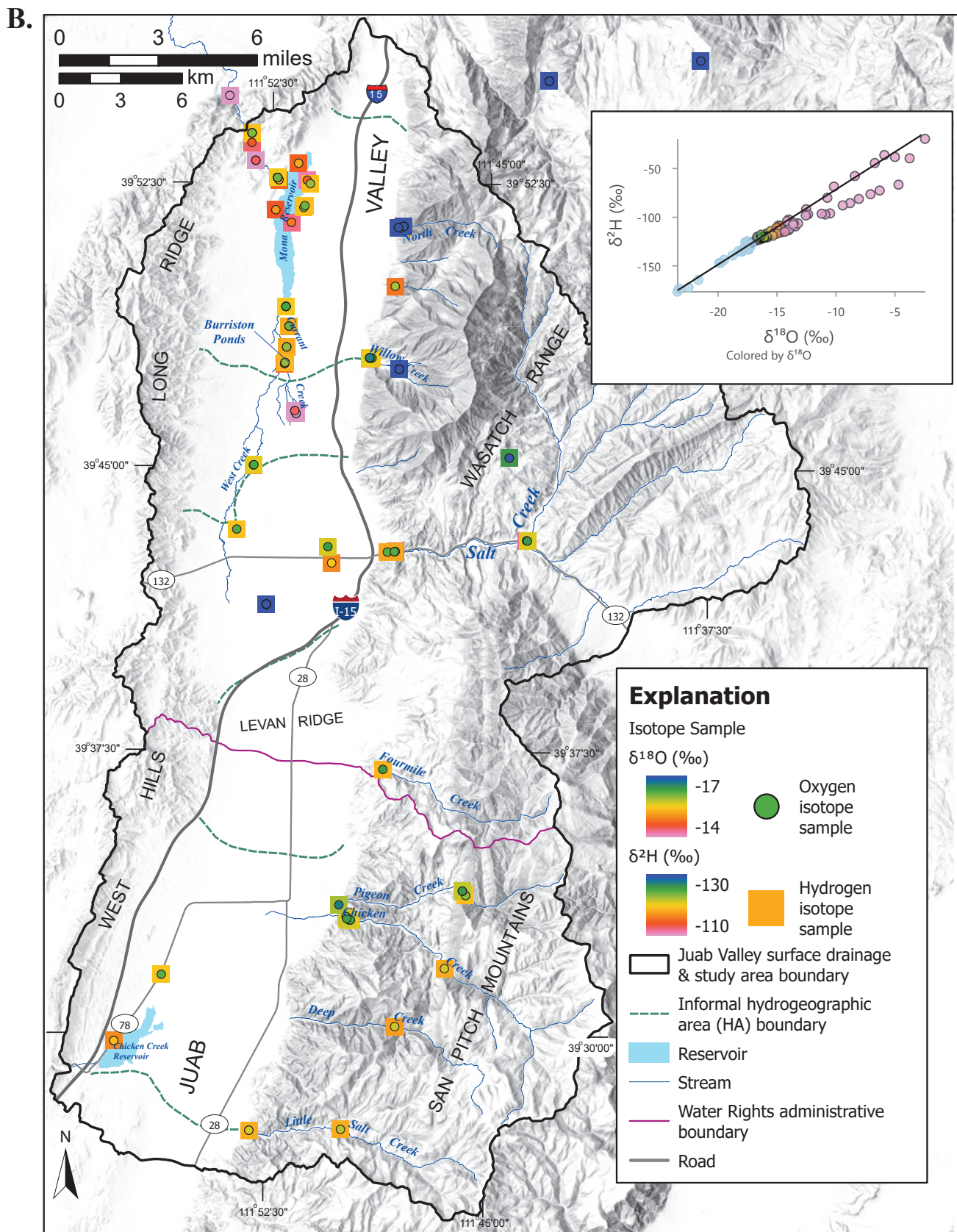
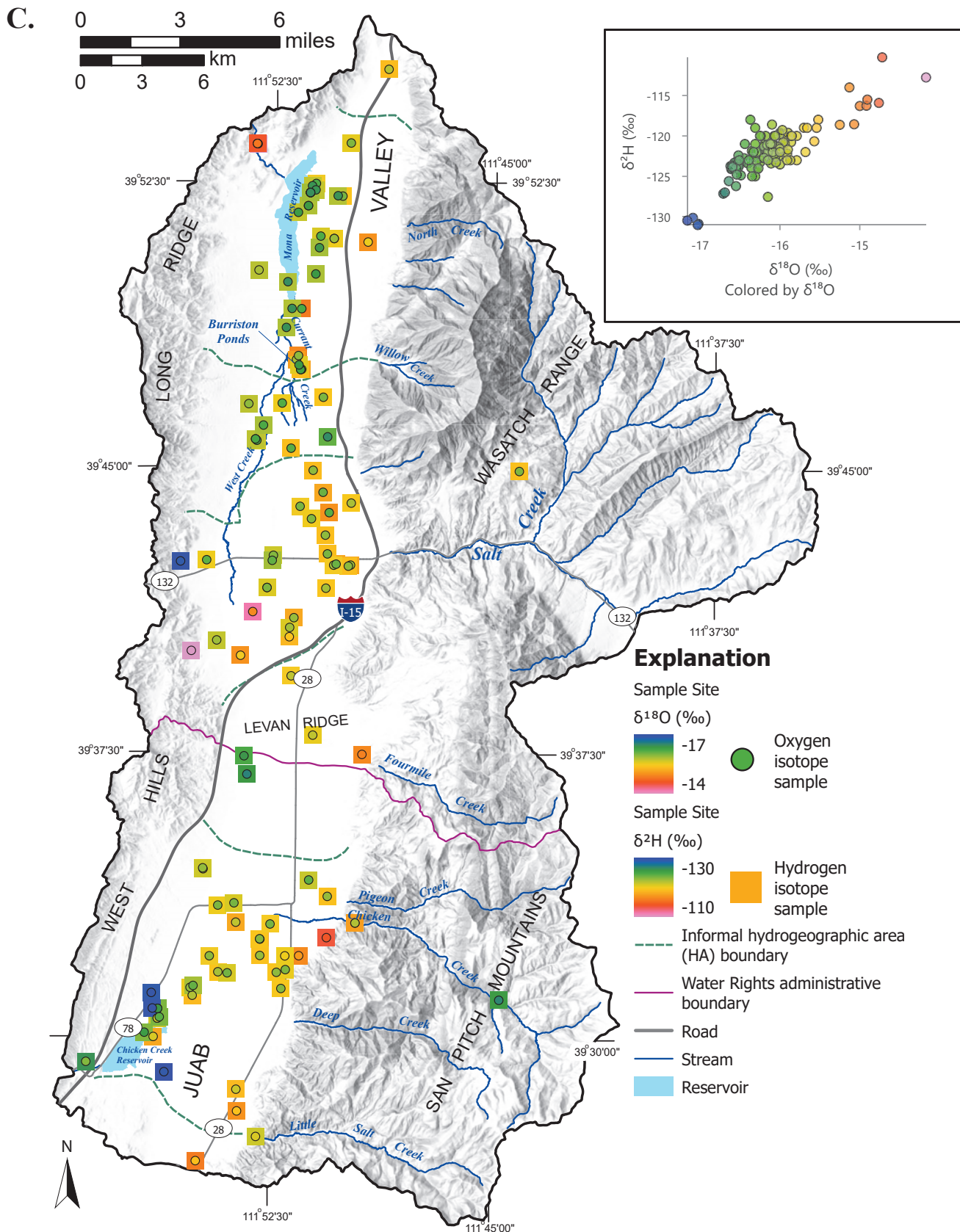


Figure 30. Cluster assignments of groundwater and surface water samples collected in 2015 and 2017 (table 5).





**Figure 31 continued.** A) Sites where stable isotope data were collected, symbolized by site type. Inset plot shows ratio of stable isotopes of hydrogen and oxygen of all the samples collected for the study. B) Location and  $\delta^2\text{H}$  and  $\delta^{18}\text{O}$  compositions for Juab Valley surface water and precipitation samples. Inset plot shows ratio of stable isotopes of hydrogen and oxygen of surface water and precipitation samples collected for the study. C) Location and  $\delta^2\text{H}$  and  $\delta^{18}\text{O}$  compositions for Juab Valley groundwater samples. Inset plot shows ratio of stable isotopes of hydrogen and oxygen of the groundwater samples collected for the study.



**Figure 31 continued.** A) Sites where stable isotope data were collected, symbolized by site type. Inset plot shows ratio of stable isotopes of hydrogen and oxygen of all the samples collected for the study. B) Location and  $\delta^2\text{H}$  and  $\delta^{18}\text{O}$  compositions for Juab Valley surface water and precipitation samples. Inset plot shows ratio of stable isotopes of hydrogen and oxygen of surface water and precipitation samples collected for the study. C) Location and  $\delta^2\text{H}$  and  $\delta^{18}\text{O}$  compositions for Juab Valley groundwater samples. Inset plot shows ratio of stable isotopes of hydrogen and oxygen of the groundwater samples collected for the study.

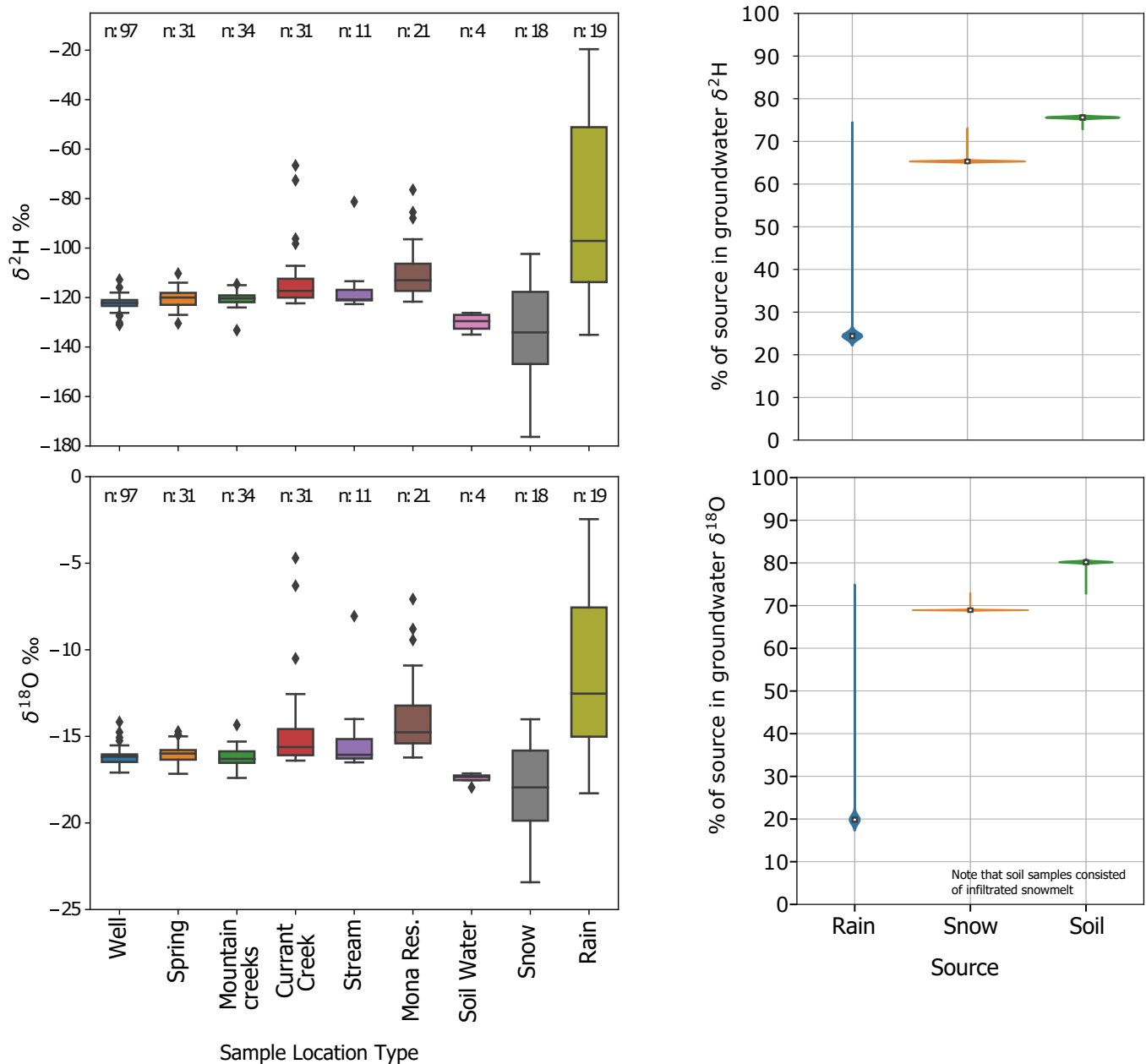


**Figure 32.** Stable-isotope compositions of groundwater and estimated seasonal precipitation end-members.

The general east-to-west progression from more enriched to more depleted stable-isotope compositions may reflect progressively lower temperature of water at the time of recharge. The recharge-temperature variations could reflect elevation, seasonal, or climatic effects. Groundwater recharged at high elevations, and/or during winter, and/or during a cooler past climate would have more depleted stable-isotope compositions. The zonation does not reflect differences in recharge elevation on either side of the valley, because the more depleted stable-isotope compositions associated with cooler temperatures are adjacent to the lower-elevation mountains. The zonation could in part represent predominance of in situ (i.e., valley-floor) recharge of snowmelt in the western part of the valley versus recharge of runoff from summer storms in the eastern part of the valley. However, the stable-isotopic

compositions of Juab Valley groundwater indicate predominance of recharge of winter precipitation valley-wide (figure 32). The general zonation of isotopic values agrees with the groundwater conceptualization of younger in the east to older in the west, where the older groundwater in the western part of the valley recharged during times of cooler climate. Groundwater-level contours (figure 16) indicate flow from Long Ridge and the West Hills toward the valley floor, and therefore suggests that some recharge occurs along the western valley margin (although if so, it is likely much slower than from the eastern valley margin). Thus, even the older groundwater in the valley center may have more than one source area. The apparent southwest-protruding lobe of more enriched groundwater from the western slope of the Wasatch Range to the Burriston Ponds area may reflect a local flow system having a

greater proportion of recharge of spring runoff and summer storm precipitation onto the alluvial fans than occurs in other parts of the valley. Conversely, this and other variations from a regular east-to-west progression may reflect the effects of local recharge and mixing.

## Radiogenic Isotopes

**Tritium:** Tritium values range from 0.1 to 5.6 tritium units (TU) (table 5). Samples having TU values less than 0.5 have mean residence times (i.e., time since recharge to the water table) greater than approximately 60 years (i.e., before above-ground testing of nuclear bombs); samples having TU values between 0.5 and 2.0 may contain mixtures of water having residence times greater and less than 60 years; and samples having TU values of 2.0 or greater were recharged less than 60 years ago. We did not collect dissolved-gas samples for this study, which would enable more precise estimates of groundwater residence times from tritium concentrations.

In the Levan hydrogeographic area, TU values consistently decrease to the southwest along the groundwater flow path suggested by Thiros and others (1996) (figure 33). In the Levan Ridge hydrogeographic area, TU values range from 0.2 to 1.0, suggesting pervasive groundwater having mean residence time of >60 years. In the Nephi, West Creek, and Mona Reservoir hydrogeographic areas, TU values generally decrease from southeast to northwest along the flow path suggested by Thiros and others (1996), with the exception of the well just east of Burrison Ponds which has the highest TU value (5.6) of the 14 samples. This sample also has stable-isotope values that more closely resemble surface water in the Wasatch Range to the east. Together, these data suggest a plume of relatively young groundwater supplies the Burrison Ponds springs.

**Radiocarbon:**  $^{14}\text{C}$  measurements have units of percent modern carbon (pmC), which is the percentage of  $^{14}\text{C}$  relative to A.D. 1950 levels. Radiocarbon values for Juab Valley groundwater are between 7.4 and 100.5 percent modern carbon (pmC) (table 5). The carbon-13 isotope ( $^{13}\text{C}$ ) is a naturally occurring stable isotope of carbon that is used to evaluate chemical reactions involving carbon (Clark and Fritz, 1997).  $^{13}\text{C}$  concentration is typically reported as a delta notation as a ratio with  $^{12}\text{C}$ , like  $\delta^{18}\text{O}$  and  $\delta^2\text{H}$ , but with the Vienna Pee Dee Belemnite as the standard reference. Values of  $\delta^{13}\text{C}$  ratios in Juab Valley groundwater range from -14.0 to -6.6‰ (table 5).

The calculation of  $^{14}\text{C}$  ages requires the determination of  $A_0$ , the initial, non-decayed  $^{14}\text{C}$  content of the groundwater.  $A_0$  is typically assumed to be 100 pmC in the absence of subsurface geochemical reactions. This assumption is, however, commonly invalid in the Great Basin, where elevated  $\text{CO}_2$  concentrations due to microbial and plant respiration in the soil causes dissolution of carbonate minerals into the vadose-zone water. Thus,  $A_0$  is generally significantly lower than 100 and can even be lower than 50 pmC (Plummer and Glynn,

2013). Several models account for geochemical reactions and exchanges to calculate  $A_0$  (Ingerson and Pearson, 1964; Mook, 1972; Tamers, 1975; Fontes and Garnier, 1979). For this study,  $A_0$  was calculated in NETPATH-Win (El-Kadi and others, 2011) using the Fontes and Garnier model (Fontes and Garnier, 1979), which models the exchange and mixing of carbon and carbon isotopes between soil-gas  $\text{CO}_2$  and carbonate minerals. End-members of radiocarbon and  $\delta^{13}\text{C}$  were assumed to be 100 pmC and  $-21.8 \pm 1.4\text{‰}$  for soil-gas  $\text{CO}_2$  (Hart, 2009), and 0 pmC and 0‰ for carbonate minerals, respectively. This model produced realistic  $A_0$  values for eight samples (table 5). The model produced unrealistic  $A_0$  values for the other eight samples. The erroneous  $A_0$  values come from samples having TU values of 2.0 or greater, indicating the input of bomb radiocarbon, which changes the radiocarbon content of the soil-gas end-member, with the exception of sample B3-17. Although the model produced an erroneous  $A_0$  value, the TU value for the sample is 0.1. Sample B3-17 is from a flowing well on the eastern margin of Mona Reservoir that is screened along most of the well depth, and thus may represent mixing of old and modern water from multiple flow paths. Although more simplistic than the Fontes and Garnier model (Fontes and Garnier, 1979), our model (figure 34) shows simple mixing between isotope end-members and differentiates between samples that contain significant bomb-peak radiocarbon versus those that do not.

The mean  $A_0$  value for the low tritium samples is  $41 \pm 6$  pmC. Radiocarbon ages for these samples range between 1200 and 15,000 years before present (B.P.). Figure 35 shows the distribution of mean radiocarbon ages, and table 3 summarizes the radiocarbon data and analyses. Samples having TU values of 2.0 or greater are not assigned radiocarbon ages but are interpreted as “modern” (younger than about 1000 years B.P.). Mean radiocarbon ages are oldest in the western part of Juab Valley. Modeling of radiocarbon and tritium data together (next section) provides additional insight into the radiogenic isotope data.

**Lumped parameter modeling:** Mixing models were chosen based on conceptualization and geometry of aquifers. For wells in unconfined aquifers, we used the exponential mixing model (EMM) or the partial exponential model (PEM) based on the depth of the screened interval below the water table.

The values of pmC were adjusted relative to 100 as required by TracerLPM (Jurgens and others, 2012). For samples having low tritium concentrations, values of  $A_0$  were adjusted using the corrected radiocarbon age. For samples that could not be corrected, the mean value of  $A_0$  (46.1 pmC) was used as an offset factor. This method proved to be too imprecise for the lumped parameter modelling. Therefore, age distributions for these samples were constrained only by tritium concentration, aquifer geometry, and well construction. Tritium and  $^{14}\text{C}$  concentrations were only used in conjunction when the sample did not have significant bomb-peak  $^{14}\text{C}$  and tritium concentrations were above the detection limit (0.2 TU).

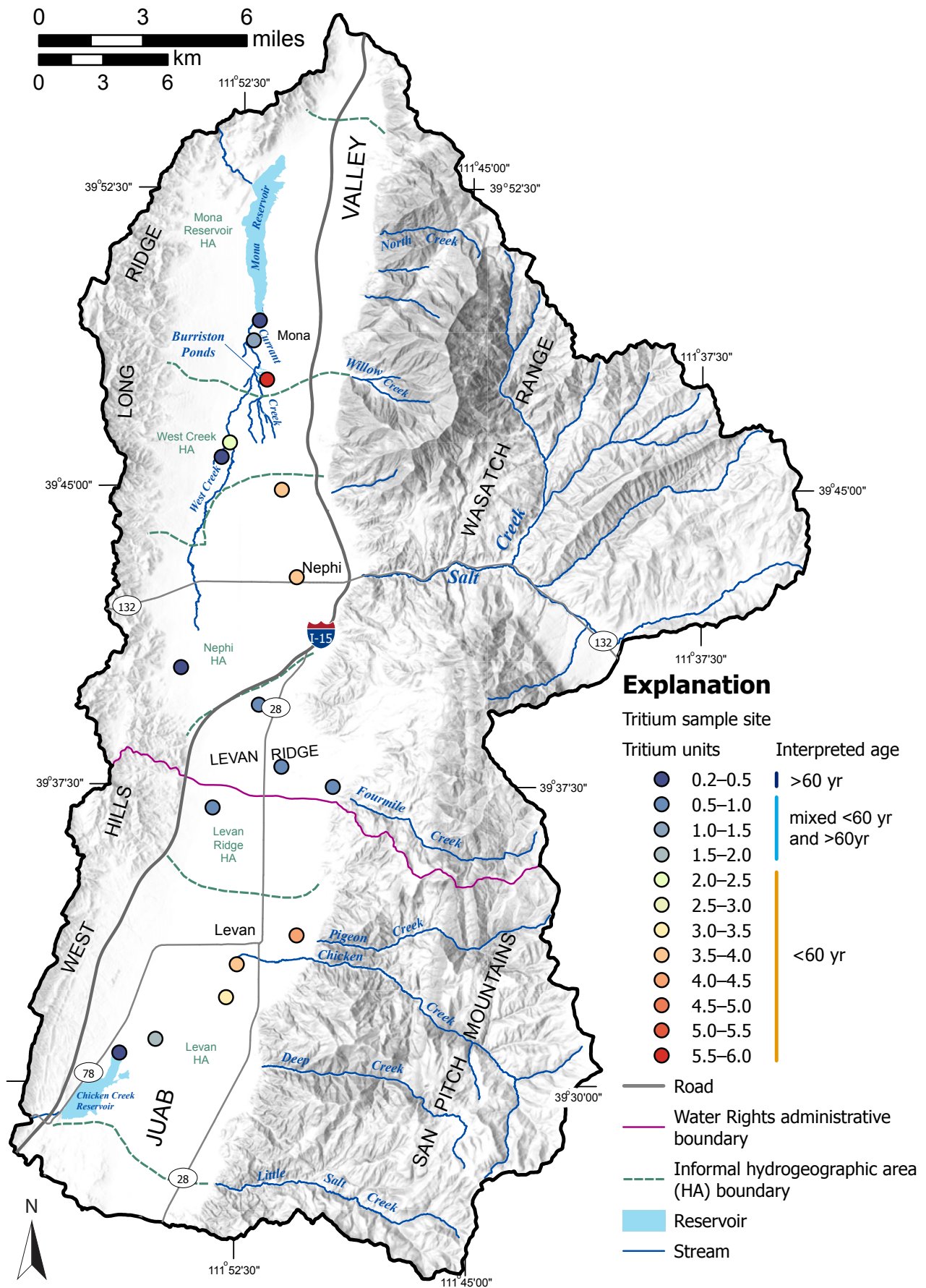
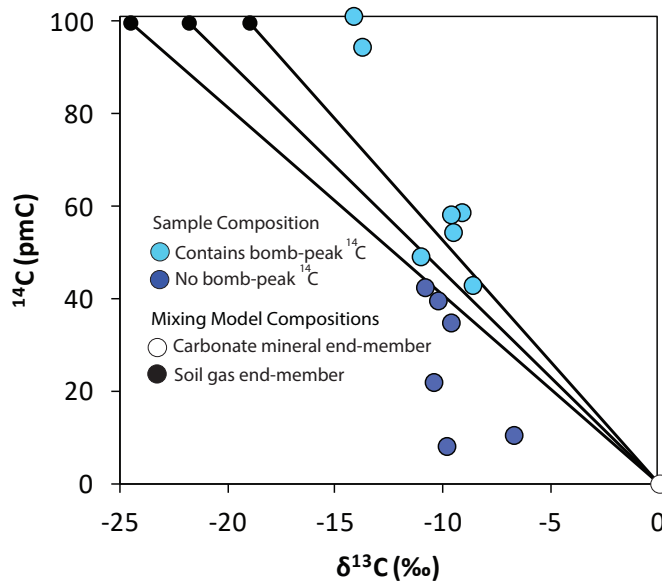


Figure 33. Tritium-unit values (TU) for Juab Valley water chemistry samples collected in 2015 and 2017 (table 3).



**Figure 34.** Carbon-isotope compositions and simple mixing lines between modern soil gas and carbonate minerals (Hart, 2009).

Mean groundwater ages are 35–210 yr B.P. for samples containing bomb peak  $^{14}\text{C}$ . Mean ages are 1370–23,200 yr B.P. for samples that apparently contain no bomb peak  $^{14}\text{C}$ .

The distribution of mean residence times within the study area is generally complicated. There is, however, a clear age progression along the southern flow line from Levan to Chicken Creek Reservoir (figure 36). Here, the model ages increase from 108 to 210 yr B.P. before jumping to 17,700 yr B.P. or sample H2-S1.

Relative contributions of basin recharge and groundwater velocity to the model ages were constrained with a simple one-dimensional flow model. Using a gridded model having cell length of 0.1 km, the groundwater age at the edge of the basin, fraction of recharge at each cell and groundwater velocity were modified to minimize misfit between the model and observations. The optimization procedure was performed using Solver in Microsoft Excel. The best fit occurs when the initial age is 42.8 yr B.P., the velocity is 11.6 m/year, and the fraction of young groundwater is 3.8% for each grid cell (figure 37).

Tritium and radiocarbon values, model ages, and lumped parameter modeling indicate a general east-to-west increase in residence time and mean groundwater age (reflecting the proportions of residence times present in the samples); however, the progressions are neither unidirectional nor linear with distance from the valley margin. This may suggest that recharge occurs within the basin, adding young water to the relatively old water that recharged in or adjacent to the Wasatch Range. Conversely, along the southern traverse from Levan to Chicken Creek Reservoir, substantially deeper, older groundwater reaches the land surface at spring H2-S1 northeast of Chicken Creek Reservoir, perhaps due to an abrupt decrease in aquifer transmissivity caused by a fault or an abrupt change in basin-

fill lithology. A similar scenario may apply to sample F2-02 in the eastern Levan Ridge hydrogeographic area having an anomalously old radiocarbon age. Stable and radiogenic isotope data can be difficult to interpret when sampling from long-screen production wells. Long-screen wells produce a mixture of water from many hydrogeologic zones, with many different flow paths and ages. Some of the lack of clear trends in the data may be due to this.

## MONA RESERVOIR WATER BUDGET

### Introduction

Mona Reservoir represents a local base level for Juab Valley and a discharge area for groundwater. Determining the water budget for the reservoir allows for a better understanding of the greater water budget for Juab Valley and may benefit future reservoir management.

### Previous Work

Woodward-Clyde International oversaw dam modifications on Mona Reservoir in 1998 (Gerhart, 1999). They included surveyed plans and a hypsometric curve as part of their modification. Thiros and others (1996) included the reservoir in their groundwater model, and estimated groundwater discharge to the it. The Utah Division of Water Rights keeps records of reservoir stages and discharges in their dam safety database.

### Methods

#### Bathymetric Survey

In the fall of 2018, Mona Reservoir was empty, and Currant Creek flowed directly into the reservoir outflow point; only a few marshy areas in the reservoir had ponding water. Using a DJI Phantom unmanned aerial vehicle, we collected 3795 high-resolution (3.34 cm/pixel) overlapping aerial photographs of the reservoir. We calibrated the photos with 37 control points having high-visibility markers. The control points were measured with a survey-grade GPS instrument, corrected using the TURN network. We used AgiSoft structure-from-motion software to process the images and control points to create a high-resolution (sub-meter) digital elevation model (DEM) of the reservoir floor. We masked areas of water cover using manually entered control points to fill the areas where shallow water was ponded. The resulting DEM covers 6.5 km<sup>2</sup> of the reservoir. We stitched the existing lidar of the southern end of the reservoir to the DEM for a complete DEM of the entire reservoir.

#### Hypsometric Curve

Using the high-resolution DEM, we created a hypsometric curve for Mona Reservoir. Hypsometric curves are functions

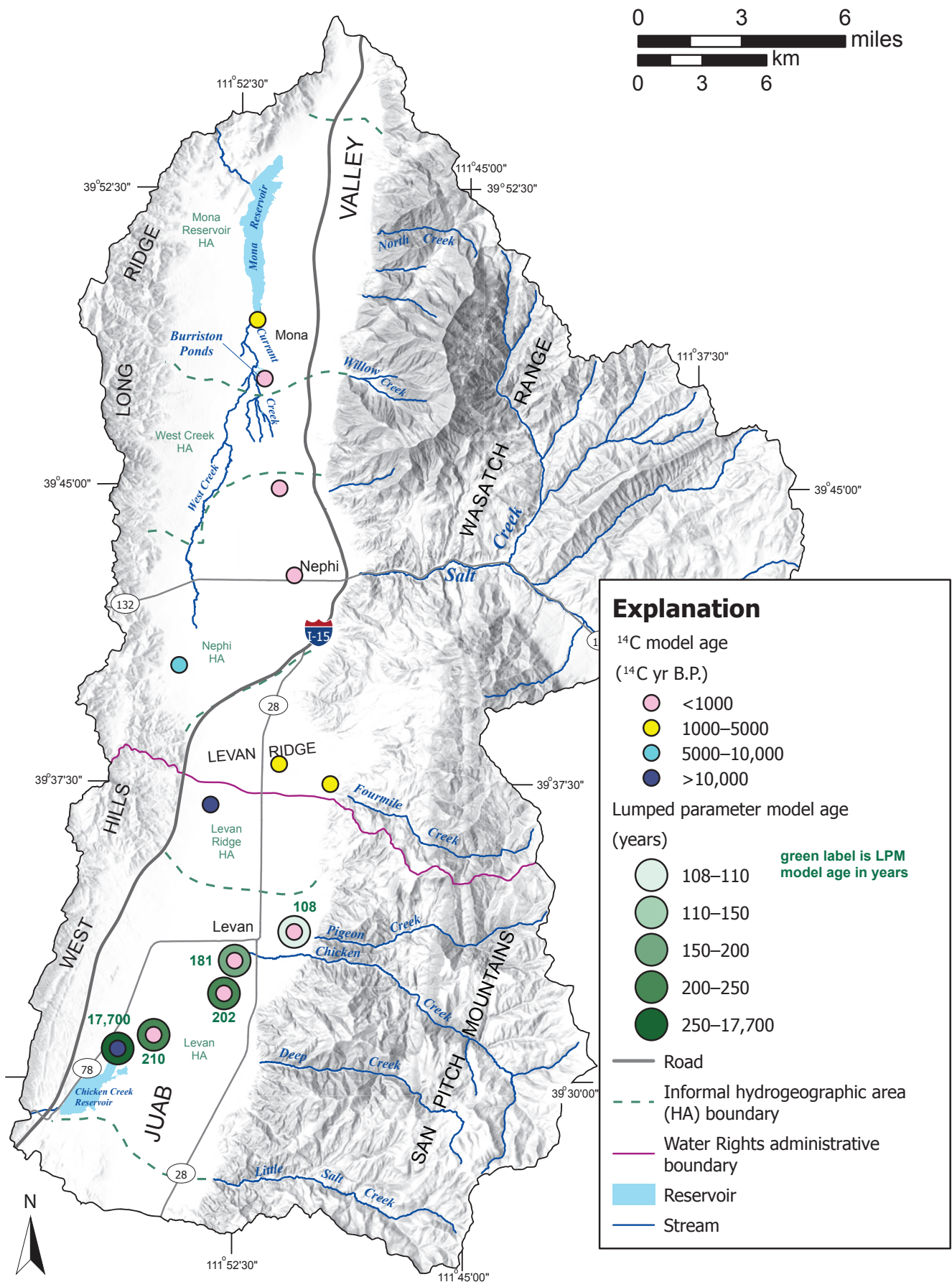


Figure 35. Lumped parameter model ages for Juab Valley water chemistry samples collected in 2015 and 2017 (table 5).

that represent the relationship between water surface elevation and reservoir volume. To create the hypsometric curve, we intersected grids of constant elevation, representing various reservoir water elevations, with the DEM. With the DEM and constant elevation grids, we conducted a cut-fill analysis in GIS, which measures the volume between two surfaces. We plotted the results of the cut-fill analysis against elevation and applied best fit curves to the data to generate equations that calculate reservoir area and volume from reservoir water elevation.

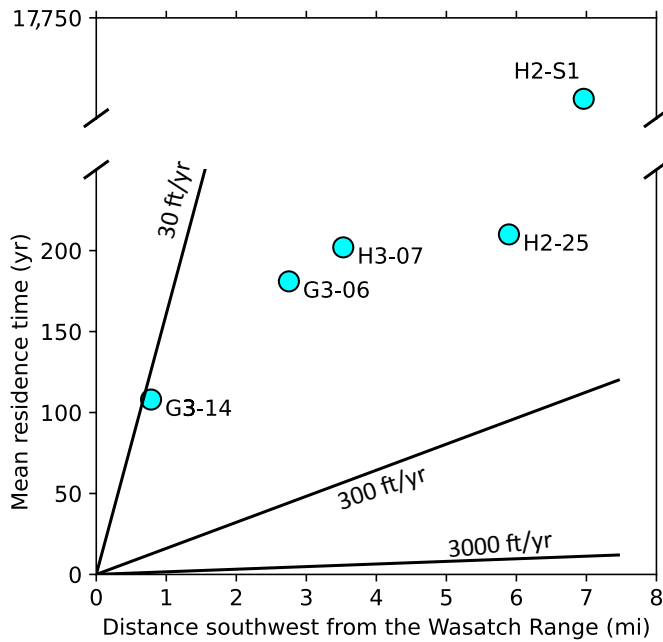


Figure 36. Mean residence time of samples and age progression with indicative flow velocities along the flow path from Levan to Chicken Creek Reservoir.

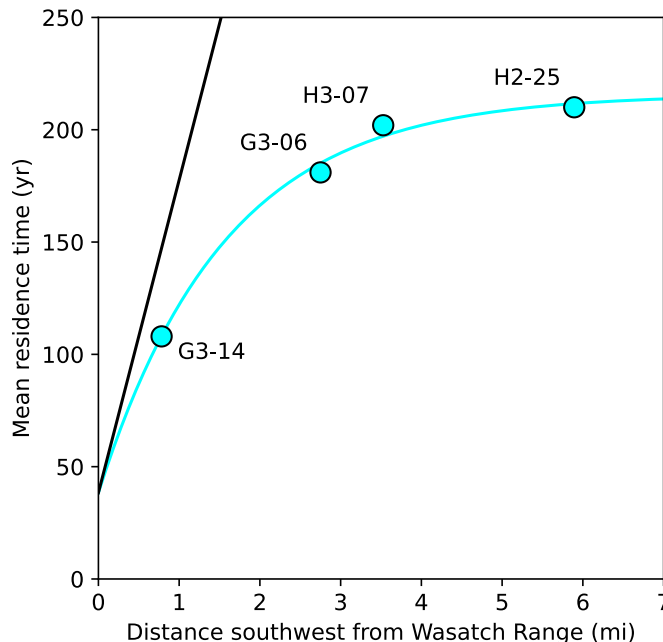


Figure 37. Best-fit model of age progression for samples along the flow path from Levan to Chicken Creek Reservoir.

### Stream Gaging

Continuous stream gaging above and below Mona Reservoir constrained the inflow and outflow components of the water budget for Mona Reservoir. We installed non-vented pressure transducers at two monitoring locations above and below the reservoir to measure flow into and out of the reservoir over time. We placed a transducer in the reservoir to measure the stage over time. All three locations included staff gages for regular manual readings, and the upstream location had a flume. We corrected the pressure time series from the transducers for barometric pressure fluctuations and converted the resulting water levels to flow estimates using manual measurement data. For the downstream side, we created a discharge stage relationship using stream velocity meter measurements, resulting in flow measurement errors as high as 20% of measurement. For the upstream side, we calculated flow in the flume based on stage using WinFlume.

### Budget Calculation

The change in storage in Mona Reservoir is based on a simple water budget approach:

$$\Delta S = Q_{gw} + Q_{in} - Q_{out} - ET + PPT \quad (2)$$

where:

$\Delta S$  = change in storage

$Q_{gw}$  = flow of groundwater into the reservoir

$Q_{in}$  = flow of surface water into the reservoir

$Q_{out}$  = flow of surface water out of the reservoir

$ET$  = evaporation of reservoir water and marginal vegetation transpiration

$PPT$  = precipitation directly into the reservoir

Using this equation, we solved for groundwater flow into the reservoir ( $Q_{gw}$ ). We calculated the daily change in reservoir storage ( $S$ ) using the hypsometric curve and hourly transducer measurements. Surface-water flow into ( $Q_{in}$ ) and out of ( $Q_{out}$ ) the reservoir was calculated using stream gaging (see above). Overland flow contributions directly into the reservoir not coming from streams were considered negligible. We calculated the evaporation from the lake ( $ET$ ) using SSEBop (Senay and others, 2013) estimates from remote sensing (see Groundwater Budget section for more information) that were temporally interpolated to daily values.  $ET$  was scaled by lake area using the hypsometric curve and lake measurements. We calculated the precipitation on the lake ( $PPT$ ) using daily PRISM data (2.5 mi [4 km] grid cells).

## Results and Discussion

The volume of water in the reservoir when pool elevation is equal to the spillway elevation of 4882.3 ft is 11,700 ac-ft, with a water surface area of 1390 acres (figure 38). The maximum capacity of the reservoir is 28,300 ac-ft when the pool elevation is at dam crest (4891.5 ft), covering 1850 acres. After adjusting the vertical datum for NAVD88, our hypsometric curve produced volume estimates that are very similar to those of Gerhart (1999) (figure 38).

Flow, temperature, and conductivity of Carrant Creek show a diurnal trend that is consistent throughout the period of measurement. Frequency analysis of the trend shows that it does not match with common Earth tide periodicities and is most likely attributable to evapotranspiration (figure 39). Flow and conductivity show an inverse relationship, where increased flow dilutes the water and decreases the conductivity. Amplitude of the trend in conductivity is higher in the summer (about 100  $\mu\text{S}/\text{cm}$ ).

During the 2019 water year, Mona Reservoir had an inflow of 5100 ac-ft of groundwater, with 2900 ac-ft being lost to

seepage, resulting in a net gain of  $2200 \pm 1000$  ac-ft (figure 40; table 6). This estimate is about 3700 ac-ft less than the amount calculated by the USGS model (Thiros and others, 1996), consistent with our observations of decreasing Carrant Creek flow and groundwater storage. Because we balanced the reservoir budget with the groundwater flow, some of this amount may be attributable to error in measurement. Previous studies did not quantify groundwater seepage out of the reservoir, but some seepage is likely occurring when reservoir levels are high (figure 40).

## GROUNDWATER BUDGET

### Previous Work

Thiros and others (1996) produced the most recent three-dimensional groundwater model of Juab Valley. Their model was made using MODFLOW-88, an early USGS groundwater model code. Brooks and Stolp (1995) constructed a three-dimensional groundwater flow model of southern Utah and Goshen Valleys, immediately downstream of the study area.

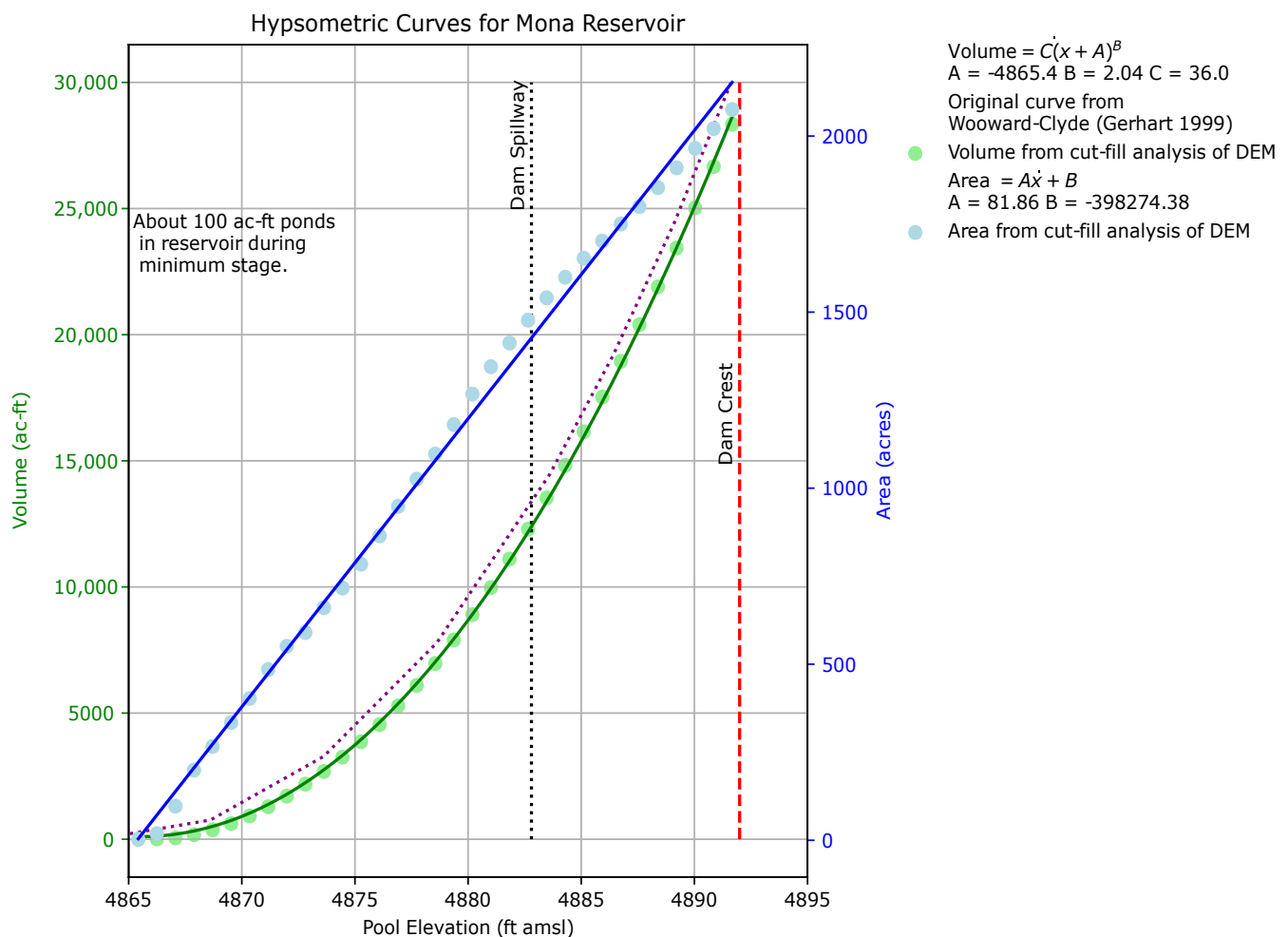


Figure 38. Hypsometric curves for Mona Reservoir.

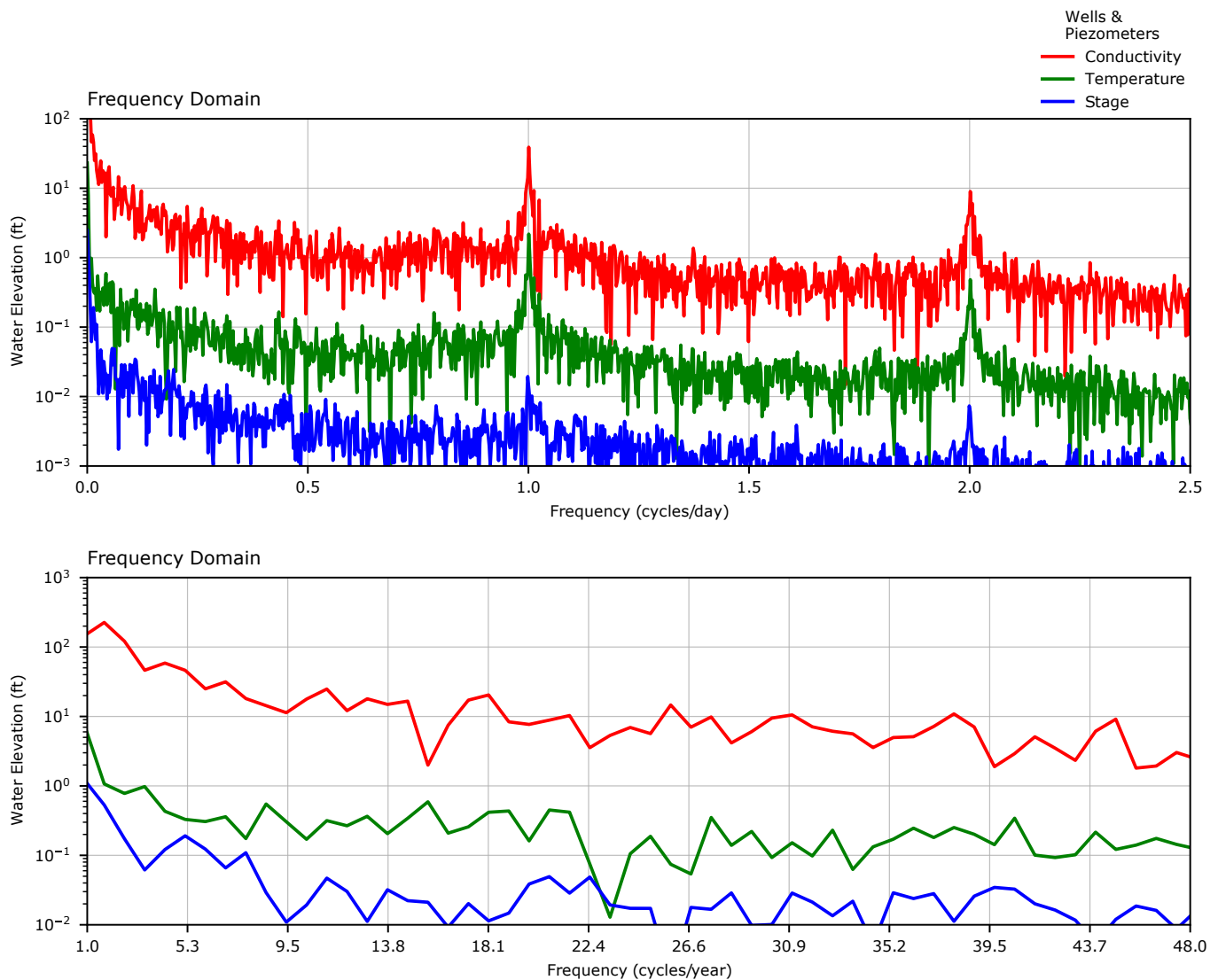


Figure 39. Frequency analysis for Currant Creek inflow data collected by the UGS.

## Methods

To satisfy the need for up-to-date water budget estimates, we calculated a water budget for Juab Valley using the results and conceptual model of our hydrogeologic framework study, an updated version of the Thiros and others (1996) model, and current water budget methodologies (Healy and others, 2007) to constrain components of recharge and discharge and their uncertainties. We assumed that the groundwater budget was not balanced, based on the observed storage and discharge changes.

## MODFLOW Model

Inkenbrandt updated the MODFLOW finite difference groundwater model of Juab Valley (Thiros and others, 1996) and used it as a tool to check the water budget and aid in groundwater system conceptualization (figure 41). To update the model, six additional stress periods were added to the long-term transient model (table 7), bringing the model to the current period of

study (2020). Specified recharge and discharge were extended using the relationships specified in Thiros and others (1996), with some adjustments. See the sections on recharge and discharge below for more information.

We tried to minimize modification to the original model outside of the addition of time steps. However, updating the model from MODFLOW-88 (McDonald and Harbaugh, 1988) to MODFLOW-2000 (Harbaugh and others, 2000) to MODFLOW-2005 (Harbaugh, 2005) requires some user input that can cause variations in the product of that conversion. For example, the original Thiros and others (1996) model had four layers, where the fourth layer had an essentially infinite thickness (see Thiros and others, 1996, p. 56–57), whereas the converted model has five layers. Because the scale of study was the same as the original model study area, we maintained the original grid spacing. To accommodate for the addition of new wells over time, we added pumping data for all wells drilled after 1993 having discharges greater than 10 ac-ft/yr.

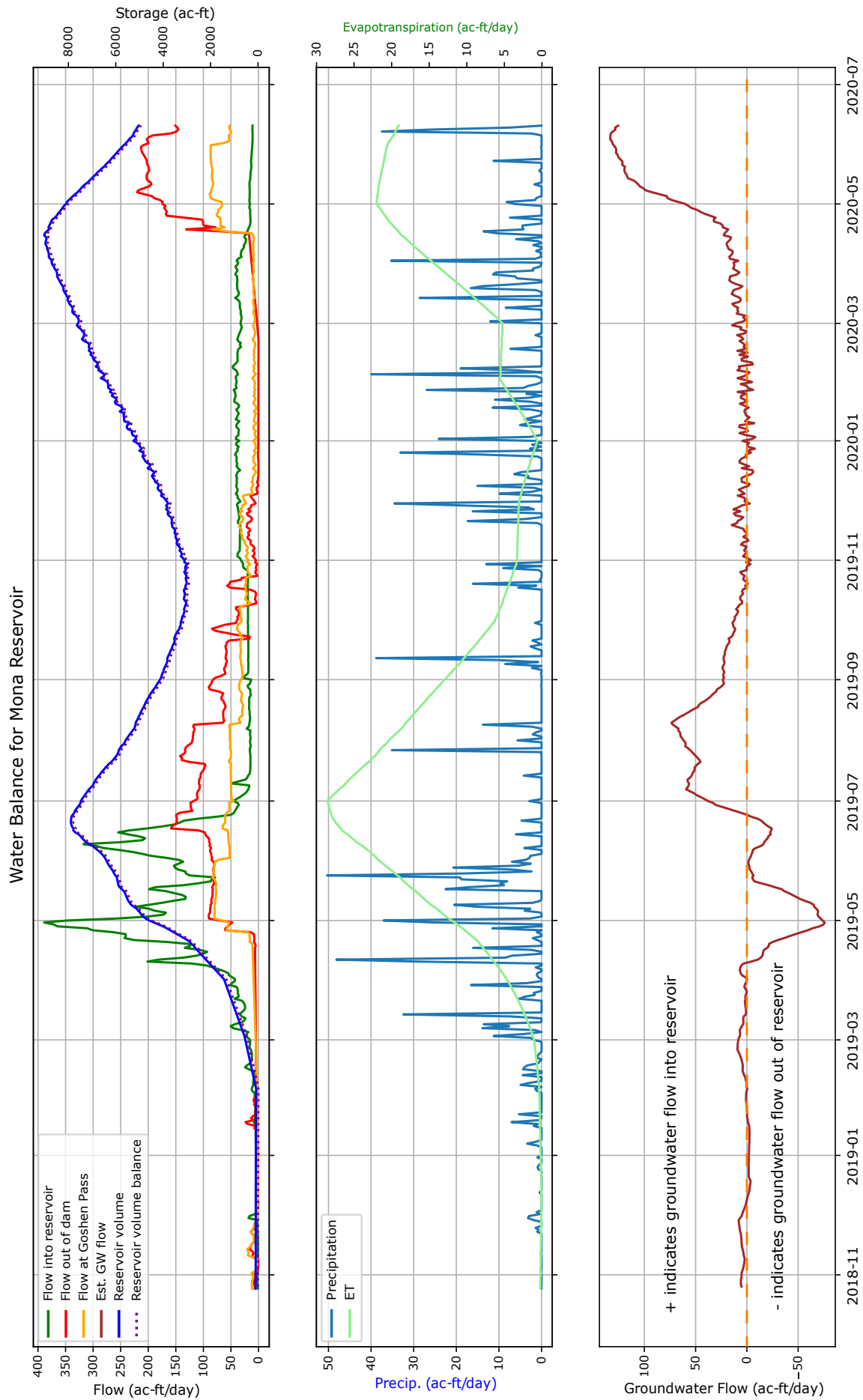


Figure 40. Flow components for the water balance of Mona Reservoir.

**Table 6.** Mona Reservoir budget for water years 2019 and 2020.

Component		Acre-feet per Water Year		Source
		2019	2020	
	Baseflow of Currant Creek	13,100	6300	Eckhart on USGS Gage
	Flow at Goshen pass	9200	6900	Measured
Inputs	Flow into dam	18,500	7600	Measured
	Precipitation into lake	800	800	PRISM and Daymet
	Groundwater flow into reservoir	2200	7200	From daily balance
	Total	21,500	15,600	
Outputs	Evaporation from lake	3200	2300	SEEBop
	Flow out of dam	15,200	11,500	Measured
	Total	18,400	13,800	
Water year input - water year output		3100	1800	
Reservoir storage change (+ increase)		3200	1800	Measured

## Recharge

### Seepage from Streamflow

To estimate flow of ungaged streams, we used output from the USGS StreamStats model, which uses regional regression equations and watershed parameters to estimate flow statistics of a given point along a stream (Ries and others, 2017). The StreamStats model can be run through a browser on any internet-connected computer, and the USGS has recently added web-service capabilities for scripted modeling.

We ran the StreamStats model for each measurable stream entering Juab Valley (figure 42). The StreamStats model does not provide year-to-year estimates, and only provides mean and quantiles of flow data for a watershed. To estimate temporal variation of each stream, we used the ratio of StreamStats data and measured annual flows at the Salt Creek (10146000) and Chicken Creek (10219200) gage sites (figure 43). The record of the Chicken Creek gage ended in 1995, so prediction of flow for years after that is not possible using the Chicken Creek records. Linear regression of the modeled flow against the measured Chicken Creek flow provided adjustment factors for flow in the southern part of the valley (figure 44).

The StreamStats model provides a good estimate of streamflow for streams in the northern half of the study area. Monthly statistics of measurements at the Salt Creek USGS gage (1014600) are within 15% of the StreamStats estimates (figure 43A). Statistics of measurements at the Salt Creek USGS gage (1014600) compared against the StreamStats statistics gives an r-squared value of 0.98, fitting along the 1 to 1 line (figure 43B). The model generally overestimates monthly measured flow at the Chicken Creek gage (10219200) by about 14% (figure 43C), but still can recreate 93% of the variance of the gaged measurements (figure 43D; figure 44).

As Thiros and others (1996) did in their study, and as we observed in our field measurements, we assumed all major eastern streams were diverted for irrigation. We aggregated

streamflow by area and used the aggregated estimates in our water budgets. To check our estimates from StreamStats, we also estimated seepage from streamflow using the approach of Thiros and others (1996), where a linear relationship was established between precipitation and stream recharge.

### Recharge and Irrigation

The bulk of groundwater recharge occurring on the valley floor is from infiltration of unconsumed irrigation water and water lost from irrigation conveyance systems. To estimate recharge from unconsumed irrigation water we calculated evapotranspiration from irrigated agriculture based on current water-related land use data, crop consumption data, and remote sensing GIS-based evapotranspiration models (Allen and others, 2007a; Senay and others, 2013; Singh and others, 2014) and subtracted this value from estimates of applied water from surface sources and well withdrawal.

**Table 7.** Stress periods for the revised Thiros and others (1996) model. Stress periods 9 to 14 were added in this study.

Stress Period	Starting Time	Ending Time	Start Year	End Year
1	0	5	1949	1953
2	5	11	1954	1959
3	11	19	1960	1967
4	19	21	1968	1969
5	21	29	1970	1977
6	29	34	1978	1982
7	34	38	1983	1986
8	38	44	1987	1992
9	44	53	1993	2001
10	53	62	2002	2010
11	62	63	2011	2011
12	63	70	2012	2018
13	70	71	2019	2019
14	71	72	2020	2020

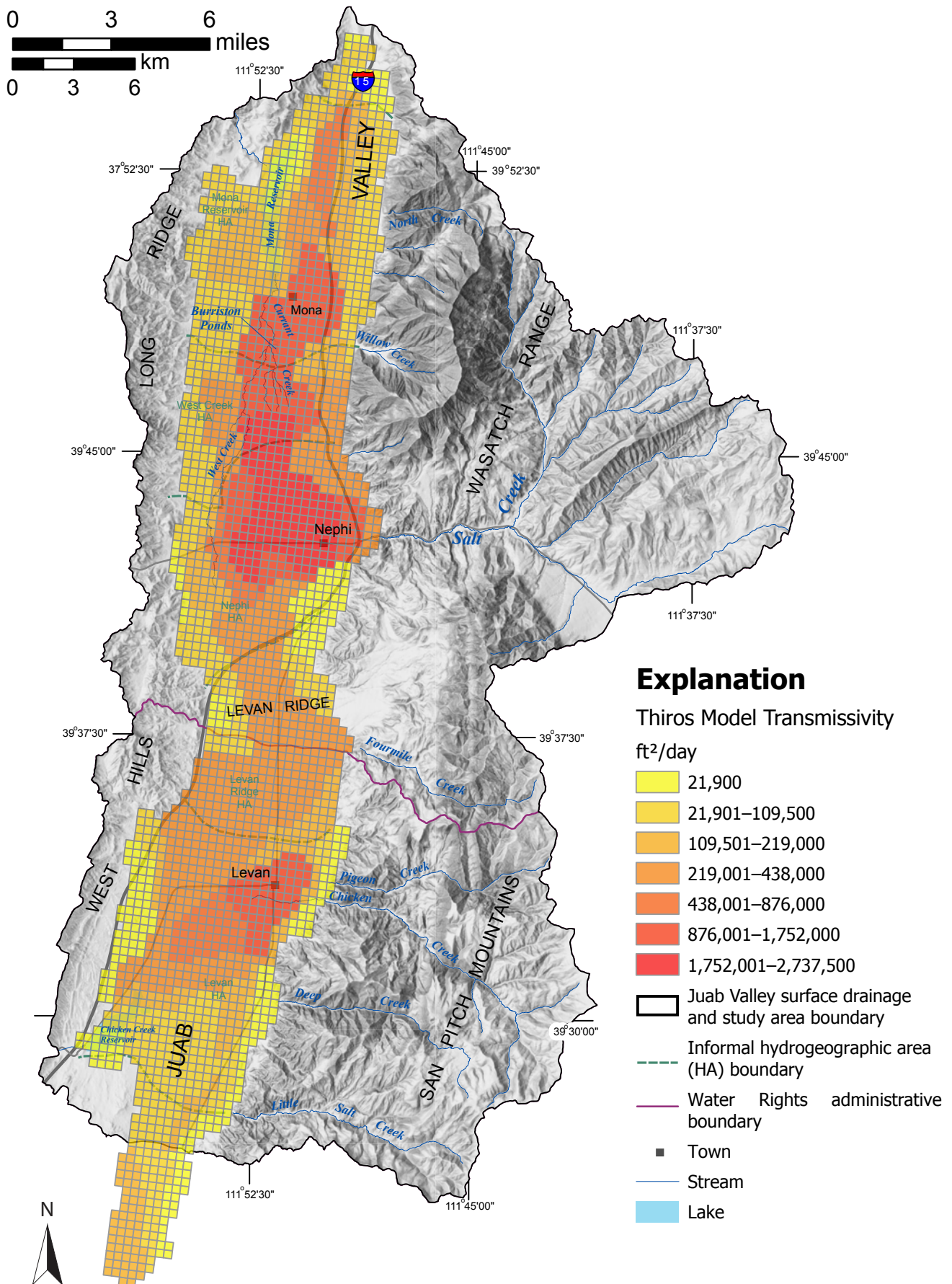


Figure 41. Model grid of the updated USGS 3-dimensional groundwater flow model.

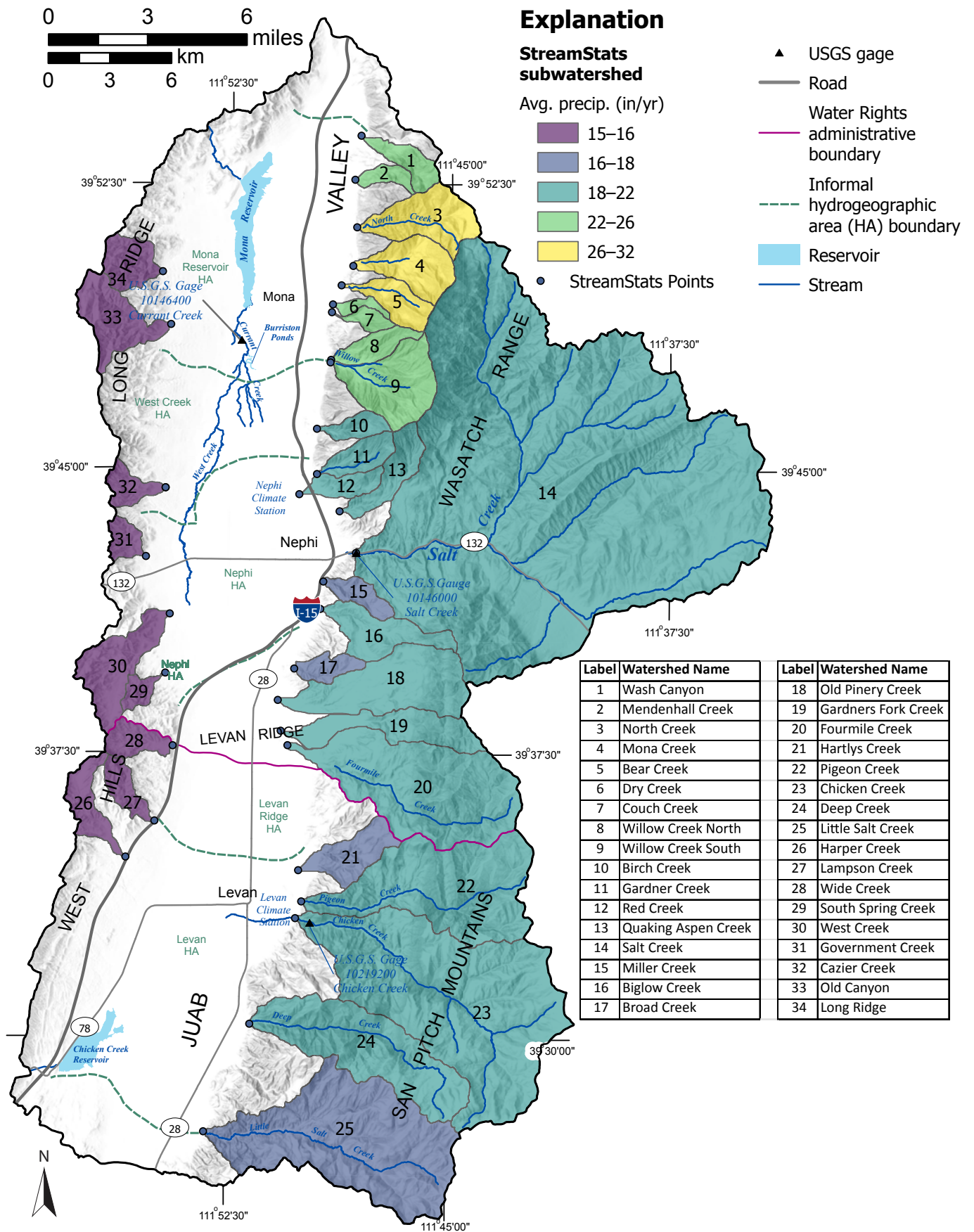
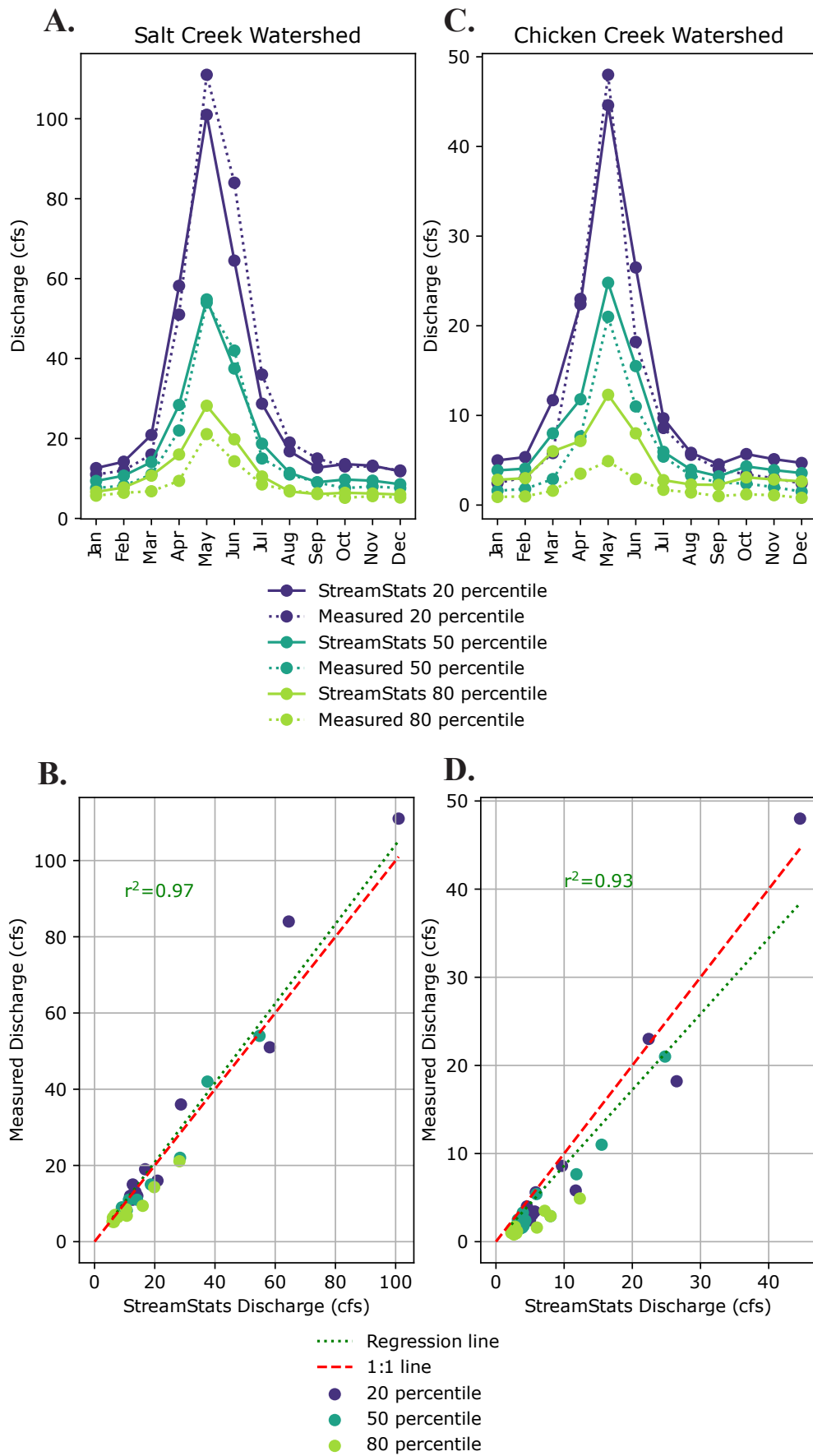


Figure 42. Subwatersheds analyzed using StreamStats. See tables 8 and A6 for a summary of flow from these subwatersheds.



**Figure 43.** Validation of StreamStats models against measured monthly flow in the Salt Creek (A and B) and Chicken Creek (C and D) watersheds.

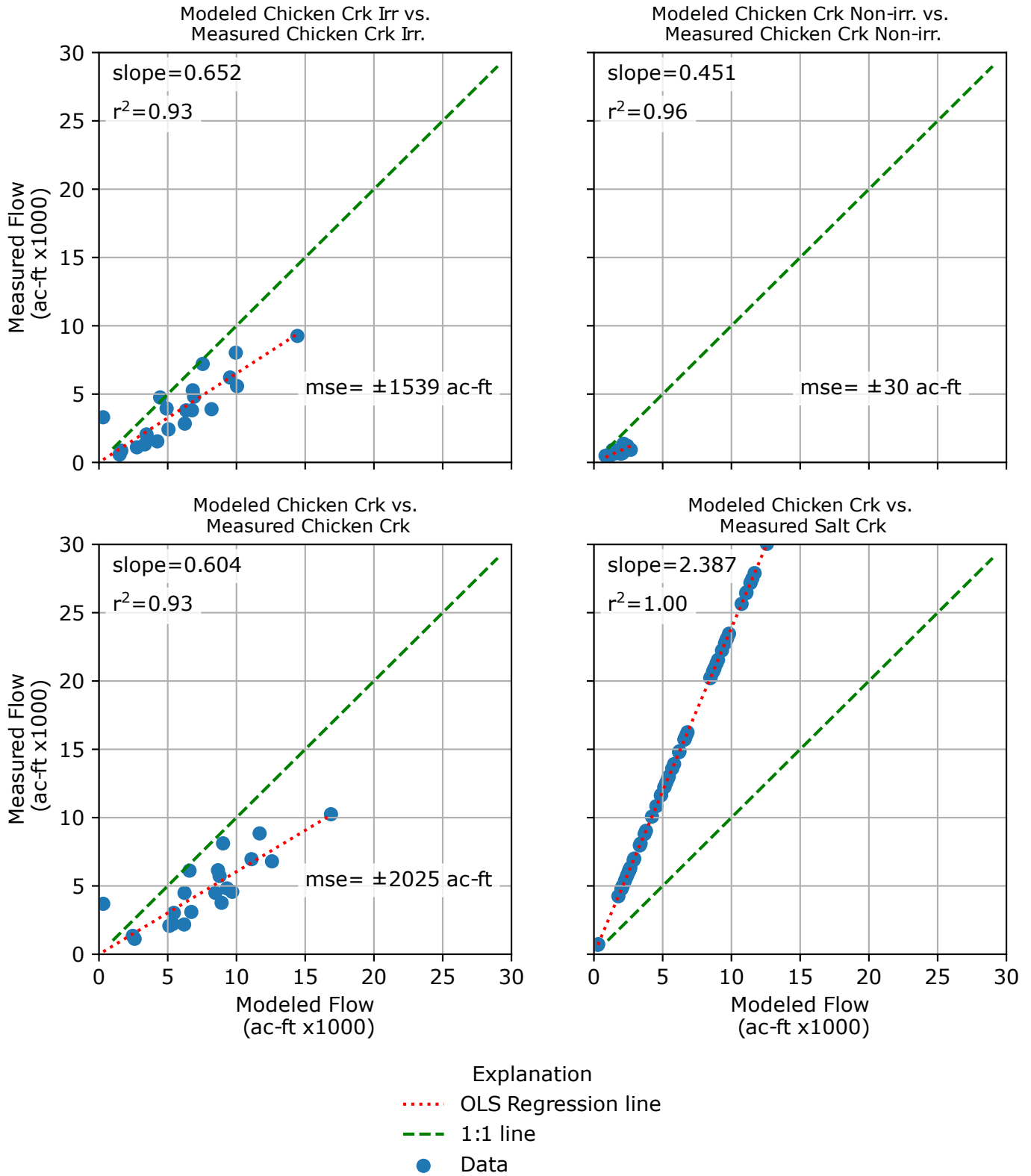


Figure 44. Regression analysis of the Chicken Creek watershed against yearly discharge estimates.

Water diverted for irrigation was calculated using a combination of StreamStats streamflow estimates for the eastern streams (table 8) and estimates of groundwater pumping for irrigation. We multiplied the water volumes diverted by an efficiency percentage to calculate the water availability (table 9). The percentage was used to account for losses from irrigation conveyance systems like leakage, canal seepage, and evaporation. Many of the irrigation systems in Juab Valley have lined or piped conveyance systems, and we assumed that this efficiency generally has improved since the 1990s. We assumed that relatively wet water years will have lower efficiencies than relatively dry water years, as many conveyance systems will be at capacity, and overflow and bypass will occur, as well as increased leakage and consumptive use by natural vegetation. During times of drought, water application and management is more conservative, overflow and bypass will be lower, and efficiencies are assumed to be higher, especially for surface water. For the 2019 water year, we used the same efficiency values as Thiros and others (1996). For the 2020 water year, we used higher efficiency, to reflect improvements in the conveyance and delivery systems (table 9), as well as conservation of water due to limited availability in the valley.

For recharge from irrigation return flow, we used numbers comparable to those of Thiros and others (1996). For the 2019 water year, we assumed that the percentage of recharge was slightly lower than that of the 1990s, due to changes in irrigation practices (switching from flood irrigation to pivots or wheel-line irrigation to pivots). For the 2020 water year, we assumed a smaller percentage of recharge due to decreased application to reflect the limited availability of water.

For this study, we did not calculate domestic water discharged to septic systems and infiltration of unconsumed landscape irrigation water by individual valley area, as domestic water recharge is relatively small compared to the total water recharged in the valley. Based on the same use data as listed in the Groundwater Pumping section, we calculated the valley-wide indoor use, which equates to a valley-wide septic recharge of 66 ac-ft/yr. Based on the average outdoor use and an infiltration amount of 20%, the average recharge from landscape watering for the entire valley would be about 44 ac-ft/yr.

Recharge from streams and adjacent mountains was assumed to be comparable to that of previous years. To reflect this, we applied the same methods used to create input for the Thiros and others (1996) MODFLOW model, which is based on precipitation quantity.

### Subsurface Inflow

Estimates of subsurface inflow were derived from the inputs for the USGS model (Thiros and others, 1996) and checked against Terra, a model based on a Thornwaite soil-water balance (Abatzoglou and others, 2018). For the Terra estimates, subsurface inflow was assumed to be equivalent to recharge, which was estimated by summing all soil moisture that exceeded the calculated soil field capacity for the regions of interest.

Thiros and others (1996) used a simple linear relationship between precipitation and subsurface inflow. When we extended the time interval of the MODFLOW model, we encountered

**Table 8.** Yearly streamflow estimates aggregated to major areas of Juab Valley and adjusted for different years. See A6 for the watersheds used in each aggregated area.

Valley Area	StreamStat Median			Adjusted for 2019			Adjusted for 2020		
	Non-Irrigation Season (ac-ft/yr)	Irrigation Season (ac-ft/yr)	Annual Flow (ac-ft/yr)	Non-Irrigation Season (ac-ft/yr)	Irrigation Season (ac-ft/yr)	Annual Flow (ac-ft/yr)	Non-Irrigation Season (ac-ft/yr)	Irrigation Season (ac-ft/yr)	Annual Flow (ac-ft/yr)
Mona East	2100	6700	8800	1100	16,500	16,900	2400	3300	5900
Mona West	400	1800	2200	200	4400	4200	400	900	1500
Nephi East	7700	20,900	28,600	4200	51,100	54,800	8800	10,300	19,300
Nephi West	600	1700	2200	300	4100	4200	600	800	1500
NE Total	9800	27,600	37,400	5300	67,600	71,700	11,200	13,600	25,200
NW Total	1000	3500	4400	500	8500	8400	1000	1700	3000
North Total	10,800	31,100	41,800	5800	76,100	80,100	12,200	15,300	28,200
Levan East	5000	12,200	17,200	1200	19,500	19,900	2600	3900	7000
Levan West	500	1200	1700	100	1900	1900	300	400	700
South Total	5500	13,400	18,900	1300	21,400	21,800	2900	4300	7700
Grand Total	16,300	44,500	60,700	7100	97,500	101,900	15,100	19,600	35,900
	Adjustment Ratios		Temporal	1.14	0.49	0.67	0.55	2.45	1.92
			South	0.45	0.65	0.60	0.45	0.65	0.60

precipitation values that resulted in zero and negative values for recharge from the mountain blocks. We can assume that the valley does not contribute water to the Wasatch Range or San Pitch Mountains based on the potentiometric gradient and relative proportions of groundwater use and recharge. To eliminate zero and negative recharge values, we estimated a best-fit exponential relationship between mountain precipitation from PRISM and the flux specified for the original time steps in the model (figure 45).

## Discharge

### Groundwater Pumping

Thiros and others (1996) estimated well discharge to be the largest source of discharge in Juab Valley. Groundwater pumping has increased significantly since the early 1990s due to increased industrial use, acreage under irrigation, population (especially in Mona and Nephi), and water-usage efficiencies. Our approach examined the spatial and temporal variation in groundwater pumping for Juab Valley.

We estimated the spatial distribution of well pumping and water use in Juab Valley using records from the Utah Division of Water Rights, the Utah Division of Water Resources, and Monte Carlo methods. First, we examined each ground-

water water right in the valley, focusing on the proof of beneficial use. When available, we noted the documented rate of pumping for each well and the place of use. We also noted the dominant use type for each well, and if multiple wells were assigned to the same water right. We compared these numbers with relevant USGS estimates.

To estimate both the total pumping for the valley and seasonal variations in pumping, we used a combination of well pumping measurements reported to the Utah Division of Water Rights and refined by the Utah Division of Water Resources, and a pumping model based on well pumping functions. If pumping data were available for the well, the median monthly pumping rate was used for that well. This rate was used because pumping rates were not reported for all relevant years. Because they are required to report use data, we used pumping measurements reported for the eight active municipal wells examined in this study. We did not include inactive municipal wells in our estimates.

If actual pumping measurements were not available, then monthly pumping values for each well were estimated using pumping functions. A function to estimate monthly water use per well was created for each use type. All the functions included a sinusoidal scaling function that decreased use in the winter and increased use during the peak demand of the

**Table 9.** Groundwater recharge in Juab Valley from distribution-system loss and unconsumed irrigation return flow. See Thiros and others' (1996) table 3 for comparison.

Location	Year	Water Diverted for Irrigation		Irrigation Water Available for Use		Irrigation Water Available for Crop Use (ac-ft)	Recharge from Water Diverted for Irrigation (ac-ft)	Irrigation Water that Recharges Groundwater (%)	Irrigated Area (ac)	Crop Consumptive Use (ac-ft)	Water Available for Crop Use - Crop Consumptive use (ac-ft)
		Groundwater (ac-ft)	Streamflow (ac-ft)	GW <sup>1</sup> (%)	SW <sup>1</sup> (%)						
<b>Northern Part</b>											
Mona Area	1990-92	5100	8000	70%	50%	7600	2780	25%	4200	8400	-800
Nephi Area	1990-92	12,900	16,100	70%	50%	17,100	6100	21%	7200	14,400	2700
Total	1990-92	18,000	24,000			25,000	9000	22%	11,400	23,000	1800
Mona Area	2019	1800	16,500	70%	50%	9500	3700	20%	3425	6900	2600
Nephi Area	2019	5100	51,100	70%	50%	29,100	10,100	18%	10,436	22,500	6600
Total	2019	6900	67,600			38,600	13,800		13,861	29,400	9200
Mona Area	2020	5200	3300	90%	80%	7300	1200	14%	3430	5500	1800
Nephi Area	2020	15,100	10,300	90%	80%	21,800	3000	12%	10,440	20,900	900
Total	2020	20,300	13,600			29,100	4200		13,870	26,400	2700
<b>Southern Part</b>											
Levan Area	1990-92	8400	12,400	70%	50%	9700	4300	24%	7400	15,000	-5300
Levan Area	2019	3800	19,200	70%	50%	12,300	4600	20%	7100	15,020	-2720
Levan Area	2020	11,400	3900	90%	80%	13,400	2100	14%	7100	10,000	3400
<b>Valley Total</b>											
	1990-92	26,400	36,400			34,700	13,300		18,800	38,000	-3500
	2019	10,700	86,800			50,900	18,400		20,961	44,420	6480
	2020	31,700	17,500			42,500	6300		20,970	36,400	6100

<sup>1</sup>GW and SW are groundwater and surface water, respectively.

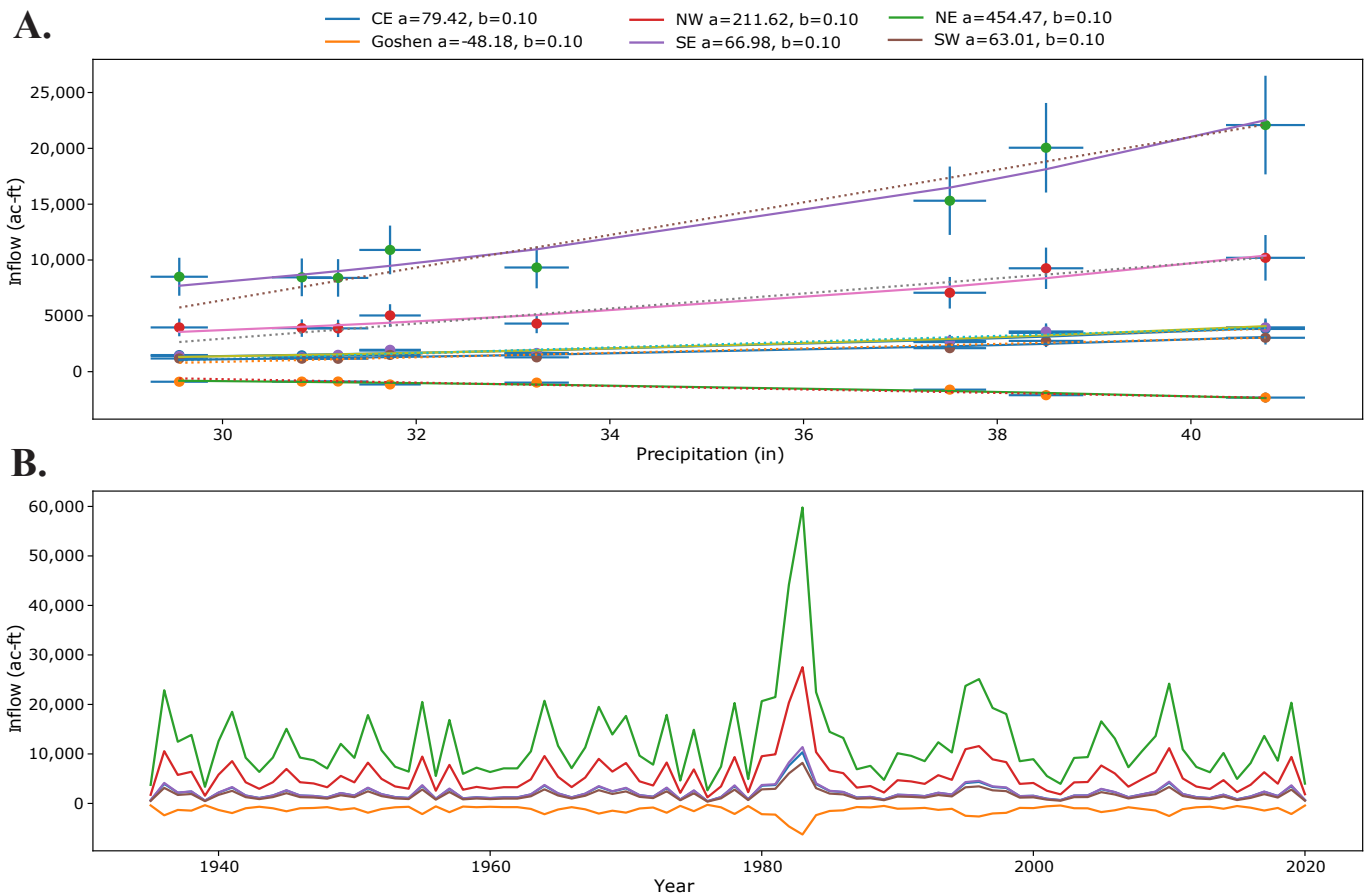


**Figure 45. A)** Exponential relationship between precipitation and subsurface inflow (solid lines) for each area of subsurface input. Original linear relationship from Thiros and others (1996) is shown as a dashed line. **B)** Resulting time-series based on the exponential relationships in A. CE = Central east south of Nephi and north of surface water divide, NE = East side of valley north of Nephi, NW = West side of valley south of Long Ridge, Goshen = Long Ridge area where groundwater is leaving the valley, SE = Southeast side of valley, south of the surface water divide, SW = Southwest side of the valley, south of the surface water divide.

summer months. To account for unmeasured variability in monthly pumping, we created an informed normal distribution for each function, where values were selected from the distribution for each month. The normal distributions were “informed,” meaning that they were assigned means, standard deviations, and limits based on available information for that well type. For the irrigation and stock categories, values selected from the normal distributions represented the percent of time that a well was pumping for each month. The range of values for these distributions was set to between 0% (no pumping that month) and 100%, when the well was pumped for the entire duration of the month. We determined the mean and standard deviation of these pumping duration percentages from drawdown observations in adjacent wells, from conversations with well operators, and from available pumping records. For the domestic wells, the normal distributions were based on the range of possible water use values derived from the Utah Division of Water Resources.

Agricultural well pumping estimates were based on a pumping function. Irrigation wells were assigned a pumping rate of zero for the months of January, February, March, November, and December. If the well had a defined water right in acre-

ft per year, we assumed that the well operator put the entire water right to beneficial use and optimized the pumping duration to reflect that water right and distributed pumping use across the active pumping months using a sinusoidal scaling factor. If a water right had multiple wells, we divided the right evenly across those wells, unless evidence in the water right documentation suggested otherwise. For wells where water rights only limited the pumping rate in cfs, we estimated the pumping duration using an informed normal distribution with an average of 50% and a standard deviation of 30%, meaning that during the peak month of July, the average irrigation well is operating 50% of the time, with some wells operating more frequently and some wells operating less frequently. For each month in the active pumping season, the pumping duration was scaled with the seasonal sinusoidal function and multiplied by the number of days in the month and the well pumping rate.

We estimated pumping from stock wells using a similar technique, except a log-normal function was applied using a mean peak pumping duration of 5% and with all months considered active pumping months. The log-normal function was applied to match the large quantity of wells that only pump part of the year, whereas only a few wells pump more frequently for stock.

Estimates of domestic well pumping should reflect estimates of water use. Water use per household depends on the number of people per household and the acreage of lawn surrounding each home. U.S. Census (2020) data indicate an average of 3.39 people per household in the rural regions of Juab Valley, where individual wells are the water source. This density is based on data from 2010 census blocks whose centroids do not overlap the current retail culinary water service areas (UGRC, 2021). A total of 1019 people and 301 housing units were in areas not serviced by the city. The total population and housing counts for Juab Valley in 2010 were 9235 and 2993, respectively. These counts were cross-checked and verified with 2010 service data provided by the Utah Division of Water Rights. We estimated the domestic indoor water use for a home in Utah by using the linear relationship of 32.1 multiplied by the number of people per home plus 88.4 for indoor water use, which for the rural Juab Valley area is 197 gallons per home per day (Klotz and Hasenyager, 2010). Outdoor water use is a function of watering area size, and for our estimates, we used 648 gallons per household per day, which is the quantity for watering areas between 0.25 and 0.5 acres. Based on these estimates, the average single-home domestic well in Juab Valley needs to pump about 845 gallons of water per day.

The Monte Carlo function used to estimate the domestic pumping of groundwater consisted of a value randomly selected from a normal distribution and multiplied by the sinusoidal

scaling function for each of the irrigation months in the year (April through October). The mean and standard deviation of the normal distribution used in the estimate function were 648 and 442 gallons per home per day, respectively (Klotz and Hasenyager, 2010). During non-irrigation months, pumping was estimated based on a random selection of a value from a normal distribution that represents indoor use, having a mean of 197 gallons per day (average indoor water use) and a standard deviation of 100 gallons per day.

We interpolated the resulting estimates of spatial distribution of pumping by conducting a kernel density interpolation. Kernel density interpolation uses point density and point values to determine the magnitude-per-unit area of a point feature. The resulting raster of interpolated pumping rates shows the acre-ft of water pumped per year per acre.

We examined how groundwater use changed over time, focusing on data recorded by the USGS (Smith and others, 2019). Plotting groundwater pumping and average precipitation over time shows an inverse relationship, where less available precipitation causes greater amounts of pumping (figure 46). About 71% of the variance in yearly groundwater pumping can be explained by variance in precipitation. As documented in previous sections, groundwater use has increased an average of 360 ac-ft/yr since 1994. We removed the linear increase of the groundwater use over time to better model the relationship

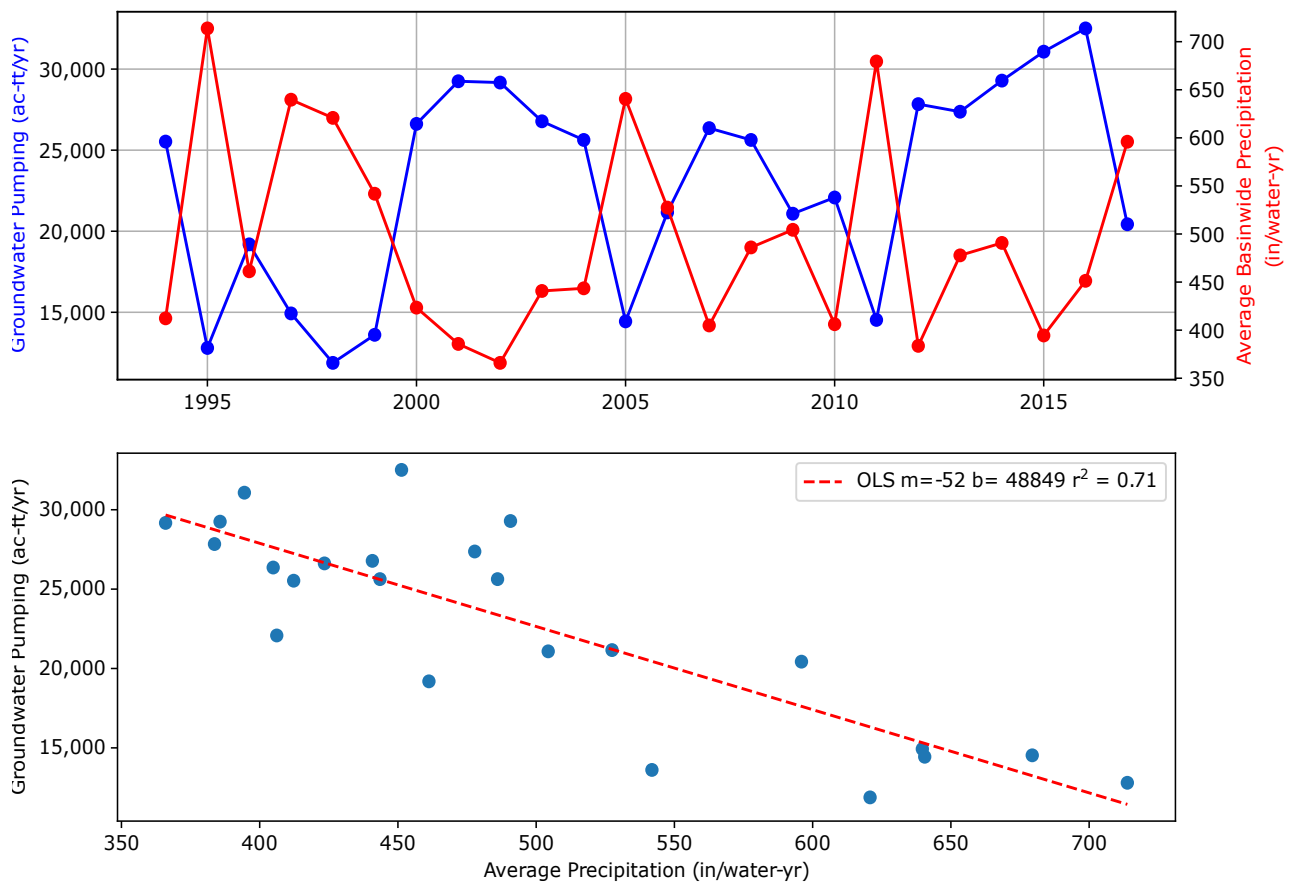


Figure 46. Relationship between valley-wide groundwater pumping and precipitation.

between precipitation and pumping. Next, we conducted an ordinary least squares regression on the PRISM precipitation data for the entire basin and the USGS pumping data. Given a specified year value and PRISM precipitation data, we can estimate annual pumping within about 3000 ac-ft of the values reported by the USGS.

### Flow to Goshen Valley

Estimates of groundwater flow to Goshen Valley are based on Darcy's Law (Freeze and Cherry, 1997):

$$Q = kA \frac{dh}{dl} \quad (3)$$

where:

- Q = groundwater flow (volume/time)
- A = cross sectional area (area)
- dh/dl = hydraulic gradient (length/length)
- k = hydraulic conductivity (length/time)

Groundwater-level contours at the northern end of the Juab Valley decrease toward Long Ridge, suggesting interbasin flow from Juab Valley north through Paleozoic carbonate rocks to Goshen Valley. Interbasin flow estimates based on Darcy's Law require hydraulic gradient, hydraulic conductivity, and an estimate of effective cross-sectional area of flow. Our potentiometric surface maps indicate a hydraulic gradient of 0.06 near the Juab–Goshen Valley boundary.

Well data were used for estimating hydraulic conductivity, while geologic data were used to estimate cross-sectional area of flow. Only two wells were drilled in the volcanic rock, both of which are in Goshen Valley (well identification numbers 29683 and 29422). Specific capacity data from these wells indicate that the transmissivity of the volcanic material ranges from 5 to 20 ft<sup>2</sup>/day. To calculate the cross-sectional area of flow, consider that Long Ridge is made up of volcanic breccia 13,000 ft to the south of Currant Creek and fractured Paleozoic carbonates 26,000 ft to the north of Currant Creek (McKean and others, 2015). Assuming an aquifer thickness of about 1000 ft (McKean and others, 2015), the hydraulic conductivity of the volcanic rocks is about 0.005 to 0.02 ft/day. Assuming a cross sectional area of 12,900,000 ft<sup>2</sup>, the effective interbasin flow from Juab Valley to Goshen Valley through the volcanic rocks would be about 100 ac-ft/yr.

Most of the groundwater flow from Juab Valley to Goshen Valley is likely through the Paleozoic rocks north of Currant Creek and south of the surface water divide between Utah Valley and Juab Valley (south of Santaquin). There are several high-angle faults in these rocks that strike perpendicular to the potentiometric surface contours (i.e., parallel to the estimated

groundwater flow direction); these faults could act as fracture conduits. This part of the ridge is 26,000 ft long, and we can assume that most of the permeability is in the top 1000 ft of the rock, resulting in a cross-sectional area of 26,000,000 ft<sup>2</sup>. Hydraulic conductivity of fractured bedrock is approximately 0.01 to 0.1 ft/day (Fetter, 1988), resulting in 100–1500 ac-ft/yr of flow to Goshen Valley from Juab Valley.

### Springs and Seeps

For the Mona area, we estimated changes in springs and seeps using the Mona Reservoir model. For the other areas including Chicken Creek, we used the results of the updated MODFLOW model to estimate current discharge values of springs and seeps. See the MODFLOW model section for information regarding how this model was extended.

### Evapotranspiration

Evapotranspiration was calculated using multiple methods, to allow for cross validation and comparison. We measured evapotranspiration from groundwater of the valley using SSEBop (Senay and others, 2013) estimates of areas mapped as wetlands and checked those values using Terra estimates (Abatzoglou and others, 2018).

Two eddy covariance stations were deployed for the study, one in an agricultural station near Nephi and one in a wetland south of Mona Reservoir. Each station was equipped with devices manufactured by Campbell Scientific, including a KH20 hygrometer, a CSAT3B+ 3D sonic anemometer, a CS106 barometer, an EE181 temperature-humidity probe, and a CR6 datalogger. Neither station had telemetry. Due to delays related to the programming of the stations, as well as issues with corrupt solid-state memory, the number of surface measurements was very limited. The limited data availability led us to rely primarily on estimates from SSEBop (Senay and others, 2013).

## Results and Discussion

We estimated the groundwater budget for Juab Valley for water years 2019 and 2020 (table 10). The water budget was in surplus by about 21,200 ac-ft in water year 2019 and in deficit by about 16,500 ac-ft for water year 2020. Water year 2019 had significantly higher precipitation than average, whereas 2020 had below-average precipitation (figure 2). Well pumping, recharge rates, and evapotranspiration all depend on the amount of precipitation (Thiros and others, 1996).

### Recharge

Recharge in Juab Valley is driven by precipitation, and all the recharge inputs specified in the MODFLOW model are ultimately derived from precipitation. Based on the geographical distribution of precipitation, and the results of groundwater

models (Thiros and others, 1996), the most significant recharge to the Juab Valley aquifer system is from the Wasatch Range to the east of the valley as ephemeral stream loss and subsurface inflow. This is also the most poorly constrained value in the budget. Terra (Abatzoglou and others, 2018) estimated recharge from the Wasatch Range for 2019 to be 23,000 ac-ft/yr, which is close to the 27,600 ac-ft/yr derived from the Thiros and others (1996) relationship presented on figure 45. However, the Terra estimate was zero for the following year, which is much lower than the estimate of 4700 ac-ft/yr used as specified flux input for the extended model.

The estimated infiltration rate for the valley floor was 4% of the precipitation estimated from Daymet, totaling 7920 ac-ft in 2019 and 2960 ac-ft in 2020. We verified this infiltration rate using soil moisture change estimates from the Terra model (Abatzoglou and others, 2018). This value was also estimated using the relationship established by Thiros and others (1996) for the setup of their model. Like with the other recharge sources, seepage from infiltration related to irrigation return flow and streams was estimated using linear relationships between recharge and precipitation, as described in Thiros and others (1996).

Unlike Thiros and others (1996), we derived our non-irrigation streamflow measurements from StreamStats. The most notable difference between the StreamStats estimate and the

estimate derived from Thiros and others (1996) was values for 2019 were lower than 2020 values (table 10), which is likely a result of calculation of precipitation during the year versus streamflow during that year. Because the Thiros and others (1996) relationship is based on yearly precipitation, an especially wet November and December may artificially inflate non-irrigation streamflow estimates.

## Discharge

**Well discharge:** More water is pumped during dry years to compensate for the lack of precipitation and divertible surface flows, as seen in the groundwater use record from the USGS. Low points in the use record correspond to years of higher-than-average precipitation and periods of higher groundwater pumping correspond to periods of drought. Regressing groundwater pumping since 1994 and PRISM precipitation (ac-ft/water year) together produces an r-squared value of 0.71 (figure 46), and a slope and intercept of -0.052 and 46,994, respectively. With the addition of a temporal correction, groundwater pumping was estimated with an r-squared of 0.8 for all pumping and 0.82 for irrigation pumping (figure 47). Based on that relationship, the total groundwater pumping in Juab Valley was  $18,000 \pm 3000$  ac-ft for the 2019 water year and  $37,000 \pm 3000$  ac-ft for the 2020 water year (table 10, figure 47). The estimate for irrigation pumping is 17,000

**Table 10.** Groundwater budget for Juab Valley. Values are in units of acre feet.

	USGS			UGS						Data Source
	1993 (Table 6)			2019			2020			
Recharge	North	South	Valley	North	South	Valley	North	South	Valley	
Nonirrigation-season streamflow loss	14,580	2920	17,500	5800	1340	7140	12,200	2800	15,000	StreamStats
Unconsumed irrigation water and distribution loss	10,000	5280	15,280	13,800	4600	18,400	4200	2100	6300	11-18% of GW <sup>1</sup> and SW <sup>1</sup> diversion (Table 9)
Irrigation-season streamflow loss	910	0	910	960	0	960	450	0	450	Relationship derived from Thiros and others (1996)
Precipitation Infiltration	4580	3240	7820	5040	2880	7920	1920	1040	2960	4% of Daymet Precip
Eastern subsurface inflow	20,910	3240	24,150	23,900	3700	27,600	4700	660	5360	Relationship derived from Thiros and others (1996)
Western ephemeral stream loss and subsurface inflow	7950	2840	10,790	8400	2410	10,810	3000	700	3700	StreamStats
<b>Total recharge</b>	<b>58,930</b>	<b>17,520</b>	<b>76,450</b>	<b>57,900</b>	<b>14,930</b>	<b>72,830</b>	<b>26,470</b>	<b>7300</b>	<b>33,770</b>	
<b>Discharge</b>	<b>North</b>	<b>South</b>	<b>Valley</b>	<b>North</b>	<b>South</b>	<b>Valley</b>	<b>North</b>	<b>South</b>	<b>Valley</b>	
Wells										
Total	12,080	8290	20,370	12,000	6000	18,000	24,000	13,000	37,000	Well model
Springs	0	380	380	0	800	800	0	800	800	Water rights
Currant Creek Seepage	13,870	0	13,870	13,100	0	13,100	6300	0	6300	Reservoir balance (table 6)
Seepage to Mona Reservoir	8880	0	8880	2200	0	2200	7200	0	7200	Reservoir balance (table 6)
Seepage to Chicken Creek Res Reservoir	0	3640	3640	0	2900	2900	0	2800	2800	Updated MODFLOW model
Evapotranspiration	5800	1660	7460	7600	3900	11,500	5300	2000	7300	Wetland SEEBop
Subsurface outflow (mostly to Goshen)	1890	0	1890	800	0	800	200	0	200	
<b>Total Discharge</b>	<b>42,520</b>	<b>13,970</b>	<b>56,490</b>	<b>35,700</b>	<b>13,600</b>	<b>49,300</b>	<b>43,000</b>	<b>18,600</b>	<b>61,600</b>	
<b>Storage Change</b>	<b>16,410</b>	<b>3550</b>	<b>19,960</b>	<b>22,200</b>	<b>1330</b>	<b>23,530</b>	<b>-16,530</b>	<b>-11,300</b>	<b>-27,830</b>	

<sup>1</sup>GW and SW are groundwater and surface water, respectively.

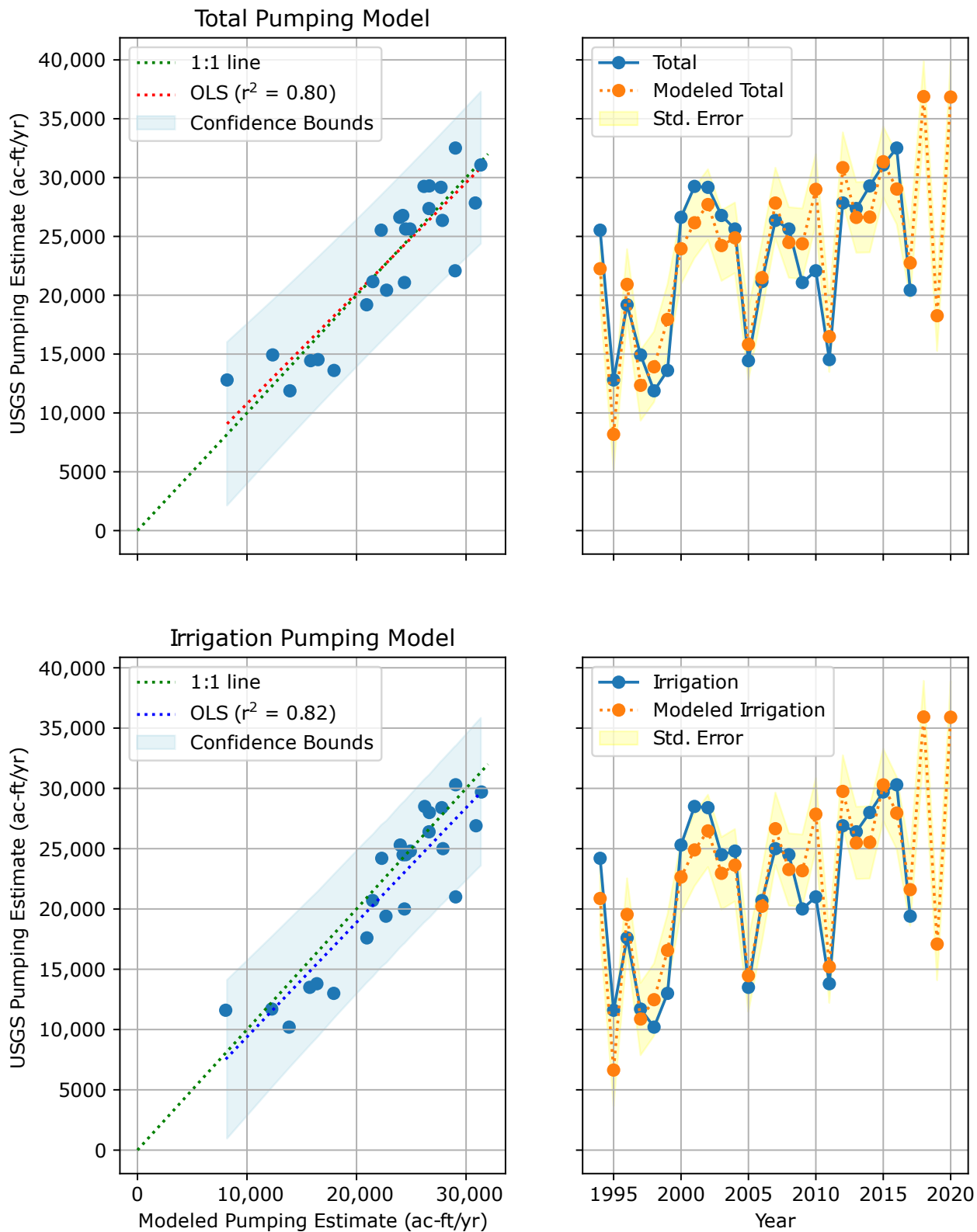


Figure 47. Regression model results for temporal groundwater pumping model.

$\pm 3000$  ac-ft for the 2019 water year and  $36,000 \pm 3000$  ac-ft for the 2020 water year (figure 47). Based on the results of a Mann Kendall analysis of pumping data from 1994 to 2017 reported by the USGS, groundwater pumping increased at a rate of approximately 362 acre-ft/yr.

For the spatial pumping model, we identified 345 actively pumped wells in Juab Valley (figure 48). There may be additional wells that are not pumped, that have not been documented by the Utah Division of Water Rights, or were drilled after this study. Of the 345 wells, 172 were domestic wells, 97 were irrigation wells, 58 were stock wells, 8 were municipal water wells, and the remaining wells were industrial and other use wells. Although some had multiple uses, the wells were organized by their dominant use. Based on estimates from the Monte Carlo pumping model, stock pumping is likely underestimated by the USGS. Assuming the average well that waters livestock only pumps 10% of the time during the peak month of July, and less frequently during the other months in the year, then the most probable amount of stock use in Juab Valley is 200 ac-ft/yr. Domestic use was estimated at 270 ac-ft/yr. Pumping density (figure 48) generally matches areas of most significant groundwater decline (figure 19). Pumping density is highest around Nephi, which corresponds to the water use reported by the city (Utah Division of Water Rights, 2020) and the distribution of large irrigation wells in that area. Based on the spatial model, the total calculated average well discharge for Juab Valley in 2020 was 32,300 ac-ft/yr, which is close to the value of 37,000 ac-ft/yr estimated from USGS data. Agricultural wells accounted for more than 90% of the total groundwater pumped in Juab Valley for the past 20 years. The estimated average irrigation pumping from this model was 30,200 ac-ft/yr.

**Evapotranspiration of groundwater:** Valley-wide evapotranspiration from wetlands (phreatophytes and shallow groundwater) was 11,500 ac-ft and 7300 ac-ft for 2019 and 2020, respectively (table 10). Based on analysis of remotely sensed data using SSEBop (Senay and others, 2013), the rate of evapotranspiration from groundwater is declining over time (figure 49). Mann Kendall analysis of the evapotranspiration trends indicates declines of 130 and 100 ac-ft/yr in the north and south parts of the valley, respectively. These estimates agree with our observations of shrinking discharge areas (figure 23). Our estimates for evapotranspiration are comparable (figure 49) to estimates derived from the extended USGS model (Thiros and others, 1996).

**Subsurface outflow:** Based on our conceptual groundwater model, potentiometric surface lines, and groundwater age data, groundwater is moving from Juab Valley to Goshen Valley, most likely through Long Ridge near Currant Creek. However, the quantity of water moving through the ridge is relatively small (table 10). Subsurface outflow from Juab Valley to Goshen Valley, based on Darcy flux, is about 800 ac-ft/yr, which is comparable to values around 1000 ac-ft/yr indicated by Thiros and others (1996). This flow likely decreases

with available precipitation, and has the potential to become zero or negative, depending on the amount of drawdown in northern Juab Valley.

**Springs and seepage:** Stable isotope and hydrograph analyses indicate that about 80% of the flow in Currant Creek is derived from groundwater seepage. Based on our Mona Reservoir balance, total seepage to Currant Creek and Mona Reservoir was about 15,300 ac-ft in water year 2019 and 13,500 ac-ft in water year 2020. Seepage to reservoirs, springs, and streams estimated using the extended model was about 4000 ac-ft lower than estimate via the reservoir model. The model indicates a decrease in seepage over time. These estimates are supported by observed changes in water area coverage (figure 23).

### Storage Change

Many changes in the Juab Valley hydrologic system have occurred since the USGS conducted their study (Thiros and others, 1996). Table 11 lists a timeline of water events in Juab Valley, including notable events after 1993. Relevant events include the start of the Young Living Lavender Farm in 1995, many farms shifting to sprinkler irrigation in 1998–2002, the completion of the Currant Creek Power Plant, and the disappearance of the Columbia spotted frog. Since the USGS study (Thiros and others, 1996), several large new wells have begun operation, including two east of Mona (WINs 29701 and 29439) and one immediately southwest of the mouth of Willow Creek canyon (WIN 24640), as well as Mona City's municipal wells (WINs 18777 and 25778).

Groundwater storage increases when the groundwater is surplus and decreases when it is in deficit. One possible contributing factor to the observed changes in storage is the changes in irrigation practices. Increases in irrigation efficiency from flood to pivot-based irrigation can increase crop production. However, this change can also decrease irrigation return flows. Increase in crop production is tied to increases in crop consumptive use. Groundwater pumping in Juab Valley has increased over time at an average rate of 360 acre-ft/yr, which is approximately equal to the average rate of storage change estimated from changes in groundwater levels. Most of the change in groundwater pumping is from increases in agricultural pumping, despite improvements in irrigation efficiency, although pumping from new municipal use and power generation has also occurred.

Operation of the Currant Creek Power Plant is not likely the primary reason for significant declines in groundwater storage and the flow of Currant Creek. The power plant was designed to be extremely efficient and uses a small amount of water relative to other power plants and municipal water providers. The cooling system is a closed-loop system and evaporation as a result is minimal. The plant pumps water from wells on the east side of Juab Valley using water rights exchanged from

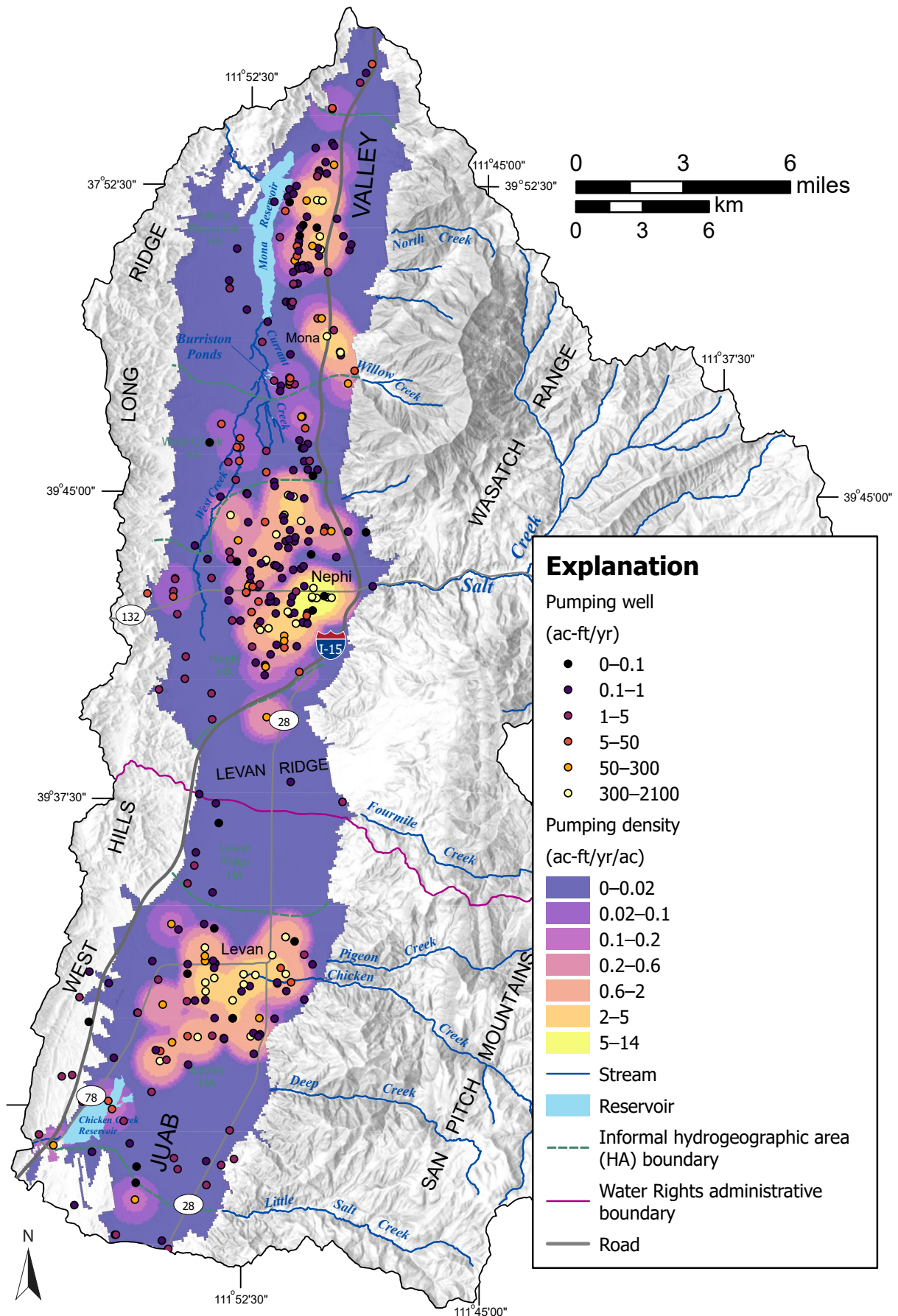


Figure 48. Distribution of pumping intensity estimated using spatial groundwater pumping model.

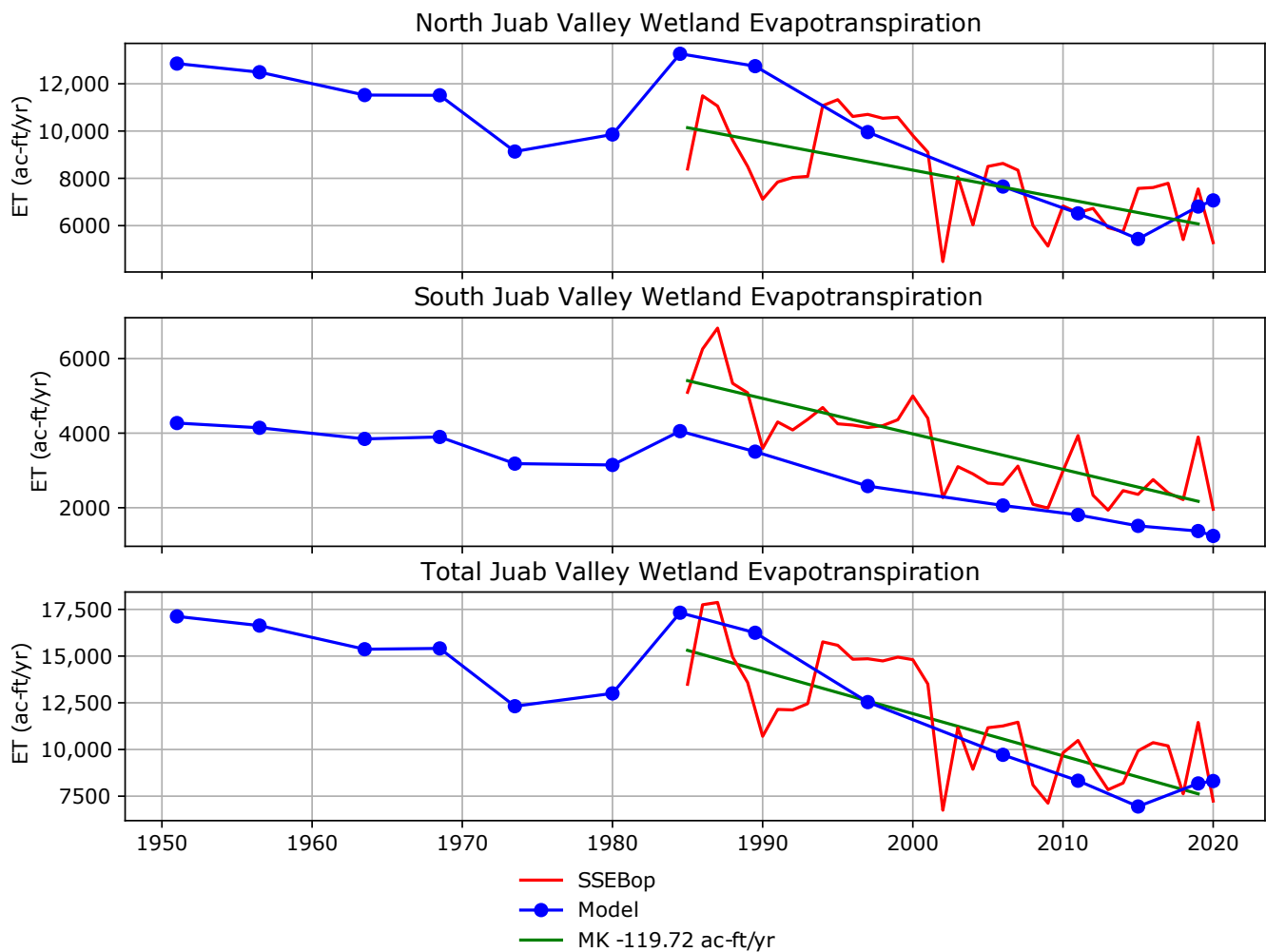


Figure 49. Estimated groundwater evapotranspiration over time.

Currant Creek. Based on our conceptual groundwater flow model, the wells do capture water that would otherwise end up in Currant Creek.

Natural groundwater discharge and aquifer storage have been decreasing in Juab Valley since the last groundwater study in 1993 (Thiros and others, 1996). Average discharge loss from Currant Creek is about 250 ac-ft/yr, in addition to loss of evapotranspiration from areas of phreatophytes, which is a total of 230 ac-ft/yr (figure 49), and the loss in storage from the aquifer system, which is 6600 ac-ft/yr. Together, these estimates indicate a long-term average groundwater-budget deficit of 7080 ac-ft/yr.

Based on the estimated decline in groundwater storage, stream discharge, and evapotranspiration, there is a general deficit in the groundwater budget. Whereas 2019 showed surplus of available water, the average condition of the groundwater budget is a deficit. This deficit is on average equivalent to 7080 ac-ft/yr, which is the sum of the above-mentioned changes. The deficit could be as high as the estimated deficit for the groundwater budget in 2020, which was 27,830 ac-ft (table 10).

The estimated surplus in the 2019 groundwater budget was 21,200 ac-ft (table 10). Subsurface inflow into the eastern part of the valley is very poorly constrained and is based on relationships derived from specified flux input data for the calibrated transient Thiros and others (1996) model. Intermittent relatively wet years like those observed in 2019 can recharge the aquifer to some extent, but the declining trends will likely continue. Long-term average subsurface flow to the eastern part of Juab Valley has likely been lower since 1993, based on overall declining precipitation. Not all the groundwater-budget surplus recharged the valley-fill aquifer; a significant but unmeasured part likely flowed through the Chicken Creek Reservoir gate.

The groundwater model indicated storage changes comparable to changes observed in wells (figure 50). Average groundwater storage change from 1992 to 2020 based on the extended model is 4400 ac-ft/yr for the north and 2800 ac-ft/yr for the south, for a total of 7200 ac-ft/yr, which is 600 ac-ft higher than storage estimates from groundwater level changes (figure 51). Although some wells showed elevation offset from the modeled values, the relative changes in water level over time

**Table 11.** Water-related events in history of Juab Valley.

Date	Event	Source
1873	First dam completed (Mona/Nebo Reservoir)	Utah State History, 2010
10/20/1877	Goshen Irr and Canal Co. files suit against Mona Canal Co	Utah State History, 2010
6/27/1879	Mona Canal Company assets auctioned off	<a href="#">Hardy, 2000 (Deseret News)</a>
1896	Mount Nebo Reservoir	<a href="#">Rae and Baker, 1971</a>
6/1/03	Nephi diversion canal of Salt Creek for hydro plant complete	A History of Juab County 148
10/22/07	Rowley Spring pipe completion for Nephi	<a href="#">Record for Utah Water Right 53-2</a>
7/1/41	Mona Irr Company completes concrete canal from Bear Canyon	A History of Juab County 236
4/16/47	Ditchworks initiated in Willow Creek	<a href="#">Scanned record of Utah Water Right 53-186</a>
1/12/87	Piping of Willow Creek complete	<a href="#">MISC from Utah Division of Water Rights Record 53-186</a>
1995	Young Living Lavender Farm started D. Gary Young	Daily Herald, 2018
11/15/95	<a href="#">Northern Juab Valley Ground Water Policy</a>	<a href="https://www.waterrights.utah.gov/wrinfo/policy/wrareas/area53.asp">https://www.waterrights.utah.gov/wrinfo/policy/wrareas/area53.asp</a>
10/1/00	Transition of Mona irrigation rights to municipal rights; New Mona well installed	<a href="#">Hardy, 2000 (Deseret News)</a>
1998-2002	Large shift to pivot sprinklers	Google Earth Imagery
10/31/03	Mona irrigation change application to Mona City	<a href="#">Scanned record of Utah Water Right 53-186</a>
6/20/05	Completion of Phase I of Currant Creek Power Plant	<a href="#">Power Magazine, 2006</a>
9/23/05	Power generation taken offline for completio	<a href="#">Power Magazine, 2006</a>
3/22/06	Currant Creek Power Plant fully operational	<a href="#">Power Magazine, 2006</a>
7/27/15	Mona Res dry; Current Creek didn't use water	<a href="#">Letter from Goshen Irrigation Co. to Utah Div. Water Rights (2016)</a>
2018	Last time Columbia Spotted Frog egg masses spotted in Mona area	DWR Wildlife Central Region: Keith Lawrence or Jordan Holcomb

matched well. The extended model was discretized into large time chunks of eight years, except for 2011, 2019, and 2020, so finer fluctuations in those large blocks of time were not reflected in the model. Modeled drawdown shows cells in the top layer of the model in the Levan area dried out. Modeled drawdown from 1950 to 2021 was highest in the Nephi and Levan areas, where each area had up to 55 ft of drawdown, and the Mona area had up to 20 ft of decline.

## Error Quantification

The largest potential error sources in the groundwater budget are subsurface flow from the Nebo mountain massif and out of the valley, as it is based on a rough relationship with precipitation. As with any measurement, the other components of the groundwater budget also include error.

Measured flow out of Mona Reservoir was generally within 2–5 cfs of the values reported to the Dam Safety Group at the Utah Division of Water Rights, except for two measurements in late 2019, which are about 20 cfs lower than Dam Safety estimates. The stage discharge equation had a good fit, though it is only based on five measurements. The biggest error in the downstream measurement was the quality of the manual discharge measurements, which would propagate to the stage discharge estimates. The transducer data is generally lower than dam safety measurements. Based on error in surface flow measurements, total error is estimated to be around 20% of measurement. Storage estimates of Mona Reservoir were well constrained. Our hypsometric curve

matched that of the dam engineers. The volume estimates from JRC data and the dam safety data correlated well with our measurements.

Overall, the extended groundwater model accurately predicted groundwater level changes within less than a foot in many of the observation wells that we set.

## SUMMARY

Lithologic data from 201 water well driller's logs obtained from the Utah Division of Water Rights were compiled into a well-management database and used to characterize variations in basin-fill lithology in the upper 400 ft of the Juab Valley basin-fill aquifer. The basin fill is characterized by interlayered predominantly fine-, mixed-, and coarse-grained deposits. Most deposits having uniform grain size are lens-shaped, so are not continuous over large areas, and are less than about 100 ft thick. The upper 100 ft and deposits below the valley center at all depth ranges are overall finer grained than other parts of the basin. Along the groundwater flow path from the recharge area on the upper Salt Creek alluvial fan east of Nephi, northwest to the discharge area at and around Burrison Ponds, overall grain size decreases abruptly just east of the discharge area. Groundwater flow is likely predominantly in the relatively coarse-grained interval from about 100 to 400 ft depth. The springs that supply Burrison Ponds likely occur where an erosional depression intersects this transmissive

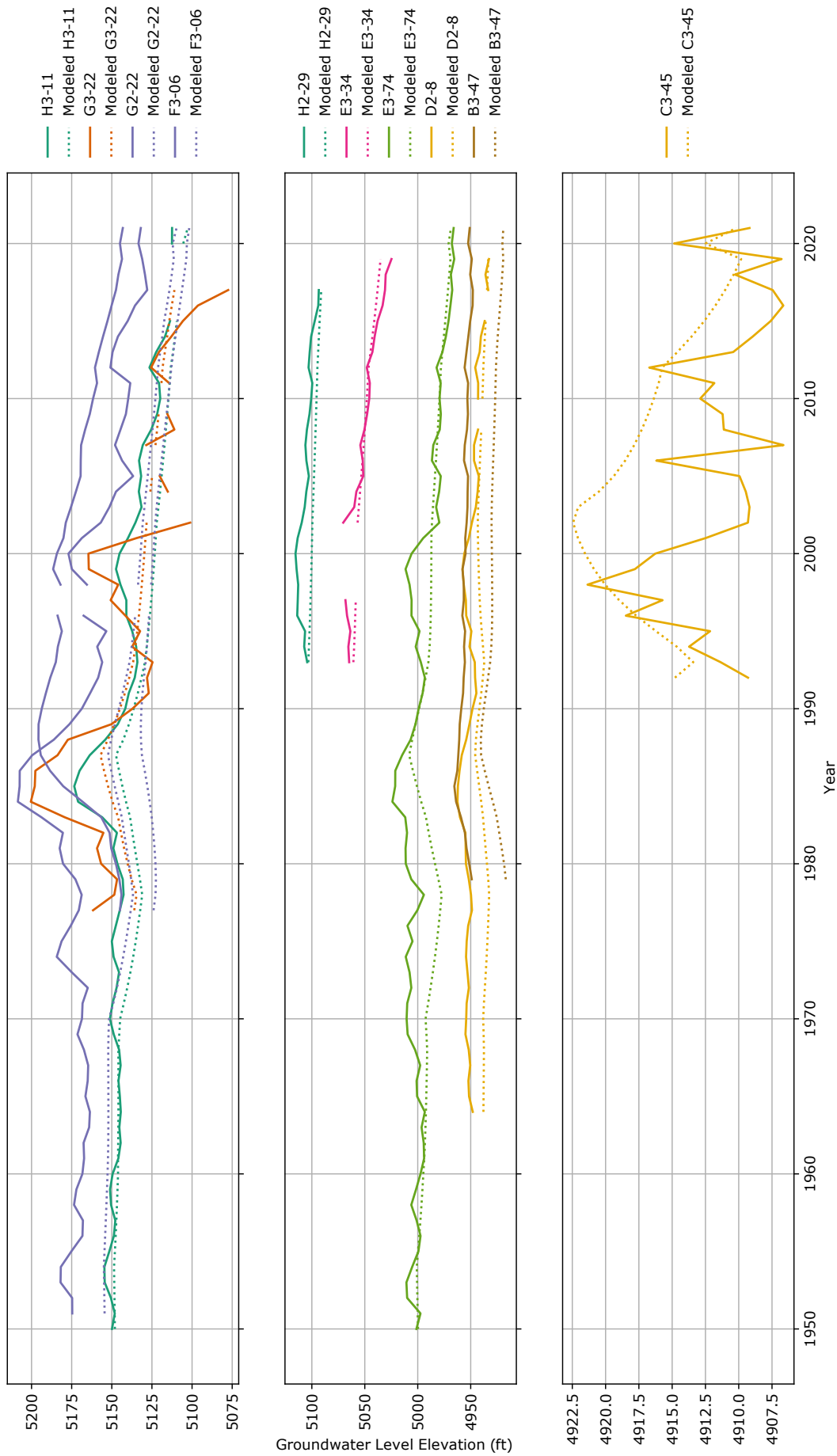
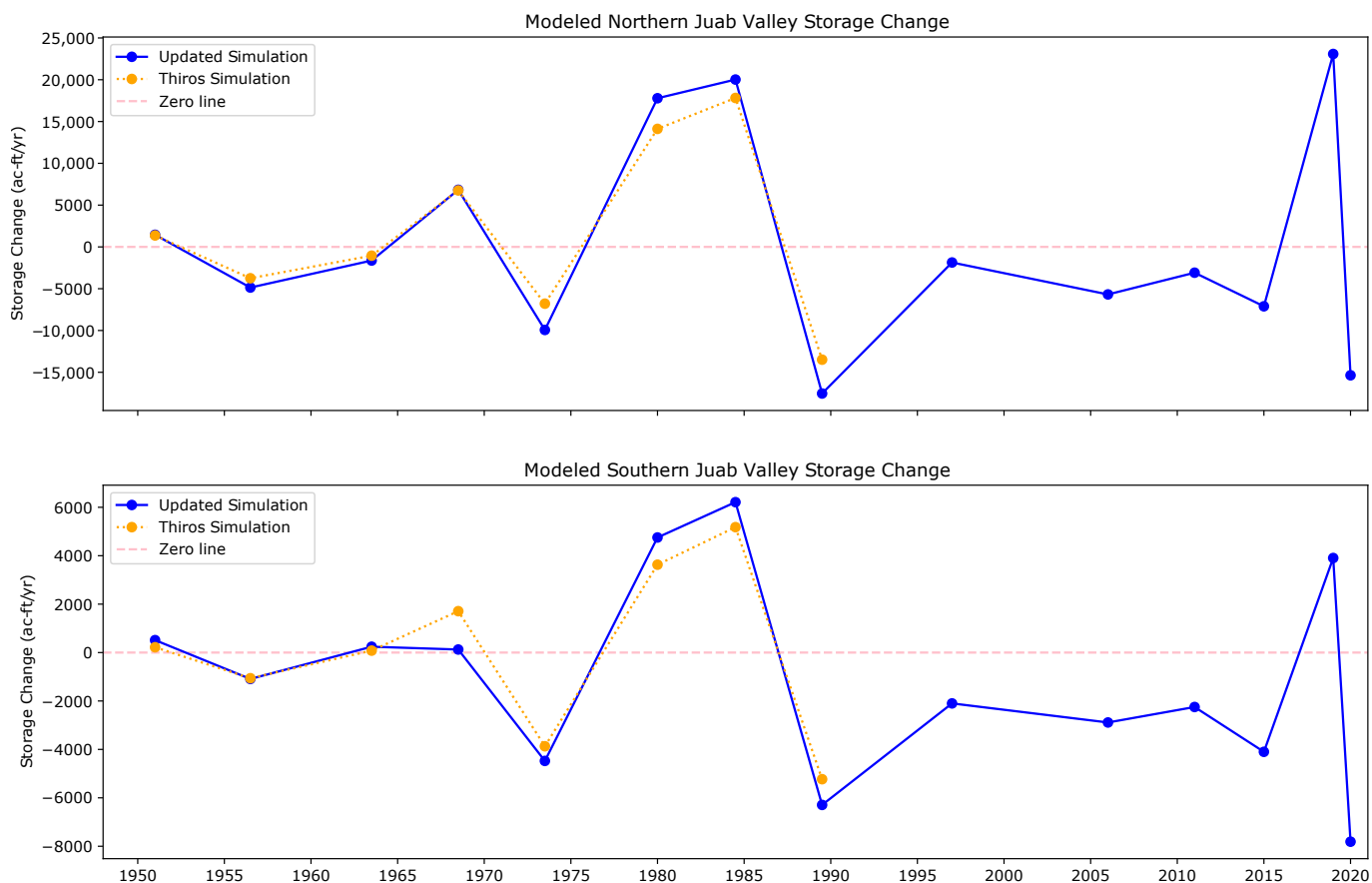


Figure 50. Hydrographs showing modeled changes (dashed) and measured changes (solid) of potentiometric surface elevation over time in select wells. See figure 9A for locations.



**Figure 51.** Modeled groundwater storage change for Juab Valley over time. Values from the updated model (solid blue) were plotted against the original Thiros and others' (1996) model (dashed orange).

zone. Along the groundwater flow path from the recharge area on the Willow Creek to North Creek alluvial fans east of Mona, west to the discharge area along the eastern margin of Mona Reservoir, overall grain size also decreases abruptly from east to west, forcing groundwater to the surface. Along the groundwater flow path from the recharge area on the Pigeon Creek and Chicken Creek alluvial fans east of Levan, southwest to the discharge area at and northeast of Chicken Creek Reservoir, overall grain size also decreases abruptly from east to west forcing groundwater to the surface, and a broad erosional depression intersects or is close to the top of the transmissive part of the basin-fill aquifer.

Well-test data from the driller's logs were used to estimate the transmissivity of the basin-fill aquifer. These rough estimates range from 14 to 116,110 ft<sup>2</sup>/day (1.3-10,787 m<sup>2</sup>/day), and the median value is 1580 ft<sup>2</sup>/day (150 m<sup>2</sup>/day). Our results are comparable to a similar effort by Thiros and others (1996) even though nearly 50 well logs available for our study did not exist for the previous work. Transmissivity is overall greatest in the proximal parts of the alluvial fans that emanate from the ranges bounding the eastern valley margin.

New gravity data collected by the UGS and previously existing data were combined with selected driller's logs and a published depth section of an east-west seismic-reflection profile through

Nephi to produce two-dimensional model profiles showing the depth and structure of the upper part of the basin fill. A prominent reflector in the middle part of the basin fill is interpreted here to represent the unconformity between younger, semiconsolidated to unconsolidated clastic basin fill above and Tertiary volcanic, volcanoclastic, and sedimentary rocks below. The basin fill above the unconformity is interpreted as the Juab Valley basin-fill aquifer, and is physically continuous with the upper 600 ft of the aquifer which is currently developed for groundwater use. An isopach map of the upper basin fill was constructed from a network of 2D gravity profiles tied to the seismic-reflection depth section. The isopach map defines a basin center that is 2000 to 3250 ft thick that trends north-south from Burrington Ponds to Levan Ridge, and trends southwest in the southern part of the study area. Gravity and isopach-contour patterns suggest structural complexity at the southern end of Mona Reservoir and below and south of Nephi. An east-west-trending bedrock ridge likely underlies the northern part of the basin along the latitude of the southern end of Mona Reservoir. The basin fill thickens to locally 2000 ft below the northern part of Mona Reservoir. Isopach contour patterns below and south of Nephi suggest a complex buried horst-graben system. This area coincides with the intersection zone between the projected trend of a Mesozoic-Cenozoic strike-slip fault zone and the Wasatch fault zone, and with the boundary zone between the Nephi and Levan segments of the Wasatch fault zone.

We measured depth to water in 157 wells throughout Juab Valley in March and early April 2015. Land-surface elevation control was from high-precision GPS or 1-m-resolution lidar. We constructed a valley-wide groundwater-level map from our measurements and 16 water levels measured by the USGS. The groundwater divide below Levan Ridge is as much as 4 miles north of its position in 1965 as determined by the USGS. Groundwater-level contours north of the divide are generally horseshoe-shaped, parallel to the eastern valley margin and convex to the north-northwest, indicating flow toward the north-northwest. Complicated contour patterns exist below and west of Nephi, an area of interspersed heavy agricultural pumping and residential development. Water-level contours at the northern end of the valley decrease toward Long Ridge, suggesting interbasin flow from Juab Valley north through Paleozoic carbonate rocks to Goshen Valley. Groundwater-level contours in eastern Levan Ridge are closely spaced and trend north-south, suggesting inflow from the Fourmile Creek drainage basin in the San Pitch Mountains and its alluvial fan along the mountain front. Groundwater-level contours below the central part of Levan Ridge form an east-west-trending saddle that defines the groundwater divide. South of the divide, contours are horseshoe-shaped and convex to the southwest indicating flow toward the southwest, with complex patterns in the agricultural-residential area southwest of Levan.

A map showing water-level changes in Juab Valley from 1993, the time of the USGS's previous valley-wide water-level survey (Steiger, 1995; Thiros and others, 1996), to 2015 was made by contouring the difference between water-level elevations for individual wells having measurements in both years. Changes ranged from -0.5 to -44 ft, excluding local anomalous values. The areas of greatest groundwater-level decline are west of Nephi, west-northwest of Levan, and northwest of Mona Reservoir. The groundwater level in one well on Levan Ridge declined by 33 ft despite its distance from the Nephi and Levan agricultural areas and few nearby wells.

Monthly monitoring of groundwater levels in unused wells in the Levan Ridge area, the southwest parts of the study area, and southwest of Burrinston Ponds shows greater detail and recent trends of water-level fluctuations. Wells on the northern and southern margins of Levan Ridge and in the southwest part of the Levan agricultural area show seasonal fluctuations related to pumping superposed on declines of 0.3 to 5 ft per year. A well in the central part of Levan Ridge near the interpreted groundwater divide declined by 2.2 ft per year. Seasonally flowing wells at the southwest end of the agricultural area southwest of the Levan area flowed during October 2017 through May 2018, after which time flow ceased and water levels decreased by as much as 17 ft during the irrigation season, and flow resumed in October 2018. Southwest of Burrinston Ponds, a well near West Creek shows seasonal fluctuations of 14 to 21 ft but four other wells to the west and northwest show only slight fluctuations.

During 2015 and 2017 we sampled 66 wells (6 flowing), 5 springs, and 12 streams for major-solute chemistry. Most water is either Mg-HCO<sub>3</sub> or mixed SO<sub>4</sub>-Cl-Ca-Mg type, and TDS of groundwater samples ranged from 232 to 2626 mg/L excluding one anomalous value, and the median value is 786 mg/L. Groundwater composition generally reflects the bedrock composition of the mountains to the east; HCO<sub>3</sub> is the dominant ion west of the Mount Nebo area in the Wasatch Range which is composed of Paleozoic carbonate rocks; SO<sub>4</sub> is the dominant ion west of the San Pitch Mountains, composed in its western part of the Jurassic Arapien Formation which includes gypsum and halite; and mixed-composition water occurs throughout the basin and in the eastern part of the valley west of the southern Wasatch Range and northern San Pitch Mountains in which carbonate, siliciclastic, and Arapien Formation rocks crop out. Statistical analysis of all major-solute data identified five distinct clusters (i.e., compositional groups) that show systematic distribution generally reflecting bedrock and basin-fill composition.

Values of the stable isotopes <sup>2</sup>H and <sup>18</sup>O generally become more depleted from east to west in the study area. More depleted values are generally associated with cooler temperatures at the time of recharge, whereas the mountains bounding Juab Valley on the west have substantially lower elevation and precipitation there would be expected to have relatively enriched stable-isotope compositions. The overall east-to-west variation may represent the presence of older groundwater that was recharged under cooler climatic conditions. Stable-isotope values of the springs that supply Burrinston Ponds and from a nearby well are similar to those in streams along the Wasatch Range front to the east and are more enriched than groundwater from nearby wells to the north and south. This anomaly may reflect a comparatively high-velocity flow path from the eastern mountain front to Burrinston Ponds. Mixing model analysis indicates that groundwater recharge in Juab Valley is most likely 78%–90% snow and 10%–22% rain.

Tritium (<sup>3</sup>H) values generally decrease from east to west, reflecting progressively greater time since recharge, consistent with the pattern observed in the stable-isotope data. Low tritium values were measured from flowing wells west of Mona (C3-19) in the Mona Reservoir–Burrinston Ponds discharge area, and from a seasonally flowing well (H2-S1) in the Chicken Creek Reservoir discharge area. Carbon-14 (<sup>14</sup>C) model ages range from about 1200 to 10,400 years for samples in the northern, western, and southwestern part of the study area; <sup>14</sup>C model ages could not be calculated for samples from the central and eastern parts of the valley near Levan and between Nephi and Mona. Modeling of the <sup>3</sup>H and <sup>14</sup>C data together show progressively decreasing ages from northeast to southwest along the flow path from the Chicken Creek–Pigeon Creek alluvial fans to the Chicken Creek Reservoir discharge area, although an abrupt increase in model age at seasonally flowing well H2-S1 indicates the addition of substantially older groundwater from greater depth.

Based on Currant Creek discharge, wetland evapotranspiration, and groundwater level measurements, the Juab Valley groundwater budget is in deficit on average of about 7080 ac-ft/yr. The biggest contributors to these declines are increased groundwater pumping over time, coupled with decreased recharge over time. Although relatively wet water years like 2019 might help contribute to groundwater recharge to the aquifer, it will not cause a complete water level recovery to levels observed prior to the 1990s. Despite groundwater discharge to Mona Reservoir, it has been completely emptied at least twice in the past decade, and if current conditions persist, this will likely happen again.

## ACKNOWLEDGMENTS

We are grateful to the numerous landowners who granted permission to access their irrigation and domestic wells for water-level measurements and sampling. David Worwoods provided invaluable information on the valley's wells and owners. Hurlow thanks Brittany Dame for collecting and organizing the well records, and for extensive fieldwork during the early stages of the project; Christian Hardwick and Will Hurlbut for collecting and processing the gravity and TEM data; Stan Smith for analyzing the 2015 groundwater stable- and radiogenic-isotope data; Ethan Payne and Emily McDermott for assuming the monthly groundwater-level duties. Thanks to the Church of Jesus Christ of Latter-day Saints and Young Living Lavender Farm for giving us access to land to take valuable measurements.

There were several key reviewers for this report. Reviews by UGS colleagues Emily McDermott and Claire Spangenberg helped improve the manuscript. We appreciate the careful technical reviews by David Pitcher (Central Utah Water Conservancy District) and David Jones (Utah Division of Drinking Water). Stephanie Carney, Mike Hylland, and Bill Keach all helped significantly improve the quality of the document.

## REFERENCES

- Abatzoglou, J.T., Dobrowski, S.Z., Parks, S.A., Hegewisch, K.C., 2018, Terraclimate, a high-resolution global dataset of monthly climate and climatic water balance from 1958–2015: *Scientific Data* v. 5, no. 170191, doi: <https://10.1038/sdata.2017.191>.
- Allen, R.G., Tasumi, M., Morse, A., Trezza, R., Wright, J.L., Bastiaanssen, W., Kramber, W., Lorite, I., and Robison, C.W., 2007a, Satellite-based energy balance for mapping evapotranspiration with internalized calibration (METRIC)—Applications: *Journal of Irrigation and Drainage Engineering*, v. 133, no. 4, p. 395–406.
- Allen, R.G., Tasumi, M., and Trezza, R., 2007b, Satellite-based energy balance for mapping evapotranspiration with internalized calibration (METRIC)—Model: *Journal of Irrigation and Drainage Engineering*, v. 133, no. 4, p. 380–394.
- Anderson, R.E., Zoback, M.L., and Thompson, G.A., 1983, Implications of selected subsurface data on the structural form and evolution of some basins in the northern Basin and Range province, Nevada and Utah: *GSA Bulletin*, v. 94, no. 9, p. 1055–1072, doi: <https://doi.org/10/df8h64>.
- Anglim, J., 2009, Factor Analysis in R | R-bloggers: Online, <https://www.r-bloggers.com/2009/10/factor-analysis-in-r/>, accessed April 2021.
- Auby, W.L., 1991, Provisional geological map of the Levan quadrangle, Juab County, Utah: Utah Geological Survey Map 135, 13 p. booklet, scale 1:24,000, <https://doi.org/10.34191/M-135>.
- Beria, H., Larsen, J.R., Michelon, A., Ceperley, N.C., and Schaeffli, B., 2020a, HydroMix v1.0—A new Bayesian mixing framework for attributing uncertain hydrological sources: *Geoscientific Model Development*, v. 13, no. 5, p. 2433–2450, doi: <https://doi.org/10/ghdwrn>.
- Best, M.G., and Christiansen, E.H., 1991, Limited extension during peak Tertiary volcanism, Great Basin of Nevada and Utah: *Journal of Geophysical Research, Solid Earth*, v. 96, no. B8, p. 13509–13528, doi: <https://doi.org/10/czp6t6>.
- Biek, R.F., 1991, Provisional geologic map of the Nephi quadrangle, Juab County, Utah: Utah Geological Survey Map 137 scale 1:24,000, doi: <https://doi.org/10.34191/M-137>.
- Bjorklund, L.J., 1967, Ground-water resources of northern Juab Valley, Utah: Utah Department of Natural Resources, Division of Water Rights Other Government Series 17, 77 p.
- Bowen, G.J., Putman, A., Brooks, J.R., Bowling, D.R., Oerter, E.J., and Good, S.P., 2018, Inferring the source of evaporated waters using stable H and O isotopes: *Oecologia*, v. 187, no. 4, p. 1025–1039, doi: <https://doi.org/10/gdxqx4>.
- Brooks, L.E., and Stolp, B.J., 1995, Hydrology and simulation of ground-water flow in southern Utah and Goshen valleys, Utah: U.S. Geological Survey Technical Publication 111, 104 p.
- Clark, D.L., 1990, Provisional geologic map of the Juab quadrangle, Juab County, Utah: Utah Geological Survey Map 132, 14 p. booklet, scale 1:24,000, doi: <https://doi.org/10.34191/M-132>.
- Constenius, K.N., 1996, Late Paleogene extensional collapse of the Cordilleran foreland fold and thrust belt: *Geological Society of America Bulletin*, v. 108, no. 1, p. 20–39, doi: <https://doi.org/10/fspdb9>.
- Daily Herald, 2018, D. Gary Young: Online, [https://www.heraldextra.com/lifestyles/announcements/obituaries/d-gary-young/article\\_2d10e786-06f6-571e-87ce-1b10d63a745f.html](https://www.heraldextra.com/lifestyles/announcements/obituaries/d-gary-young/article_2d10e786-06f6-571e-87ce-1b10d63a745f.html), accessed May 2021.

- DeCelles, P.G., and Coogan, J.C., 2006, Regional structure and kinematic history of the Sevier fold-and-thrust belt, central Utah: *Geological Society of America Bulletin*, v. 118, no. 7–8, p. 841–864, doi: <https://doi.org/10/dhc629>.
- Effimoff, I., and Pinezich, A.R., 1986, Tertiary structural development of selected basins—Basin and Range Province, northeastern Nevada: *Geological Society of America Special Paper*, v. 208, p. 31–42, doi: <https://doi.org/10/gjp7sm>.
- El-Kadi, A.I., Plummer, L.N., and Aggarwal, P., 2011, NETPATH-WIN—An interactive user version of the mass-balance model, *NETPATH: Groundwater*, v. 49, no. 4, p. 593–599, doi: <https://doi.org/10/fsz2rz>.
- Evans, J.P., and Oaks, R.Q., 1996, Three-dimensional variations in extensional fault shape and basin form—The Cache Valley basin, eastern Basin and Range province, United States: *Geological Society of America Bulletin*, v. 108, no. 12, p. 1580–1593, doi: <https://doi.org/10/dstqj>.
- Fetter, C., 1988, *Applied Hydrogeology*: Columbus, Ohio, Merrill Publishing Company, 592 p.
- Felger, T.J., Machette, M.N., and Sorensen, M.L., 2004, Provisional geologic map of the Mona quadrangle, Juab and Utah Counties, Utah: *Utah Geological Survey Open-File Report 428*, scale 1:24,000, doi: <https://doi.org/10.34191/OFR-428>.
- Fontes, J.C., and Garnier, J.M., 1979, Determination of the initial  $^{14}\text{C}$  activity of the total dissolved carbon—A review of the existing models and a new approach: *Water Resources Research*, v. 15, no. 2, p. 399–413, doi: <https://doi.org/10/fmc26m>.
- Freeze, R.A., and Cherry, J.A., 1979, *Groundwater*: Englewood Cliffs, New Jersey, Prentice-Hall, 604 p.
- Friedman, I., Smith, G.I., Johnson, C.A., and Moscati, R.J., 2002, Stable isotope compositions of waters in the Great Basin, United States part 2. Modern precipitation: *Journal of Geophysical Research—Atmospheres*, v. 107, no. D19, p. ACL 15-1-ACL 15-22., doi: <https://doi.org/10.1029/2001jd000566>.
- Frisbee, M.D., Phillips, F.M., Campbell, A.R., Hendrickx, J.M.H., and Engle, E.M., 2010, Modified passive capillary samplers for collecting samples of snowmelt infiltration for stable isotope analysis in remote, seasonally inaccessible watersheds 2—field evaluation: *Hydrological Processes*, v. 24, no. 7, p. 834–849, doi: <https://doi.org/10/cpg5ht>.
- Gerhart, P.C., 1999, Construction drawings Mona dam rehabilitation Juab County, Utah: Woodward-Clyde International Unpublished consultant's report 97U108, 15 p.
- Güler, C., and Thyne, G.D., 2006, Statistical clustering of major solutes—use as a tracer for evaluating interbasin groundwater flow into Indian Wells Valley, California: *Environmental and Engineering Geoscience*, v. 12, no. 1, p. 53–65, doi: <https://doi.org/10/bnvcv2>.
- Harbaugh, A.W., 2005, MODFLOW-2005, the U.S. Geological Survey modular ground-water model—the Ground-Water Flow Process: *U.S. Geological Survey Techniques and Methods 6-A16*, 253 p.
- Harbaugh, A.W., Banta, E.R., Hill, M.C., and McDonald, M.G., 2000, MODFLOW-2000, The U.S. Geological Survey modular ground-water model—User guide to modularization concepts and the ground-water flow process: *U.S. Geological Survey Open-File Report 00-92*, 130 p.
- Hardy, R.L., 2000, Mona residents seek to protect water shares: Online, <https://www.deseret.com/2000/9/5/19527324/mona-residents-seek-to-protect-water-shares>, accessed May 2021.
- Hart, R., 2009, Isotopic evaluation of carbon dioxide in soil gas in Utah for a more accurate input variable in ground-water age determining models: Provo, Utah, Brigham Young University, M.S. thesis, 69 p.
- Harty, K.M., Mulvey, W.E., and Machette, M.N., 1997, Surficial geologic map of the Nephi segment of the Wasatch fault zone, eastern Juab County, Utah: *Utah Geological Survey Map 170*, scale 1:50,000, doi: <https://doi.org/10.34191/M-170>.
- Healy, R.W., Winter, T.C., LaBaugh, J.W., and Franke, O.L., 2007, *Water budgets—foundations for effective water-resources and environmental management*: U. S. Geological Survey Circular 1308, 90 p.
- Hintze, L.F., and Kowallis, B.J., 2009, *Geologic history of Utah*: Brigham Young University Geology Studies, Special Publication, 225 p.
- Hurlow, H., 2014, Hydrogeologic studies and groundwater monitoring in Snake Valley and adjacent hydrographic areas, west-central Utah and east-central Nevada: *Utah Geological Survey Bulletin 135*, 304 p., doi: <https://doi.org/10.34191/B-135>.
- Hurlow, H.A., 2017, Hydrogeology of the Malad-Lower Bear River basin, north-central Utah and south-central Idaho: *Utah Geological Survey Special Study 157*, 39 p., doi: <https://doi.org/10.34191/SS-157>.
- Hylland, M.D., and Machette, M.N., 2008, Surficial geologic map of the Levan and Fayette segments of the Wasatch fault zone, Juab and Sanpete Counties, Utah: *Utah Geological Survey Map 229* scale 1:50,000, <https://doi.org/10.34191/M-229>.
- Ingraham, N.L., and Taylor, B.E., 1991, Light stable isotope systematics of large-scale hydrologic regimes in California and Nevada: *Water Resources Research*, v. 27, no. 1, p. 77–90.
- Ingerson, E., and Pearson, F.J., 1964, Estimation of age and rate of motion of groundwater by  $^{14}\text{C}$  method, in Miyake, Y. and Koyama, T., editors, *Recent research in field of hydrosphere, atmosphere and nuclear geochemistry*: Maruzen, Tokyo, p. 263–283.

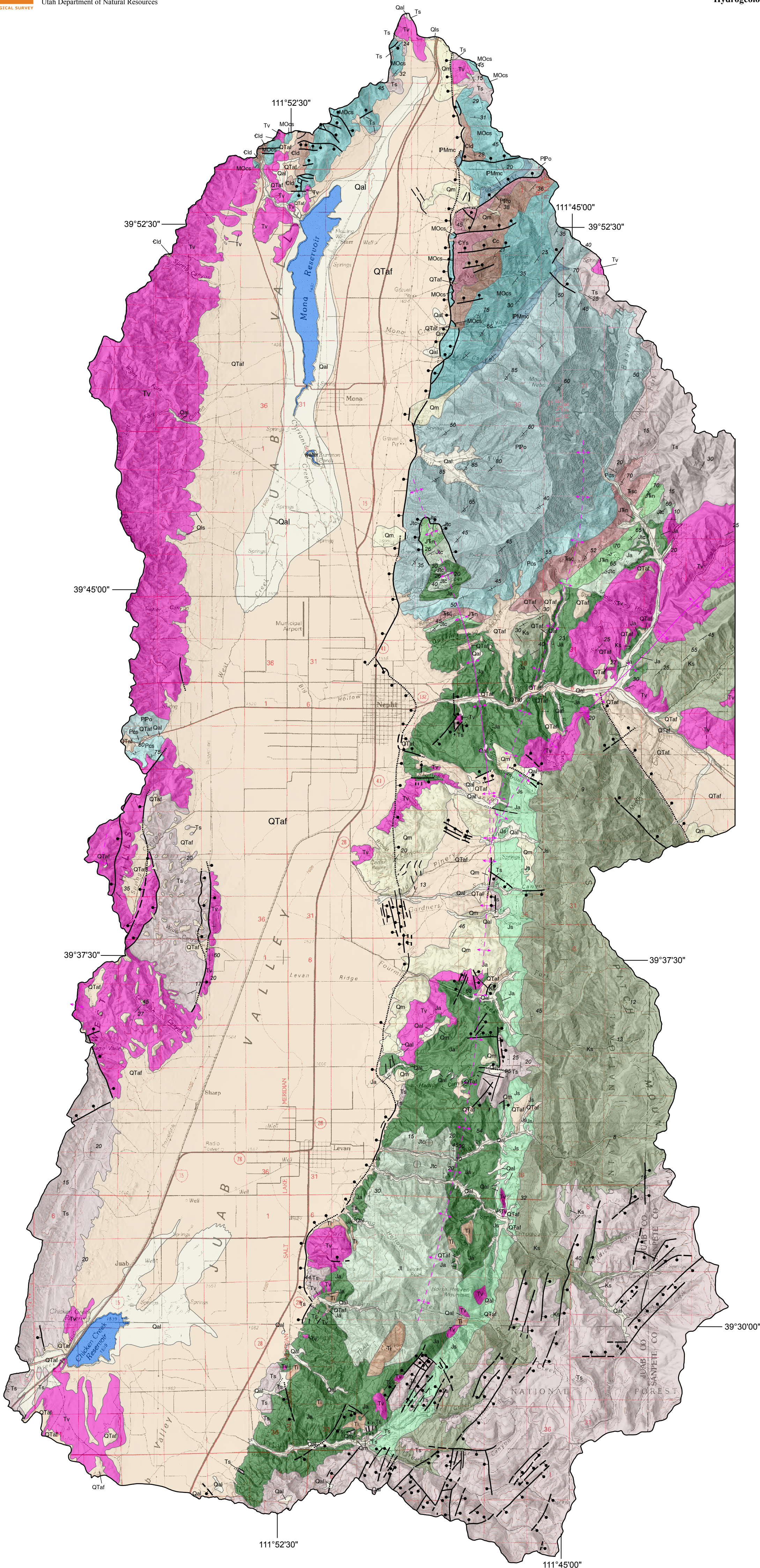
- Jurgens, B.C., Böhlke, J.K., and Eberts, S.M., 2012, TracerLPM (Version 1)—An Excel Workbook® for interpreting groundwater age distributions from environmental tracer data: U.S. Geological Survey Techniques and Methods Report 4-F3, 60 p.
- Kirby, S.M., 2012, Statistical analysis and geochemical evolution of groundwater in the Snake Valley area of western Utah—Implications for regional groundwater flow: Utah Geological Association Publication, v. 41, p. 115–134.
- Klotz, E., and Hasenyager, C., 2010, 2009 residential water use: Utah Division of Water Resources Water Use Report, 48 p.
- Kodali, T., 2016, Hierarchical Clustering in R | R-bloggers: Online, <https://www.r-bloggers.com/2016/01/hierarchical-clustering-in-r-2/>, accessed April 2021.
- Liberty, L.M., Heller, P.L., and Smithson, S.B., 1994, Seismic reflection evidence for two-phase development of Tertiary basins from east-central Nevada: Geological Society of America Bulletin, v. 106, no. 12, p. 1621–1633, doi: <https://doi.org/10/cqfvvc>.
- Mace, R., 2001, Estimating transmissivity using specific-capacity data: Bureau of Economic Geology, University of Texas at Austin Geological Circular 01–2, 44 p.
- Macfarlane, P.A., 2000, Revisions to the nomenclature for Kansas aquifers: Midcontinent Geoscience, no. 244, p. 1–14.
- Machette, M.N., Personius, S.F., Nelson, A.R., Bucknam, R.C., and Hancock, P., 1992, The Wasatch fault zone, U.S.A: Annales Tectonicae, v. 6, p. 5–39.
- McDonald, M.G., and Harbaugh, A.W., 1988, A modular three-dimensional finite-difference ground-water flow model: U.S. Geological Survey Techniques of Water-Resources Investigations, Book 6, 588 p.
- McKean, A.P., Solomon, B.J., and Kirby, S.M., 2015, Geologic map of the Goshen quadrangle, Utah and Juab Counties, Utah: Utah Geological Survey Map 272, scale 1:24000, doi: <https://doi.org/10.34191/M-272dm>.
- Miller, O.L., 2020, Quantifying trends in arsenic, nitrate, and dissolved solids from selected wells in Utah: U.S. Geological Survey USGS Numbered Series 2020–5047, 80 p., doi: 10.3133/sir20205047.
- Mook, W.G., 1972, On the reconstruction of the initial 14C content of groundwater from the chemical and isotopic composition, in Eighth International Conference on Radiocarbon Dating – Royal Society of New Zealand, p. 342–352.
- Neuman, S.P., 1982, Statistical characterization of aquifer heterogeneities, in Recent Trends in Hydrogeology: Boulder, Colorado, Geological Society of America Special Paper 189, p. 81–103.
- Pan-American Center for Earth and Environmental Studies (PACES), 2012, Gravity database of the US: Online, <http://research.utep.edu/paces>, accessed June 2012.
- Pekel, J.-F., Cottam, A., Gorelick, N., and Belward, A.S., 2016, High-resolution mapping of global surface water and its long-term changes: Nature, v. 540, no. 7633, p. 418–422, doi: <https://doi.org/10/f9gkxn>.
- Plummer, L., and Glynn, P., 2013, Radiocarbon dating in groundwater systems, in Isotope Methods for Dating Old Groundwater: International Atomic Energy Agency, Vienna, p. 33–90.
- Power Magazine, 2006, Currant Creek power plant, Mona, Utah: Power Magazine.
- PRISM Climate Group, 2012, 30-year normal precipitation—annual, period 1981–2010: Online, <http://prism.oregon-state.edu>.
- Quick, J., 2012, R tutorial series—Centering variables and generating z-scores with the scale() function: Online, <https://www.r-bloggers.com/2012/03/r-tutorial-series-centering-variables-and-generating-z-scores-with-the-scale-function/>, accessed April 2021.
- Rae, S., and Baker, T.L., 1971, Mount Nebo dam and reservoir: National Park Service Historical American Engineering Record UT-95, 3 p.
- Ries, K.G., III, Newson, J.K., Smith, M.J., Guthrie, J.D., Steeves, P.A., Haluska, T., Kolb, K.R., Thompson, R.F., Santoro, R.D., and Vraga, H.W., 2017, StreamStats, version 4: U.S. Geological Survey USGS Numbered Series 2017–3046, doi: 10.3133/fs20173046.
- Saltus, R.W., and Jachens, R.C., 1995, Gravity and basin-depth maps of the Basin and Range Province, Western United States: U.S. Geological Survey Geophysical Investigations Map GP-1012, scale 1:2,500,000, doi: <https://doi.org/10/gjp7sk>.
- Schlische, R.W., and Anders, M.H., 1996, Stratigraphic effects and tectonic implications of the growth of normal faults and extensional basins: Reconstructing the History of Basin and Range Extension Using Sedimentology and Stratigraphy, p. 183–203.
- Scholl, M.A., Ingebritsen, S.E., Janik, C.J., and Kauahikaua, J.P., 1996, Use of precipitation and groundwater isotopes to interpret regional hydrology on a tropical volcanic island—Kilauea volcano area, Hawaii: Water Resources Research, v. 32, no. 12, p. 3525–3537.
- Seaber, P.R., 1988, Hydrostratigraphic units, in Back, W., Rosenshein, J.S., and Seaber, P.R., editors, Hydrogeology: Geological Society of America, Geology of North America, v. O-2, p. 9–14., doi: <https://doi.org/10.1130/DNAG-GNA-O2.9>.
- Senay, G.B., Bohms, S., Singh, R.K., Gowda, P.H., Velpuri, N.M., Alemu, H., and Verdin, J.P., 2013, Operational evapotranspiration mapping using remote sensing and weather datasets—A new parameterization for the SSEB approach: JAWRA Journal of the American Water Resources Association, v. 49, no. 3, p. 577–591, doi: <https://doi.org/10.1111/jawr.12057>.

- Singh, R.K., Senay, G.B., Velpuri, N.M., Bohms, S., and Verdin, J.P., 2014, On the downscaling of actual evapotranspiration maps based on combination of MODIS and Landsat-based actual evapotranspiration estimates: *Remote Sensing*, v. 6, no. 11, p. 10483–10509, doi: <https://doi.org/10.3390/rs61110483>.
- Smith, L., Birken, A.S., Klebba, P.H., Jones, K.K., Derrick, V.N., Downhour, P., Eacret, R.J., Gibson, T.L., Slaugh, B.A., Whittier, N.R., Douglas, B.P., LaBonte, D.V., and Fisher, M.J., 2019, Groundwater conditions in Utah, spring of 2018: Utah Department of Natural Resources Other Government Series, 117 p.
- Smith, R.B., and Bruhn, R.L., 1984, Intraplate extensional tectonics of the eastern Basin-Range—Inferences on structural style from seismic reflection data, regional tectonics, and thermal-mechanical models of brittle-ductile deformation: *Journal of Geophysical Research, Solid Earth*, v. 89, no. B7, p. 5733–5762, doi: <https://doi.org/10.1029/J089B07057>.
- Sprinkel, D., Doelling, H., Kowallis, B., Waanders, G., and Kuehne, P., 2011, Early results of a study of Middle Jurassic strata in the Sevier fold and thrust belt, Utah, *in* Sprinkel, D., Yonkee, W.A., and Chidsey, T.C., Jr., *Sevier thrust belt—northern and central Utah and adjacent areas*: Utah Geological Association Publication 40, p. 151–172.
- Steiger, J.I., 1995, Selected hydrologic data for Juab Valley, Utah, 1935–94: U.S. Geological Survey USGS Numbered Series 95–101, 89 p., doi: <https://doi.org/10.3133/ofr95101>.
- Tamers, M.A., 1975, Validity of radiocarbon dates on ground water: *Geophysical Surveys*, v. 2, no. 2, p. 217–239, doi: <https://doi.org/10.1080/00141801.1975.10644477>.
- Thiros, S.A., Stolp, B.J., Hadley, H.K., and Steiger, J.I., 1996, Hydrology and simulation of ground-water flow in Juab Valley, Juab County, Utah: Utah Department of Natural Resources, Division of Water Rights 114, 100 p.
- U.S. Census Bureau, 2020, Population and housing unit estimates: Online, <http://www.census.gov/popest/>, accessed November 2021.
- U.S. Geological Survey (USGS), 2021, National Water Information System (NWIS) database: Online, <http://water-data.usgs.gov/nwis>, accessed November 2021.
- Utah Climate Center Climate data for Nephi and Levan stations: Online, <https://climate.usurf.usu.edu/>, accessed November 2021.
- Utah Division of Water Rights, 2020, Water use data from the Utah Water Use Program: Online, <https://waterrights.utah.gov/distinfo/wuse.asp>, accessed December 2020.
- Utah Division of Water Rights, 2021, Utah Well Logs: Online, <https://opendata.gis.utah.gov/>, accessed November 2021.
- Utah Foundation, 2014a, An analysis of projected population change in Utah: Utah Foundation Research Report 720, 17 p.
- Utah Foundation, 2014b, Flowing toward 2050—Utah’s water outlook: Utah Foundation Research Report 723, 20 p.
- Utah Geospatial Resource Center (UGRC), 2021, Retail culinary water suppliers dataset: Online, <https://gis.utah.gov/data/utilities/retail-culinary-water-suppliers/>, accessed November 2021.
- Utah State History, 2010, The Goshen and Mona water dispute, 1873—1881—A case study of the struggle between ecclesiastical and secular authority in Utah: *Utah Historical Quarterly*, v. 78, no. 4.
- Witkind, I.J., and Weiss, M.P., 1991, Geologic Map of the Nephi 30' x 60' Quadrangle, Carbon, Emery, Juab, Sanpete, Utah, and Wasatch Counties, Utah: U.S. Geological Survey Miscellaneous Investigation Series, Map I-1937 16 p. pamphlet, scale 1:100,000.
- Witkind, I.J., Weiss, I.J., and Brown, T.L., 1987, Geologic map of the Manti 30' x 60' Quadrangle, Carbon, Emery, Juab, Sanpete and Sevier counties, Utah: U.S. Geological Survey Miscellaneous Investigation Series, Map I-1631, scale 1:100,000, doi: <https://doi.org/10.3133/i1631>.
- Zoback, M.L.C., 1992, Superimposed late Cenozoic, Mesozoic, and possible Proterozoic deformation along the Wasatch fault zone in central Utah, *in* Gori, P.L., and Hays, W.W., editors, *Assessment of regional earthquake hazards and risk along the Wasatch Front, Utah*: U.S. Geological Survey Professional Paper 1500-A-J, p. E1–E20.

**APPENDIX**

Tables A1–A6:

[https://ugspub.nr.utah.gov/publications/special\\_studies/ss-170/ss-170-a.pdf](https://ugspub.nr.utah.gov/publications/special_studies/ss-170/ss-170-a.pdf)



## SIMPLIFIED HYDROGEOLOGIC MAP OF JUAB VALLEY, UTAH

### Symbols

- Normal fault, dashed where approximately located, dotted where concealed; bar and ball on down-dropped side
- Fault, unknown, dashed where approximately located, dotted where concealed
- Anticline, dashed where approximately located
- Bedding, horizontal
- Bedding, vertical
- Bedding, inclined
- Bedding, overturned

### Geologic Units

- Alluvial deposits
- Mass-movement deposits
- Lacustrine deposits
- Alluvial-fan deposits
- Intrusive rocks
- Volcanic (pyroclastic and volcanoclastic) rocks
- Tertiary sedimentary rocks
- Cretaceous siliclastic rocks
- Jurassic siliclastic and carbonate rocks
- Jurassic Arapian Formation
- Twin Creek limestone
- Nugget Sandstone (siliclastic rocks)
- Triassic siliclastic and carbonate rocks
- Permian carbonate and siliclastic rocks
- Oquirrh Formation
- Manning Canyon Shale
- Mississippian, Ordovician, and Devonian carbonate and siliclastic rocks
- Cambrian carbonate rocks
- Cambrian and Proterozoic siliclastic rocks
- water

